(27)

Theoretical and Experimental Studies of Vesicle Formation in Surfactant Mixtures

by

Pak K. Yuet
M.Sc., Chemical Engineering (1990)
Queen's University
B.Eng., Chemical Engineering (1988)
Technical University of Nova Scotia

Submitted to the Department of Chemical Engineering
in partial fulfillment of the requirements for the degree of

Doctor of Philosophy

at the

MASSACHUSETTS INSTITUTE OF TECHNOLOGY

June 1996

Author . .....
Department of Chemical Engineering
May 16, 1996

Certified by .....
Daniel Blankschtein
Associate Professor
Thesis Supervisor

Accepted by .....
Robert E. Cohen
Chairman, Departmental Committee on Graduate Students

Theoretical and Experimental Studies of Vesicle Formation in Surfactant Mixtures

by

Pak K. Yuet

M.Sc., Chemical Engineering (1990)

Queen's University

B.Eng., Chemical Engineering (1988)

Technical University of Nova Scotia

Submitted to the Department of Chemical Engineering
on May 16, 1996, in partial fulfillment of the
requirements for the degree of
Doctor of Philosophy

Abstract

A fundamental understanding of vesicle formation and stability in mixed surfactant systems is important for the description of their phase behavior, for the application of vesicles as encapsulating devices, and for the elucidation of cholesterol gallstone formation in bile, where the solubilization of cholesterol in vesicles has been suggested to correlate with the metastability of bile. To gain a better understanding of vesiculation, a molecular-thermodynamic theory was developed to describe the formation of mixed surfactant vesicles. The theory incorporates a detailed modeling of the various free-energy contributions associated with vesiculation, including a mean-field calculation of the free-energy contribution associated with packing of the surfactant tails in the vesicle bilayer, an estimation of the surfactant-head steric repulsions using an equation of state for hard-disk mixtures, in the context of the scaled-particle theory, and a calculation of the electrostatic free energy of a vesicle using approximate analytical expressions for the surface potentials. By knowing only the molecular structure of the surfactants involved in vesicle formation and the solution conditions, the theory can predict a wealth of vesicle properties, including vesicle size and composition distribution, surface charge densities, surface potentials, and compositions of vesicle leaflets. More importantly, this theory is able to reveal the relative importance of, as well as the interplay between, the various free-energy contributions to vesiculation. In particular, it was found that: (i) the distribution of surfactant molecules between the two vesicle leaflets plays a major role in vesiculation, (ii) vesicles that are stabilized by the entropy of mixing, such as those containing surfactants of similar tail lengths,

are large and widely distributed in size, and (iii) mixed surfactant vesicles, which are characterized by small sizes and a narrow size distribution, can be stabilized energetically in highly asymmetric surfactant mixtures. In addition, it was found that vesicle composition is determined by the interplay between the entropy of mixing and the free energy of vesiculation. Specifically, decreasing surfactant tail-length asymmetry reduces the energetic influence, as compared to the entropic one, by decreasing the surfactant tail transfer free energy, thus producing an effect on vesicle composition similar to that produced by adding salt, which reduces the electrostatic free-energy contribution associated with vesiculation.

In the experimental study of cholesterol solubilization in model bile, a systematic comparison of ultracentrifugation and gel chromatography was first conducted regarding their ability to separate vesicles and mixed micelles in model bile. It was found that ultracentrifugation overestimates vesicular cholesterol content, mainly due to the creation of a bile salt depletion zone. This technique was then modified by reducing the mobility of mixed micelles in a centrifugal field. The distribution of cholesterol measured by the modified technique was found to agree well with that measured using gel chromatography. This modified technique and gel chromatography were then used in a two-level factorial experiment to investigate the effects of several physiological variables, including total lipid content, bile salt (BS) to egg-yolk phosphatidylcholine (EYPC) ratio [BS/(BS+EYPC)], cholesterol (Ch) content, and bile salt hydrophobicity, on two responses: the distribution of cholesterol and the vesicular Ch/EYPC ratio. The results show that: (i) the total lipid content has a significant but opposite effect on the two responses, (ii) increasing total lipid content reduces the percentage of cholesterol in vesicles while raising the vesicular Ch/EYPC ratio, (iii) the BS/(BS+EYPC) ratio is the most important variable in determining the vesicular Ch/EYPC ratio, but does not seem to affect the distribution of cholesterol, and (iv) the bile salt hydrophobicity affects both responses, presumably through the interactions with the hydrophobic moieties of the phospholipids. Total lipid content was also found to interact strongly with the BS/(BS+EYPC) ratio and with the bile salt hydrophobicity in determining the distribution of cholesterol. In addition, the effect of bile salt hydrophobicity on the vesicular Ch/EYPC ratio was found to depend on total lipid content, as well as on the BS/(BS+EYPC) ratio. These findings suggest that the metastability of bile may be correlated to the vesicular Ch/EYPC ratio, but not to the distribution of cholesterol, and that it is possible to effectively alter the two responses by varying several physiological variables simultaneously.

The theoretical and experimental findings of this thesis should contribute to our fundamental knowledge on surfactant mixtures, as well as on the formation of cholesterol gallstones in bile. It is also hoped that this thesis will serve as a gateway for further exciting and rewarding discoveries in the area of mixed surfactant systems.

Thesis Supervisor: Daniel Blankschtein
Title: Associate Professor

Acknowledgments

I dedicate this thesis to my parents. Without their encouragement, I would not have pursued my Ph.D. degree. I thank them for their love; I thank them for everything.

I would also like to thank Professor Blankschtein for his guidance and advice. He is always there when I need him, both academically and personally. In fact, after six years, he is more than just a thesis advisor; he is a good friend of mine. And, of course, Ginger is always there to listen to my complaints and to talk to me; without her, my final year at MIT would have been very different.

Thanks also go to Dr. Joanne Donovan for her advice on the experimental program of this thesis, to Dr. Sudhakar Puvvada for his help in getting me started on this work, to Irene Kotok for her assistance in the experimental work, to Monika Leonard for teaching me the laboratory skills, and to Dr. Martin Carey for many helpful discussions.

And now the crew. I would like to thank Dr. Leo Lue for the many late-night intellectual discussions, the Ashdown desserts, and some very "deep" conversations on the meaning of life, Nancy Zoeller for sharing the cubicle for over three years (without complaint), Anat Shiloach for the coffee run, Dr. Chia-li Liu for just being there (when I thought nobody was around), and Ayal Naor for introducing me to the "real" music.

Finally, I would like to express my gratitude to the National Institute of Health (NIH) Biotechnology Training Grant and the American Liver Foundation for financial support.

Contents

List of Figures

List of Tables

Chapter 1

Introduction

Surfactants, or surface active agents, are molecules that contain both hydrophilic ("water-loving") and hydrophobic ("water-fearing") moieties. The hydrophilic moiety, usually referred to as the "head", prefers to be surrounded by water molecules, whereas the hydrophobic moiety, usually referred to as the "tail", tends to repel water molecules. Because of this dual affinity (sometimes referred to as "amphiphilicity"), when surfactants are placed in water which is in contact with air, they migrate to the water/air surface, with their hydrophobic tails protruding into the air and their hydrophilic heads immersed in the water. Similarly, when surfactants are placed in a system containing water and hydrocarbon, they collect at the macroscopic water/hydrocarbon interface, with their hydrophobic tails now residing in the hydrocarbon phase. By collecting at surfaces or interfaces, surfactants have the ability to lower surface or interfacial tensions. This property has been widely exploited in detergents, shampoos, and other cleansing agents, which are an indispensable part of our modern life. The physical origin of the migration of surfactants to the surface of an aqueous system, or to the interface of a water/hydrocarbon system, is simply the minimization of the system free energy. When a surfactant molecule is placed in water, the water molecules surrounding the hydrophobic tail are forced to adopt a more ordered arrangement, as compared to that in pure water. By transferring the surfactant molecule to the surface or interface, and removing the tail out of the aqueous phase, the previously ordered water molecules can be released, thus gaining

entropy and lowering the free energy of the system. This is, indeed, the so-called "hydrophobic effect" [162].

1.1 Self-Assembly of Surfactants

As the surface or interface gets more crowded, it becomes increasingly difficult to transfer additional surfactant molecules to that location, and therefore, the free-energy gain associated with this transfer process diminishes as the solution becomes more concentrated in surfactant. Beyond a certain threshold surfactant concentration, known as the critical micelle concentration (CMC) [1], therefore, the surfactant molecules prefer to self-assemble in the aqueous phase, forming microstructures that contain both hydrophobic and hydrophilic regions. The hydrophobic region is composed of the surfactant tails, and is shielded from water by the hydrophilic region composed of the surfactant heads. Self-assembling thus constitutes another vehicle to accommodate for the hydrophobic effect.

Surfactants can self-assemble in dilute aqueous solutions into a variety of microstructures, including micelles, vesicles, and lamellae. In particular, unilamellar vesicles, which are composed of a closed bilayer that separates an inner aqueous compartment from the outer aqueous environment, are often found in various aqueous surfactant systems. Figure 1-1 shows a schematic representation of a two-component unilamellar surfactant vesicle, with the two types of surfactant heads represented by the black and white circles. Note that the vesicle hydrophobic region may be viewed as composed of an outer and an inner leaflet. The outer and inner leaflets correspond to those regions formed by the surfactant molecules anchoring at the outer and inner hydrocarbon/water interfaces, respectively. Because of their unique morphology, vesicles have been used as encapsulating agents in diverse practical applications, including the controlled delivery of drugs, of active substances in cosmetics, and of functional food ingredients such as enzymes [59, 96, 97]. In many cases, for example,

[1] In a surfactant mixture, this threshold concentration depends on the relative composition of the surfactants.

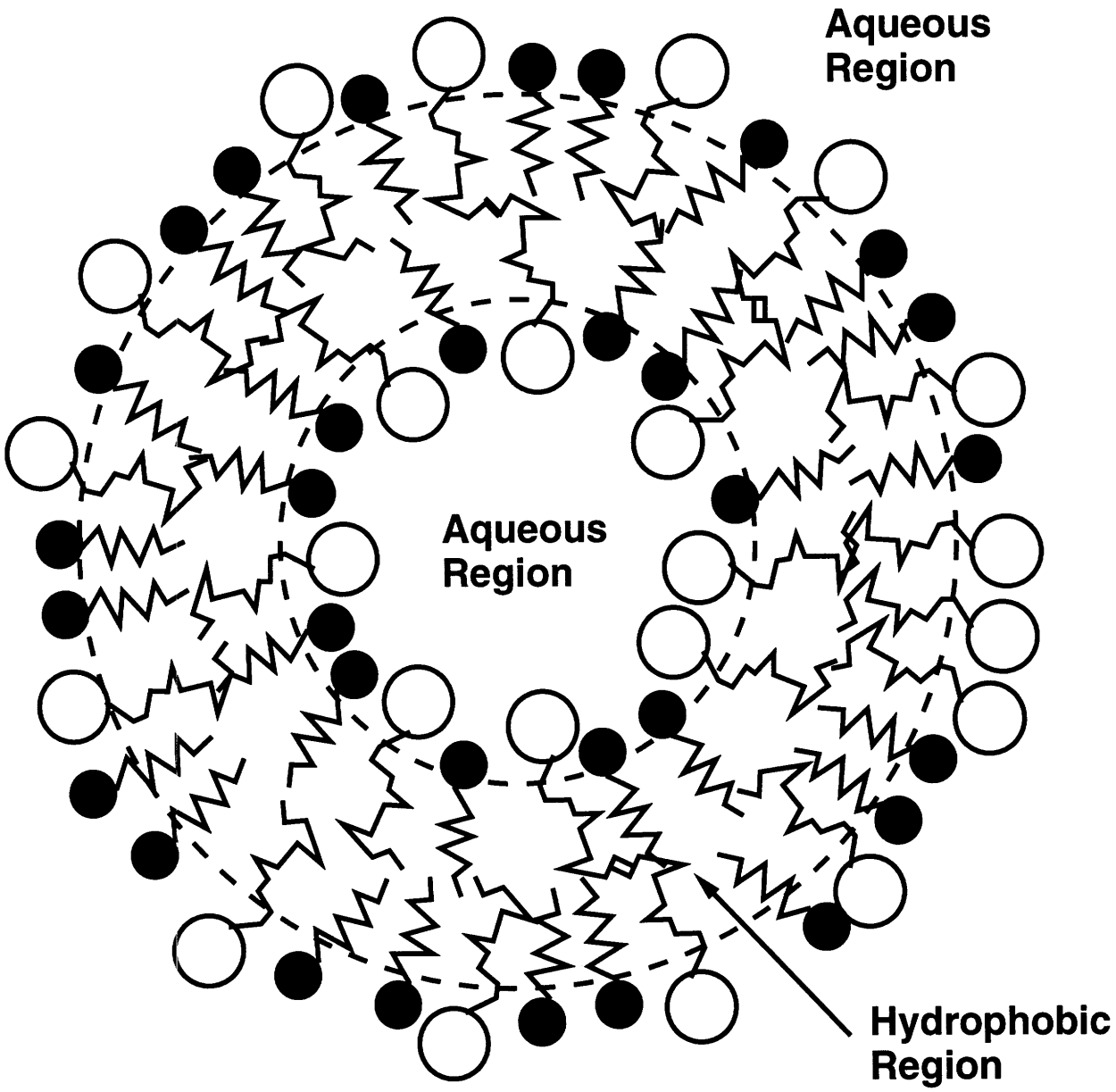

Figure 1-1: Schematic diagram of a two-component unilamellar surfactant vesicle. The two surfactant molecules are represented by the black and white heads with hydrophobic tails of different lengths. The hydrophobic region of the vesicle, which is bounded by the two dashed lines, is composed of the hydrophobic tails of the two surfactants.

that of phospholipid vesicles, the formation of vesicles requires the input of some form of energy, such as sonication [100]. These vesicles often aggregate and fuse to form large multilamellar structures within days, and are believed to be thermodynamically unstable. On the other hand, vesicles have been found to form spontaneously in some aqueous surfactant systems, including solutions containing: (i) mixtures of lecithin and lysolecithin [69], (ii) mixtures of long- and short-chain lecithins [57], (iii) mixtures of AOT and choline chloride [120], (iv) dialkyldimethylammonium hydroxide surfactants [18, 68, 129, 130, 161], (v) cationic siloxane surfactants [102], and (vi) mixtures of cationic and anionic surfactants [19, 75, 86, 87, 92]. These spontaneously-forming vesicles are believed to be thermodynamically stable in the sense that they are more resistant to aggregation and fusion, and that no energy input, besides gentle mixing, is required for their formation.

1.2 Biomedical Implication of Vesicles

In addition to the industrial applications mentioned above, vesicles formed by surfactant mixtures also have a very important implication in the medical field. Besides being used as model cell membranes because of their unique closed bilayer structure [51], vesicles play an important role in the formation of cholesterol gallstones in bile.

1.2.1 Bile and Cholesterol Gallstones

Human bile is formed in the liver as a solution of bile salt, phospholipid, cholesterol, electrolytes, and other components such as proteins [21]. A major fraction the bile secreted by the liver passes into the gallbladder, where it is concentrated as water is absorbed through the wall of the gallbladder. In addition to facilitating the digestion and absorption of fats, bile is also the only means by which cholesterol is excreted out of the body. The three major lipid components in bile: bile salt, phospholipid, and cholesterol, are all amphiphilic molecules, which can self-assemble to form aggregates, such as, simple micelles, mixed micelles, and vesicles, in bile [21, 111, 152]. Indeed, biliary cholesterol is solubilized by these aggregates [25], resulting in an extraordinarily

high cholesterol concentration in bile compared to its solubility in water [145]. Figure 1-2 depicts the general structure of a taurine-conjugated bile acid molecule. The hydroxyl groups, whose positions are indicated by R1, R2, and R3, and the ionic end of the taurine group (SO_3^-) form the hydrophilic regions, while the fused hydrocarbon ring structure forms the hydrophobic region. The structure of a phosphatidylcholine molecule is shown in Figure 1-3. The hydrophilic head of this molecule consists of a negatively charged phosphate group, a positively charged choline group, and the glycerol backbone. It is referred to as a zwitterionic, or dipolar, head (containing both a cation and an anion). The hydrophobic group contains two hydrocarbon chains which belong to two fatty acids. The structure of a cholesterol molecule is shown in Figure 1-4. The hydroxyl group at the number 3 carbon position on ring A forms the hydrophilic moiety. Note that the cholesterol molecule has a nearly planar structure, as opposed to the buckled structure of a bile acid molecule.

In lithogenic biles, cholesterol nucleates and precipitates as monohydrate crystals, which then agglomerate to form macroscopic cholesterol gallstones. Cholesterol gallstone is a common disease in most western countries. About 20 % of the population over the age of 65 have gallstones, and it is estimated that about $8 billion is spent every year on the treatment of this disease. In the past decades, significant research effort has been devoted to understanding the formation of cholesterol gallstones, and much attention has been devoted to elucidate the effects of the physico-chemical properties of bile, including the molecular structures of the lipid components (bile salt, phospholipid, and cholesterol), the composition of the bile, and the aggregation state of the lipids, on the stability of bile with respect to cholesterol nucleation [25, 94]. In particular, it has been suggested that the distribution of cholesterol between vesicles and mixed micelles, as well as the vesicle composition, play an important role in cholesterol nucleation [66, 67, 136].

1.2.2 Model Biliary System

Since native bile is such a complex system containing over forty components [21], and is not readily available, a model biliary system is often used in the experimental

Bile acid	R1	R2	R3
Cholic Acid	α-OH	α-OH	α-OH
Ursodeoxycholic Acid	α-OH	β-OH	H
Chenodeoxycholic Acid	α-OH	α-OH	H
Deoxycholic Acid	α-OH	H	α-OH
Lithocholic Acid	α-OH	H	H

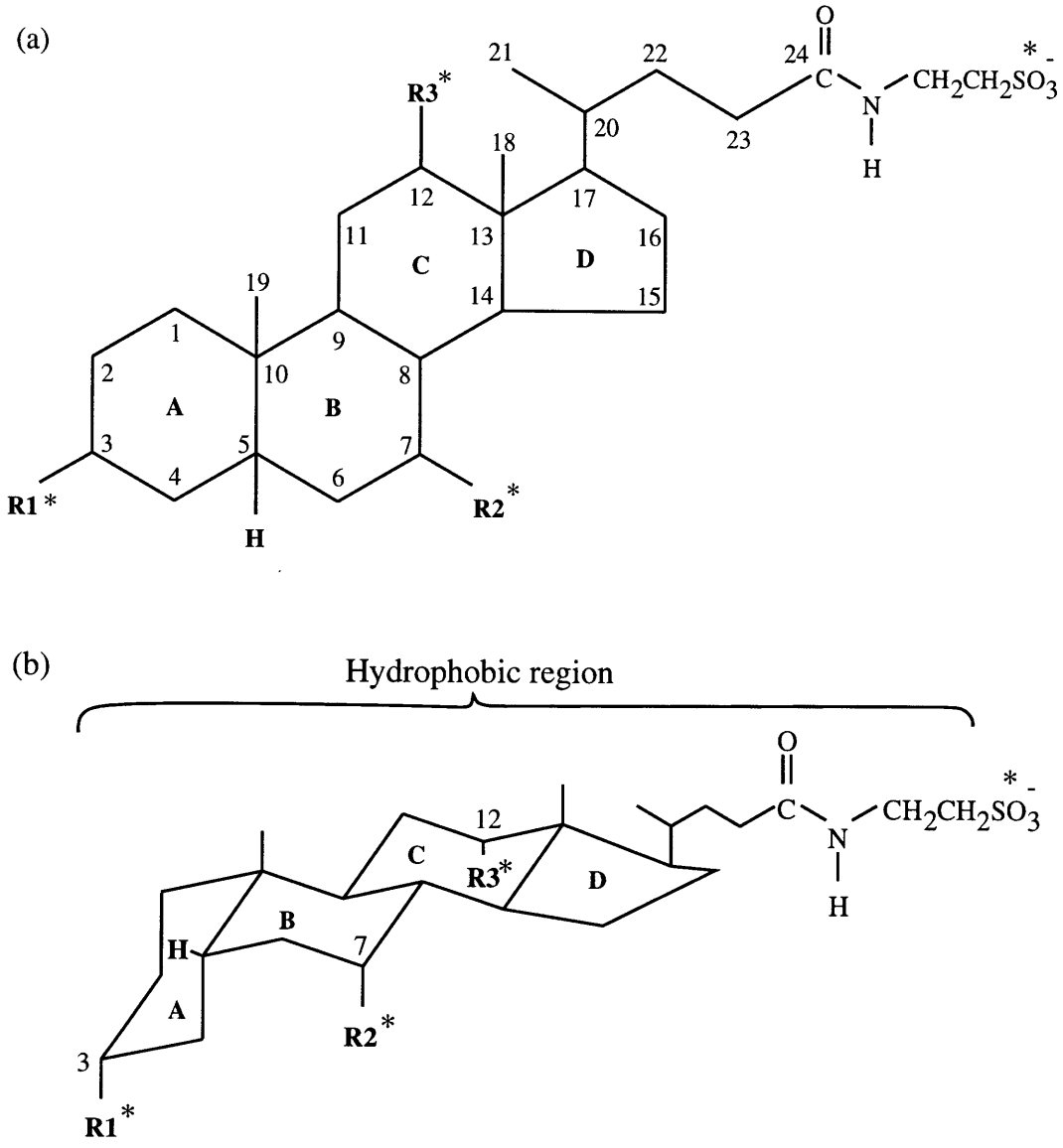

Figure 1-2: Molecular structure of taurine-conjugated bile acids. (a) "Top-view" of the molecule. (b) "Side-view" of the molecule showing the buckled structure of rings A and B. The hydrophilic regions are marked by "*".

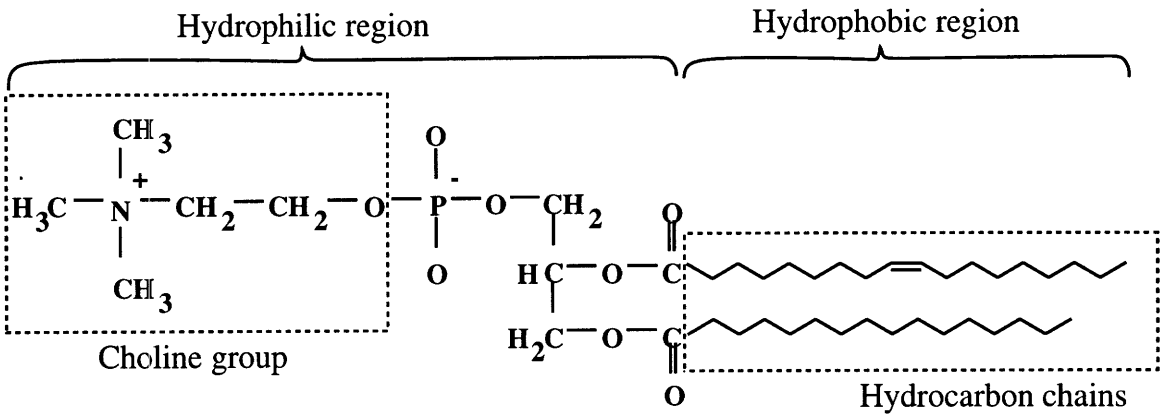

Figure 1-3: Molecular structure of 1-palmitoyl-2-oleoyl phosphatidylcholine.

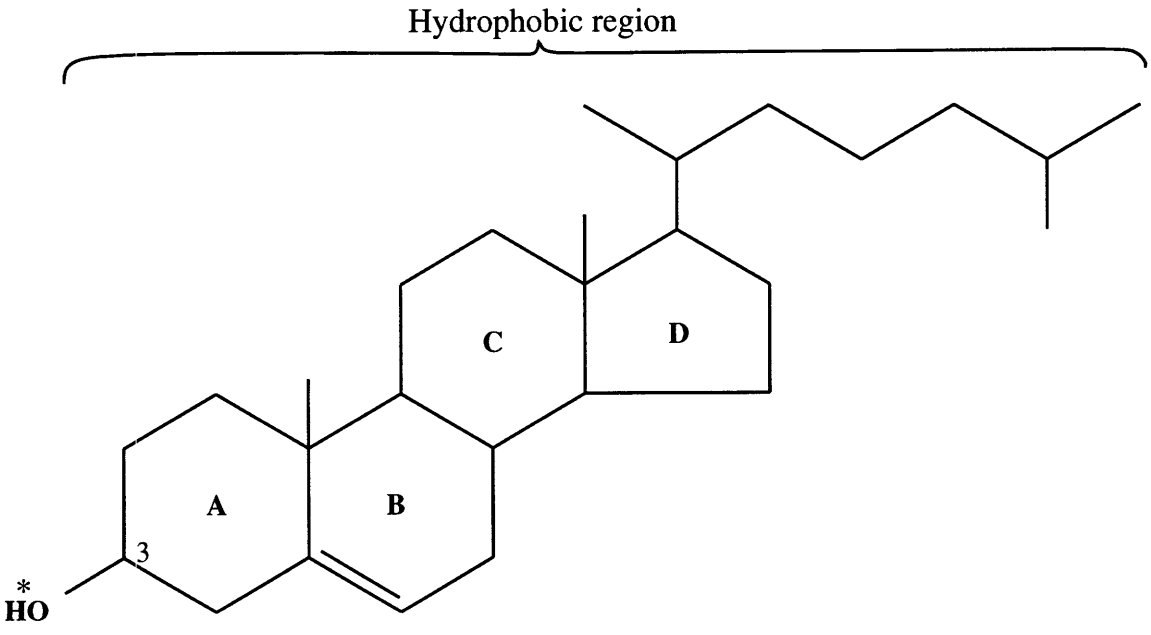

Figure 1-4: Molecular structure of cholesterol. The hydrophilic region is marked by "*".

studies of cholesterol gallstone formation. Such a system, often referred to as "model bile" in the area of bile research, consists of bile salt, phospholipid, cholesterol, water, sodium chloride, and a small amount of sodium azide to prevent bacterial growth. While native bile contains a mixture of bile salts, as shown in Figure 1-2, the "bile salt" component in a model bile is usually represented by a specific species of bile salt, such as sodium taurocholate (TC). Egg-yolk phosphatidylcholine (EYPC) is usually used to make up the "phospholipid" component because native bile contains mostly phosphatidylcholine, and the hydrocarbon chain-length distribution in EYPC is similar to that in native bile. The concentration of sodium chloride ranges from 0.1 M to 0.2 M, corresponding to the physiological concentration of sodium chloride in native bile. In addition to the components described here, other substances such as proteins or calcium salt may be included, depending on the objectives of a particular study.

The phase behavior of model bile was first studied by Carey and Small [26] using various mixtures of bile salts, phospholipids, and cholesterol. They developed the equilibrium phase diagram for a ternary model biliary system having a fixed water content. A schematic representation of this phase diagram is shown in Figure 1-5. Mapping of the compositions obtained from native biles onto the phase diagram has revealed that many native bile samples fall within the three-phase region (see Figure 1-5), in which a solution of micelles and vesicles should be at equilibrium with cholesterol crystals, yet not all of them contain cholesterol crystals or gallstones [79]. This observation, together with the concept of cholesterol supersaturation index (CSI)[2], has advanced the idea of metastability in bile. The phase diagram, however, is not complete. Although the single-phase micellar solution region, that is, the region bounded by the solid line in the phase diagram (see bottom region of Figure 1-5), is quite well-defined, the boundaries involving two-phase and three-phase equilibria (regions bounded by the light dashed lines) are still unclear.

[2]The cholesterol supersaturation index is a measure of the amount of cholesterol in a bile sample relative to the solubility of cholesterol in a model bile of corresponding lipid (bile salt, phospholipid, and cholesterol) composition [23].

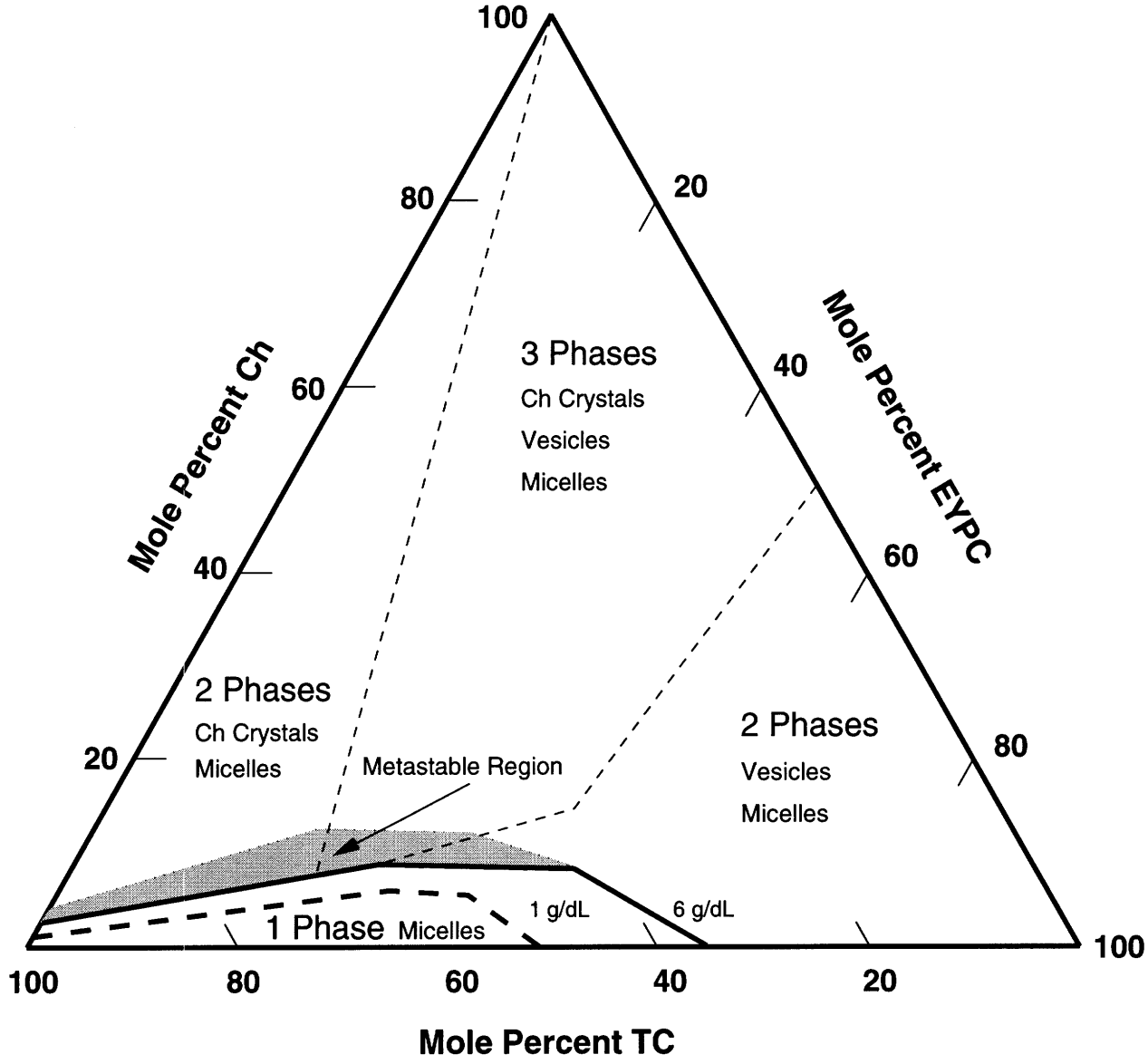

Figure 1-5: Schematic equilibrium phase diagram for the pseudo-ternary system containing taurocholate (TC), egg-yolk phosphatidylcholine (EYPC), cholesterol (Ch), and a fixed proportion of water. The boundary of the one-phase micellar solution is denoted by the solid line for 6 g/dL total lipid content (heavy dashed line for 1 g/dL total lipid content). The two light dashed lines are the approximate boundaries separating the various multi-phase regions as indicated in the diagram. The two-phase (vesicles and micelles) metastable region is denoted approximately by the shaded region above the one-phase micellar solution. (Phase diagram adapted from Ref. 26).

1.3 Research Motivation

In light of the background information given above, fundamental research on vesicle formation in surfactant mixtures will benefit many different areas, including colloid and interface science, complex fluids, encapsulation and drug delivery, and cholesterol gallstone formation in bile. The research described in this thesis addresses several important theoretical and experimental aspects of mixed vesicular systems, and the motivation for the studies to be conducted as part of this thesis is presented below.

1.3.1 Theoretical Studies of Mixed Vesicles

In spite of the practical importance of mixed surfactant vesicles, as reflected in the various industrial and drug delivery applications described above, as well as in the intimate relation between vesicles and cholesterol gallstone formation in bile, there is still a lack of theoretical understanding regarding the formation of mixed surfactant vesicles. Consequently, the theoretical analysis of mixed surfactant vesicles represents an important step towards developing a better fundamental understanding of the problems encountered in the different areas cited above. More specifically,

1. In the general areas of colloid and interface science and complex fluids, vesicles represent an important class of self-assembling microstructures, as alluded to earlier. Accordingly, in order to understand the global phase behavior, as well as to rationalize the fundamental principles involved in the self-assembly of surfactant mixtures, a theoretical description of mixed vesicles is essential. In addition, as mentioned earlier, the traditional phospholipid vesicles and the spontaneously-forming cationic/anionic vesicles exhibit rather different behaviors in terms of their formation and their thermodynamic stability. This has posed challenging problems in understanding how vesicles are formed in various surfactant systems. Moreover, by carefully studying the interplay between the various free-energy contributions responsible for vesicle formation, one can also shed light on the physics and chemistry of other surfactant microstructures such as mixed micelles.

2. The practical implementation of vesicles as encapsulating devices in industry and in the drug delivery area also demands a more fundamental knowledge of the formation and stability of mixed surfactant vesicles. Vesicle size and size distribution, for example, play an important role in determining the amount of substances that can be encapsulated, as well as in affecting the kinetics of the release of these substances. As will be shown in chapters 4 and 5, a detailed examination of the relative importance of the various free-energy contributions associated with the process of vesiculation[3], including their interplay, can reveal valuable information regarding the factors controlling vesicle size and size distribution.

3. In the context of cholesterol gallstone formation in bile, a theoretical analysis of mixed surfactant vesicles should provide insights into the mechanism of cholesterol solubilization in bile, which may, in turn, lead to a better understanding of the problem of cholesterol nucleation in bile. Since bile can be treated as a complex fluid containing vesicles and mixed micelles, the development of a theoretical framework aimed at describing the behavior of vesicular systems can provide a starting point for the fundamental study of biliary systems.

Two major theoretical approaches are currently used to study the formation of unilamellar vesicles: the curvature-elasticity approach and the molecular approach. The curvature-elasticity approach, which is by far the more popular of the two theoretical approaches, describes the vesicle bilayer as a continuous membrane characterized by the spontaneous curvature and the elastic bending modulus [72, 90]. In this approach, the formation of finite-sized vesicles depends on the interplay between these two quantities [73, 147]. The theory provides an elegant, simple way to describe the formation of vesicles, and it has been utilized in many theoretical studies to describe vesicle shape deformation and phase behavior [5, 6, 88, 119, 148, 163, 164], as well as electrostatic effects on membrane rigidity [54, 55, 117, 175]. However, because

[3] "Vesiculation" refers to the process by which surfactant monomers self-assemble in an aqueous environment to form a vesicle.

this approach is based on a curvature expansion of the free energy of a membrane, it breaks down for small vesicles, for which the curvature is quite pronounced. In addition, within the framework of this theory, the spontaneous curvature and the elastic bending modulus are treated as phenomenological parameters, thus limiting its quantitative predictive ability. May and Ben-Shaul have recently calculated [109] these parameters for mixed bilayers using a mean-field molecular theory for chain packing, and phenomenological expressions for the head group and interfacial free-energy contributions. They concluded that, for surfactant mixtures containing 16- and 8-carbon tails, the planar bilayer is energetically favorable, and that the addition of short tails considerably reduces the bending rigidity. Bergström and Eriksson have performed similar calculations for a mixture of sodium dodecyl sulfate and dodecanol [9] using empirical expressions for chain packing and head-group interactions. They also concluded that the addition of a long-chain alcohol can significantly reduce the bending constant and therefore promote spontaneous vesicle formation. However, since these calculations are also based on the curvature-expansion approach, their conclusions are applicable only to large vesicles (small curvatures), and, therefore, the effect of surfactant tail-length asymmetry on the stabilization of small vesicles remains unclear. Nevertheless, the curvature-elasticity approach has been very successful in guiding experimental studies and explaining, at least qualitatively, many experimental observations.

The molecular approach was pioneered by Israelachvili, Mitchell, and Ninham [81, 82, 115], who developed a geometric packing argument that permits one to predict the shape of self-assembling microstructures, including spheroidal, cylindrical or discoidal micelles, vesicles, and bilayers. Using a simple model based on the principle of opposing forces proposed by Tanford [162], Israelachvili and co-workers [82] predicted a near-Gaussian distribution of vesicle sizes. The theory was later extended to describe two-component vesicles [30], such as those formed from mixtures of phospholipid and cholesterol, and yielded similar results. Nagarajan and Ruckenstein also developed a molecular model for vesicles [124] using a statistical-thermodynamic approach. Their model included the free-energy changes associated with the loss of

translational and rotational degrees of freedom of the molecules in the aggregate, and treated the electrostatic interactions between ionic or zwitterionic surfactant heads at the Debye-Hückel approximation level [123]. Their work represents the first serious attempt to develop a predictive model for the formation of vesicles. Recently, a molecular theory based on the cell model [63] has been developed for cationic/anionic mixed vesicles [19], which predicts surface charge densities, including salt effects, in good agreement with experimental data. However, this theory does not account for the packing of the surfactant tails in the vesicle hydrophobic region, and it is not completely predictive in the sense that the vesicle radius is an input parameter determined experimentally.

In order to elucidate the complex mechanism involved in the process of vesiculation, it is quite clear that a detailed molecular theory is required. A satisfactory molecular theory should be applicable over the entire vesicle size range, and allow for an estimation of the various free-energy contributions associated with vesiculation so that one can examine their relative importance and interplay in determining the vesicle properties, such as size and composition distribution. The ability to cover the entire vesicle size range is particularly important in the sense that, as mentioned in the preceding paragraph, the theoretical analysis should be capable of incorporating other microstructures, regardless of their sizes, in the study of the global phase behavior of surfactant mixtures. In developing such a theory, therefore, the various free-energy contributions associated with vesiculation must be accounted for carefully. More specifically,

1. Since the surfactant tails are constrained within the vesicle hydrophobic region, the tail packing must be treated accordingly to reflect the free-energy difference between the tails in a vesicle and those in the bulk solution. In addition, because a vesicle possesses a finite curvature, as opposed to a planar bilayer, one needs to account explicitly for the effect of curvature on the packing of the surfactant tails in a vesicle bilayer, particularly when the vesicle is very small (see chapters 2, 4, and 5).

2. The presence of a finite vesicle curvature poses additional challenges in the computation of the free energy of vesiculation. In particular, a curved bilayer consisting of two surfactant components requires five variables for its characterization (see chapter 2), and therefore, in the minimization of the vesicle free energy, one must sample a large configurational space. In addition, in the calculation of the electrostatic free-energy contribution, a relation between the surface potentials and the surface charge densities is required. The Poisson-Boltzmann (PB) equation can, in principle, provide such a relation, but since no analytical solution for the PB equation is available for the vesicle spherical geometry, the direct application of the PB equation, which would entail a tedious numerical integration procedure, would be quite prohibitive. Consequently, a more efficient method must be developed for the evaluation of the electrostatic free energy of a charged vesicle (see chapter 3).

3. The calculation of the steric free energy associated with the surfactant heads usually involves the estimation of the head area, which, in some cases, can be a rather ambiguous quantity. In addition, the traditional calculation of this free-energy contribution, which is based on the two-dimensional van der Waals equation of state, is known to overestimate the surface pressure at high packing densities (see discussion in chapter 2). In order to obtain a more accurate expression, therefore, an alternate formulation should be adopted in the estimation of the steric free energy (see chapter 2).

1.3.2 Experimental Studies of Biliary System

Since the nucleation of cholesterol crystals represents the initial step in a sequence of events that leads to the formation of cholesterol gallstones in bile, it will be beneficial, from a medical standpoint, to be able to identify a set of physiological variables that can most likely alter the propensity towards cholesterol nucleation in bile. As mentioned earlier, previous studies have linked the distribution of cholesterol and the vesicle composition to the metastability of bile, and therefore, it is important to

understand how certain physiological variables, including total lipid content, bile salt to phospholipid ratio, and cholesterol content, influence the distribution of cholesterol and the vesicle composition.

In all previous studies of cholesterol distribution, however, the so-called "one-variable-at-a-time" strategy[4] [89, 135, 149, 158, 170] was used. This strategy is limited by the amount of time and materials required, and, more importantly, by its inability to identify the simultaneous effects of several variables on a particular response. In a complex system like bile, it is highly probable that physiological variables, such as those cited above, interact with each other. Accordingly, a more systematic methodology is required to provide more information, particularly with respect to the interactions between various physiological variables, on the vesicular composition, as well as on the distribution of cholesterol between vesicles and mixed micelles. A very useful and efficient way to study the simultaneous effects of a large number of variables on a particular response is through the use of *statistically-designed experiments* (see chapter 7). Although widely used in the chemical process industry, statistical experimental design is rarely applied in medical research. In brief, statistical experimental design is simply a systematic way of setting the experimental conditions, that is, the values of each variable under consideration. The responses at each experimental condition are measured, and a regression analysis can then be performed to estimate the coefficient associated with each variable. The values of the coefficients reflect the individual effects of the variables, as well as the interactions among them.

To study the vesicle composition and the distribution of cholesterol between vesicles and mixed micelles, however, one needs to separate these biliary aggregates while preserving the original distribution. Two techniques are currently used to separate vesicles and mixed micelles in bile: ultracentrifugation and gel chromatography. Ultracentrifugation separates the biliary aggregates based on the difference in their densities, while gel chromatography separates them based on the difference in their sizes. Although both techniques are widely used in biliary research, there is yet no sys-

[4] A "one-variable-at-a-time" strategy is one where, at each experimental condition, only one variable is changed while all the other variables are kept constant.

tematic comparison between these two techniques. A major problem which may have caused confusion in this area is that, in using gel chromatography, the eluant should contain the correct monomeric and simple micellar bile salt concentration, known as the inter-mixed micellar / vesicular bile salt concentration (IMC) [35, 40, 43], so that the dynamic equilibrium between the lipid monomers and the lipid aggregates can be maintained during separation. In previous studies using gel chromatography, however, an arbitrary bile salt concentration has been used in the eluant [see Ref. 40 and references cited therein], rendering the interpretation of those results very difficult. In light of these problems, a logical first step in the experimental studies of vesicle composition and the distribution of cholesterol will involve a systematic comparison between the two separation techniques, using the correct IMC in gel chromatography (see chapter 6). Depending on the outcome of this comparison, modification of the current techniques may be required in order to develop a reliable method for separating vesicles and mixed micelles (see chapter 7).

1.4 Research Objectives

With the research motivation in mind, the central objectives of this thesis are twofold:

1. To develop a theoretical description of the formation of vesicles in surfactant mixtures. This objective is aimed at gaining fundamental knowledge on complex fluids in general, as well as at providing a starting point for the fundamental study of the formation of cholesterol gallstones in bile. A molecular theory for the formation of mixed surfactant vesicles will be constructed through a detailed modeling of the various free-energy contributions associated with vesiculation. This molecular theory will then be combined with a thermodynamic framework to describe the entire vesicle suspension in order to predict vesicle properties, such as, size and composition distribution, the distribution of molecules between the outer and inner vesicle leaflets, surface charge densities, and surface potentials.

2. To apply the statistical experimental design methodology to study the simultaneous effects of several physiological variables, such as, total lipid content, cholesterol content, and type of bile salt, on vesicle composition and the distribution of cholesterol between vesicles and mixed micelles in bile. In the development of a reliable method for separating vesicles and mixed micelles in model bile, the two current techniques, ultracentrifugation and gel chromatography, will be compared systematically to ascertain their compatibility, and, if necessary, the techniques will be modified to provide an accurate tool for the separation of the biliary aggregates.

The thesis is organized as follows. In chapter 2, the details of the development of a molecular-thermodynamic theory for the formation of mixed surfactant vesicles is presented. In chapter 3, approximate expressions for the surface potentials of a charged vesicle are derived, based on the nonlinear Poisson-Boltzmann equation, which are subsequently used to evaluate the electrostatic free energy of a vesicle. In chapter 4, the theory is applied to a cationic/anionic surfactant mixture, and the theoretical predictions for this system, including vesicle size and composition distribution and surface potentials, are presented. In chapter 5, the theory is utilized to study the effect of surfactant tail-length asymmetry on the formation and stabilization of mixed surfactant vesicles. In chapter 6, ultracentrifugation and gel chromatography are compared systematically regarding their ability to separate vesicles and mixed micelles in a biliary system. In chapter 7, a modification of ultracentrifugation is developed, followed by the application of factorial experimental design to the study of cholesterol distribution and vesicular composition in model bile. Finally, conclusions and a discussion of future research directions are presented in chapter 8.

Chapter 2

Molecular-Thermodynamic Theory of Mixed Vesicles

This chapter presents the details of the development of a molecular-thermodynamic theory to describe the formation of two-component mixed surfactant vesicles, with particular emphasis on cationic/anionic surfactant mixtures [178]. The central quantity in this theory is the free energy of vesiculation, which is calculated by carefully modeling the various free-energy contributions associated with vesiculation. By knowing only the molecular structures of the surfactants involved in vesicle formation and the solution conditions, the theory can predict a wealth of vesicle properties, including vesicle size and composition distribution, surface potentials, surface charge densities, and compositions of vesicle leaflets. A notable difference between the present theory and all the theoretical approaches mentioned in chapter 1 is in the level of detail associated with the calculation of the free-energy change of vesicle formation. More specifically: (i) the packing of the surfactant tails in the vesicle hydrophobic region is estimated through a mean-field calculation, which explicitly accounts for the conformational degrees of freedom of the tails, (ii) the electrostatic interactions between the charged surfactant heads are estimated by explicitly solving the corresponding nonlinear Poisson-Boltzmann equations, and (iii) a more accurate equation of state is adopted in the calculation of the steric repulsions between the surfactant heads. In addition, details such as the location of the outer and inner steric-repulsion surfaces

in a vesicle, the curvature correction to the interfacial tensions at the outer and inner hydrocarbon/water vesicle interfaces, and the existence of four charged surfaces associated with a two-component cationic/anionic vesicle are also carefully accounted for. More importantly, the theory allows for an in-depth analysis of the mechanisms of vesicle stabilization, and of the interplay between the various free-energy contributions to the free energy of vesiculation. The present molecular-thermodynamic theory also has the ability to cover the entire range of vesicle sizes (or curvatures), thus enabling a description of small, energetically stabilized, vesicles. In addition, this theory can be extended to account for the presence of other self-assembling structures possessing relatively small sizes, such as mixed micelles. The latter point is particularly important for the prediction of the global phase behavior of mixed surfactant systems that can form both mixed micelles and mixed vesicles, such as in the case of bile.

2.1 Thermodynamic Framework to Describe a Vesicle Suspension

The molecular-thermodynamic theory presented in this chapter can be viewed as a generalization of the theories developed by Puvvada and Blankschtein to describe single and mixed micellar solutions [138, 139, 140]. In this theory, the total Gibbs free energy of the solution, G, is written as a sum of three contributions [10]: the standard-state free energy, G_o, the free energy of mixing, G_{mix}, and the interaction free energy, G_{int}, that is,

$$G = G_o + G_{mix} + G_{int} \tag{2.1}$$

The chosen standard state corresponds to one in which all the surfactant monomers and the surfactant aggregates, in this case the vesicles, exist in isolation at infinite dilution, and are "fixed" in space, that is, without mixing. The free energy of mixing, G_{mix}, then accounts for the free-energy change due to the configurational entropy associated with mixing the aggregates, the monomers, and the water molecules. The interaction free energy, G_{int}, accounts for the interactions among the aggregates and

the monomers, which can play an important role in, for example, phase separation of a micellar solution [10, 138, 140]. In most systems in which spontaneous vesiculation has been observed, the total surfactant content is only about 1 to 2 wt% [74], and the mole fraction of vesicles in these cases can be as low as 10^{-10} (see chapter 4). Accordingly, in the present study, it is assumed that: (i) the mixing contributing to G_{mix} is ideal, and (ii) the vesicle suspension is so dilute that the interaction free-energy contribution, G_{int}, can be neglected. Of note is that the precise mathematical form of the entropy of mixing can affect the quantitative predicted size and composition distribution. In this respect, different models for the entropy of mixing have been utilized to model micellar solutions [81, 122, 124, 139], and the reader is referred to these references for further details.

Consider a system containing three components: surfactant A, surfactant B, and water. Based on assumptions (i) and (ii) above, the size and composition distribution in a vesicle suspension can be expressed as follows (see appendix A for details of the derivation of Eq. (2.2))

$$X(n,F) = X_{1A}^{nF} X_{1B}^{n(1-F)} \exp(-n g_{ves}/kT) \tag{2.2}$$

where $X(n,F)$ is the mole fraction of vesicles having aggregation number, n, and composition, F, which is defined as the mole fraction of component A in the vesicle, T is the absolute temperature, and k is the Boltzmann constant[1]. In Eq. (2.2), X_{1A} and X_{1B} are the mole fractions of the surfactant A and B monomers, respectively, g_{ves} is the free energy of vesiculation , defined as

$$g_{ves} = \tilde{\mu}_{n,F}^{o} - F\mu_{1A}^{o} - (1-F)\mu_{1B}^{o} \tag{2.3}$$

[1]A note of caution here is that the size and composition distribution given in Eq. (2.2) is only an approximate expression. Indeed, statistical-mechanical arguments show that, within the context of ideal mixing, a pre-exponential factor proportional to $n^{-1/2}$ should be present in Eq. (2.2) [166]. However, the value of this factor is typically very small ($< 10^{-4}\ kT$), compared to the uncertainties involved in the calculation of g_{ves} ($\approx 10^{-2}\ kT$), and therefore can be neglected for the purpose of the present study.

where $\tilde{\mu}^o_{n,F}$ is the standard-state chemical potential per molecule in a vesicle, and μ^o_{1A} and μ^o_{1B} are the standard-state chemical potentials of the surfactant A and B monomers, respectively. From a physical viewpoint, the free energy of vesiculation, g_{ves}, is the total free-energy change per molecule associated with the process by which nF surfactant A monomers and $n(1-F)$ surfactant B monomers are transferred from the aqueous environment to a vesicle having aggregation number, n, and composition, F. Equation (2.2) indicates that $X(n,F)$ depends on the interplay of two factors: an entropic factor, $X_{1A}^{nF}X_{1B}^{n(1-F)}$, and an energetic (Boltzmann) factor, $\exp(-ng_{ves}/kT)$. The entropic factor reflects the penalty associated with localizing the surfactant A and B monomers at a certain position in space, that is, in a vesicle, while the energetic factor reflects the propensity of the surfactant A and B monomers to aggregate.

2.2 Molecular Model of Vesicle Formation

To evaluate the vesicle size and composition distribution, $X(n,F)$ in Eq. (2.2), one needs an explicit model for the free energy of vesiculation, g_{ves}. The free energy of vesiculation can be viewed as composed of the following five contributions: (1) the transfer free energy, g_{tr}, (2) the packing free energy, g_{pack}, (3) the interfacial free energy, g_σ, (4) the steric free energy, g_{steric}, and (5) the electrostatic free energy, g_{elec} (see Figure 2-1). Mathematically, one can therefore write

$$g_{ves} = g_{tr} + g_{pack} + g_\sigma + g_{steric} + g_{elec} \tag{2.4}$$

These five free-energy contributions account for the essential features that differentiate a surfactant molecule in the vesicle and in the monomeric state. The transfer free energy, g_{tr}, reflects the so-called hydrophobic effect [162], which constitutes the major driving force for surfactant self-assembly in water. Indeed, the transfer free energy is the only favorable free-energy contribution to molecular aggregation, with the other four free-energy contributions described in Eq. (2.4) working against this process. The hydrophobic region in a vesicle, however, is different from bulk hydro-

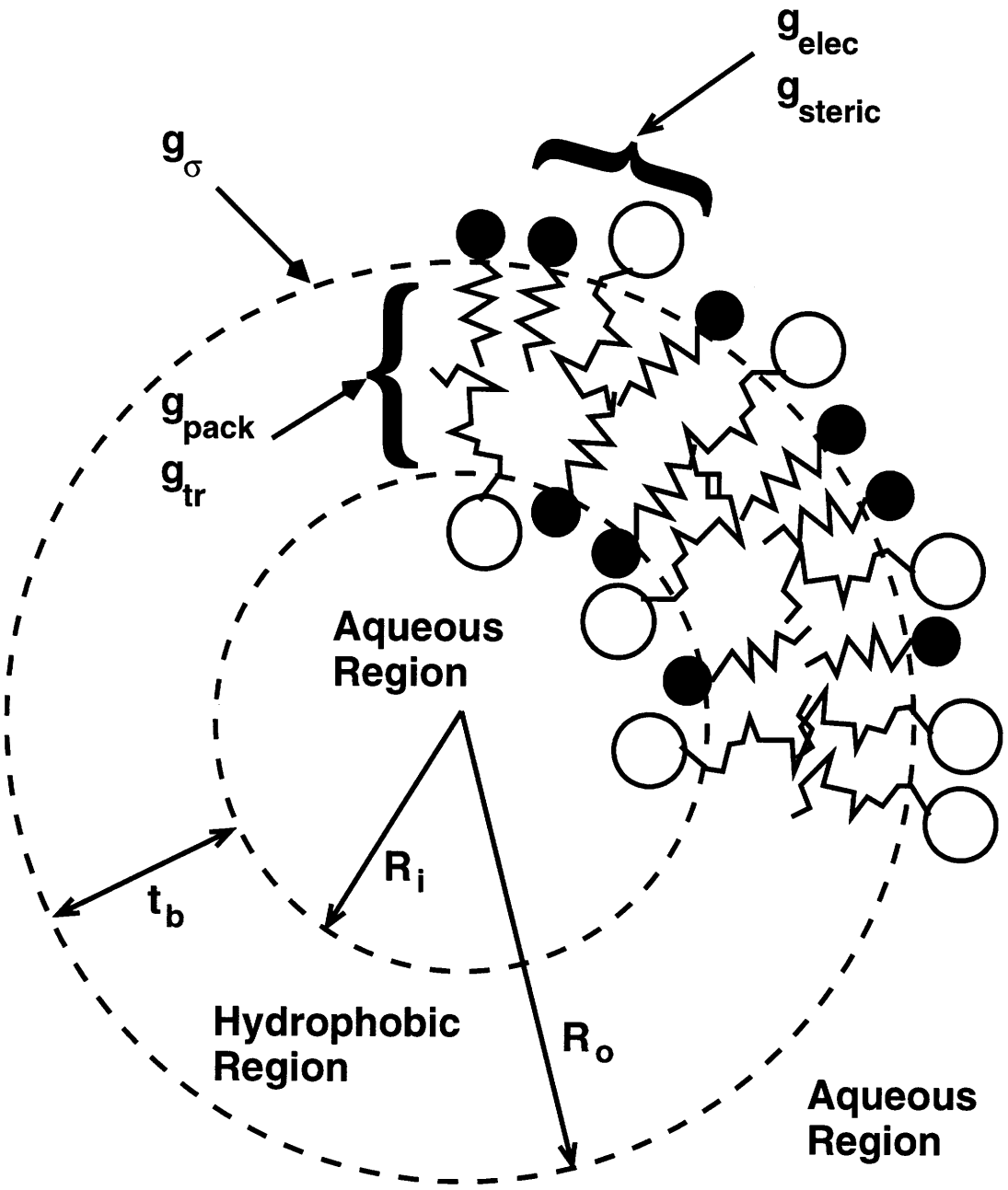

Figure 2-1: Schematic representation of a two-component (represented by the black and white heads) unilamellar vesicle showing: (i) part of the hydrophobic bilayer region composed of the surfactant tails of both surfactant species, (ii) the location of the outer and inner hydrocarbon/water interfaces, and (iii) the various regions with which the free-energy contributions, g_{tr}, g_{pack}, g_{σ}, g_{steric}, and g_{elec}, are associated.

carbon. In a vesicle, the surfactant tails are anchored at one end on either the outer or inner interfaces, which restricts the number of conformations that each surfactant tail can adopt while still maintaining a uniform liquid hydrocarbon density in the vesicle hydrophobic region. This subtle difference between a bulk hydrocarbon phase and the hydrophobic region in a vesicle is captured by the packing free energy, g_{pack}. In addition, free-energy penalties are imposed, upon aggregation, by the creation of the outer and inner hydrocarbon/water interfaces, captured in g_{σ}, and by the steric repulsions and electrostatic interactions between the surfactant heads, captured in g_{steric} and g_{elec}, respectively. The following paragraphs briefly describe each free-energy contribution, including their estimation based on knowledge of the molecular structures of the surfactant molecules involved in vesicle formation and the solution conditions.

2.2.1 Transfer Free Energy

The process by which the surfactant tails are transferred from the aqueous environment to the hydrophobic vesicle bilayer upon aggregation can be viewed as being composed of three steps: (i) the surfactant tails are transferred from the aqueous environment to their corresponding *pure* hydrocarbon phases, (ii) the surfactant tails are then mixed to form the outer and inner hydrocarbon mixtures, corresponding to the outer and inner "leaflets", or monolayers, that constitute the vesicle bilayer, and (iii) the surfactant tails are anchored at one end on the outer or inner vesicle interfaces (see Figure 2-1). The free-energy change associated with the third step can be accounted for by the packing free energy, g_{pack}, as will be discussed in (2) below. The free-energy changes associated with the first two steps are captured by the transfer free energy, g_{tr}. Accordingly, for a vesicle having aggregation number, n, and composition, F, g_{tr} can be expressed as

$$g_{tr} = F\Delta\mu_{tr,A} + (1-F)\Delta\mu_{tr,B} + g_m \tag{2.5}$$

where $\Delta\mu_{tr,A}$ and $\Delta\mu_{tr,B}$ are the free-energy changes associated with transferring the tails of surfactants A and B from the aqueous environment to their corresponding *pure* liquid hydrocarbon phases, respectively, and g_m is the free-energy change per molecule due to mixing of the tails of surfactants A and B in the outer and inner vesicle leaflets. Strictly speaking, because of the proximity of the surfactant heads in a vesicle, the environment surrounding a surfactant head in a vesicle can also be different from that in the aqueous environment. However, the effect on vesiculation due to this difference is likely to be much smaller than that caused by transferring the surfactant tails, particularly for long-chain hydrocarbons, and it is therefore reasonable to neglect this difference as a first approximation.

The free-energy change, $\Delta\mu_{tr,k}$ ($k = A$ or B), arises mainly from the rearrangement of water molecules surrounding the surfactant tails when they are transferred from the aqueous environment to the pure hydrocarbon phase. This free-energy change can be estimated directly from solubility data, since the process of dissolution can be viewed as the reverse of the transferring process described above. In particular, for alkyl tails, empirical relations based on experimental solubility data are available, which express $\Delta\mu_{tr,k}$ as a function of carbon number and temperature [1]. Specifically,

$$\frac{\Delta\mu_{tr,k}}{kT} = (3.04 - 1.05n_{c,k})\frac{298}{T} - (5.06 + 0.44n_{c,k}) \tag{2.6}$$

where $n_{c,k}$ is the carbon number of the tail of component k (A or B) in the hydrophobic region. In this formulation, the hydrocarbon/water interface is located between the first and second carbon atoms in the tail. Accordingly, $n_{c,k}$ should be one less than the total number of carbon atoms in the tail. For example, for a surfactant tail containing 16 carbon atoms, such as that corresponding to cetyltrimethylammonium bromide (CTAB), $n_{c,k}$ is equal to 15. This choice of the location of the interface is mainly due to possible water penetration into the hydrophobic region [138]. In other words, the first carbon atom of the tail is allowed to come into contact with water.

The free-energy change per molecule associated with mixing the tails of surfactants A and B in each vesicle leaflet is estimated using ideal mixing as a first approximation,

that is

$$\frac{g_m}{kT} = f \sum_{k=A,B} X_{ok} \ln X_{ok} + (1-f) \sum_{k=A,B} X_{ik} \ln X_{ik} \tag{2.7}$$

where X_{ok} and X_{ik} are the mole fractions of component k ($k = A$ or B) in the outer and inner leaflets, respectively, and f is the mole fraction of surfactant molecules in the outer leaflet, that is,

$$f = \frac{\text{Number of surfactant molecules in the outer leaflet}}{\text{Total number of surfactant molecules in the vesicle}} \tag{2.8}$$

The mole fraction, f, thus characterizes the distribution of surfactant molecules between the outer and inner leaflets in a vesicle. As will be shown in chapter 4, f is perhaps the most important variable affecting the thermodynamics of vesiculation.

2.2.2 Packing Free Energy

In the hydrophobic region of a vesicle, the surfactant tails are anchored at one end on the outer and inner vesicle interfaces, which impose restrictions on the conformations of the surfactant tails. This packing penalty is captured in this molecular model by the packing free energy, g_{pack}, which is estimated as the free-energy difference between a surfactant tail packed in a vesicle and a surfactant tail dispersed in bulk hydrocarbon, that is,

$$g_{pack} = \mu_{pack} - \mu^f_{pack} \tag{2.9}$$

where μ_{pack} is the free energy per molecule due to packing of a surfactant tail in a vesicle, and μ^f_{pack} is the packing free energy corresponding to a "free" surfactant tail (see appendix B). In this study, the mean-field approach developed by Szleifer and co-workers is generalized [160] to calculate this free-energy contribution. Briefly, μ_{pack} can be written as follows

$$\mu_{pack} = \sum_{k=A,B} [f X_{ok} \mu_{ok} + (1-f) X_{ik} \mu_{ik}] \tag{2.10}$$

where μ_{ok} (μ_{ik}) is the packing free energy per molecule of component k in the outer (inner) leaflet, which can be written in terms of the single-chain probability distribution of chain conformations. For example, for component k in the outer leaflet, one has

$$\mu_{ok} = \sum_{\alpha_k} P(\alpha_k) E_k(\alpha_k) - kT \sum_{\alpha_k} P(\alpha_k) \ln P(\alpha_k) \tag{2.11}$$

where $P(\alpha_k)$ is the probability of component k in the outer leaflet adopting a conformation, α_k, and $E_k(\alpha_k)$ is the internal energy of the chain corresponding to the conformation, α_k. The probability, $P(\alpha_k)$, can be related to the volume of the hydrophobic region through the following relation

$$\sum_{k=A,B} [f X_{ok} \langle \phi_{ok}(r) \rangle + (1-f) X_{ik} \langle \phi_{ik}(r) \rangle] = a(r) \tag{2.12}$$

where $\langle \phi_{ok}(r) \rangle$ and $\langle \phi_{ik}(r) \rangle$ are the configurational-average segment volume densities (volume per unit length) at position, r, due to component k in the outer and inner leaflets, respectively. For example, for component k in the outer leaflet, one has

$$\langle \phi_{ok}(r) \rangle = \sum_{\alpha_k} P(\alpha_k) \phi_{ok}(\alpha_k, r) \tag{2.13}$$

A similar expression can be written for $\langle \phi_{ik}(r) \rangle$. The quantity, $a(r)$, in Eq. (2.12) is the volume density *available* at position, r. Here, the density of the vesicle hydrophobic region is assumed to be uniform and equal to that of liquid hydrocarbon. Accordingly, for given values of f, X_{ok}, X_{ik}, R_o, and R_i, $a(r)$ depends only on the geometry of the vesicle, and the probability distribution can be obtained by solving Eq. (2.12). The constraint of uniform liquid density in the vesicle hydrophobic region should be a valid assumption based on a comparison with experimental observations [61, 62], although simulations of phospholipid bilayers have shown that the density may decrease towards the center of the bilayer [107]. This constraint can, in fact, be relaxed, provided that the density profile in the hydrophobic region is known. However, using an explicit non-uniform density profile in this calculation will certainly introduce some ambiguities, since the profile is not known *a priori* in most cases.

Consequently, rather than using the density profile as an arbitrary parameter, the density is kept uniform in all the calculations which follow.

Knowing $P(\alpha_k)$, μ_{pack} can then be calculated using Eqs. (2.10) and (2.11). The general procedure for solving Eq. (2.12), including the discretization of the vesicle hydrophobic region, can be found in Refs. 159 and 160, and it will not be detailed here. However, some useful formulas that are specific for the vesicle geometry are presented in appendix B. These formulas should be helpful to readers who are interested in actually performing such calculations.

A noteworthy point here is that, instead of treating the vesicle bilayer as a planar bilayer, the theory explicitly accounts for its curvature. Consequently, five variables (f, X_{ok}, X_{ik}, R_o, and R_i) are needed to characterize a vesicle bilayer in the packing calculations, as opposed to only two variables (thickness and composition) in the planar case[2]. In the present study, the packing free energies are generated for a fixed number of combinations of these five variables, and for other combinations of these variables, the corresponding packing free energies are obtained by interpolation. This somewhat tedious packing free-energy calculation is necessary to ensure the applicability of this theory to the entire range of vesicle sizes. As will be shown in chapter 4, the effects of curvature and the freedom with respect to the distribution of surfactant molecules between the two vesicle leaflets, reflected in the variable, f, are particularly important as the vesicle size becomes small. In a rigorous calculation of the free energy of vesiculation, then, the packing contribution must be able to reflect these effects in the small vesicle size range. Nevertheless, for systems that are dominated by large vesicles, the packing free energy may be approximated by that corresponding to a planar bilayer without a significant loss of accuracy.

2.2.3 Interfacial Free Energy

As the surfactant molecules self-assemble to form the vesicle, the outer and inner interfaces between the hydrophobic region and the aqueous environments are created

[2]In a planar bilayer, $f = 0.5$, $X_{ok} = X_{ik}$, and the absolute values of R_o and R_i are irrelevant, since only their difference, that is, the planar bilayer thickness, is important.

(see Figure 2-1). The free-energy change per molecule, g_σ, required to create these two interfaces can be captured in the following expression

$$g_\sigma = f\bar{\sigma}_o(a_o - \bar{a}_o^*) + (1-f)\bar{\sigma}_i(a_i - \bar{a}_i^*) \tag{2.14}$$

where a_o (a_i) and $\bar{a}_o^*$ ($\bar{a}_i^*$) are the area per molecule and the molar-average shielded area per molecule at the outer (inner) interface, respectively. The shielded area is the area occupied by the surfactant tail at the interface, and it reduces the area of contact between the hydrophobic region and water. The molar-average shielded areas are defined as follows

$$\bar{a}_o^* = \sum_{k=A,B} X_{ok} a_k^* \tag{2.15}$$

$$\bar{a}_i^* = \sum_{k=A,B} X_{ik} a_k^* \tag{2.16}$$

where a_k^* is the shielded area of component k. In Eq. (2.14), $\bar{\sigma}_o$ and $\bar{\sigma}_i$ are the curvature-corrected molar-average interfacial tensions at the outer and inner interfaces, respectively. The curvature correction to the interfacial tension can be estimated using the Tolman equation [167]. In particular, for the range of vesicle sizes considered here,

$$\bar{\sigma}_o = \bar{\sigma}_{op}(1 - \frac{2\delta}{R_o}) \tag{2.17}$$

$$\bar{\sigma}_i = \bar{\sigma}_{ip}(1 - \frac{2\delta}{R_i}) \tag{2.18}$$

where δ is the Tolman length, and R_o (R_i) is the outer (inner) vesicle radius, measured from the center of the vesicle to the outer (inner) hydrocarbon/water interface. In Eq. (2.17) (Eq. (2.18)), $\bar{\sigma}_{op}$ ($\bar{\sigma}_{ip}$) is the molar-average planar interfacial tension associated with the outer (inner) interface, estimated, as a first approximation, as

$$\bar{\sigma}_{op} = \sum_{k=A,B} X_{ok}\sigma_k \tag{2.19}$$

$$\bar{\sigma}_{ip} = \sum_{k=A,B} X_{ik}\sigma_k \tag{2.20}$$

where σ_k is the planar interfacial tension between component k ($k = A$ or B) and water. If, for example, component A consists of a 16-carbon tail and component B consists of a 8-carbon tail, then σ_A and σ_B should be the interfacial tensions between water and pentadecane, and water and heptane, respectively[3].

The effect of curvature on interfacial tension is, in fact, not a trivial issue. Indeed, significant research effort has been devoted since the derivation of Eqs. (2.17) or (2.18) by Tolman [167], particularly regarding the estimation of the Tolman length,δ[52, 77, 91, 126, 144, 167]. The simplest definition of the Tolman length, δ, is the distance between the surface of tension and the Gibbs dividing surface. The existence of a finite curvature results in a non-zero value of this distance, as opposed to zero in the planar case, and effectively enhances or reduces the interfacial tension from its planar value, depending on the sign of δ, or more specifically, depending on the densities of the two phases involved. Because the Tolman length, δ, only comes into play in systems containing droplets having very small sizes, it is usually difficult to obtain an accurate experimental measurement of δ. Theoretical studies and simulations of Lennard-Jones fluids have set the value of δ between -0.2d to -0.4d for droplets, where d is the hard-sphere diameter [52, 70, 83, 127]. In this study, δ is estimated to be 1.4 Å and -1.4 Å for the outer and inner interfaces, respectively. The estimation is based on a linear density profile across an interfacial region having a thickness of about 2.5 Å, which corresponds approximately to twice the projected length of a carbon-carbon bond, in accordance with the water-penetration region (see section 2.2.1). The linear profile is just a simplifying assumption; indeed, other profiles, such as sigmoidal, have yielded no significant difference. Interestingly, the estimated δ value of 1.4 Å agrees well with the simulation results discussed earlier, if we treat the hydrophobic region as composed of "spheres" of methylene segments ($d \approx 4$ Å). It is beyond the scope of this work to provide a thorough investigation on the Tolman

[3]Recall that, as stressed earlier, the number of carbons in the hydrophobic region is one less than that in the actual surfactant tail.

length. Instead, we treat δ as a fixed parameter which reflects the influence of finite curvature in the calculation of the interfacial free energy, g_σ. An interesting point to note here is that the Tolman length for the inner interface has a sign opposite to that for the outer interface because the phases involved (hydrocarbon and water) are reversed in this case. Consequently, the effect of curvature works to reduce the interfacial tension at the outer interface, whereas it increases the interfacial tension at the inner interface.

2.2.4 Steric Free Energy

Surfactant heads have a finite size, and therefore, when they are brought together to form a vesicle, the steric repulsions between these heads will invariably incur a free-energy penalty to the process. This steric free-energy contribution can be estimated as the free-energy change associated with the process by which the surfactant heads are brought from infinitely apart to the state corresponding to the vesicle interfaces. For example, for the outer interface, this can be expressed as

$$G_{steric,o} = -\int_{\infty}^{A_o} (\Pi - \Pi^{id}) dA_o \tag{2.21}$$

where $G_{steric,o}$ is the total outer steric free energy, A_o is the total area of the outer steric-repulsion surface, Π is the surface pressure, and Π^{id} is the ideal surface pressure. The outer (inner) steric-repulsion surface is defined as the surface located at a distance, $\bar{d}_{ch,o}$ ($\bar{d}_{ch,i}$), from the outer (inner) hydrocarbon/water interface, where

$$\bar{d}_{ch,o} = \sum_{k=A,B} X_{ok} d_{ch,k} \tag{2.22}$$

$$\bar{d}_{ch,i} = \sum_{k=A,B} X_{ik} d_{ch,k} \tag{2.23}$$

and $d_{ch,k}$ is the charge distance of component k, which is the distance between the location of the charge in the head of component k and the hydrocarbon/water interface. An expression similar to Eq. (2.21) can be written for the total inner steric free energy, $G_{steric,i}$, and the total steric free energy of the vesicle is simply

$G_{steric} = G_{steric,o} + G_{steric,i}$. In the present theory, it is assumed that the surfactant heads are compact, so that they can be modeled as hard disks which are characterized by fixed diameters. Note, however, that for chain-like surfactant heads such as those of the poly(ethylene oxide) variety, this hard-disk approach is probably not applicable since the heads may be quite flexible in that case. The treatment of flexible surfactant heads is beyond the scope of the present study, and the interested reader is referred to Ref. 22 and references therein for a description of various ways to deal with such flexible heads.

Traditionally, the two-dimensional repulsive van der Waals (vdW) equation of state has been used to evaluate G_{steric} [19, 121, 123, 124, 125, 139, 140]. Using this equation of state to express the surface pressure, Π, in Eq. (2.21), one would obtain the familiar logarithmic form of the steric free energy. The problem with using the vdW equation of state is that the estimation of the so-called head area of the surfactant molecule is quite ambiguous. Theoretically speaking, in order to be consistent with the description of the vdW equation of state, the head area should really be the excluded area per molecule. However, estimates of this quantity vary within a wide range, even for a simple surfactant head such as a sulfate [19, 121, 123, 124, 125, 139, 140]. In addition, the vdW equation of state is known to overestimate the surface pressure for a hard-disk system [112], particularly when the hard disks approach a high packing density. This behavior may prevent the surfactant heads from coming too close to each other in a vesicle, thus resulting in an overestimation of the area per molecule. To overcome this difficulty, and in an attempt to obtain a more accurate expression for G_{steric}, the scaled-particle theory (SPT) equation of state for hard-disk mixtures [56, 98, 128] is used in the present study. In addition to its simplicity, the choice of the SPT equation of state is mainly due to two reasons: (i) in the SPT equation of state, it is the hard-disk area that comes into the formulation, thus eliminating the ambiguity discussed above, and (ii) the behavior of surface pressure at high packing densities is more realistic than that predicted by the vdW equation of state, which should result in a more reliable estimate of the area per molecule. Performing the integration in Eq. (2.21) using the SPT equation of state

(see appendix C for details), one obtains

$$\frac{g_{steric}}{kT} = f\left[\frac{\pi \bar{d}_o^2/4}{a'_o - \bar{a}_{ho}} - \ln\left(1 - \frac{\bar{a}_{ho}}{a'_o}\right)\right] + (1-f)\left[\frac{\pi \bar{d}_i^2/4}{a'_i - \bar{a}_{hi}} - \ln\left(1 - \frac{\bar{a}_{hi}}{a'_i}\right)\right] \quad (2.24)$$

where $g_{steric} = G_{steric}/n$ is the steric free energy per molecule, $\bar{d}_o$ ($\bar{d}_i$) and $\bar{a}_{ho}$ ($\bar{a}_{hi}$) are the molar-average hard-disk diameter and hard-disk area (see appendix C for definitions) of the surfactant heads at the outer (inner) interface, respectively, and a'_o (a'_i) is the outer (inner) area per molecule calculated at the outer (inner) steric-repulsion surface. Note that a'_o and a'_i are different from a_o and a_i used in Eq. (2.14), which are the area per molecule at the outer and inner hydrocarbon/water interfaces, respectively. Indeed, a'_o and a'_i are related to a_o and a_i through geometric considerations by the following relations

$$a'_o = a_o\left(1 + \frac{\bar{d}_{ch,o}}{R_o}\right)^2 \quad (2.25)$$

$$a'_i = a_i\left(1 - \frac{\bar{d}_{ch,i}}{R_i}\right)^2 \quad (2.26)$$

This correction to the area per molecule reflects the fact that the steric repulsions between the surfactant heads occur at slightly different locations away from the outer and inner hydrocarbon/water interfaces. As in the case of the curvature correction to the interfacial tension (see Eqs. (2.17) and (2.18)), this correction becomes significant only in the case of small vesicles.

2.2.5 Electrostatic Free Energy

As stated earlier, vesicles form spontaneously in certain mixtures of cationic and anionic surfactants. In order to account for the electrostatic interactions between the oppositely-charged surfactant heads in the vesicle, one needs to calculate the electrostatic free energy, g_{elec}, which acts to oppose the self-assembling process. Several methods may be used to estimate g_{elec}, including the simple "capacitor" model [30, 81, 82], and the calculation of the internal energy and the entropy of demixing the

ions in aqueous solution [63, 106]. A more direct approach involves the calculation of the reversible work required to charge all the surfaces involved. In a two-component vesicle, there can be four such surfaces, since the distances, $d_{ch,A}$ and $d_{ch,B}$, need not be the same. Accordingly, a rigorous calculation requires charging the four surfaces simultaneously (see Figure 2-2(a)). To charge a surface, the relation between the surface potential and the surface charge density must be known. The Poisson-Boltzmann (PB) equation provides such a relation, but there is as yet no analytical solution to the PB equation in spherical geometry. Consequently, the direct application of the PB equation to the charging process can be tedious since a numerical solution is required at each charging step. Furthermore, as will be discussed in section 2.3, the configuration of an isolated vesicle, which is characterized by such variables as the distribution of molecules, f, the outer and inner leaflet compositions, X_{ok} and X_{ik}, and the thickness of the hydrophobic region, t_b, is obtained by minimizing the free energy of vesiculation with respect to these variables. Such a minimization procedure will invariably sample a large configuration space, which makes the numerical solution of the PB equation quite prohibitive.

To simplify the calculation of g_{elec}, an approximate charging approach is adopted in the present study. Instead of charging the four surfaces simultaneously as shown in Figure 2-2(a), we estimated g_{elec} as the free energy corresponding to charging an outer and inner spherical capacitor, depicted in Figure 2-2(b), plus that corresponding to placing the net charges on two surfaces, depicted in Figure 2-2(c). The outer spherical capacitor consists of the two surfaces defined by R_3 and R_4, with an electric charge of Q_{3f}, while the inner spherical capacitor is composed of the surfaces defined by R_2 and R_1, with an electric charge of Q_{2f}. Mathematically, therefore, g_{elec} can be expressed as follows

$$ng_{elec} = \frac{Q_{2f}^2 D}{2\epsilon_w R_1^2(1+D/R_1)} + \frac{Q_{3f}^2 D}{2\epsilon_w R_3^2(1+D/R_3)} + \int_0^1 [\psi_i(\lambda)Q_i' + \psi_o(\lambda)Q_o']d\lambda \quad (2.27)$$

where $Q_o' = Q_{3f} + Q_{4f}$ ($Q_i' = Q_{1f} + Q_{2f}$) is the final net charge on the outer (inner)

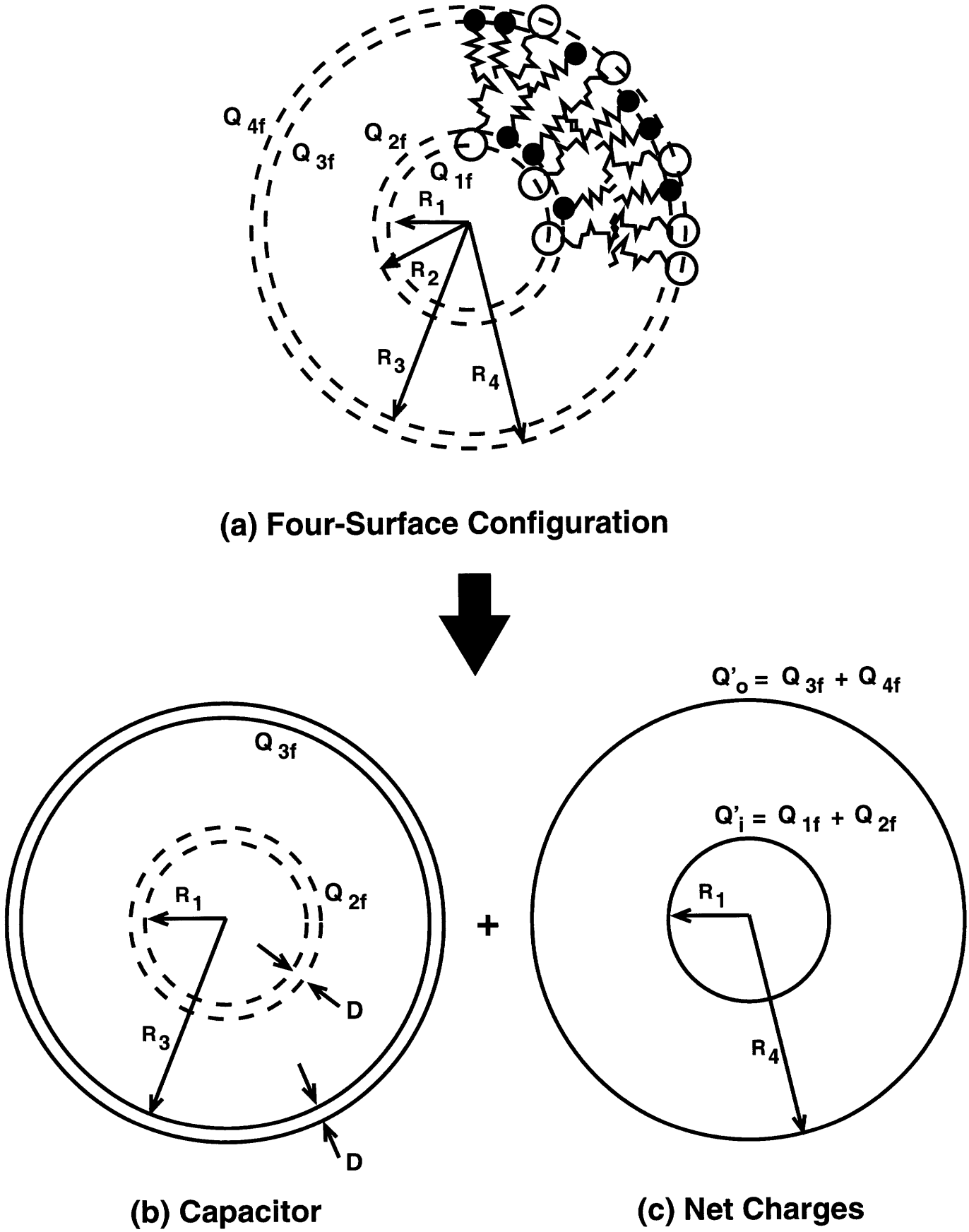

Figure 2-2: Schematic diagram depicting the approximation used in the calculation of the electrostatic free energy, g_{elec}. The four-surface configuration in (a) is replaced by a configuration that consists of an outer and inner capacitor in (b), plus the net charges on the outer and inner interfaces in (c). The charge on each surface is denoted by $Q_{jf}, j = 1, \ldots, 4$, and D is defined as $D = R_2 - R_1 = R_4 - R_3$.

charged surface[4], ψ_o (ψ_i) is the outer (inner) surface potential, $Q_{jf}, j = 1, \ldots, 4$ is the final charge at R_j, ϵ_w is the permittivity in water, λ is the charging parameter, and D is the so-called gap distance, which is defined as

$$D = |d_{ch,A} - d_{ch,B}| \tag{2.28}$$

The final charge on each surface can, of course, be calculated by knowing the aggregation number, n, the distribution of molecules, f, and the mole fraction of each component. For example, Q_{3f} can be expressed as $Q_{3f} = nfX_{oA}ez$, where e is the elementary charge and z is the valence of component A[5]. The first two terms on the right-hand side of Eq. (2.27) are the inner and outer capacitor terms, and the integral term corresponds to the charging of the inner and outer charged surfaces from zero to the total net charges. The derivation of Eq. (2.27), including the approximations involved in this approach, can be found in appendix D. Note that the charged surfaces are not the same as the hydrocarbon/water interfaces, which are located at R_o and R_i (see Figure 2-1 and section 2.2.1), nor are they the same as the steric-repulsion surfaces, which are located at $\bar{d}_{ch,o}$ and $\bar{d}_{ch,i}$ (see section 2.2.4). To further facilitate the calculation of g_{elec}, approximate expressions have been developed for the two surface potentials, ψ_o and ψ_i, based on the nonlinear PB equation. The derivation of these expressions is given in chapter 3.

2.3 Computational Procedure

Many equations are involved in the present molecular-thermodynamic model for the description of mixed cationic/anionic vesicles. Before we proceed to discuss the com-

[4]Note that the term "final", as used here, does not imply the minimum-energy configuration of the vesicle. Instead, it refers to the charging stage in the calculation of g_{elec}. In other words, the term "final" corresponds to the state at which $\lambda = 1$. As discussed in section 2.3, g_{ves} is minimized by sampling a large configuration space, and each sampled vesicle configuration will have a "final" charge on each surface.

[5]Here, it is assumed that the distance between the location of the charge on the surfactant head of component A and the hydrocarbon/water interface, $d_{ch,A}$, is smaller than that corresponding to component B, $d_{ch,B}$.

putational procedure involved in the implementation of these equations, it will be beneficial to the reader to present a summary of these equations. Such a summary is given in appendix E, in which references to other expressions required in these model equations are also provided.

A total of variables are involved in the calculation of g_{ves}. In addition to n and F, there are two areas per molecule, a_o and a_i, the distribution of molecules between the two leaflets, f, the composition of each leaflet, X_{oA} and X_{iA}, the outer and inner radii, R_o and R_i, and the thickness of the hydrophobic region, t_b (see Figure 2-1). These variables are not totally independent, but are, instead, related through constraints imposed by the geometry of the vesicle. Indeed, as shown in appendix F, there are five such geometric relations among the ten variables cited above. These geometric relations can be used to eliminate five variables. Specifically, at each n and F, one can calculate the free energy of vesiculation by minimizing g_{ves}, as given in Eq. (2.4), with respect to three independent variables: X_{oA}, f, and t_b. The choice of these three variables is mainly based on the convenience in solving the geometric constraints. From a physical standpoint, this procedure of calculating the free-energy surface implies that, at given values of n and F, an isolated vesicle will seek a minimum free-energy configuration, and it will not be affected by the presence of other vesicles in the suspension. This procedure is valid under the assumption of negligible inter-vesicular interactions, captured in G_{int}, as stated in section 2.1. If G_{int} is not negligible, however, the minimum free-energy configuration of an isolated vesicle may be different from that of a vesicle in suspension, since the interactions may depend on vesicle size, which, in turn, may be influenced by the vesicle configuration. In this case, then, the free energy of the entire vesicular suspension, G, should be minimized (see Eq. (2.1)).

Since one can now compute g_{ves} at every n and F, Eq. (2.2) can be used to express $X(n, F)$ as a function of X_{1A} and X_{1B}. This relation can then be inserted in the mass balance equations, which state that, for a two-component vesicular system,

$$X_{At} = X_{1A} + \sum_n n \int_0^1 F X(n, F) dF \tag{2.29}$$

$$X_{Bt} = X_{1B} + \sum_n n \int_0^1 (1-F) X(n,F) dF \tag{2.30}$$

where X_{At} and X_{Bt} are the total mole fractions of components A and B in the system, respectively. Since X_{At} and X_{Bt} are experimental inputs, the only unknowns in Eqs. (2.29) and (2.30) are the monomer mole fractions, X_{1A} and X_{1B}, which can be solved for by using a simple trial and error procedure. After obtaining the monomer mole fractions, X_{1A} and X_{1B}, the quantity $X(n,F)$ can be calculated directly using Eq. (2.2). A noteworthy point here is that, in the calculation of g_{elec}, the ion concentration, which plays an important role in the screening of the surface potentials, includes the monomer concentrations, X_{1A} and X_{1B}. This implicit relation calls for an iterative procedure, thus making any rigorous calculation rather tedious. In some cases, however, one may be able to make certain approximations so as to simplify this calculation. For example, when there is a large amount of added salt present in the system, compared to the surfactant concentration, the concentration of added salt will simply swamp out the monomer concentration, rendering it insignificant as far as the calculation of g_{elec} is concerned.

2.4 Concluding Remarks

In summary, this chapter has presented a thermodynamic framework to describe a vesicle suspension, and discussed thoroughly the estimation of the various free-energy contributions to the free energy of vesiculation, g_{ves}. When compared to previous molecular approaches, this theory provides a more precise account of the various free-energy contributions to vesiculation, including an evaluation of the packing free energy associated with the surfactant tails and the steric free energy associated with the surfactant heads. Unlike the widely used continuum or curvature-elasticity approach, the present theory accounts explicitly for the molecular nature of the aggregates, and therefore provides many more details about the configuration of the vesicles over *the entire range of radii or curvatures.* In chapter 4, this theory will be applied to study vesicle formation in a cationic/anionic surfactant mixture. In addition to

demonstrating the ability of the theory to predict vesicle properties, such as, size and composition distribution and surface potentials, the study presented in chapter 4 also illustrates how the interplay between the various free-energy contributions associated with vesiculation affects the formation of mixed vesicles. The theory will then be utilized in chapter 5 to study the effect of surfactant tail-length asymmetry on the formation and stabilization of mixed surfactant vesicles. As stated in section 2.2.5, however, in order to estimate the electrostatic free energy, g_{elec}, of a charged vesicle via the reversible charging process, a relation between the surface potentials and the surface charge densities must be established. Therefore, before proceeding with the applications of the theory, the following chapter will first detail the derivation of the approximate analytical expressions used in the calculation of the surface potentials of a charged vesicle.

Chapter 3

Approximate Expressions for the Surface Potentials of Charged Vesicles

In this chapter, approximate relations between the surface potentials and the surface charge densities are derived for the purpose of evaluating g_{elec} of a charged vesicle [177]. The surface potentials of a charged vesicle may, in principle, be calculated by solving the Poisson-Boltzmann (PB) equation (see section 3.1). Unfortunately, an analytical solution of the PB equation in spherical geometry is not yet available, and, therefore, an often tedious numerical integration procedure is required [50, 113]. Consequently, it is quite prohibitive, from a computational standpoint, to utilize the PB equation in the minimization of g_{ves}. In this respect, several approximate analytical solutions of the PB equation have been developed for a single charged sphere in an electrolyte solution [8, 108, 132, 174]. In particular, Evans, Mitchell, and Ninham (EMN) derived [48, 49, 116] an analytical expression for the electrostatic free energy of ionic micelles in their development of the dressed-ionic micelle theory. Mitchell and Ninham later extended [117] this formulation to charged vesicles, where they assumed that the interior of the vesicle is electrically neutral, and that the electrostatic potential at the center of the vesicle is zero. Although these assumptions simplify the mathematical complexities, they can be restrictive under conditions of

low ionic strength and/or small vesicle radius where the potential in the interior of the vesicle may not decay to zero at the center. In addition, the assumption of an electrically neutral interior implies that the electrostatic potential does not vary across the hydrophobic region, which is valid only when the vesicle has similar outer and inner surface charge densities.

In the present derivation of approximate expressions for the surface potentials, no assumption of zero center-point potential and electroneutrality in the interior of the vesicle is made. Consequently, a solution strategy different from that of EMN is required, since the outer and inner surface potentials are coupled through the potential profile in the hydrophobic region. The derivation of the approximate relations is presented in two stages. First, in section 3.1, we derive a set of three approximate algebraic equations describing the relations between the surface potentials, the center-point potential, and the surface charge densities, based on a generalization of the approach of EMN. The two boundary conditions at the outer and inner surfaces of the vesicle serve as the backbone of this derivation. This set of equations can then be solved numerically, and the resulting surface potentials can be used in Eq. (2.27) in chapter 2 to evaluate the electrostatic free energy of the charged vesicle. In the second stage (see section 3.2), other approximations are introduced in order to obtain analytical expressions for the surface potentials. Using these analytical expressions, the surface potentials can be calculated directly without any numerical procedure, and, therefore, g_{elec} in Eq. (2.27) can be calculated much more efficiently. Accordingly, the derivation in the second stage represents an additional improvement on the efficiency of utilizing Eq. (2.27), as compared to simply utilizing the approach of EMN. A detailed derivation of the analytical expressions for the vesicle surface potentials is presented in the appendix G.

3.1 Implicit Relations between Surface Potentials and Surface Charge Densities

In what follows, the charged vesicle is modeled as composed of three regions, which are separated by two charged surfaces (see Figure 3-1). Regions 1 and 3 are the aqueous domains containing water and ions, and Region 2 is the hydrophobic domain made up of the surfactant tails. It is assumed that the ions can cross freely, but not accumulate in, the hydrophobic region [50, 113, 165]. Assuming that both the surfactant and the added salt are symmetric electrolytes having the same valence, z, and that the system is spherically symmetric, the nonlinear PB equation for each of the three regions can be written as follows

1. Region 1 ($0 \leq r \leq R_i$):

$$\frac{d^2y_1}{dx^2} + \frac{2}{x}\frac{dy_1}{dx} = \sinh(y_1) \tag{3.1}$$

2. Region 2 ($R_i < r \leq R_o$):

$$\frac{d^2y_2}{dx^2} + \frac{2}{x}\frac{dy_2}{dx} = 0 \tag{3.2}$$

3. Region 3 ($r > R_o$):

$$\frac{d^2y_3}{dx^2} + \frac{2}{x}\frac{dy_3}{dx} = \sinh(y_3) \tag{3.3}$$

where

$$y_j = ez\psi_j/kT \quad , \qquad j = 1, 2, 3 \tag{3.4}$$

$$x = \kappa_w r \tag{3.5}$$

$$\kappa_w = \sqrt{\frac{8\pi n_o e^2 z^2}{\epsilon_w kT}} \tag{3.6}$$

In Eqs. (3.1) – (3.6), ψ_j is the electrostatic potential in Region j (1, 2, or 3), y_j is the reduced potential in Region j, r is the radial coordinate, κ_w is the inverse of the Debye screening length, $\epsilon_w = 4\pi\eta_w\epsilon^o$ is the permittivity of water, where η_w is the dielectric constant of water and ϵ^o is the permittivity in vacuum, k is the Boltzmann

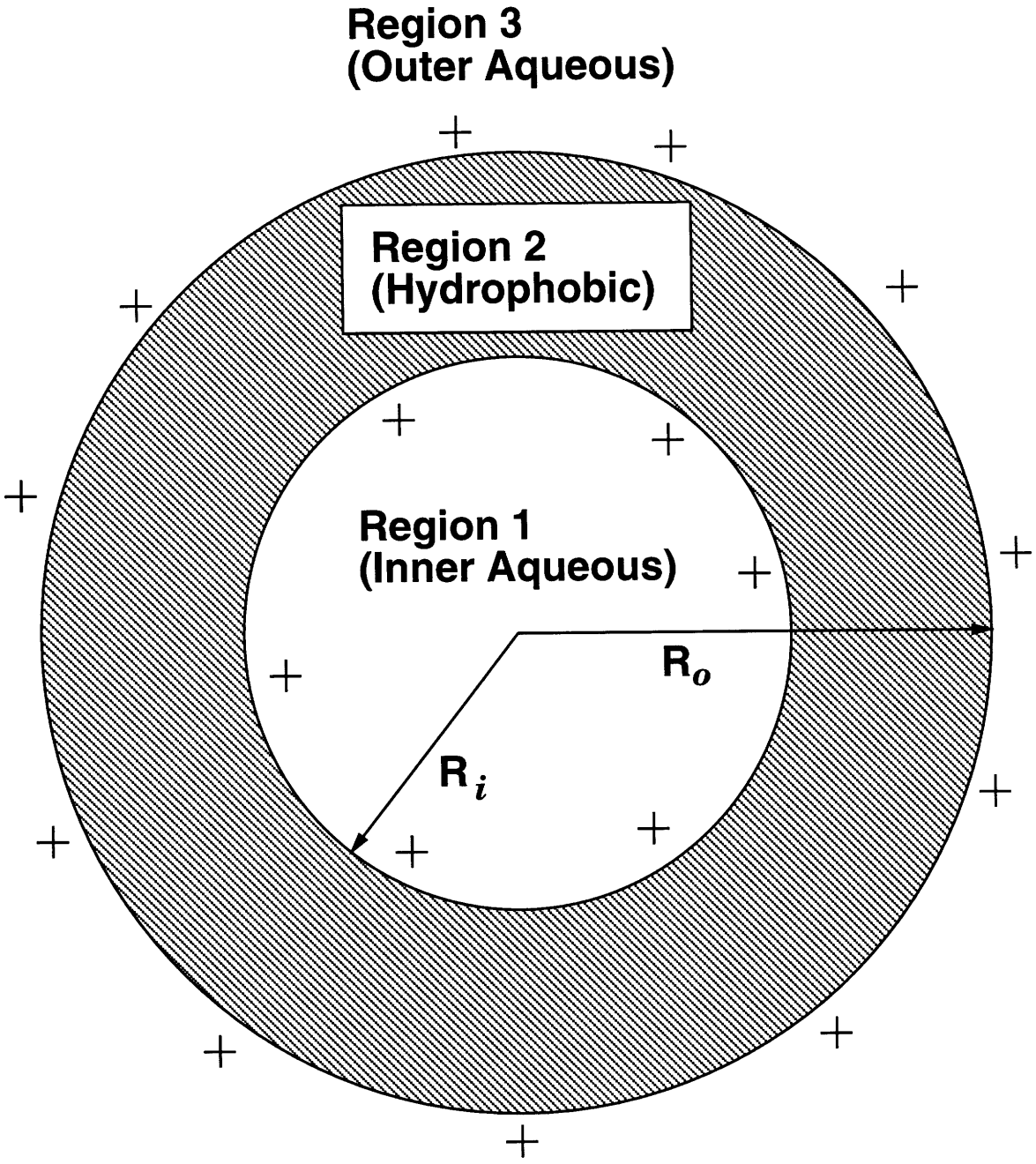

Figure 3-1: Schematic diagram of a positively-charged vesicle showing the inner and outer aqueous regions, separated by the hydrophobic region composed of the surfactant tails. The vesicle is assumed to be spherical, and the charges are assumed to be smeared on the surfaces at R_i and R_o, the inner and outer radii, respectively.

constant, e is the elementary charge, T is the absolute temperature, and n_o is the average ion concentration, which is the sum of the concentrations of the surfactant monomers and the added salt present in Regions 1 and 3[1]. The homogeneous nature of Eq. (3.2) is a consequence of the assumption that there is no ion accumulation in the hydrophobic region (Region 2), which implies that the charge density in the hydrophobic region is zero.

Note that in utilizing the PB equation, we are making the usual assumptions of smeared surface charges and point-sized ions [12]. The smearing of charges may be viewed as resulting from the rapid motion of the molecules within each leaflet of the bilayer, and therefore, from a time-averaging point of view, appears to be a reasonable description. The assumption of point-sized ions does not appear to be too restrictive, as compared to the case of micelles, since the radius of a cationic-anionic vesicle is typically larger than 300 Å [87], whereas the size of a counterion is of the order of 1 to 2 Å. In addition, for simplicity, it is also assumed that the dielectric constants, both in water and in the hydrophobic region, are constant, and neglect other effects such as dielectric saturation (the reader is referred to Ref. 14 for a detailed discussion of these effects).

The boundary conditions for the set of differential equations (3.1) – (3.3) can be written as follows

1. At $x = 0$:

$$\frac{dy_1}{dx} = 0 \tag{3.7}$$

$$y_1 = y_o \tag{3.8}$$

2. At $x = \kappa_w R_i \equiv X_i$:

$$\epsilon_1 \kappa_w \frac{dy_1}{dx} - \epsilon_2 \kappa_w \frac{dy_2}{dx} = \frac{4\pi\sigma_i ez}{kT} \tag{3.9}$$

$$y_1 = y_2 \tag{3.10}$$

[1]Note that the equilibrium surfactant monomer concentration is typically not known *a priori*. In order to obtain the surfactant monomer concentration, from which n_o can then be computed, one needs to calculate the overall free energy of the vesicular solution iteratively subject to the constraint of surfactant mass balance.

3. At $x = \kappa_w R_o \equiv X_o$:

$$\epsilon_2 \kappa_w \frac{dy_2}{dx} - \epsilon_3 \kappa_w \frac{dy_3}{dx} = \frac{4\pi\sigma_o ez}{kT} \tag{3.11}$$

$$y_2 = y_3 \tag{3.12}$$

4. As $x \to \infty$:

$$\frac{dy_3}{dx} = 0 \tag{3.13}$$

$$y_3 = 0 \tag{3.14}$$

where σ_o and σ_i are the charge densities at the outer and inner surfaces, respectively, $\epsilon_j = 4\pi\eta_j\epsilon^o$ is the permittivity in Region j (1, 2, or 3), where η_j is the dielectric constant in Region j, and y_o is the reduced center-point potential, that is, the reduced potential at the center of the vesicle. Although Regions 1 and 3 contain ionic solutions, and may therefore have lower dielectric constants than pure water [12], ϵ_1 and ϵ_3 are assumed to be equal to ϵ_w for simplicity. Equations (3.9) and (3.11) describe the variation of the electric field across the inner and outer surfaces, respectively, according to Gauss law. Equations (3.10) and (3.12) state the continuity of the electrostatic potentials at the inner and outer surfaces, respectively. Equation (3.7) is the requirement of spherical symmetry, while Eq. (3.13) ensures that the entire system, that is, the charged vesicle and the aqueous solution in Regions 1 and 3, is electrically neutral.

As mentioned earlier, the potential profiles in the three regions can be obtained by numerically integrating Eqs. (3.1), (3.2), and (3.3), subject to the boundary conditions given in Eq. (3.7) through Eq. (3.14). This integration starts at the center of the vesicle, that is, at $x = 0$, and the solution then propagates across the three regions until it approaches infinity. However, in the calculation of the electrostatic free energy, G_{elec}, using the charging process, the only relevant quantities are the two potentials at the outer (ψ_o) and inner (ψ_i) surfaces, as shown in Eq.(2.27 in chapter 2). In other words, *in order to evaluate G_{elec}, one does not need to know how the potential varies with the radial distance.* Accordingly, a numerical integration of the PB equation will require unnecessary efforts spent on calculating the entire spatial potential profile.

Indeed, Eqs. (3.9) and (3.11), which relate the potential gradients at the outer and inner surfaces through the surface charge densities, may be used to obtain the two surface potentials directly. More specifically, the PB equations presented in Eqs. (3.1) – (3.3) may be used simply to express the surface potential gradients in terms of the surface potentials, which can then be calculated by solving Eqs.(3.9) and (3.11).

Following the derivation in Ref. 48, one obtains an approximate expression for the potential gradient at X_o in Region 3 from Eq. (3.3), that is,

$$\left.\frac{dy_3}{dx}\right|_{X_o} \approx -2\sinh\left(\frac{y_{3,o}}{2}\right)\left[1+\frac{2}{X_o}\frac{1}{\cosh(y_{3,o}/2)+1}\right] \tag{3.15}$$

where $y_{3,o}$ denotes the reduced potential (see Eq. (3.4)) at $x = X_o$, that is, at the outer surface of the vesicle. Two approximations are involved in deriving Eq.(3.15), and the reader is referred to Ref. 116 for complete details. One of the approximations, namely, the replacement of the first derivative, dy_3/dx, in Eq. (3.3) with the result from planar geometry, leads to an inconsistency which has already been discussed by Hayter [71], and its validity can only be judged *a posteriori*. Similar approximations can be applied to Eq. (3.1). Specifically, incorporating Eqs. (3.7) and (3.8), the approximate equation for the potential gradient at $x = X_i$ in Region 1 can be written as

$$\left.\frac{dy_1}{dx}\right|_{X_i} \approx [g(y_{1,i})]^{1/2}\left[1-\frac{2}{X_i g(y_{1,i})}\int_{y_o}^{y_{1,i}}[g(y_1)]^{1/2}dy_1\right] \tag{3.16}$$

where

$$g(y_1) = 2(\cosh y_1 - \cosh y_o) \tag{3.17}$$

and $y_{1,i}$ denotes the reduced potential at $x = X_i$, that is, at the inner surface of the vesicle. The difference between Eqs.(3.16) and (3.15) originates from the different boundary conditions used in their derivation. To further simplify Eq. (3.16) by carrying out the integration, the function $g(y_1)$ in the integrand is replaced by $2(\cosh y_1 - 1)$, that is, the integration is carried out by treating y_o as zero (see Eq. (3.17)). This approximation should be valid for high ionic strengths, since in this case y_o is essentially

zero due to strong screening. Applying this approximation, Eq. (3.16) becomes

$$\left.\frac{dy_1}{dx}\right|_{X_i} \approx 2\sinh\left(\frac{y_{1,i}}{2}\right)\left[1-\frac{2}{X_i}\frac{\cosh(y_{1,i}/2)-\cosh(y_o/2)}{\sinh^2(y_{1,i}/2)}\right] \tag{3.18}$$

Equation (3.2), which is a homogeneous differential equation, can be solved exactly to give the potential gradients at the two surfaces. Specifically,

$$\left.\frac{dy_2}{dx}\right|_{X_i} = \frac{1}{X_i^2}\left(\frac{1}{X_i}-\frac{1}{X_o}\right)^{-1}(y_{3,o}-y_{1,i}) \tag{3.19}$$

$$\left.\frac{dy_2}{dx}\right|_{X_o} = \frac{1}{X_o^2}\left(\frac{1}{X_i}-\frac{1}{X_o}\right)^{-1}(y_{3,o}-y_{1,i}) \tag{3.20}$$

There are now expressions for the four derivatives at the outer and inner surfaces, given by Eqs. (3.15), (3.18), (3.19), and (3.20). These four derivatives are related by the two boundary conditions, Eqs. (3.9) and (3.11), through the outer and inner surface charge densities. Therefore, substituting these expressions for the four derivatives in Eqs. (3.9) and (3.11), one obtains the following two equations

$$\frac{4\pi\sigma_o e z}{\epsilon_3\kappa_w kT}-\frac{\epsilon_2}{\epsilon_3}\frac{1}{X_o^2}\left(\frac{1}{X_i}-\frac{1}{X_o}\right)^{-1}(y_{3,o}-y_{1,i}) = 2\sinh\left(\frac{y_{3,o}}{2}\right)\left[1+\frac{2}{X_o}\frac{1}{\cosh(y_{3,o}/2)+1}\right] \tag{3.21}$$

$$\frac{4\pi\sigma_i e z}{\epsilon_1\kappa_w kT}+\frac{\epsilon_2}{\epsilon_1}\frac{1}{X_i^2}\left(\frac{1}{X_i}-\frac{1}{X_o}\right)^{-1}(y_{3,o}-y_{1,i}) = 2\sinh\left(\frac{y_{1,i}}{2}\right)\left[1-\frac{2}{X_i}\frac{\cosh(y_{1,i}/2)-\cosh(y_o/2)}{\sinh^2(y_{1,i}/2)}\right] \tag{3.22}$$

Note that Eq. (3.21) can be easily reduced to EMN's expression for a micelle (Eq. (11) in Ref. 116). This can be seen as follows. In a micelle, Region 1 is also hydrophobic, which implies that there is no ion accumulation, and, therefore, the potential gradient at the inner surface in Region 1 (at $x = X_i$) is zero. In addition, there is no charge on the inner surface; indeed, the inner surface does not exist in a micelle, and the outer surface corresponds to the aqueous/hydrocarbon core interface. Consequently, dy_1/dx and σ_i can be set to zero in Eq. (3.9), which results in dy_2/dx at $x = X_i$ being zero. From Eq. (3.19), then, $y_{3,o}$ becomes equal to $y_{1,i}$, and Eq. (3.21) becomes

identical to Eq. (11) in Ref. 116.

Since the center-point potential, y_o, is not known *a priori*, there are three unknowns, y_o, $y_{1,i}$, and $y_{3,o}$, and two equations, Eqs. (3.21) and (3.22). Consequently, one needs another relation in order to calculate the potentials at the outer and inner surfaces. This additional relation can be obtained by considering only the inner aqueous region (Region 1). This region may be viewed as a spherical aqueous cavity surrounded by a charged surface of radius R_i. Several expressions can be found in the literature which describe the potential profile within such a cavity [39, 95, 165]. The relation given by Tenchov and co-workers [165], which is adopted in the present work because of its simplicity, expresses the inner surface potential, $y_{1,i}$, in terms of the center-point potential, y_o, that is,

$$y_{1,i} = y_o Y_1 + y_o^3 Y_3 \tag{3.23}$$

where

$$Y_1 = \frac{\sinh(X_i)}{X_i} \tag{3.24}$$

$$Y_3 = \sum_{n=1}^{\infty} [\alpha_n X_i^{2n-1} \sinh(X_i) - \beta_n X_i^{2n} \cosh(X_i)] \tag{3.25}$$

$$\alpha_n = \frac{2^{2n}(2^{2n}-1)}{24n(2n)!} \tag{3.26}$$

$$\beta_n = \frac{2^{2n}(2^{2n}-1)}{3(2n+1)^2(2n)!} \tag{3.27}$$

Equation (3.23) is accurate for a surface charge density of up to about 2.4×10^{-21} C/Å^2 (1.5 e/nm^2) [165]. Note that in a cationic-anionic vesicle, because of the mixing of positive and negative charges, the surface charge density is typically less than 0.16×10^{-21} C/Å^2 (0.1 e/nm^2) [33].

For given values of σ_i^f, σ_o^f, n_o, R_i, and R_o, Eqs. (3.21), (3.22), and (3.23) can be solved simultaneously to find y_o, $y_{1,i}$, and $y_{3,o}$. Although a numerical procedure is still required because of the implicit nature of these equations, it is much less computationally intensive than that involved in the direct numerical integrations of the PB equations in the three regions, particularly when one of the boundaries is

at infinity (see Eqs. (3.13) and (3.14)). *The three approximate algebraic equations, (3.21), (3.22), (3.23), thus represent the initial improvement in the efficiency of using the PB equation for the calculation of the electrostatic free energy of a charged vesicle.* It is important to emphasize at this point that *it is the accuracy of the surface potentials, $y_{1,i}$ and $y_{3,o}$, and not of the center-point potential, y_o, that we are interested in.* As shown in Eq. (2.27) in chapter 2, only the surface potentials are involved in the calculation of the electrostatic free energy using the charging process, with the center-point potential never playing an explicit role. Consequently, in determining the validity of the approximate solutions with respect to the electrostatic free energy, the accuracy of the surface potentials, and not of the center-point potential, should be of primary importance.

3.2 Approximate Analytical Expressions for the Surface Potentials

The computational efficiency of utilizing the PB equation may be further improved if one can obtain analytical expressions for $y_{1,i}$ and $y_{3,o}$ so that they can be evaluated directly from other known quantities such as the surface charge densities and the outer and inner radii of the vesicle. This section briefly discusses the derivation of such approximate expressions. A more detailed derivation can be found in the appendix G.

Consider Eqs. (3.21) and (3.22). The hyperbolic functions appearing in these two equations may be linearized around the surface potentials which correspond to a vesicle having an electrically neutral interior and zero center-point potential. This reference configuration is chosen mainly for convenience. Indeed, as shown in appendix G, such a vesicle will have the two surface potentials and the center-point potential completely decoupled, such that the two surface potentials can then be evaluated separately. By choosing this reference configuration, it is assumed that the surface potentials of a charged vesicle do not deviate much from those of the reference

vesicle. Equations (3.21) and (3.22) thus become

$$(s_o - A_3) - y_{3,o}\left(\frac{\gamma}{X_o^2} + \frac{1}{X_o} + B_3\right) + y_{1,i}\frac{\gamma}{X_o^2} = 0 \tag{3.28}$$

and

$$s_i + \frac{\gamma}{X_i^2}(y_{3,o} - y_{1,i}) = A_1 + B_1 y_{1,i} - \frac{y_{1,i}}{X_i} + \frac{y_o^2}{X_i(A_1 + B_1 y_{1,i})} \tag{3.29}$$

respectively, where s_o, s_i, γ, and the coefficients A_1, B_1, A_3, and B_3 are given in appendix G (see Eqs. (G.3), (G.4), (G.5), (G.13), (G.14), (G.10), and (G.11), respectively). The outer surface potential, $y_{3,o}$, can be expressed in terms of the inner surface potential, $y_{1,i}$, using Eq. (3.28). The center-point potential, y_o, can also be expressed in terms of $y_{1,i}$ by inverting Eq. (3.23). Substituting the resulting expressions in Eq. (3.29) and rearranging the terms, one obtains a polynomial in $\tilde{y}_1 = y_{1,i}/Y_1$. Specifically,

$$\hat{Y}_3^2\tilde{y}_1^6 - 2\hat{Y}_3\tilde{y}_1^4 - (B_1 F Y_1^2 X_i - 1)\tilde{y}_1^2 - (A_1 F + B_1 E)X_i Y_1 \tilde{y}_1 - A_1 E X_i = 0 \tag{3.30}$$

where Y_1 is given in Eq. (3.24), and the coefficients $\hat{Y}_3$, E, and F are given in appendix G (see Eqs. (G.20), (G.22), and (G.23), respectively). Equation (3.30) may be solved numerically to obtain $\tilde{y}_1$, or equivalently, $y_{1,i}$. However, for small $\tilde{y}_1$, the fourth- and sixth-order terms in Eq. (3.30) can be neglected, and $\tilde{y}_1$ can then be expressed approximately as follows

$$\tilde{y}_1 \approx -\frac{(A_1 F + B_1 E)Y_1}{2(B_1 F Y_1^2 - 1/X_i)} \pm \frac{1}{2}\left\{\left[\frac{(A_1 F + B_1 E)Y_1}{(B_1 F Y_1^2 - 1/X_i)}\right]^2 - \frac{4A_1 E}{(B_1 F Y_1^2 - 1/X_i)}\right\}^{\frac{1}{2}} \tag{3.31}$$

The selection of the + or - sign in Eq. (3.31) is discussed in appendix G following Eq. (G.25). Once $\tilde{y}_1$ is known, $y_{3,o}$ can be obtained from Eq. (3.28), namely,

$$y_{3,o} = \frac{X_o^2(s_o - A_3)}{\gamma + X_o + B_3 X_o^2} + \frac{\gamma Y_1 \tilde{y}_1}{\gamma + X_o + B_3 X_o^2} \tag{3.32}$$

Since now $y_{1,i}$ and $y_{3,o}$ can be *evaluated analytically* for given outer and inner vesicle radii and surface charge densities, the integration in Eq. (2.27) can be performed

much more rapidly. In other words, *at each charging stage, the instantaneous surface potentials can now be calculated analytically using Eqs. (3.31) and (3.32), rather than by solving the three algebraic equations, Eqs. (3.21), (3.22), and (3.23), numerically.* Equations (3.31) and (3.32) should therefore provide a much faster route, as compared to the numerical solution of Eqs. (3.21), (3.22), and (3.23), in the calculation of the electrostatic free energy of a charged vesicle. However, as detailed in appendix G, in going from the implicit relations described by Eqs. (3.21), (3.22), and (3.23) to the analytical expressions given by Eqs. (3.31) and (3.32), more approximations are introduced, which, as shown in the next section, may cause a loss in accuracy in some cases.

3.3 Results and Discussions

The surface potentials obtained by solving Eqs. (3.21), (3.22), and (3.23) [Solution I], and by using Eqs. (3.31) and (3.32) [Solution II], are shown in Tables 3.1 to 3.3 for three different ionic strengths. The results of a direct numerical integration of Eqs. (3.1), (3.2), and (3.3) [Solution III] are also shown in the corresponding tables. As emphasized earlier, we are interested mainly in the outer and inner surface potentials, since they are directly involved in the calculation of the electrostatic free energy (see Eq. (2.27) in chapter 2). Accordingly, attention should be focused on the accuracy of $\psi_o = kTy_{3,o}/ez$ and $\psi_i = kTy_{1,i}/ez$. The center-point potential, $\psi_c = kTy_o/ez$, is also shown for completeness. Note that in using the analytical expressions, Eqs. (3.31) and (3.32), one needs not evaluate the center-point potential, and, therefore, ψ_c corresponding to Solution II is not shown in the tables. The following typical parameter values were used in all the calculations: $T = 25$ °C, $R_o = 265$ Å, $R_i = 220$ Å, $\eta_w = 78.54$, and $\eta_2 = 2.5$ [50].

As shown in Tables 3.1 and 3.2, at the higher ionic strengths ($n_o = 0.1$ and 0.01 M), the agreement between the approximate solutions (I and II) and the results of the numerical integration (III) are excellent. The largest error is less than 1 %. This is to be expected because, as explained in appendix G, most of the approximations

Table 3.1: Comparison between the approximate solutions and the numerical integration of the PB equations for $n_o = 0.1$ M ($\kappa_w R_i = 22.9$). I: numerical solution of Eqs. (3.21), (3.22), and (3.23), II: solution of Eqs. (3.31) and (3.32), and III: numerical integration of the PB equations ($\psi_c = kTy_o/ez$).

$\sigma_i^f \times 10^{21}$ (C/Å^2)	$\sigma_o^f \times 10^{21}$ (C/Å^2)	ψ_c (mV)		ψ_i (mV)			ψ_o (mV)		
		I	III	I	II	III	I	II	III
2.4	2.4	0	0	132.5	132.7	132.4	131.4	131.1	131.4
	0.3	0	0	132.3	132.6	132.3	37.4	37.3	37.4
	0.07	0	0	132.3	132.6	132.3	10.0	10.0	10.0
	0.01	0	0	132.3	132.6	132.3	2.0	2.0	2.0
0.3	2.4	0	0	39.8	39.9	39.8	131.3	131.1	131.3
	0.3	0	0	39.2	39.3	39.2	37.0	36.9	37.0
	0.07	0	0	39.1	39.1	39.0	9.5	9.5	9.5
	0.01	0	0	39.0	39.1	39.0	1.5	1.5	1.5
0.01	2.4	0	0	2.6	2.5	2.6	131.3	131.0	131.3
	0.3	0	0	1.7	1.7	1.7	36.8	36.8	36.8
	0.07	0	0	1.5	1.5	1.5	9.3	9.3	9.3
	0.01	0	0	1.4	1.4	1.4	1.3	1.3	1.3

Table 3.2: Comparison between the approximate solutions and the numerical integration of the PB equations for $n_o = 0.01$ M ($\kappa_w R_i = 7.2$). I: numerical solution of Eqs. (3.21), (3.22), and (3.23), II: solution of Eqs. (3.31) and (3.32), and III: numerical integration of the PB equations ($\psi_c = kTy_o/ez$).

$\sigma_i^f \times 10^{21}$ (C/Å^2)	$\sigma_o^f \times 10^{21}$ (C/Å^2)	ψ_c (mV)		ψ_i (mV)			ψ_o (mV)		
		I	III	I	II	III	I	II	III
2.4	2.4	1.3	0.95	191.4	192.1	191.4	190.2	189.7	189.6
	0.3	1.3	0.95	191.3	191.9	191.3	83.5	82.9	83.5
	0.07	1.3	0.95	191.2	191.9	191.2	28.8	28.8	28.8
	0.01	1.3	0.95	191.2	191.8	191.2	6.9	6.9	6.9
0.3	2.4	0.8	0.7	90.1	91.0	90.1	190.1	189.6	190.1
	0.3	0.8	0.7	89.2	90.0	89.1	82.8	82.2	82.8
	0.07	0.8	0.7	88.7	89.5	88.6	27.4	27.3	27.4
	0.01	0.8	0.7	88.5	89.3	88.4	5.3	5.3	5.3
0.01	2.4	0.1	0.1	10.4	10.4	10.4	190.1	189.5	190
	0.3	0.08	0.08	7.3	7.3	7.3	82.3	81.7	82.2
	0.07	0.06	0.06	5.7	5.7	5.7	26.2	26.1	26.2
	0.01	0.05	0.05	5.0	5.0	5.0	3.9	3.9	3.9

Table 3.3: Comparison between the approximate solutions and the numerical integration of the PB equations for $n_o = 0.001$ M ($\kappa_w R_i = 2.3$). I: numerical solution of Eqs. (3.21), (3.22), and (3.23), II: solution of Eqs. (3.31) and (3.32), and III: numerical integration of the PB equations ($\psi_c = kTy_o/ez$).

$\sigma_i^f \times 10^{21}$	$\sigma_o^f \times 10^{21}$	ψ_c (mV)		ψ_i (mV)			ψ_o (mV)		
(C/Å^2)		I	III	I	II	III	I	II	III
2.4	2.4	58.5	36.6	250.6	251.6	250.6	249.4	248.5	249.3
	0.3	58.5	36.6	250.5	251.4	250.5	139.9	137.6	139.7
	0.07	58.5	36.6	250.4	251.4	250.4	66.2	65.1	66
	0.01	58.5	36.6	250.3	251.3	250.3	19.4	19.6	19.4
0.3	2.4	44.2	34.5	148.6	151.2	148.6	249.3	248.4	249.3
	0.3	44.1	34.5	147.6	150.2	147.6	139.1	136.9	139
	0.07	43.9	34.4	146.9	149.4	146.9	63.6	62.5	63.4
	0.01	43.9	34.4	146.5	149	146.5	15.4	15.6	15.4
0.01	2.4	17.5	17.9	40.5	41.6	42.4	249.2	248.3	249.2
	0.3	13.9	14.6	31.4	31.3	33.4	138.2	136	138.1
	0.07	11	11.7	24.2	24.3	26.1	60.3	59.4	60.2
	0.01	8.8	9.6	19.3	19.5	21	10.5	10.5	10.5

made in the present formulation are based on large $X_i = \kappa_w R_i$ values, that is, large vesicle radii or high ionic strengths (see Eq. (3.6)). In particular, at the higher ionic strengths, the charges on the inner surface are screened so strongly that the center-point potential, y_o, is essentially zero for a range of charge densities that covers two orders of magnitude. Consequently, the approximations used to effect Eq. (3.18), namely $y_o = 0$, and the linearization involved in the derivation of the analytical expressions, introduce negligible errors in this case, and, therefore, both formulations provide excellent agreement. The effect of the approximations becomes more noticeable as the ionic strength decreases. With the ion concentration, n_o, equal to 0.001 M (see Table 3.3), one begins to observe small discrepancies in the inner surface potentials at low surface charge densities. The largest error in ψ_i is about 8 %, which occurs at σ_o^f and σ_i^f equal to 0.01×10^{-21} C/Å^2. The effect of the ionic strength depends very much on the inner surface charge density. If the inner surface charge density is high, the importance of y_o diminishes because in this case $y_{1,i}$ is large compared to y_o, and the dependence of y_o in Eq. (3.22) becomes negligible. Therefore, even when there is significant discrepancy in y_o, one still obtains very good agreement in the two surface potentials. As the inner surface charge density becomes very low (for example, 0.01×10^{-21} C/Å^2), the magnitude of the center-point potential becomes comparable to that of the inner surface potential, $y_{1,i}$. The approximation involved in Eq. (3.18) may no longer be valid, and one sees a deviation in the inner surface potential from the results of a direct numerical integration. Note that, as shown in Eq. (3.32), the accuracy of ψ_i also determines that of ψ_o. As can be seen in Table 3.3, the values of ψ_o, corresponding to Solutions I and II, are in very good agreement with those corresponding to Solution III, even at low ionic strengths.

The electrostatic free energy per molecule, g_{elec}, calculated as $g_{elec} = G_{elec}/n$, where n is the total number of amphiphilic molecules in the vesicle, is shown in Table 3.4 for two ionic strengths (0.01 M and 0.001 M). Note that n is calculated as $n = (A_o + A_i)/a_1$, where a_1 is the average area per molecule, and is assigned a typical value of 67 Å^2 [80], and G_{elec} is calculated by carrying out the integration in Eq. (2.27) numerically. As before, the agreement between the approximate formula-

Table 3.4: Electrostatic free energies per molecule, $g_{elec} = G_{elec}/n$. The surface potentials are calculated using I: numerical solution of Eqs. (3.21), (3.22), and (3.23), II: solution of Eqs. (3.31) and (3.32), and III: numerical integration of the PB equations.

$\sigma_i^f \times 10^{21}$	$\sigma_o^f \times 10^{21}$	$n_o = 0.01$ M			$n_o = 0.001$ M		
(C/Å^2)		I	II	III	I	II	III
2.4	2.4	5.534	5.532	5.533	7.767	7.761	7.766
	0.3	2.422	2.434	2.422	3.467	3.488	3.467
	0.07	2.29	2.302	2.29	3.222	3.247	3.222
	0.01	2.28	2.292	2.279	3.197	3.222	3.197
0.3	2.4	3.353	3.341	3.353	4.769	4.742	4.769
	0.3	0.246	0.246	0.246	0.473	0.473	0.473
	0.07	0.116	0.117	0.116	0.231	0.235	0.232
	0.01	0.107	0.108	0.107	0.207	0.212	0.208
0.01	2.4	3.241	3.227	3.241	4.553	4.521	4.552
	0.3	0.137	0.136	0.137	0.261	0.256	0.261
	0.07	0.0092	0.0092	0.0092	0.0225	0.0223	0.0226
	0.01	0.00035	0.00036	0.00036	0.00115	0.00117	0.00122

tions (I and II) and the direct integration of the PB equation (III) is very good, with the largest error being about 4 %. Based on these results and other calculations, the two approximate formulations should be applicable for $X_i \geq 2.3$ (corresponding to $n_o \approx 0.001$ M for $R_i = 220$ Å), for a range of surface charge densities from 0.01×10^{-21} to 2.4×10^{-21} C/Å^2. The limit for X_i also depends on the inner radius, R_i, of the vesicle. With $X_i \geq 2.3$, the error in the surface potentials is within 10 % for a value of R_i down to about 40 Å ($n_o \approx 0.03$ M). In general, the surface potentials and the electrostatic free energies obtained with the analytical expressions (Eqs. (3.31) and (3.32)) are slightly less accurate than those obtained from the numerical solution of Eqs. (3.21), (3.22), and (3.23), mainly because of the additional linearization involved. However, *for most cationic-anionic vesicular systems, where the ion concentration is typically of the order of 0.01 M, the errors in the electrostatic free energies calculated using the analytical expressions are within 1 % of those obtained by a direct numerical integration of the PB equation (see Table 3.4)*, which is quite acceptable considering the improved efficiency associated with using the analytical expressions.

3.4 Concluding Remarks

Using the approximate expressions developed in this chapter, the electrostatic free energy, g_{elec}, can be evaluated readily as shown in Eq. (2.27) in chapter 2. In the following chapter, the molecular-thermodynamic theory developed in chapter 2 is applied to a cationic/anionic surfactant mixture. In addition to demonstrating the validity of this theory by comparing the predicted results to experimental data, chapter 4 will also illustrate how the detailed model presented in chapter 2, coupled with the results of chapter 3, can reveal the relative importance of the various free-energy contributions, as well as their interplay, in determining various vesicle properties, such as, vesicle size and composition, as well as the distribution of molecules between the outer and inner vesicle leaflets.

Chapter 4

Application of the Theory: I. Cationic/Anionic Surfactant Mixture

In this chapter, the molecular-thermodynamic theory developed in chapter 2, including the results obtained in chapter 3, is applied to an aqueous mixture of cetyltrimethylammonium bromide (CTAB) and sodium octyl sulfate (SOS), a system which has been studied experimentally [19, 74]. Spontaneous formation of vesicles has been observed in this system within a narrow range of compositions, and properties such as average vesicle size and zeta potentials have been measured experimentally [19, 74]. Accordingly, the application of the present theory to this system should also serve as some test of its range of validity and applicability. Our attention is focused on the composition range over which only vesicles are observed, since at this stage, this theory can only describe vesicles. In order to describe the complete phase behavior, however, one has to calculate the free energies associated with other self-assembling structures, such as mixed micelles, which is beyond the scope of this work. The main goal here is to predict the vesicle properties in solution, namely, the distribution of molecules between the outer and inner vesicle leaflets, the composition of each leaflet, surface potentials, surface charge densities, as well as size and composition distribution.

4.1 Model System

A summary of the molecular properties of the two surfactant components (CTAB and SOS) required in the theory, namely, the carbon number in the vesicle bilayer, $n_{c,k}$, the valence, z_k, the head area, $a_{h,k}$, the shielded area, a_k^*, the charge distance, $d_{ch,k}$, and the planar interfacial tension, σ_k, is provided in Table 4.1. For clarity, CTAB is denoted as component A ($k = A$) and SOS as component B ($k = B$). As discussed in chapter 2, the head area corresponds to the cross-sectional hard-disk area of the surfactant head. This quantity was estimated using both a space-filling atomic model and a computer-generated model, which yielded the same result. Another important molecular property is the charge distance, $d_{ch,k}$, of component k. Recall, from Eq. (2.28), that the values of $d_{ch,k}$ for the two components determine the gap distance, D, used in the calculation of g_{elec}. In addition, the dielectric constant is set at 2.5 for the hydrophobic region and 78.5 for water, and all the calculations are carried out at 25 °C. As can be seen, these input parameters depend only on the chemical structures of the surfactant molecules involved and the solution conditions.

4.2 Free Energy of Vesiculation

Using these molecular properties, one can generate a surface of g_{ves} as a function of n and F. As shown in Figure 4-1, g_{ves} shows a near-parabolic dependence on F, having a minimum between 0.6 and 0.7. This behavior is mainly due to the interplay between the transfer free energy, g_{tr}, and the electrostatic free energy, g_{elec}. The predicted variations of these two free-energy contributions as a function of F are depicted in Figure 4-2 for a large vesicle (approximating a planar bilayer). Intuitively, g_{elec} should attain a minimum at $F = 0.5$, since the opposite charges almost cancel each other in this case, and the electrostatic free energy is mostly due to the capacitor contribution. In other words, at $F = 0.5$, the electrostatic contribution resulting from the net charges (Figure 2-2(c)) is negligible compared to that resulting from the capacitors (Figure 2-2(b)). On the other hand, g_{tr} decreases (more negative) monotonically

Table 4.1: Molecular properties of cetyltrimethylammonium bromide (CTAB) and sodium octyl sulfate (SOS).

Molecular Properties	CTAB ($k = A$)	SOS ($k = B$)
Carbon number in bilayer, $n_{c,k}$	15	7
Valence, z_k	1	-1
Head area, $a_{h,k}$ (Å^2)	23	16
Shielded area, a_k^* (Å^2)	21	21
Charge distance, $d_{ch,k}$ (Å)	2.5	3.8
Planar hydrocarbon/water interfacial tension [101], σ_k (dyne/cm)	53	51

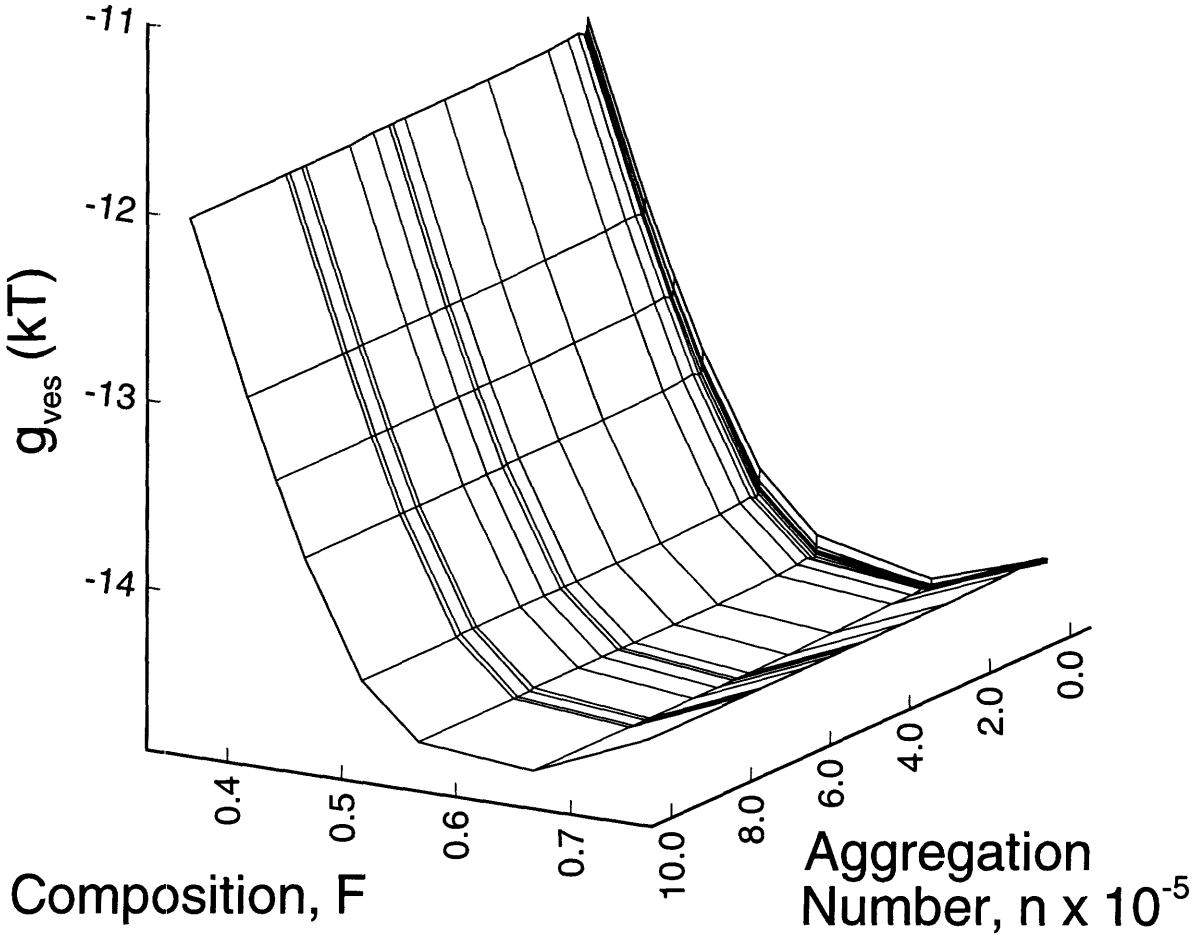

Figure 4-1: Predicted variation of the free energy of vesiculation, g_{ves}, as a function of vesicle aggregation number, n, and composition, F.

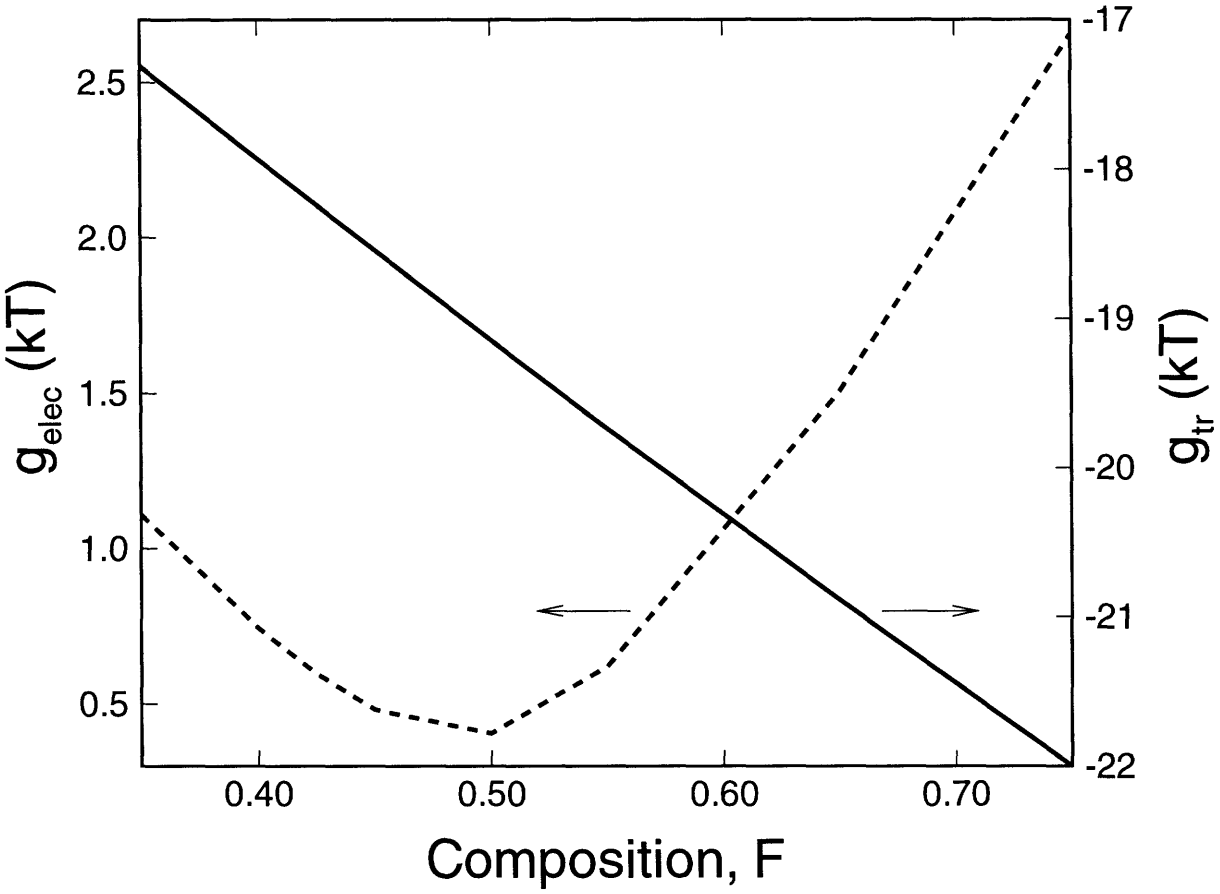

Figure 4-2: Predicted variations of the transfer free energy, g_{tr} (solid line), and the electrostatic free energy, g_{elec} (dashed line), as a function of F for a planar bilayer.

with F because of the more favorable condition of having the longer hydrocarbon chain of CTAB in the vesicle (recall that $F = 1$ corresponds to pure CTAB). The interplay of these two free-energy contributions results in the dependence of g_{ves} on F shown in Figure 4-1, with the minimum shifted to a value slightly higher than 0.5. In addition to the chain-length asymmetry between the two components, which determines the slope of g_{tr} as a function of F, the precise location of the minimum g_{ves} also depends on the ionic strength of the solution. A higher ionic strength would reduce the electrostatic penalty, causing the transfer free energy to be more dominant, and shifting F to a higher value. Note, however, that the actual composition of a vesicle in suspension may not correspond to the composition of an isolated vesicle, since, as discussed in section 2.1 (see Eq. (2.2)), the entropic factor also plays an important role in the process of vesiculation.

Also shown in Figure 4-1 is the behavior of g_{ves} as a function of n. At a fixed value of F, g_{ves} remains quite constant for large values of n, or equivalently large radii. This simply indicates that the vesicle configuration, that is, the distribution of molecules, f, the outer and inner leaflet compositions, X_{ok} and X_{ik}, the thickness of the hydrophobic region, t_b, etc., in this size range is very similar to that of a planar bilayer, which is a necessary consequence as the vesicle radius approaches infinity. On the other hand, when the values of n are very small, g_{ves} increases rapidly with decreasing n, as indicated by the sharp upturn in the energy surface as $n \to 0$. This increase in g_{ves} reflects a very different configuration for small vesicles, as compared to the planar bilayer case. Indeed, as the vesicle radius, or n, becomes very small, it is no longer feasible for a vesicle to maintain a configuration that is similar to that of a planar bilayer in the search for a minimum g_{ves} at given n and F. The variation of g_{ves} with vesicle size can be seen more clearly in Figure 4-3, in which the predicted free-energy difference, $g_{ves} - g_{bilayer}$, and the distribution of molecules, f, are plotted against the dimensionless mean curvature, $\bar{c}$, for $F = 0.5$. The dimensionless mean curvature is defined as $\bar{c} = 2\ell_{max,A}/(R_o + R_i)$, where $\ell_{max,A} = 20.5$ Å is the fully-extended length of component A (CTAB). The quantity, $g_{bilayer}$, is the free energy of "vesiculation" of a planar bilayer. By plotting these quantities versus the curvature,

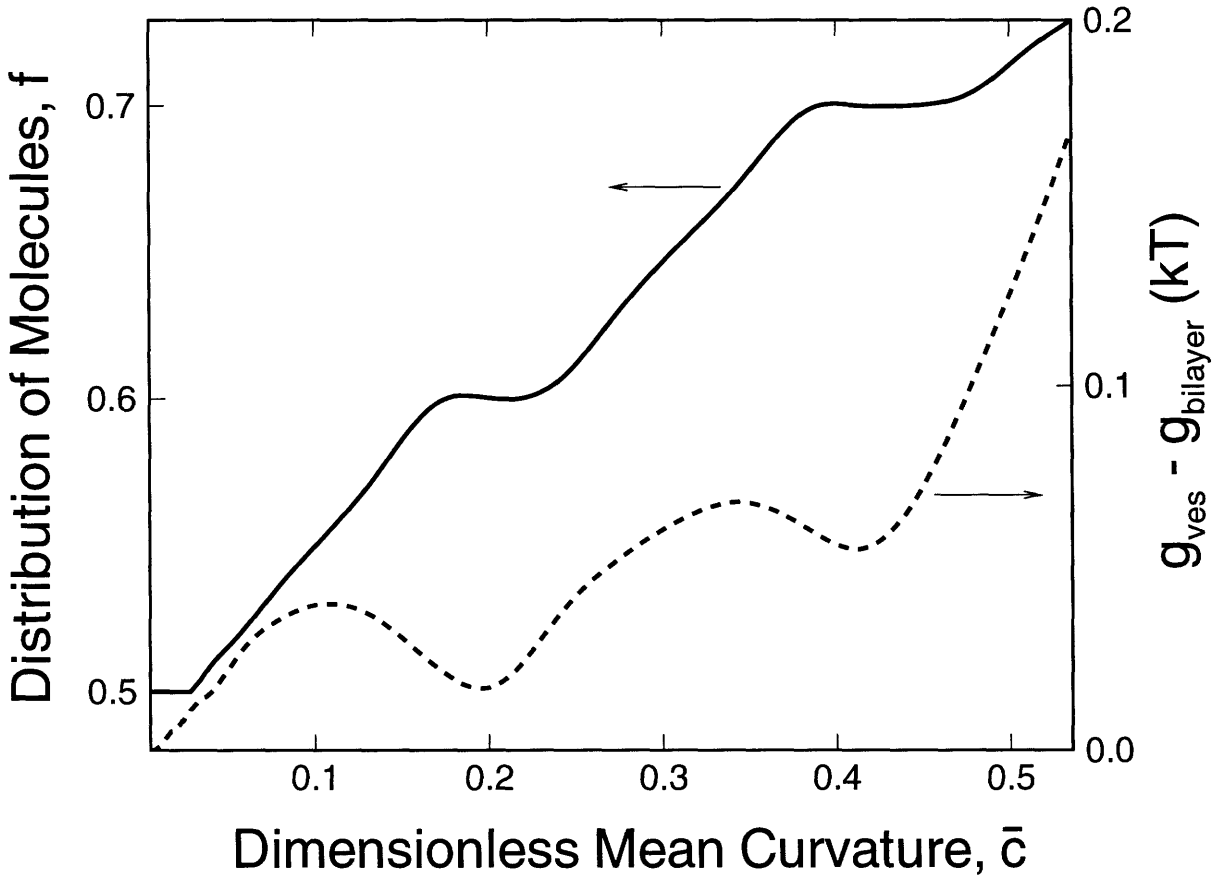

Figure 4-3: Predicted variation of the distribution of molecules, f (solid line), and the free-energy difference, $g_{ves} - g_{bilayer}$ (dashed line), as a function of the dimensionless mean curvature, $\bar{c} = 2\ell_{max,A}/(R_o + R_i)$. The vesicle composition, F, is fixed at 0.5. The distribution of molecules, f, is defined as the mole fraction of molecules in the outer leaflet.

$\bar{c}$, instead of versus the vesicle aggregation number, n, one effectively stretches out the abscissa and reveals more details in the small vesicle range. Note that increasing $\bar{c}$ is equivalent to decreasing n, that is, reducing the vesicle size. As shown in Figure 4-3, as $\bar{c} \to 0$, $f = 0.5$ and $g_{ves} - g_{bilayer} = 0$. At $\bar{c} \approx 0.025$, corresponding to a vesicle radius of about 800 Å, f begins to increase beyond 0.5, that is, more molecules are being placed in the outer leaflet. This increase in f is mainly due to the increase in the interfacial free energy, g_σ. More specifically, as shown in Figure 4-4, when f is fixed at 0.5, that is, in the absence of molecular rearrangement, the area per molecule at the outer interface, a_o, would have increased rapidly with increasing $\bar{c}$ (see solid line), thus incurring a high interfacial free-energy penalty for the formation of the vesicle. In contrast, when f is allowed to vary, a_o remains quite constant throughout the entire size range (see dash-dotted line), thus minimizing the interfacial free-energy penalty. *Consequently, for a small-radius vesicle ($\bar{c} > 0.025$), the process of vesiculation will proceed in such a way that more molecules are placed in the outer leaflet, as depicted in Figure 4-3, so that the interfacial free-energy penalty can be alleviated in the minimization of g_{ves} at given n and F.* Interestingly, when f is fixed at 0.5, the area per molecule at the inner interface, a_i, remains rather constant at approximately 35 Å^2 for $F = 0.5$ (see dashed line in Figure 4-4), indicating that g_{ves} is more sensitive to the variations in a_i in this case.

The predicted variations of g_σ, g_{steric}, g_{pack}, and g_{elec} as a function of $\bar{c}$ for $F = 0.5$ are depicted in Figure 4-5. Note that g_{steric} actually decreases with increasing curvature. This behavior is due to a combination of two effects: (i) the correction for the location of the steric-repulsion surfaces, as described in Eqs. (2.25) and (2.26), and (ii) the enhanced contribution to g_{steric} from the outer interface, as described in Eq. (2.24). As discussed in section 2.2, when the vesicle size becomes very small (that is, at large $\bar{c}$ values), the curvature correction for steric repulsions becomes more important. Indeed, when R_o is small, a_o' can be much larger than a_o (see Eq. (2.25)), which, in effect, *reduces* the steric free energy at the outer interface. Although there is a corresponding *increase* in the steric free energy at the inner interface due to a reduction in a_i', as indicated by Eq. (2.26), this increase is less significant than the

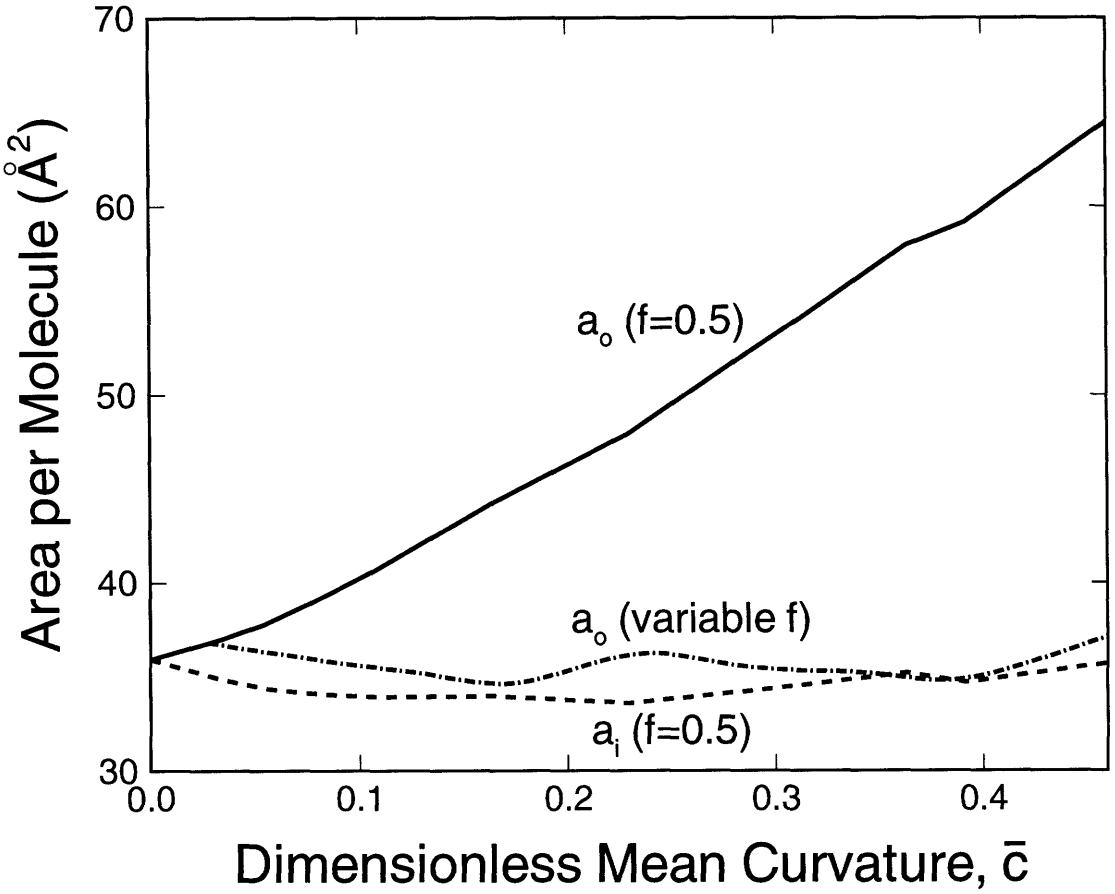

Figure 4-4: Predicted variations of the outer, a_o, and inner, a_i, areas per molecule as a function of the dimensionless mean curvature, $\bar{c}$. Solid line: a_o for $f = 0.5$, dashed line: a_i for $f = 0.5$, and dash-dotted line: a_o for varying f. The vesicle composition, F, is fixed at 0.5.

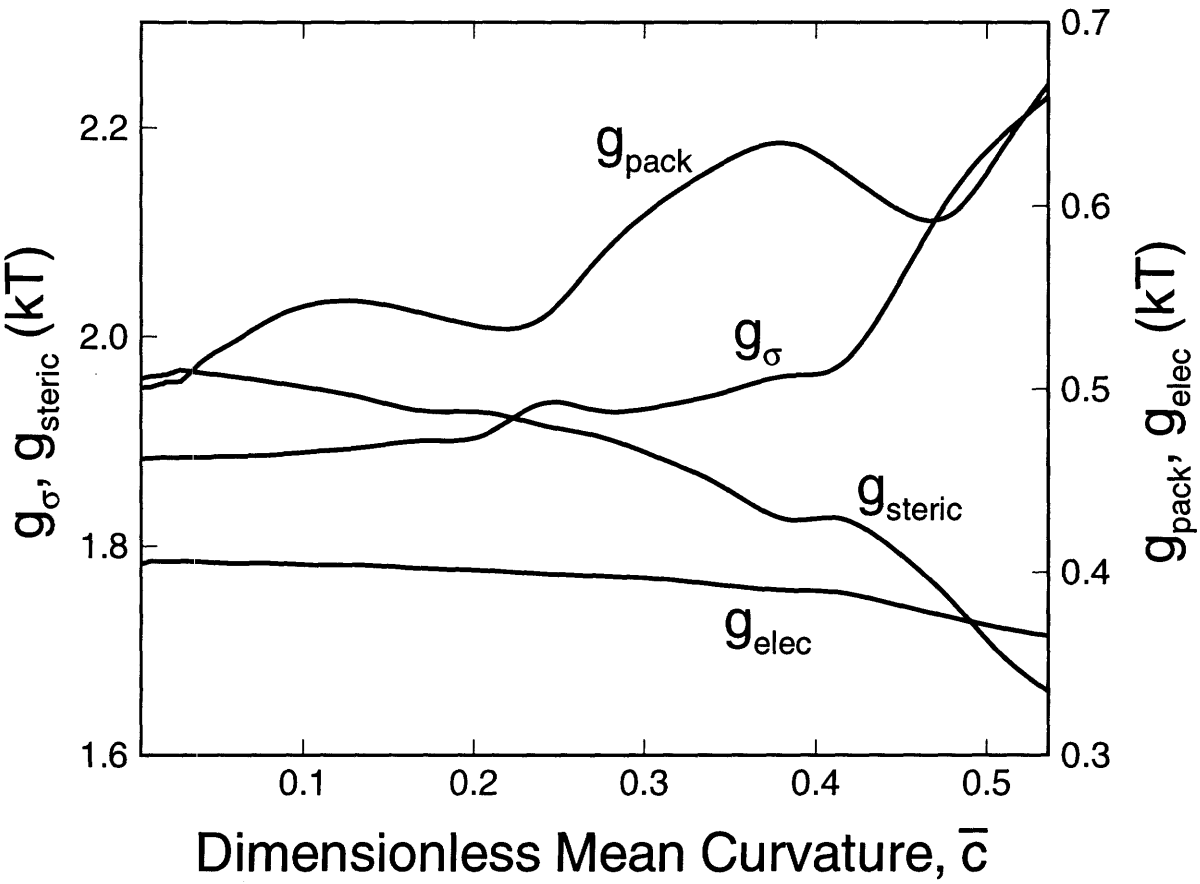

Figure 4-5: Predicted variation of the free-energy contributions, g_σ, g_{steric}, g_{pack}, and g_{elec}, as a function of the dimensionless mean curvature, $\bar{c}$. The vesicle composition, F, is fixed at 0.5.

reduction in the steric free energy at the outer interface since f also increases (and $(1-f)$ decreases) at small radii (see Eq. (2.24)). Note that the electrostatic free energy remains quite constant throughout the range of curvatures considered. This is because the compositions of the outer and inner vesicle leaflets are related through Eq. (F.4) in Appendix F, and, for a given value of F, any electrostatic effect associated with a deviation of X_{oA} from F will be more or less compensated by that associated with a similar but opposite deviation of X_{iA} from F. Consequently, the compositions in the outer and inner leaflets remain rather constant, resulting in a small variation of g_{elec} (see Figure 4-5).

A very interesting feature in Figure 4-5 is the occurrence of two local minima in g_{pack} at finite radii (or $\bar{c}$), which seems to indicate that there exist some preferred curvatures at which the packing of the surfactant tails is more favorable, at least locally. The key point to note here is that the increase in curvature is associated with a steady increase in f, as shown in Figure 4-3. In other words, as the curvature increases, more molecules are placed in the outer leaflet during the formation of the vesicles. In particular, as shown in Figure 4-3, at the two curvatures where the local minima in g_{pack} appear ($\bar{c} \approx 0.25$ and 0.45), the values of f are rather constant at about 0.6 and 0.7, respectively. Since there is simply more molecules in the outer leaflet than in the inner leaflet, the surfactant molecules would prefer to pack at a particular curvature that best accommodates this molecular arrangement. At $f \approx 0.6$, for example, this particular curvature is found at $\bar{c} \approx 0.25$ (see Figure 4-5). The shape of $g_{ves} - g_{bilayer}$, as shown in Figure 4-3, follows closely that of g_{pack}. Note that the locations of the two local minima in $g_{ves} - g_{bilayer}$, particularly at $\bar{c} \approx 0.4$, are not identical to those of g_{pack}. This is mainly due to the presence of other free-energy contributions in g_{ves}. More specifically, at $\bar{c} < 0.4$, the variations of g_{steric} and g_{σ} tend to cancel each other, and g_{pack} is quite dominant in determining the shape of $g_{ves} - g_{bilayer}$. As $\bar{c}$ increases beyond 0.4, however, the variations of g_{steric} and g_{σ} begin to play a role, thus shifting the minimum in $g_{ves} - g_{bilayer}$ in this size range to a lower value of $\bar{c}$ as compared to that corresponding to g_{pack}.

Although local minima in g_{ves} are found at finite radii (or $\bar{c}$), they are still higher

than that corresponding to a planar bilayer, as reflected by the positive values of $g_{ves} - g_{bilayer}$ over the entire vesicle size range (see Figure 4-3). The global minimum is located at $\bar{c} \rightarrow 0$, or as the vesicle approaches a planar bilayer. This indicates that, with CTAB and SOS, the most favorable configuration at $F = 0.5$ is not a finite-radius vesicle, but instead, an infinite planar bilayer. A similar behavior is found at other values of F. As will be seen later, large CTAB/SOS vesicles having configurations similar to that of a planar bilayer, as discussed above, *are stabilized by the entropy of mixing*, that is, by the mixing of vesicles and monomers in solution.

As exemplified by the preceding analysis, the free energy of vesiculation, g_{ves}, indeed arises from complex interactions among all the free-energy contributions involved in the self-assembling process. Accordingly, the minimization of g_{ves} at a given n and F represents a subtle balance between contributions associated with packing of the hydrophobic tails, formation of the the outer and inner interfaces, and steric and electrostatic interactions between the surfactant heads, all mediated through a delicate manipulation of the vesicle configuration. The different responses of the free-energy contributions to the three minimization variables, X_{oA}, f, and t_b, as discussed in section 2.3, highlights the importance of the molecular nature of self-assembling structures, even as large as vesicles. The key message here is that the internal degrees of freedom in a vesicle, namely the distribution of molecules between the outer and inner leaflets, the outer and inner leaflet compositions, the thickness of the bilayer, etc., play an extremely important role in the process of vesiculation, and one needs to account carefully for these features in order to decipher this complex and intricate process.

4.3 Size and Composition Distribution

The predicted size and composition distribution for a CTAB/SOS system containing 2 wt% surfactant, a CTAB/SOS ratio of 3/7 by weight, and no added salt is depicted in Figure 4-6 . Note that the distribution with respect to the composition, F, is very narrow, indicating that the majority of the vesicles contains the same proportion of

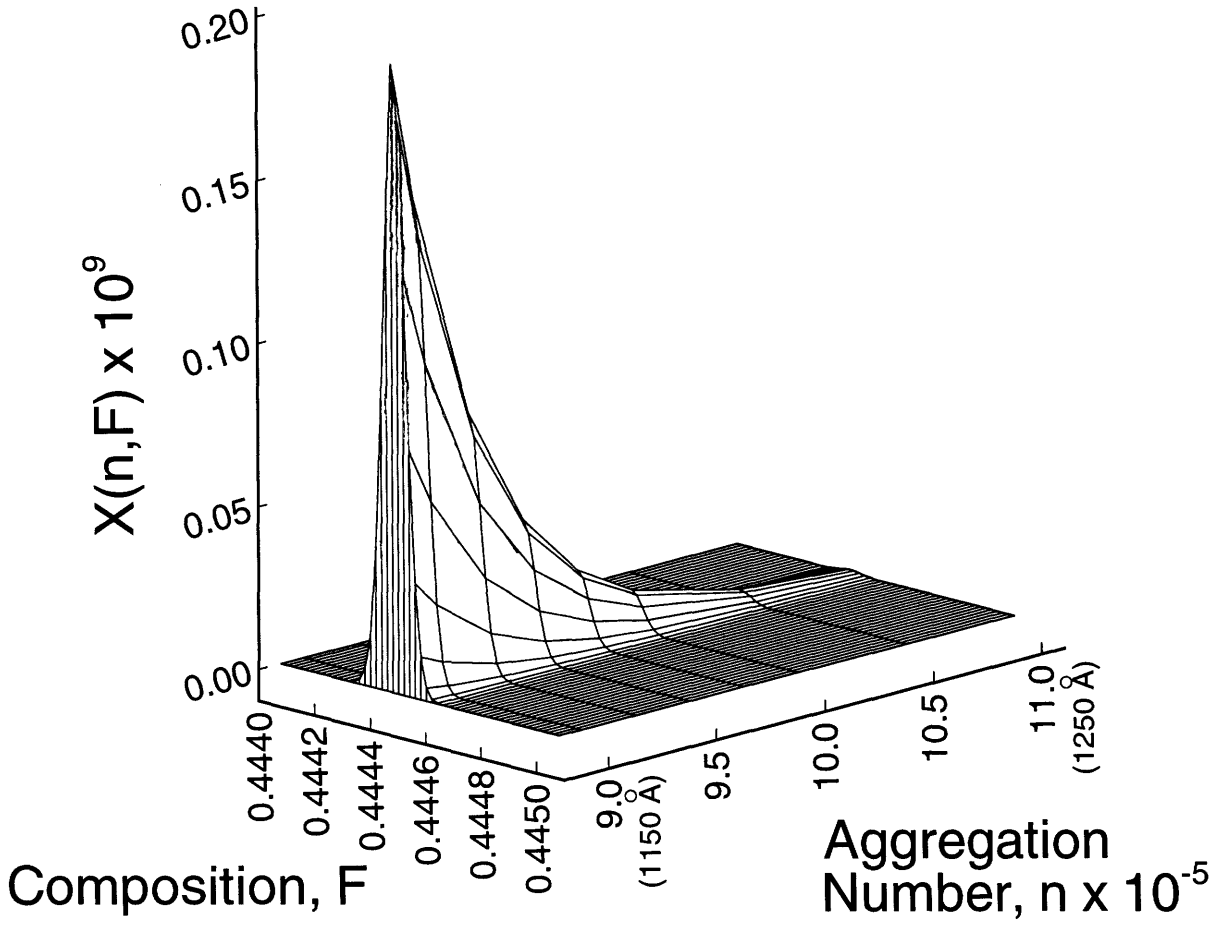

Figure 4-6: Predicted size and composition distribution, $X(n, F)$, for a CTAB/SOS aqueous system containing 2 wt% surfactant and a CTAB/SOS ratio of 3/7 by weight.

the two components. The distribution with respect to the aggregation number, n, however, shows a very different behavior. The value of $X(n, F^*)$, where $F^* = 0.44$ is the vesicle composition corresponding to the peak in the distribution in F, rises sharply at $n \approx 900000$, and then decays slowly towards large n. This size distribution can be understood mathematically by considering Eq. (2.2) and Figure 4-3. In a system containing CTAB and SOS at the conditions examined, the planar bilayer always has the lowest standard-state free energy. Small vesicles (large $\bar{c}$ in Figure 4-3) are associated with high g_{ves} (less negative) values, which makes the energetic (Boltzmann) factor in Eq. (2.2) small compared to the entropic factor, resulting in a negligible $X(n, F)$. As g_{ves} begins to level off towards a planar bilayer (shown more clearly in Figure 4-1 as $n \rightarrow \infty$), however, the energetic term becomes essentially constant. Consequently, the size distribution, $X(n, F)$, decays as C^n, where C is a constant equal to $X_{1A}^{F} X_{1B}^{(1-F)} \exp(-g_{ves}/kT)$. From a physical point of view, the existence of vesicles of large, yet finite, radii is due entirely to the entropy of mixing, G_m. In other words, although the planar bilayer has the lowest standard-state free energy, the existence of a single planar bilayer containing all the surfactant molecules in the system is entropically unfavorable. Since the free energy of vesiculation at large radii approaches that of a planar bilayer, it will be entropically more favorable to have many finite-sized vesicles. Note that the shape of the size distribution predicted by our theory for a CTAB/SOS mixture is quite similar to that predicted by Morse and Milner [119]. However, in their formulation, an arbitrary size cut-off is required to eliminate small vesicles, mainly due to the fact that the curvature-elasticity approach is not valid in the small vesicle size range.

Other predicted vesicle properties, including vesicle radius, bilayer thickness, and outer and inner surface potentials and areas per molecule, are shown in Table 4.2. In general, these predicted values compare quite favorably with the available experimental data. The measured average vesicle radius, using quasi-elastic light scattering, is approximately 1300 Å, and the zeta potential deduced from electrophoretic mobility measurements is about -58 mV [19]. However, since the zeta potential is measured at a position away from the vesicle surface, it is less negative than the actual sur-

Table 4.2: Predicted values of some average vesicle properties in the CTAB/SOS aqueous system (2 wt% surfactant, CTAB/SOS = 3/7 by weight). The average properties were evaluated for vesicles having a number-average aggregation number, $< n >_N = 930000$, and peak composition, $F^* = 0.44$.

Average Vesicle Properties	Predicted Values
Outer radius † (Å)	1200
Bilayer thickness ‡ (Å)	23
Outer (inner) surface potential * (mV)	-72 (-74)
Outer (inner) area per molecule (Å^2)	36 (35)

† Experimental value is approximately 1300 Å[19].

‡ Includes the head regions at the outer and inner interfaces.

∗ Zeta potential based on electrophoretic mobility measurement is -58 mV [19].

face potential due to ion screening, and the predicted value of -72 mV is certainly very reasonable. As stated in section 2.1, the precise predicted size and composition distribution depends on, among other assumptions, the model for the entropy of mixing, G_m. The distribution curve presented in Figure 4-6 is based on ideal mixing, and, as such, it is not meant to match any particular experimental size distribution, which in itself is a difficult property to measure. Nevertheless, Figure 4-6 does display the salient features of an entropically-stabilized vesicular system, particularly with respect to the sharp rise that is followed by a slow decay. More importantly, Figure 4-6 should be viewed as an example to illustrate how this detailed molecular model of vesicle formation can be used in conjunction with a selected entropy model to quantitatively predict vesicle properties.

4.4 Effect of Added Salt

As mentioned above, the composition, F, in a cationic/anionic vesicle is partly controlled by the electrostatic free energy, which, in turn depends on the ionic strength of the solution. Indeed, experimental observations have shown variations in vesicle size and surface potential with concentration of added salt, and the addition of about 1.4 wt% sodium bromide, corresponding to about 0.14 M, to a mixture containing 2 wt% surfactant and a CTAB/SOS ratio of 3/7 by weight induces a phase transition from vesicles to mixed micelles [19]. It is therefore of interest to test whether the molecular-thermodynamic theory presented here can capture this behavior.

Figure 4-7 depicts the predicted variations in the outer surface potential and outer surface charge density of vesicles in a system containing 2 wt% surfactant and a CTAB/SOS ratio of 3/7 by weight. The added salt (NaBr) concentration spans a range from 0 (no added salt) to 0.14 M, which is the experimentally-determined phase limit for vesicles at this composition. As shown in Figure 4-7, over this range of salt concentration, the outer surface potential changes from -74 mV to -63 mV, while the outer surface charge density changes from -0.05 to about -0.08 C/m^2, that is, the vesicle is enriched in SOS. The variation of the predicted surface potential

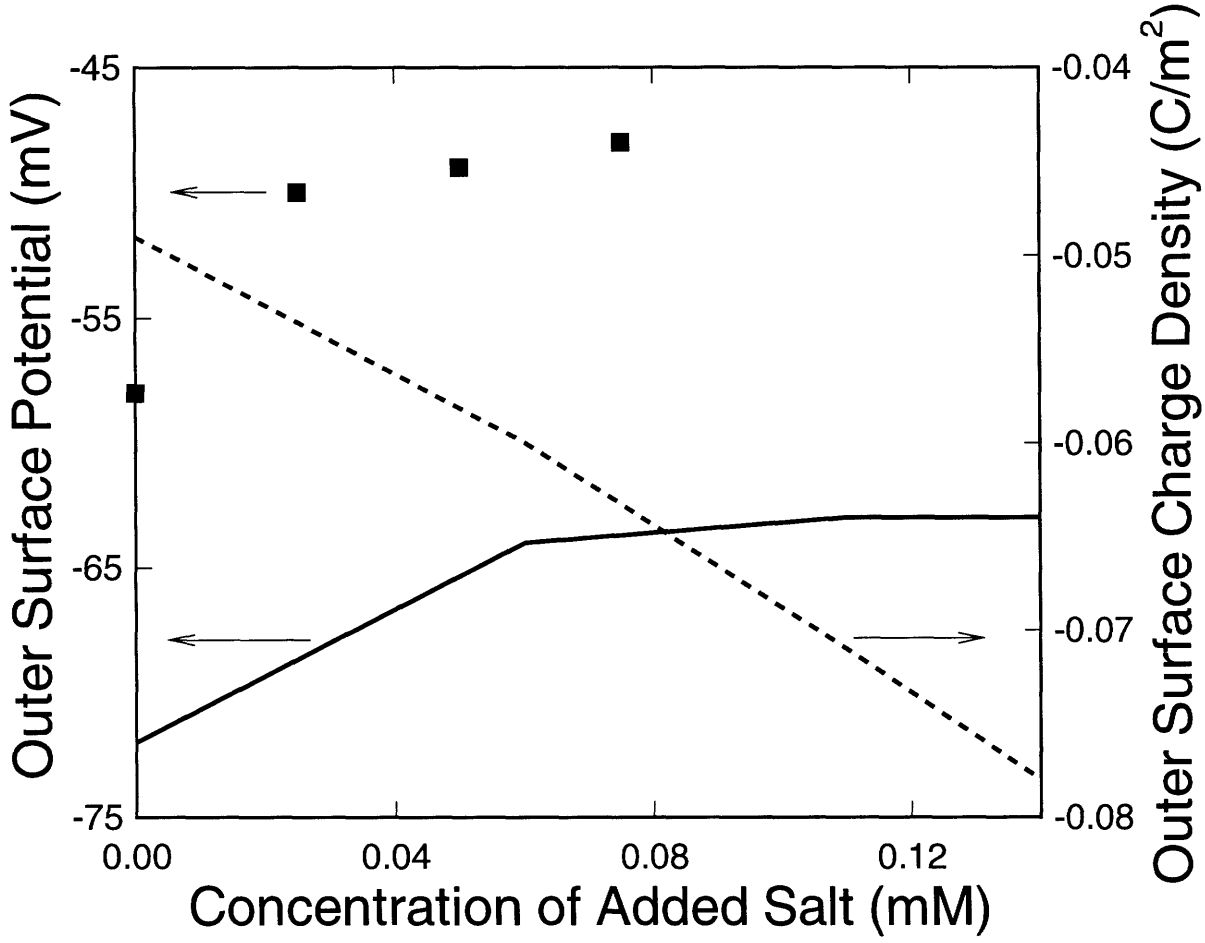

Figure 4-7: Predicted effect of concentration of added salt on the outer surface potential (solid line) and on the outer surface charge density (dashed line) of vesicles in the CTAB/SOS aqueous system. The system contains 2 wt% surfactant and a CTAB/SOS ratio of 3/7 by weight. Zeta potentials deduced from electrophoretic-mobility measurements (filled squares) are also shown for comparison [19].

as a function of added salt concentration closely follows that of the measured zeta potential, shown as filled squares in Figure 4-7 for comparison. As stressed earlier, however, the magnitude of the zeta potential is lower than that of the actual surface potential due to ion screening in solution. The predicted variation in surface charge density is mainly due to an enrichment in SOS (anionic surfactant) in the vesicles, as reflected by the decreasing value of the peak composition, F^*, shown in Figure 4-8. As the concentration of added salt increases from 0 to 0.14 M, the theory predicts a reduction in vesicle radius, which agrees nicely with experimental observations [19] (see filled circles in Figure 4-8). Concomitantly, the peak composition, F^*, decreases from 0.44 to 0.41 with increasing concentration of added salt. This behavior can, indeed, be understood quite easily from a physical standpoint. As stated in section 2.1, the size and composition distribution is determined by an energetic factor, which depends on the free energy of vesiculation, g_{ves}, and an entropic factor, which depends on the monomeric surfactant concentrations. Recall that the composition, F, of an isolated vesicle is more or less controlled by two factors: the electrostatic free energy and the transfer free energy. At low ionic strengths, the electrostatic free energy is so strong that deviations from a nearly equimolar cationic/anionic surfactant mixture in the vesicle would result in a large free-energy penalty. In this case, therefore, the energetic factor in the distribution would dominate, and the vesicle composition would remain close to that of an equimolar mixture. As the ionic strength increases, however, the importance of the electrostatic free energy diminishes. The dominance in the distribution then begins to shift from the energetic part to the entropic part, that is, how easy it is to localize a certain number of molecules in the formation of the vesicles. The entropic penalty in localizing the surfactant molecules in the process of vesiculation is, again, related to the monomeric concentrations; that is, if one component exists in a smaller amount in the bulk, it would be less probable to find it in the vesicle. Consequently, at high ionic strength, the composition of the vesicle would reflect the difference in monomeric surfactant concentrations. In this example, CTAB and SOS are mixed at a bulk ratio of 3/7, which means that the concentration of CTAB in the solution is lower than that of SOS. Accordingly, as the the ionic

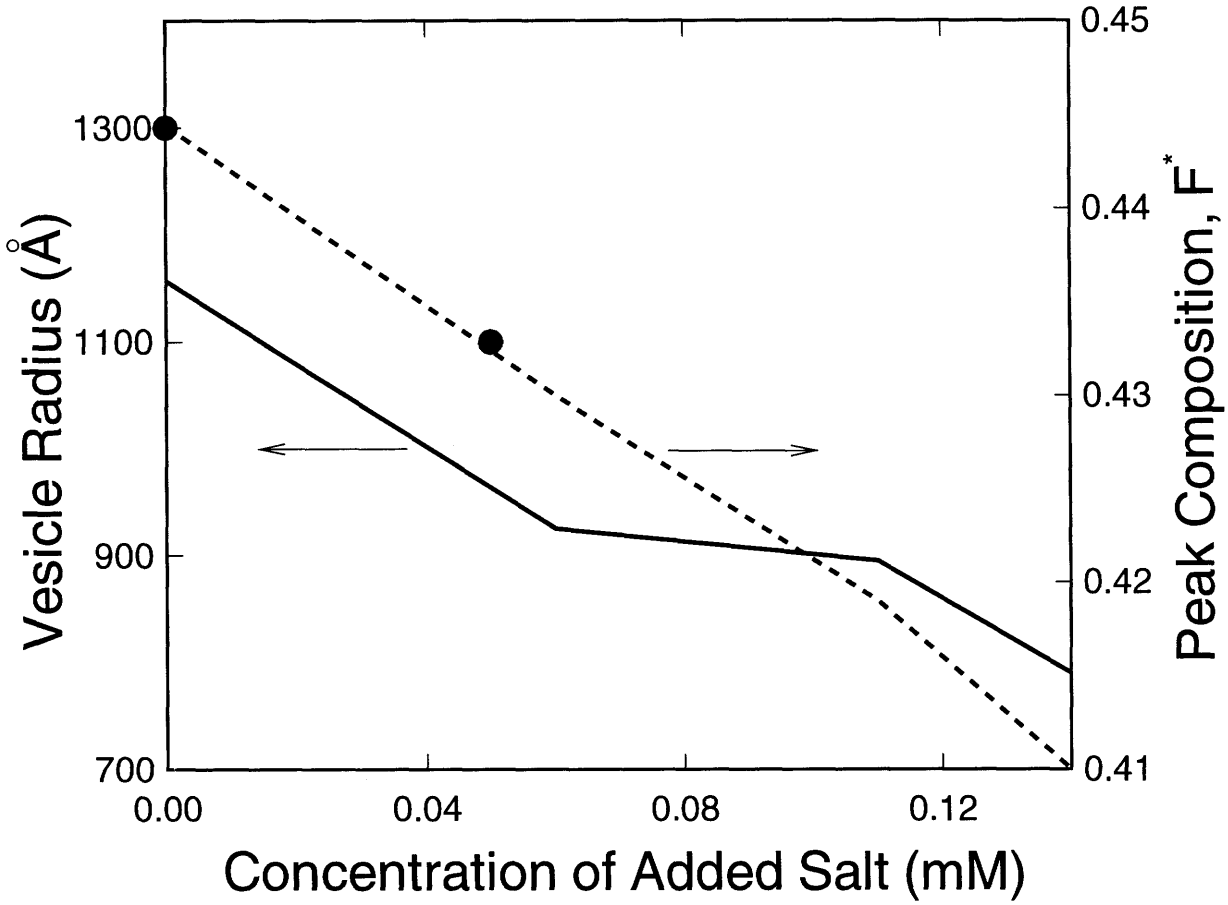

Figure 4-8: Predicted effect of concentration of added salt on vesicle radius (solid line) and on peak composition in vesicles, F^* (dashed line). The solution conditions are the same as those in Figure 4-7. Experimental values of the vesicle radius (filled circles) measured by quasi-elastic light scattering are also shown for comparison [19].

strength in the solution increases, the vesicles will be enriched in SOS, resulting in a decrease in F^*.

4.5 Concluding Remarks

This chapter has demonstrated the ability of the molecular-thermodynamic theory developed in chapter 2 to reveal the underlying mechanism, including the relative importance of the various intra-vesicular free-energy contributions, and their interplay, associated with the formation of mixed surfactant vesicles. The theory reveals that: (i) the distribution of surfactant molecules between the two vesicle leaflets plays an essential role in minimizing the vesiculation free energy of a finite-sized vesicle, and (ii) the composition of a mixed vesicle is mainly determined by three factors: the transfer free energy of the surfactant tails, the electrostatic interactions between the charged surfactant heads, and the entropic penalty associated with the localization of the surfactant molecules upon aggregation. In addition, in the context of this theory, one can predict, using only the molecular structure of the surfactants involved and the solution conditions, vesicle properties, including vesicle size and size distribution, vesicle composition, surface potentials, and surface charge densities. The theory also permits us to investigate the effect of added salt in a cationic/anionic surfactant mixture, and the results agree very well with the experimental observations. It is perhaps correct to argue that this kind of modeling detail is not necessary in the particular example considered here, since the structures of small vesicles do not come into play in the final size distribution after all. However, as shown in the following chapter, where the theory is used to study the effect of surfactant tail-length asymmetry on vesicle formation, the ability of the present theoretical approach to encompass a full range of aggregate sizes becomes very important . Moreover, this theoretical approach can be applied to both vesicles and mixed micelles, thus providing a unified approach for the prediction of the phase behavior of self-assembling systems where both types of microstructures can form and coexist.

Chapter 5

Application of the Theory: II. Effect of Surfactant Tail-Length Asymmetry on the Formation of Mixed Surfactant Vesicles

As mentioned in chapter 1, the spontaneous formation of vesicles in cationic/anionic surfactant mixtures is in sharp contrast with the formation of the traditional phospholipid vesicles. Indeed, spontaneously-forming vesicles require no input of energy for their formation, and are believed to be thermodynamically stable, while phospholipid vesicles form only upon input of some form of energy, for example, sonication, and tend to aggregate and fuse within days. This contrasting behavior has sparked significant interest, and led to several theoretical studies of mixed surfactant vesicles [30, 81, 82]. In an attempt to provide a theoretical basis for the spontaneous formation of vesicles in surfactant mixtures, Safran and co-workers [146, 147, 148] suggested that mixed vesicles can form as a result of the energetic advantage of finite-sized vesicles over a planar bilayer, a mechanism referred to as "energetic stabilization". In partic-

ular, specific interactions between the hydrophilic heads of the surfactant molecules in a mixture of cationic and anionic surfactants may lead to a difference in composition between the outer and inner vesicle leaflets. This composition difference can, in turn, alter the spontaneous curvature of the vesicle bilayer, causing a finite-sized vesicle to have a lower free energy than that corresponding to a planar bilayer. As shown in chapter 4, CTAB/SOS vesicles are *stabilized entropically.* In other words, CTAB/SOS vesicles are not energetically preferred, but rather, their formation is due to the entropic advantage associated with a multiplicity of finite-sized vesicles over that corresponding to one large planar bilayer. More importantly, it was found, in chapter 4, that surfactant-tail packing in the vesicle bilayer plays an important role in determining the behavior of the free energy of vesiculation. This indicates that, in addition to specific interactions between the surfactant heads, other mechanisms, such as, surfactant-tail packing, may also be responsible for the spontaneous formation of vesicles in surfactant mixtures. In this chapter, the molecular-thermodynamic theory developed in chapter 2 is applied to study the formation of vesicles in mixtures containing CTAB and sodium alkyl sulfates of various tail lengths [179]. In particular, we are interested in understanding how the asymmetry between the hydrophobic tails of the cationic and anionic surfactants affects the formation and stability of mixed vesicles in these complex fluids, as well as the roles of the various free-energy contributions to g_{ves} in determining the size and size distribution of these vesicles.

5.1 Model Systems and Molecular Parameters

The theory is applied to four aqueous cationic/anionic surfactant mixtures at 25 °C with no added salt. The cationic surfactant (component A) in all the four mixtures is cetyltrimethylammonium bromide (CTAB). The anionic surfactants (component B) are sodium pentadecyl sulfate (SPDS), sodium octyl sulfate (SOS), and sodium pentyl sulfate (SPS). Specifically, CTAB has 16 carbon atoms in its hydrophobic tail, while SPDS, SOS, and SPS have 15, 8, and 5 carbon atoms in their hydrophobic tails, respectively. In this theory, however, the first carbon atom of the tail is allowed to

come into contact with water [138], thus making the number of carbon atoms in the vesicle hydrophobic region one less than the total number of carbon atoms in the tail. Note that the CTAB/SOS mixture has already been studied quite thoroughly as an illustration for this theory in chapter 4. In order to highlight the asymmetry in surfactant tail length in the following discussion, CTAB, SPDS, SOS, and SPS are hereafter referred to as "C16", "C15", "C8", and "C5", respectively. The molecular properties of the various surfactants required as inputs in the theory are tabulated in Table 5.1. The values of the head area, $a_{h,k}$, the shielded area, a_k^*, and the charge distance, $d_{ch,k}$ ($k = A$ and B), were estimated using both the space-filling atomic model and computer-generated model, which yielded similar results. The corresponding planar hydrocarbon/water interfacial tensions are also included in Table 5.1.

5.2 Effect of Surfactant Tail-Length Asymmetry on Vesicle Composition

Using the molecular parameters of the surfactants and the solution conditions given above, one can calculate g_{ves} as a function of aggregation number, n, and composition, F, according to the molecular model described in section 2.2. Since the configuration of a mixed vesicle can be specified by five variables[1], at any given n and F, then, g_{ves} is obtained by minimization with respect to three configurational variables. Here, mainly for computational convenience, the following three variables are selected: the distribution of molecules, f, the outer leaflet composition, X_{oA}, and the thickness of the vesicle hydrophobic region, t_b. Figure 5-1 depicts the quantity, $g_{ves} - g_{ves}^{min}$, as a function of vesicle composition, F, for a large isolated vesicle ($n = 10^7$), which approximates a planar bilayer. Note that g_{ves}^{min} is the minimum value of g_{ves} with respect to F, and its location, F_{min}, for each curve is indicated by an arrow in Figure 5-1. The fact that there is a minimum in g_{ves} with respect to F is mainly a

[1]Recall that the configuration of a two-component mixed vesicle can be specified by five variables: the fraction of molecules in the outer leaflet, f, the composition of the outer and inner leaflets, X_{oA} and X_{iA}, respectively, and the outer and inner radii, R_o and R_i, respectively.

Table 5.1: Molecular properties of cetyltrimethylammonium bromide (CTAB), sodium pentadecyl sulfate (SPDS), sodium octyl sulfate (SOS), and sodium pentyl sulfate (SPS).

Molecular Properties	CTAB	SPDS	SOS	SPS
Carbon number in bilayer, $n_{c,k}$	15	14	7	4
Valence, z_k	1	-1	-1	-1
Head area, $a_{h,k}$ (Å^2)	23	16	16	16
Shielded area, a_k^* (Å^2)	21	21	21	21
Charge distance, $d_{ch,k}$ (Å)	2.5	3.8	3.8	3.8
Planar hydrocarbon/water interfacial tension [101], σ_k (dyne/cm)	53	53	51	51

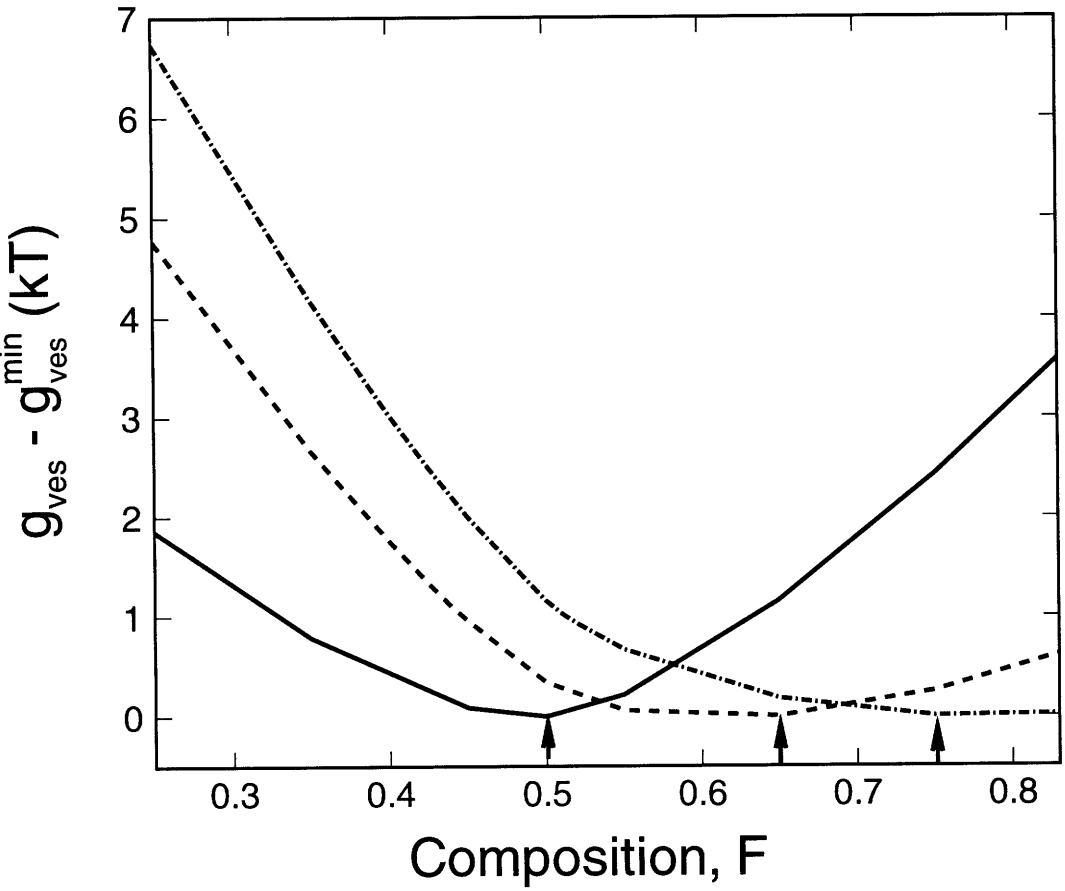

Figure 5-1: Predicted variation of $g_{ves} - g_{ves}^{min}$ as a function of vesicle composition, F, for a large vesicle ($n = 10^7$). Note that g_{ves}^{min} is the minimum free energy of vesiculation with respect to composition, F. The composition, F_{min}, corresponding to g_{ves}^{min} in each surfactant mixture is marked by an arrow. Solid line: C16/C15, dashed line C16/C8, dash-dotted line: C16/C5.

result of the competition between the electrostatic free energy, g_{elec}, and the transfer free energy, g_{tr} (see chapter 4). In brief, g_{elec} is a nearly parabolic function of F, since deviations from $F \approx 0.5$ would cause an increase in surface charge densities. On the other hand, g_{tr} decreases monotonically with increasing F, since increasing F implies that more of surfactant A (CTAB) is present in the vesicle, with CTAB having the longest hydrophobic tail (C16) among all the surfactants examined. As a result, $\Delta\mu_{tr,A}$ is more negative than $\Delta\mu_{tr,B}$. The combination of g_{elec} and g_{tr} therefore results in a minimum in g_{ves} as shown in Figure 5-1. Note that the values of F_{min} for the three surfactant mixtures are quite different. In a highly asymmetric mixture, such as C16/C5 (dash-dotted line), g_{tr} decreases rapidly with increasing F, thus pushing the value of F_{min} far to the right ($F_{min} = 0.75$). In the C16/C15 mixture (solid line), however, since the tail lengths of the two components are quite similar, the variation of g_{tr} with respect to F is less pronounced, and therefore F_{min} is approximately equal to 0.5.

Figure 5-2 depicts the vesicle size and composition distribution in a C16/C15 mixture containing 2 wt% surfactant and a C16/C15 ratio of 3/7 by weight. The distribution with respect to composition, F, is very sharp and narrow around an optimum value, $F^* \approx 0.288$, which is identical to the bulk composition in the solution[2]. On the other hand, as shown in Figure 5-3, F^* in the C16/C5 mixture containing 2 wt% surfactant and a C16/C5 ratio of 3/7 by weight is approximately 0.514, while that in the C16/C8 mixture of identical composition is about 0.44 (see chapter 4). The fact that the optimum composition of the vesicles in the suspension, F^*, does not correspond to F_{min} of an isolated vesicle, is mainly due to the interplay between the energetic and entropic factors in the size and composition distribution (see Eq. (2.2)). Specifically, the Boltzmann factor in Eq. (2.2), which contains the free energy of vesiculation, g_{ves}, reflects the energetics of forming a vesicle, while the pre-exponential factor, $X_{1A}^{nF} X_{1B}^{n(1-F)}$, accounts for the entropic penalty incurred in localizing nF surfactant A monomers and $n(1-F)$ surfactant B monomers upon vesiculation. Since the entropic factor is related to the monomer concentrations in

[2]Note that F is a molar composition, while the C16/C15 ratio of 3/7 in the bulk is by weight.

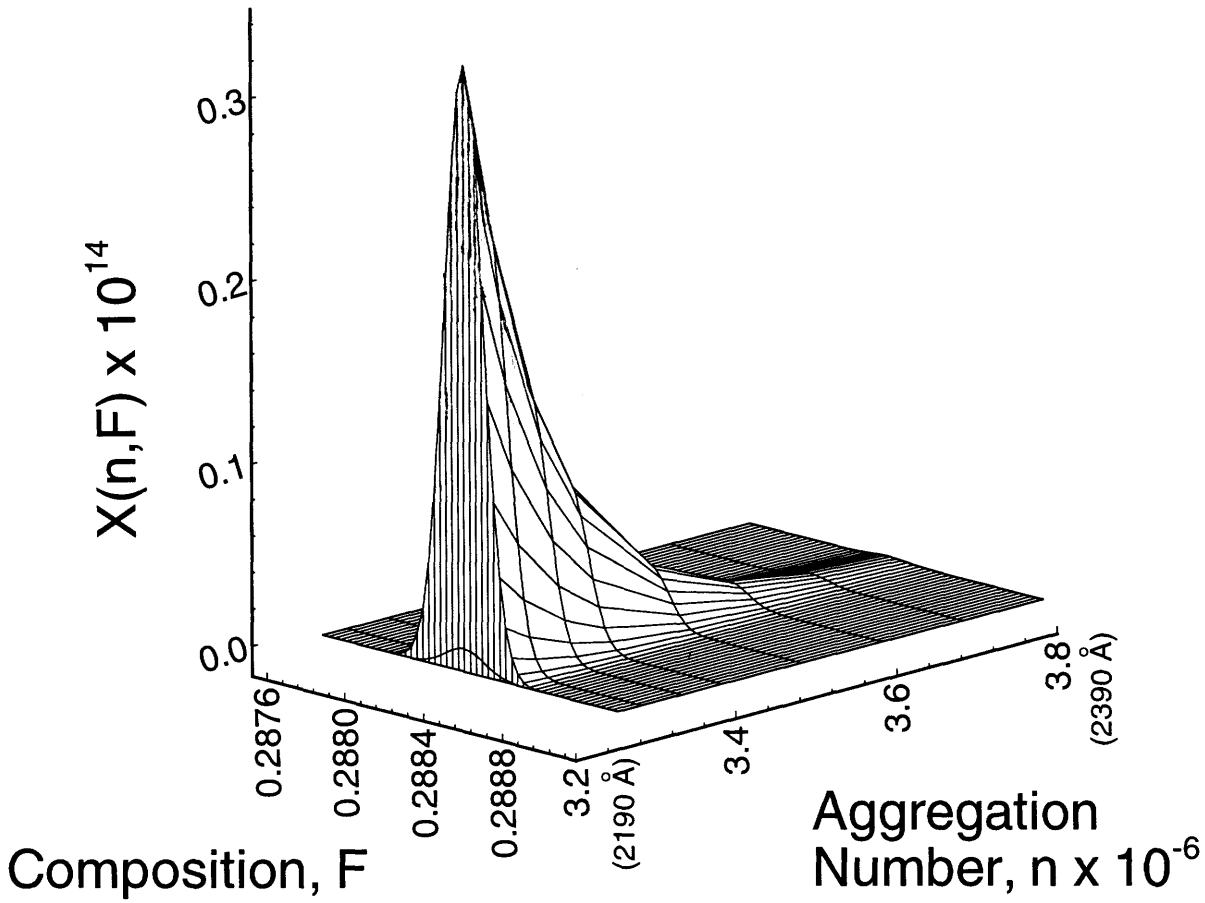

Figure 5-2: Predicted size and composition distribution, $X(n, F)$, for a C16/C15 aqueous system containing 2 wt% surfactant and a C16/C15 ratio of 3/7 by weight.

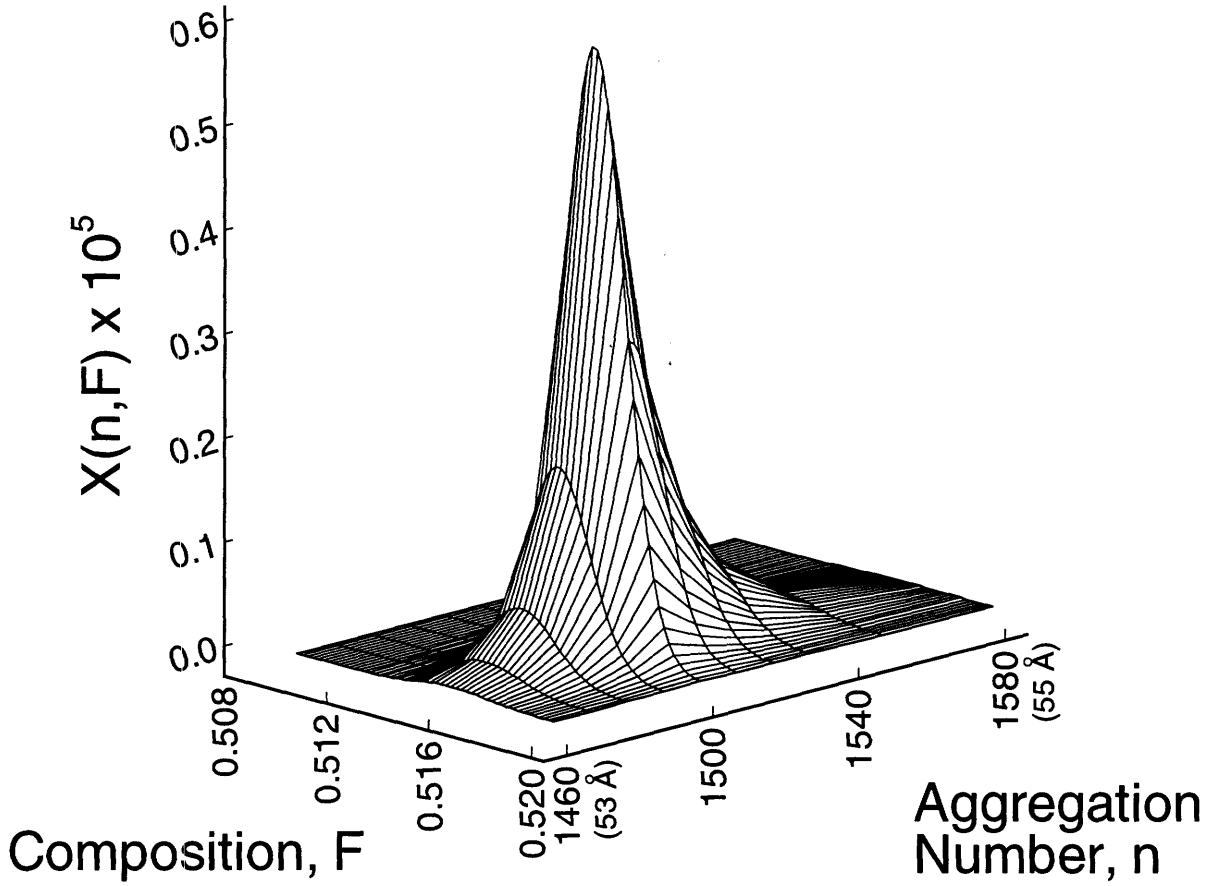

Figure 5-3: Predicted size and composition distribution, $X(n, F)$, for a C16/C5 aqueous system containing 2 wt% surfactant and a C16/C5 ratio of 3/7 by weight.

the bulk, the less concentrated component (C16 in this case) will have a lower probability of being found in a vesicle. In other words, the entropic factor will always drive the vesicle composition towards that of the bulk solution, which is usually different from the optimum composition of an isolated vesicle, F_{min}. Consequently, the system will seek a "compromise" for the vesicle composition, which depends on how g_{ves} varies with F. In the C16/C5 mixture having a C16/C5 ratio of 3/7 by weight, corresponding to a molar composition of 0.183, shifting the vesicle composition towards that of the bulk solution ($F = 0.183$) would cause an increase in both g_{elec} and g_{tr}, as discussed previously, resulting in a large increase in g_{ves}, as shown in Figure 5-1. In this case, therefore, a significant "energetic resistance" prevents F^* from decreasing from $F_{min} = 0.75$ to the bulk value. The situation in the C16/C15 mixture is rather different. As mentioned above, since the tail-length asymmetry between C16 and C15 is far less than that between C16 and C5, g_{tr} changes only slightly with F in the C16/C15 mixture. As shown in Figure 5-1, for $F < F_{min}$, g_{ves} increases much less rapidly with decreasing F in the C16/C15 mixture (solid line) than in the C16/C5 mixture (dash-dotted line). Consequently, F^* in the C16/C15 mixture can shift towards the composition of the bulk solution without incurring a high energetic penalty. Indeed, in the C16/C15 mixture having a C16/C15 weight ratio of 3/7, the entropic factor is so dominant that the vesicle composition is exactly equal to the bulk composition. The effect of decreasing surfactant tail-length asymmetry on the vesicle composition is therefore similar to that of increasing salt concentration in the vesicle suspension (see chapter 4). Specifically, with decreasing surfactant tail-length asymmetry, the energetic contribution to the composition distribution is decreased via a reduction in g_{tr}, whereas with added salt, this is effected through a reduction in g_{elec}.

5.3 Effect of Surfactant Tail-Length Asymmetry on Vesicle Size

Figure 5-4 shows the predicted difference between g_{ves} and the free energy of "vesiculation" of a planar bilayer, $g_{bilayer}$, for various cationic/anionic surfactant mixtures as a function of the dimensionless mean curvature, $\bar{c} = 2\ell_{max,A}/(R_o + R_i)$, where $\ell_{max,A}$ is the fully-extended length of the tail of component A (C16) ($\approx$ 20.5 Å), and R_o (R_i) is the outer (inner) vesicle radius, measured from the center of the vesicle to the outer (inner) hydrocarbon/water interface. Note that, for illustration purposes, the vesicle composition, F, is fixed at 0.5, with a similar behavior found at other compositions. Since the absolute values of g_{ves} are quite different for the various surfactant mixtures examined, mainly because of the difference in g_{tr}, the free-energy differences are plotted in Figure 5-4 so that these can be compared on the same scale. In addition, using curvature instead of aggregation number effectively stretches the abscissa, a feature that can reveal more details in the small vesicle size range. Note that $\bar{c} \to 0$ corresponds to the planar bilayer, and that as $\bar{c}$ increases, the vesicle size (or the aggregation number, n) becomes smaller. A common feature in all the three curves shown in Figure 5-4 is that two local minima appear at finite curvatures. The occurrence of these minima is mainly due to the packing of the surfactant tails in the vesicle hydrophobic region (see chapter 4). Specifically, as the vesicle curvature increases, the outer area per molecule, a_o, increases rapidly, resulting in a higher interfacial free-energy at the outer hydrocarbon/water interface (see chapter 4). In order to alleviate this free-energy penalty, the vesicle rearranges by placing more molecules in the outer vesicle leaflet, thus reducing a_o and, in turn, the outer interfacial free energy. However, since there are more molecules in the outer leaflet than in the inner leaflet, the molecules would prefer to pack at a particular curvature, depending on the distribution of molecules, that can best accommodate this configuration. The locations of the minima in $g_{ves} - g_{bilayer}$ thus reflect the local optimum curvatures with respect to the packing of the surfactant tails.

In the C16/C15 (solid line) and C16/C8 (dashed line) mixtures, $g_{ves} - g_{bilayer}$

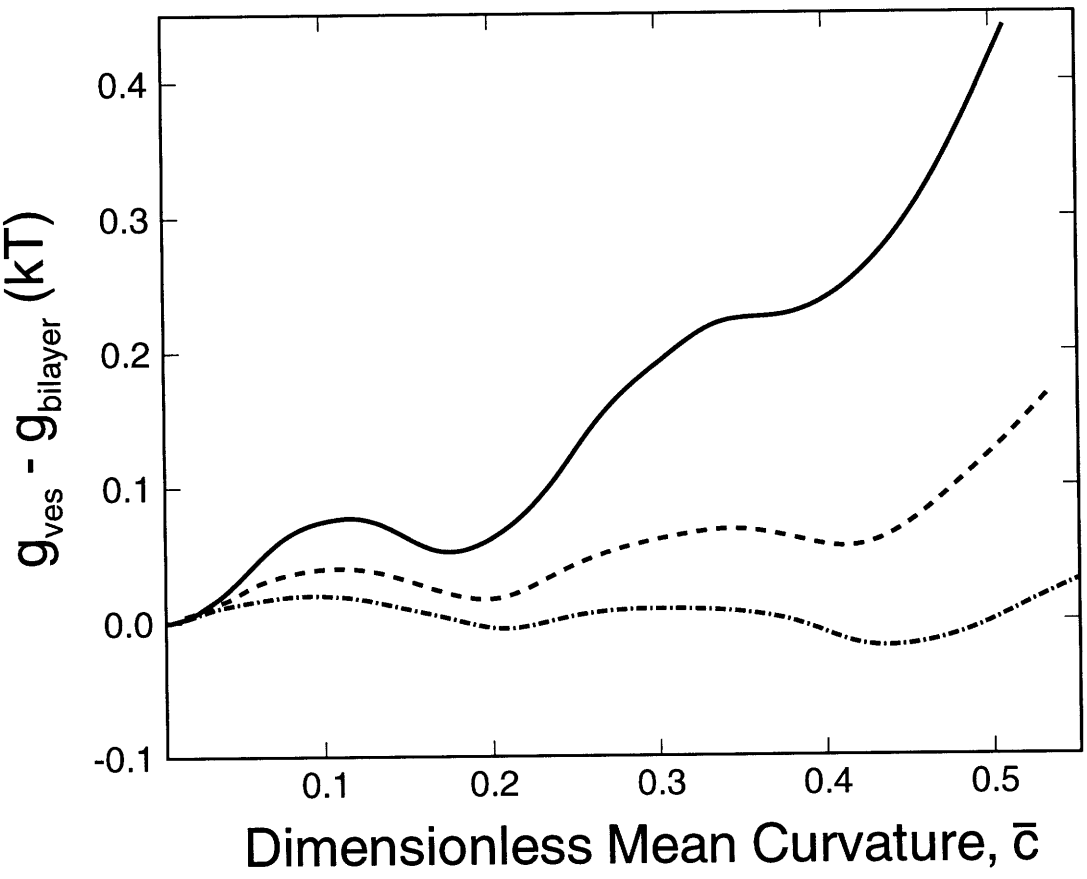

Figure 5-4: Predicted variation of the free-energy difference, $g_{ves} - g_{bilayer}$, as a function of the dimensionless mean curvature, $\bar{c} = 2\ell_{max,A}/(R_o + R_i)$, for various cationic/anionic surfactant mixtures. The vesicle composition, F, is fixed at 0.5. Solid line: C16/C15, dashed line: C16/C8, dash-dotted line: C16/C5.

remains positive throughout the entire range of curvatures, indicating that, in both cases, the global minimum corresponds to the planar bilayer ($\bar{c} = 0$). Any finite-sized vesicles that form in these two mixtures are therefore not due to any energetic advantage, but rather because of the large gain in the entropy of mixing, G_{mix}, as compared to a large planar bilayer. As shown in Figure 5-2, the distribution with respect to aggregation number, n, rises sharply at $n \approx 3.3 \times 10^6$, corresponding to $R_o \approx 2200$ Å, and then decays slowly towards large n or vesicle radii. The characteristics of this size distribution can, again, be attributed to the subtle balance between the entropic and energetic factors involved in the process of vesiculation (see chapter 4). In the case of C16/C15 and C16/C8 mixtures, when the vesicles are small (large $\bar{c}$ values), g_{ves} is much higher (less negative) than $g_{bilayer}$ (see Figure 5-4). Since both X_{1A} and X_{1B} are much smaller than unity, the entropic factor becomes dominant in this vesicle size range, thus making $X(n, F)$ negligibly small (see Eq. (2.2)). At $n \approx 3.3 \times 10^6$, or $R_o \approx 2200$ Å, in the C16/C15 mixture, g_{ves} levels off and approaches $g_{bilayer}$ (see Figure 5-4, where $g_{ves} - g_{bilayer}$ approaches zero as $\bar{c} \to 0$). In that limit, the value of $X(n, F)$ becomes finite, and as n increases (or $\bar{c}$ decreases) further, the distribution with respect to n, $X(n)$, decays as C^n, where $C = X_{1A}^F X_{1B}^{(1-F)} \exp(-g_{ves}/kT)$ is a constant.

As the asymmetry between the lengths of the surfactant tails increases, the values of $g_{ves} - g_{bilayer}$ at the local minima decrease. In the C16/C5 mixture (dash-dotted line in Figure 5-4), the values of both local minima in $g_{ves} - g_{bilayer}$ are negative, indicating that vesicles with those curvatures have a lower standard-state free energy than that corresponding to a planar bilayer. Consequently, any vesicles formed in the C16/C5 mixture will be *stabilized energetically.* As shown in Figure 5-3, the corresponding size distribution is nearly Gaussian and very narrow, and is centered at $n \approx 1500$ (or $R_o \approx 54$ Å). This R_o value corresponds to a dimensionless mean curvature, $\bar{c}$, of approximately 0.43, which is, indeed, the location of one of the minima in $g_{ves} - g_{bilayer}$ (see dash-dotted line in Figure 5-4). This size distribution is in sharp contrast with the size distribution associated with the C16/C15 mixture, where the peak vesicle size is about 2200 Å, and the size distribution is much wider (see Figure 5-

2). *Indeed, small vesicle sizes and a sharp size distribution are quite characteristic of energetically-stabilized vesicles, while entropically-stabilized vesicles are characterized by large vesicle sizes and a wide size distribution.* The fact that the size distribution in the C16/C5 mixture peaks at the smaller vesicles ($\bar{c} \approx 0.43$) instead of at the larger ones ($\bar{c} \approx 0.2$) is due to the more favorable entropy of mixing, G_{mix}, in the former case.

One very important point to bear in mind is that this theory does not predict that vesicles of such small size *will actually form spontaneously* in this system; rather, it predicts that: (i) *if vesicles form spontaneously* in this system, they will be small and narrowly distributed in their size, and (ii) surfactant tail-length asymmetry can be an important mechanism for stabilizing vesicles in a mixed surfactant system. Indeed, the fact that small vesicles are more stable than the planar bilayer does not necessarily imply that such vesicles will actually form in solution, since the surfactant components can form other microstructures such as mixed micelles. Consequently, in order to predict what microstructures will actually form in a given surfactant mixture at certain solution conditions, one needs to compare the free energies of formation of different microstructures, including vesicles, mixed micelles, and lamellae. Work along these lines is in progress.

Why then would an increase in surfactant tail-length asymmetry stabilize finite-sized vesicles? This phenomenon stems from a complex interplay between the free-energy contributions described in Eq. (2.4). As explained above, the formation of small vesicles, characterized by large curvatures, proceeds in such a way that more molecules are placed in the outer vesicle leaflet in order to reduce the interfacial free-energy penalty caused by a larger outer area per molecule. This, however, also implies that more molecules need to be packed in the outer leaflet. In a C16/C15 mixture, this presents a serious problem with respect to chain packing. Figure 5-5 depicts the methylene (CH_2) segment density distribution for a C16 tail in the hydrophobic region of a finite-sized vesicle having $\bar{c} = 0.37$ and $f = 0.7$ at a fixed composition, $F = 0.5$. This vesicle configuration corresponds to the location of the minimum in $g_{ves} - g_{bilayer}$ at the larger curvature (see solid line in Figure 5-4). Note that the distribution profile

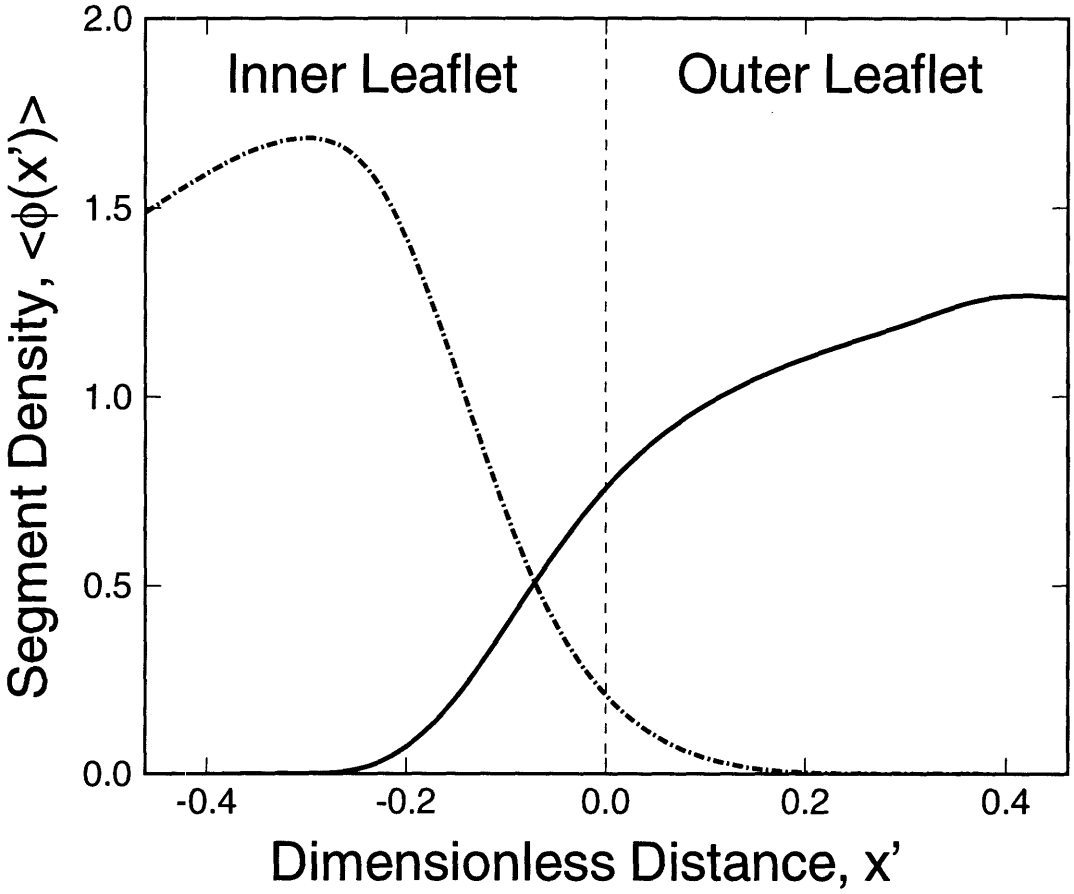

Figure 5-5: Predicted methylene segment density distributions, $\langle\phi(x')\rangle$, for a C16 tail in the vesicle hydrophobic region of a C16/C15 vesicle having $\bar{c} = 0.37$, $F = 0.5$, and $f = 0.7$. The dimensionless distance, x', is defined as $x' = x/t_b$, where x is the distance from the mid-plane of the vesicle bilayer and t_b is the thickness of the vesicle hydrophobic region. Solid line: methylene groups (CH_2) of the tail in the outer leaflet, dash-dotted line: methylene groups of the tail in the inner leaflet.

in the outer leaflet (see solid line in Figure 5-5) is quite flat compared to that in the inner leaflet (see dash-dotted line in Figure 5-5). In addition, as shown in Figure 5-6, the lateral pressure in the outer leaflet is, in general, higher than that in the inner leaflet (see solid line). Recall that the lateral pressure can be viewed as the pressure required to straighten the tails in the hydrophobic region in order to maintain uniform density. Figure 5-6 reveals that the surfactant tails in the outer leaflet are forced to take an extended configuration in order to satisfy the uniform-density constraint. The tails in the inner leaflet, on the other hand, display a higher degree of flexibility, which suggests that the surfactant tails in the inner vesicle leaflet are in a much more favorable packing environment than those in the outer leaflet. Consequently, in the minimization of g_{ves} in the C16/C15 mixture, the drive to reduce the interfacial free energy is countered by the difficulty in packing more chains in the outer leaflet, and the final g_{ves} of a finite-sized vesicle, therefore, represents a subtle balance between these two free-energy contributions. Figure 5-7 depicts the predicted variation of the interfacial (g_σ, dash-dotted line), packing (g_{pack}, solid line), and steric (g_{steric}, dashed line) free energies for a C16/C15 mixture ($F = 0.5$) as a function of $\bar{c}$. Note that g_{pack} attains its maximum value at $\bar{c} = 0.37$. As the curvature increases beyond 0.37, it is no longer beneficial to place more molecules in the outer leaflet for the purpose of relieving the interfacial free energy, since the packing free energy would have increased rapidly due to chain overcrowding. In this case, the vesicle curvature will increase at the expense of the interfacial free energy, with an associated decrease in g_{pack}. Despite the fact that more molecules are being placed in the outer leaflet as the curvature increases, the steric free energy per molecule, g_{steric}, actually decreases gradually. This decrease is caused by a combination of two effects: (i) the correction for the steric-repulsion surfaces, and (ii) a reduced contribution to g_{steric} from the inner leaflet. As shown in Eq. (2.24), g_{steric} depends on a_o' and a_i', which are calculated at the outer and inner steric-repulsion surfaces, respectively. Since a_o' increases with increasing curvature (see chapter 2), the steric free energy at the outer interface is reduced. Although a_i' decreases with increasing curvature, causing an increase in steric free energy at the inner interface, this increase is compensated by a reduction in $(1 - f)$,

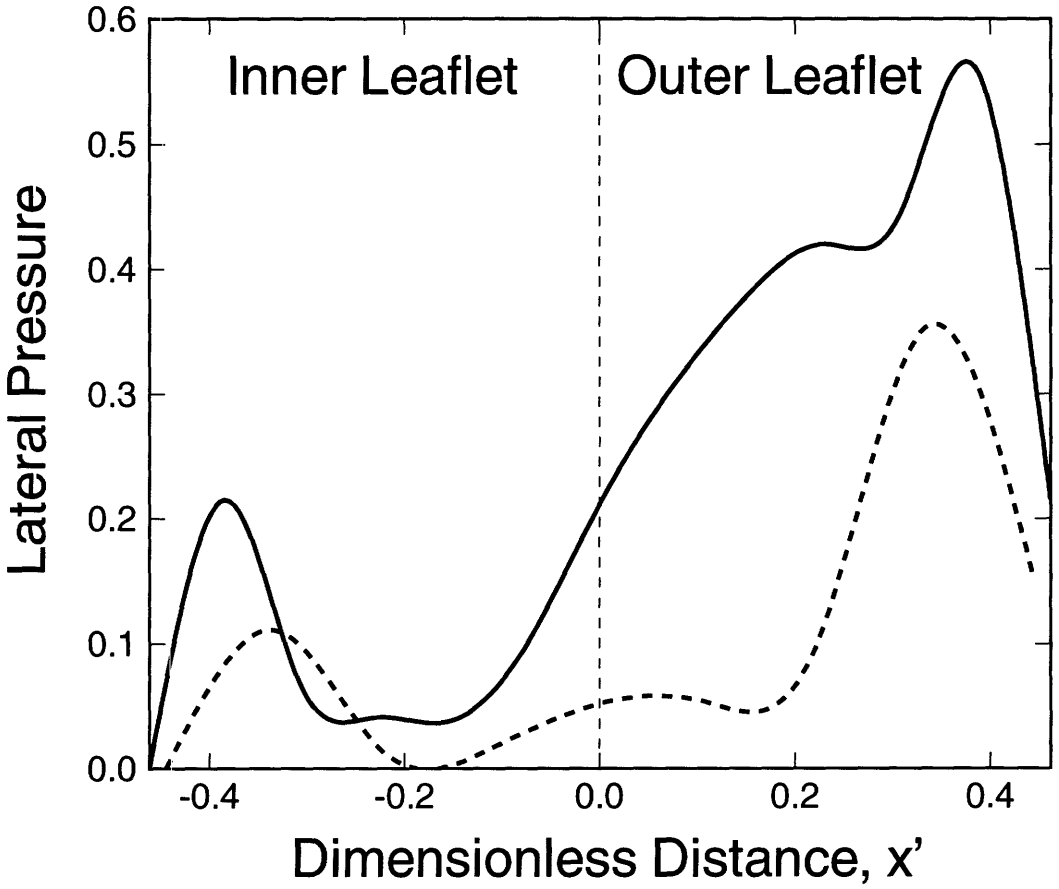

Figure 5-6: Predicted lateral pressure in the hydrophobic region of a C16/C15 vesicle having $\bar{c} = 0.37$, $F = 0.5$, and $f = 0.7$ (solid line), and a C16/C5 vesicle having $\bar{c} = 0.43$, $F = 0.5$, and $f = 0.7$ (dashed line).

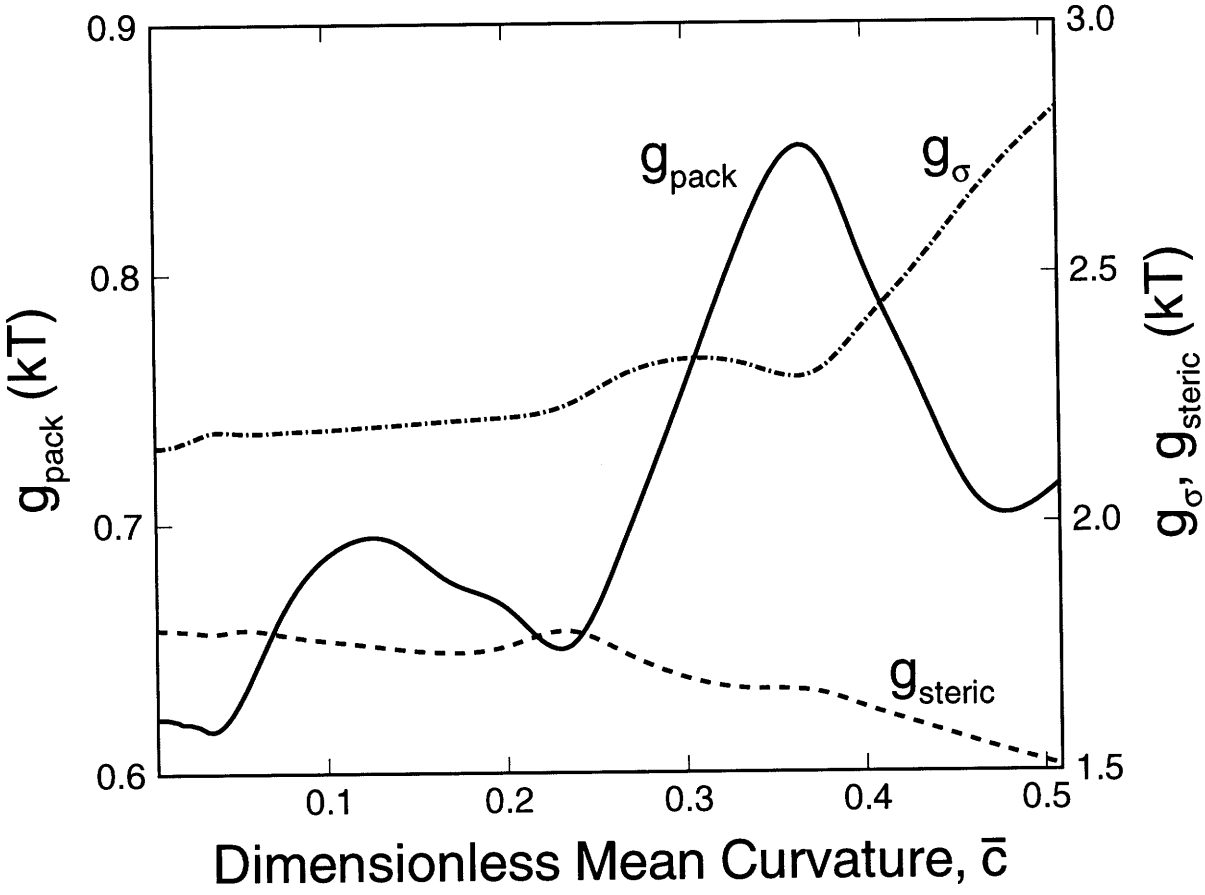

Figure 5-7: Predicted variation of the free-energy contributions, g_σ (dash-dotted line), g_{steric} (dashed line), and g_{pack} (solid line), for a C16/C15 mixture as a function of the dimensionless mean curvature, $\bar{c}$. The vesicle composition, F, is fixed at 0.5.

since, as stated above, f increases as the vesicles become smaller (or as the curvature increases) (see chapter 4). Although g_{steric} decreases with curvature, this decrease is not sufficient to compensate for the penalties in g_{σ} and g_{pack}, resulting in a high g_{ves} at this curvature. More specifically, at $\bar{c} = 0.37$, g_{σ} and g_{pack} are 0.23 kT and 0.1 kT, respectively, higher than the corresponding values for a planar bilayer, whereas g_{steric} is only 0.1 kT lower than that for the planar bilayer. The electrostatic free energy, g_{elec}, remains quite constant throughout the entire vesicle size range, and therefore is not shown in Figure 5-7. The reason for this behavior of g_{elec} is that the electrostatic free energy is largely affected by the compositions of the outer and inner leaflets, which, in turn, determine the outer and inner surface charge densities. However, the compositions of the two leaflets are related through the mass balance of component A in the vesicle (see chapter 4), that is, $F = fX_{oA} + (1 - f)X_{iA}$. Consequently, for a given overall vesicle composition, F, any increase in X_{oA} will be associated with a similar decrease in X_{iA}, and therefore, any electrostatic effect caused by a deviation of X_{oA} from F will be more or less compensated by a similar but opposite effect due to X_{iA}. As a result, g_{elec} does not vary significantly as a function of vesicle size.

The situation in a C16/C5 mixture is quite different. Figure 5-8 shows the methylene (CH_2) segment density distribution for a C16 tail in the vesicle hydrophobic region of a finite-sized vesicle having $\bar{c} = 0.43$ and $f = 0.7$ at a fixed composition, $F = 0.5$. Again, this configuration corresponds to the minimum in $g_{ves} - g_{bilayer}$ at the larger curvature for the C16/C5 mixture (see dash-dotted line in Figure 5-4). Note that, comparing Figure 5-8 and Figure 5-5, there is a marked difference in the distribution profiles in the outer leaflet between the two surfactant mixtures. In particular, the tails in the outer leaflet of a C16/C5 vesicle are not as stretched as those in a C16/C15 vesicle, and display a flexibility similar to that in the inner leaflet, in contrast to the situation in a C16/C15 vesicle. In addition, as shown in Figure 5-6, the lateral pressure throughout the C16/C5 vesicle bilayer is relatively low compared to that in the C16/C15 vesicle bilayer, indicating that the outer leaflet in a small C16/C5 vesicle provides a much more favorable environment for chain packing.

The packing environments of C16/C15 and C16/C5 vesicles can be compared more

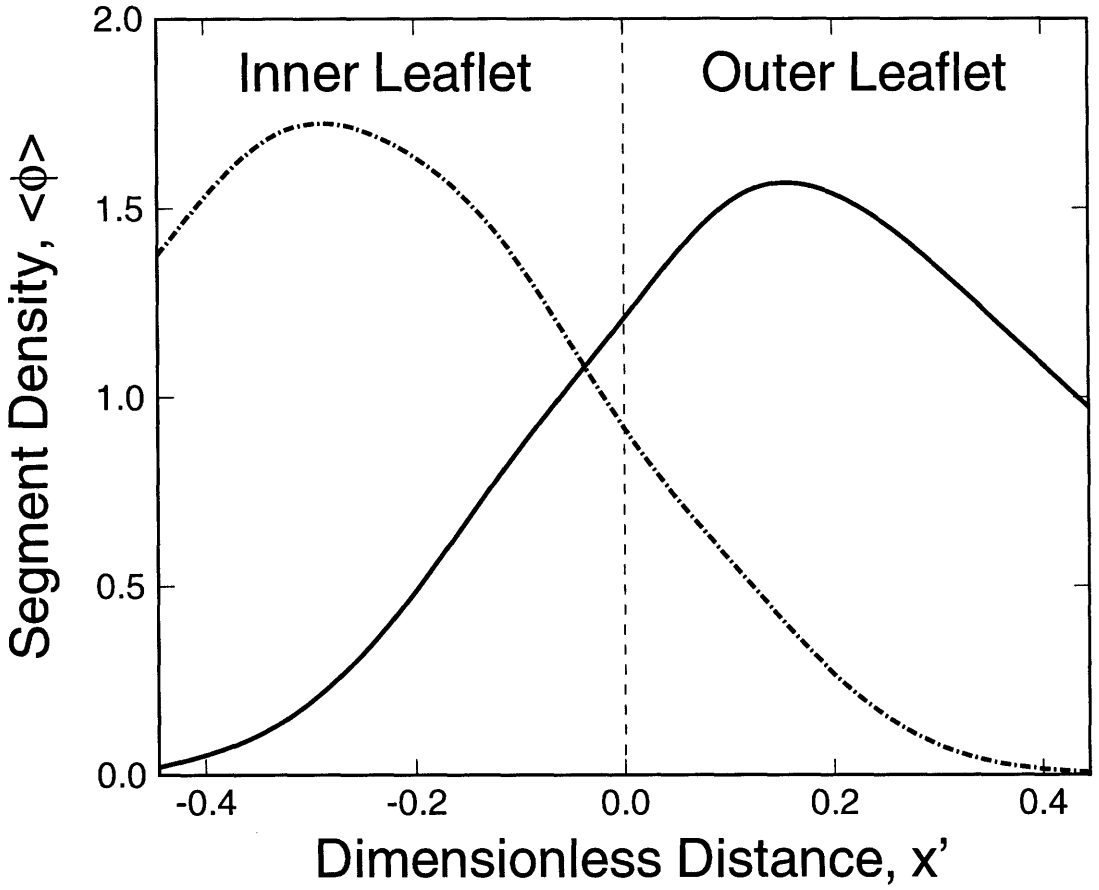

Figure 5-8: Predicted segment density distributions, $\langle\phi(x')\rangle$, for a C16 tail in the vesicle hydrophobic region of a C16/C5 vesicle having $\bar{c} = 0.43$, $F = 0.5$, and $f = 0.7$. The notation is the same as that in Figure 5-5.

directly using the order parameter for the tails, which is defined as [47]

$$S_z = \frac{1}{2}\langle 3\cos^2\theta_z - 1\rangle \tag{5.1}$$

where θ_z is the angle between the vector from C_{n-1} to C_{n+1} in the tail and the bilayer normal. Equation (5.1) indicates that: (i) $S_z = 1$ corresponds to a fully-ordered chain along the bilayer normal, (ii) $S_z = 0$ corresponds to a completely isotropic chain, and (iii) $S_z = -0.5$ corresponds to a chain perpendicular to the bilayer normal. Figure 5-9 shows the theoretically predicted order parameter of a C16 tail in the C16/C15 and C16/C5 vesicles, having configurations corresponding to the minima in $g_{ves} - g_{bilayer}$ at the larger curvatures (see Figure 5-4). Note that the C16 tails in the inner leaflet (open symbols) of the two types of vesicles have very similar order parameters, indicating that the packing environments in the inner leaflets are indeed quite similar. In the outer leaflets, the C16 tails in the two types of vesicles are, in general, more ordered than those in the inner leaflets, as shown by the higher order parameters (filled symbols), but they are also quite different from each other. More specifically, because the tail in the outer leaflet of the C16/C15 vesicle is more "crowded", it is more stretched along the bilayer normal, thus making it more ordered than the tail in the outer leaflet of the C16/C5 vesicle.

Because of the more favorable packing environment in the C16/C5 case, the competition between the interfacial and packing free energies in the minimization of g_{ves} encountered in a C16/C15 mixture is not found in a C16/C5 mixture. Indeed, by placing more molecules in the outer leaflet, the vesicle can be relieved of the interfacial free-energy penalty without incurring a high packing free-energy penalty. This can be seen more clearly in Figure 5-10, where the predicted variation of g_σ (dash-dotted line), g_{pack} (solid line), and g_{steric} (dashed line) for a C16/C5 mixture ($F = 0.5$) is shown as a function of $\bar{c}$. Recall, from Figure 5-7, that g_σ and g_{pack} for a C16/C15 vesicle having $\bar{c} = 0.37$ are 0.23 kT and 0.1 kT, respectively, higher than the corresponding values for the planar bilayer. Here, for a C16/C5 vesicle having $\bar{c} = 0.43$, where the second minimum in $g_{ves} - g_{bilayer}$ occurs (see Figure 5-4), g_σ and g_{pack} are

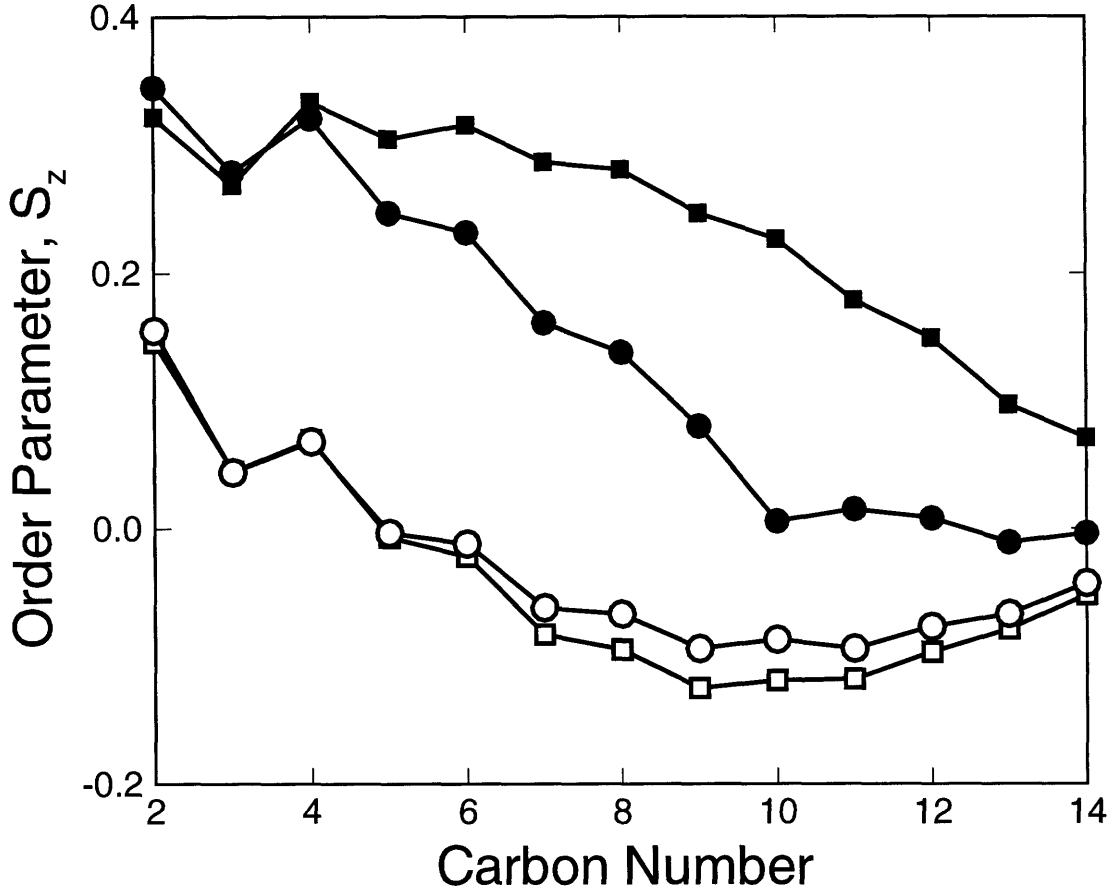

Figure 5-9: Predicted order parameters, S_z, for a C16 tail in a C16/C15 vesicle having $\bar{c} = 0.37$, $F = 0.5$, and $f = 0.7$ (squares), and a C16/C5 vesicle having $\bar{c} = 0.43$, $F = 0.5$, and $f = 0.7$ (circles). Filled symbols denote the tails in the outer leaflet, and open symbols denote the tails in the inner leaflet.

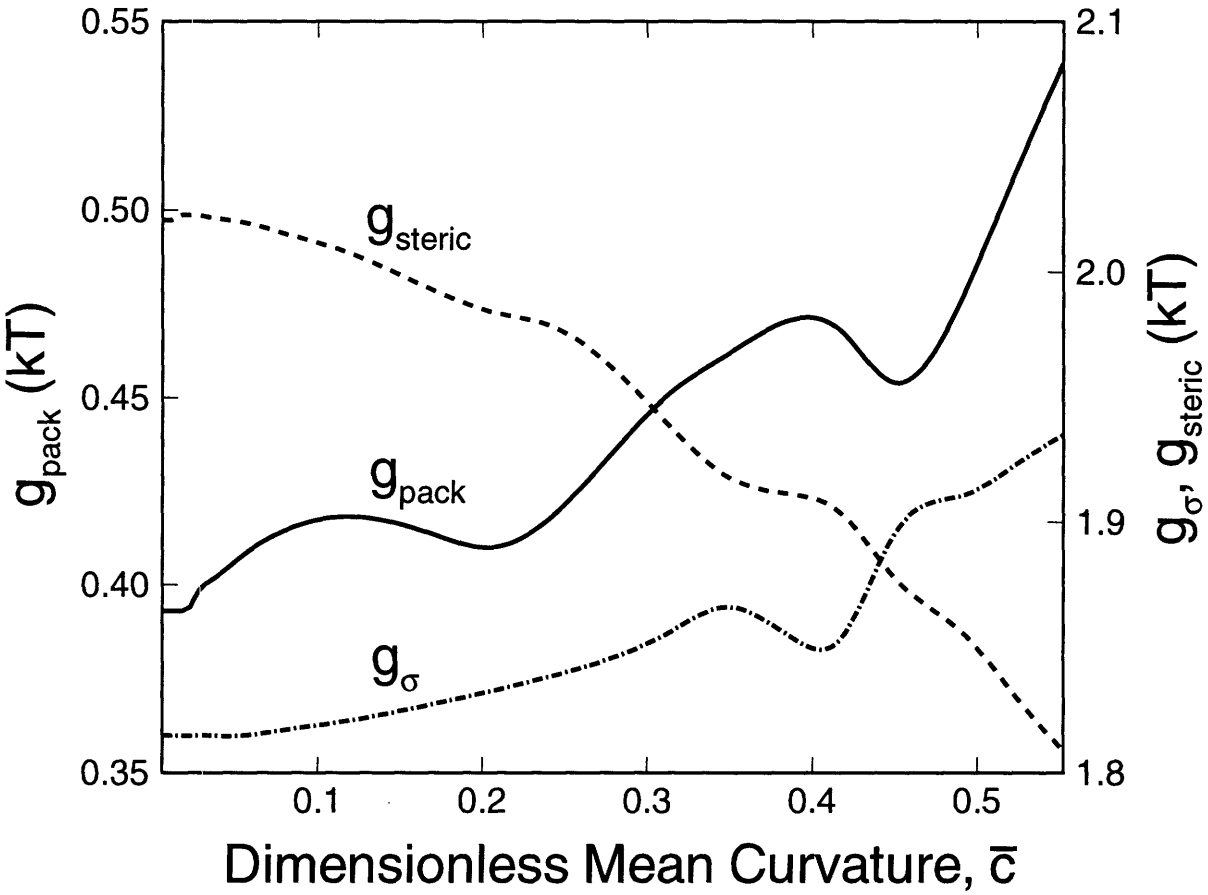

Figure 5-10: Predicted variation of the free-energy contributions, g_σ (dash-dotted line), g_{steric} (dashed line), and g_{pack} (solid line), for a C16/C5 mixture as a function of dimensionless mean curvature, $\bar{c}$. The vesicle composition, F, is fixed at 0.5.

only about 0.05 kT and 0.07 kT, respectively, higher than those for a planar bilayer. On the other hand, g_{steric} of a vesicle having a value of $\bar{c} = 0.43$ is 0.13 kT lower than that of a planar bilayer ($\bar{c} \to 0$). Therefore, in the case of C16/C5, the gain in g_{steric} exceeds the penalty due to g_{pack} and g_{σ}, resulting in a negative $g_{ves} - g_{bilayer}$ at $\bar{c} = 0.43$. As in the case of C16/C15, the contribution of g_{elec} to the variation of g_{ves} with $\bar{c}$ is insignificant when compared to the other free-energy contributions.

5.4 Concluding Remarks

The molecular-thermodynamic theory for vesicles has been applied in this chapter to investigate the effect of surfactant tail-length asymmetry on the formation of mixed vesicles. In a mixture of cationic and anionic surfactants, vesicles can be stabilized energetically by the tail-length asymmetry between the two components. By energetic stabilization, we imply that the free energy of vesiculation of a finite-sized vesicle is lower than that of a planar bilayer, thus making it a more energetically favorable structure. The effect of surfactant tail-length asymmetry can, indeed, be understood from a physical point of view. In the case of small C16/C15 vesicles, while it is true that the interfacial free-energy penalty can be relieved by placing more molecules in the outer leaflet, this also requires pushing more tails into the vesicle hydrophobic region, thus making the outer leaflet more crowded. In the case of small C16/C5 vesicles, however, the shorter C5 tails can fit nicely into the space near the outer hydrocarbon/water interface, without protruding deeply into the hydrophobic region. Consequently, the C5 tails can "cover" the outer interface without interfering significantly with the packing environment in the hydrophobic region. While the composition distributions are sharply peaked for both C16/C15 and C16/C5 mixtures, their optimum values, F^*, are quite different, Specifically, decreasing surfactant tail-length asymmetry (from C16/C5 to C16/C15) reduces the influence of g_{tr}. This, in turn, decreases the energetic contribution to vesicle formation, thus allowing the entropic contribution to play a more dominant role in determining the optimum composition. In this sense, therefore, decreasing surfactant tail-length asymmetry is similar to adding salt to the

vesicle suspension, where the energetic contribution is decreased through a reduction of g_{elec}. Entropically-stabilized vesicles, as in the case of C16/C15, tend to be large and widely distributed in size, whereas energetically-stabilized vesicles, if they form, tend to be small and narrowly distributed in size. As mentioned earlier, the present theory does not predict that C16/C5 vesicles will actually form spontaneously upon mixing, since one still needs to compare the free energy of vesiculation with those corresponding to other possible microstructures, including mixed micelles. However, in one medically relevant system, namely, an aqueous solution of bile salt, phospholipid, and cholesterol, vesicles do form spontaneously in bile. The present work suggests that the asymmetry between the hydrophobic moieties of bile salt, cholesterol, and phospholipid may play an important role in the formation and stabilization of such vesicles.

This chapter concludes the theoretical studies of mixed surfactant vesicles. In the following two chapters, I will turn my attention to the experimental part of this thesis, which includes an examination of the model biliary system. Model bile is an aqueous solution composed of bile salt, phospholipid, and cholesterol. By studying this simple, better characterized, system, instead of the much more complex system of native bile, it is hoped that one can shed light on the problem of cholesterol gallstone formation in bile. In particular, two responses, the vesicle composition and the distribution of cholesterol between vesicles and mixed micelles in model biles, will be investigated using factorial experimental design (see chapter 7). To study these two responses, however, one needs to separate vesicles and mixed micelles without altering the distribution of cholesterol. To this end, therefore, the following chapter is devoted to a systematic comparison between two commonly used separation techniques: ultracentrifugation and gel chromatography.

Chapter 6

Separation of Biliary Aggregates

Cholesterol (Ch) is solubilized in bile by three types of lipid aggregates: (i) simple bile salt / cholesterol micelles, (ii) mixed micelles containing bile salt, phospholipid (PL), and cholesterol, and (iii) unilamellar or multilamellar vesicles, which consist mainly of phospholipid and cholesterol, with a small amount of bile salt [21, 24]. Cholesterol also exists in bile as monomers at very low concentrations. Both the proportion of cholesterol in vesicles and their Ch/PL ratio appear to be inversely correlated with the nucleation time[1] [31, 64, 66, 89]. Consequently, understanding how certain physiological variables, such as total lipid content and bile salt/phospholipid ratio, alter the cholesterol distribution between biliary lipid aggregates is likely to give insights into mechanisms modulating cholesterol gallstone formation.

To study the cholesterol distribution in model and native biles, the cholesterol contents of lipid aggregates must be measured accurately, either *in situ* if possible, or by quantitative separation and chemical analysis of the lipid aggregates. Two separation techniques are currently used for this purpose: ultracentrifugation and gel chromatography. In density-gradient ultracentrifugation, a gradient in a liquid medium is pre-formed by inert substances such as sucrose, cesium chloride, or metrizamide [3, 4, 99, 154, 169]. Under a centrifugal field, particles suspended in such a medium float or sediment in a narrow band corresponding to their densities. Amigo and col-

[1]Nucleation time is the time required for the first cholesterol monohydrate crystal to appear under a microscope [78].

leagues [4, 3] described a simpler ultracentrifugation approach, in which, instead of using a pre-formed density gradient, the overall density of the bile was adjusted to 1.06 g/mL using metrizamide. Theoretically, though not demonstrated explicitly by floatation or sedimentation of the individual aggregates, the lower-density vesicles float while the higher-density mixed micelles sediment. A potential drawback of ultracentrifugation is incomplete separation of lipid aggregates, as suggested by the high bile salt content in the fractions believed to contain only vesicles [4, 169]. In fact, the compositions of these "vesicular" fractions lie within the two-phase region of the TC-PL-Ch pseudo-ternary equilibrium phase diagram [26], indicating that micelles are present in addition to vesicles . Clearly, incomplete separation leading to the contamination of the vesicular fraction with mixed micelles would result in an overestimation of the amount of cholesterol in vesicles.

Alternatively, gel chromatography separates suspended particles based on their sizes [153], but invariably dilutes the bile with eluant. Since bile salt monomers, simple micelles, mixed micelles, and vesicles exist in dynamic equilibrium, dilution alters the distribution of lipid components between the various aggregates [37]. Theoretically, if the eluant contains the correct IMC[2], the dynamic equilibrium between the lipid monomers and the lipid aggregates can be maintained during separation, and the distribution of lipid components such as Ch can thus be preserved. In contrast to the case for bile salts, cholesterol and phospholipid monomers are present in such minute amounts (about 10^{-8} and 10^{-10} M, respectively [40, 43]) that dilution does not shift significant amounts of these lipids into the monomeric phase. Indeed, it has been demonstrated that rechromatography of micellar and vesicular fractions using the correct IMC does not alter aggregate size or composition [43]. Because IMC values differ for model biles of various concentrations and compositions [42, 43], separation of lipid aggregates by gel chromatography is time-consuming, and ultracentrifugation offers a more convenient alternative. To see if the two separation techniques are compatible with each other, therefore, we first compare ultracentrifugation with gel

[2]Recall, from chapter 1, that the IMC (inter-mixed micellar / vesicular bile salt concentration) is the monomeric and simple micellar bile salt concentration in the bile sample.

chromatography using the correct IMC in the eluant [181].

6.1 Materials and Methods

Sodium taurocholate was obtained from Sigma (St. Louis, MO) and was purified by the method of Pope [137]. Grade I egg-yolk phosphatidylcholine (Lipid Products, South Nutfield, UK), cholesterol (Nu-Check Prep, Elysian, MN), and sucrose (Mallinckrodt, Paris, KY) were used as received. Purity was confirmed by thin layer chromatography, HPLC, or gas chromatography as previously described [41]. Sodium chloride was roasted at 600 °C for over 6 hrs. Other chemicals were of ACS quality or highest reagent grade. Glassware was alkali-washed overnight in ethanol / 1 N sodium hydroxide 1:1 (vol:vol), and acid-washed in 1 M nitric acid for 24 hrs, followed by thorough rinsing with Milli-Q water (Millipore, Bedford, MA).

6.1.1 Model Bile Preparation

All model biles were prepared by the method of coprecipitation [26]. Briefly, stock solutions (in methanol and chloroform) of the three lipid components were mixed in appropriate amounts. Mixtures were dried under a stream of nitrogen and then under vacuum for 24 hrs. Dried lipid films were resuspended in 0.15 M sodium chloride / 3 mM sodium azide aqueous solution, and the suspensions were vortex-mixed, flushed with argon, heated at about 75 °C for approximately 2 hrs, and incubated at 37 °C for 30 minutes. Model biles of various compositions were used in this study: (i) Ch-unsaturated model bile containing 3 g/dL total lipid, 2 mol% Ch, and a TC/(TC+EYPC) ratio of 0.7 ([TC] = 34.1 mM, [EYPC] = 14.6 mM, [Ch] = 1.0 mM, CSI = 0.30), hereafter referred to as *type A micellar bile*, for preliminary ultracentrifugation studies to examine the separation of lipid aggregates, (ii) supersaturated model biles containing 3 g/dL total lipid, 10 mol% Ch, and a TC/(TC+EYPC) ratio of 0.6 ([TC] = 26.6 mM, [EYPC] = 17.8 mM, [Ch] = 4.9 mM) and 0.7 ([TC] = 32.2 mM, [EYPC] = 13.8 mM, [Ch] = 5.1 mM) for comparison between ultracentrifugation and gel chromatography, and (iii) Ch-unsaturated model biles containing

3 g/dL total lipid, 7 mol% Ch, and a TC/(TC+EYPC) ratio of 0.7 ([TC] = 32.9 mM, [EYPC] = 14.1 mM, [Ch] = 3.5 mM, CSI $\approx$ 0.97), hereafter referred to as *type B micellar bile* [26], for studies of the effect of ultracentrifugation on the phase behavior of model bile.

Vesicles were prepared by extrusion through 0.1 micron polycarbonate membranes (Nuclepore, Pleasenton, CA). A Ch/EYPC (molar ratio 1:1) coprecipitate was resuspended in 0.15 M sodium chloride / 1 mM sodium azide aqueous solution (pH 7.4) to yield multilamellar vesicles with a final concentration of 10 mg/mL. Repeated (8 times) extrusion through two 0.1-μm polycarbonate membranes, in a High Pressure Vesicle Extruder (Model HPVE-S, Sciema Technical Services, Ltd., Richmond, BC, Canada) produced unilamellar vesicles of approximately 1050 Å in diameter, as confirmed by quasi-elastic light scattering [36]. The vesicle suspension was diluted to a concentration of 1 mg/mL ([EYPC] = [Ch] = 0.86 mM) prior to ultracentrifugation.

6.1.2 Ultracentrifugation

The densities of the model biles were adjusted to 1.03, 1.05, and 1.07 g/mL by direct addition of 8, 13, and 17.5 wt% sucrose, respectively [141]. Samples were ultracentrifuged in 0.8-mL Ultra-Clear tubes (Beckman Instruments, Palo Alto, CA) at 42,000 rpm (Beckman L8-55 ultracentrifuge, SW50.1 horizontal swinging bucket rotor, maximum $g \approx$ 200,000) and 37 °C for 6, 8, 10, or 13 hrs. Immediately after ultracentrifugation, four fractions [from top to bottom: 50 μL, 100 μL, 200 μL, and remainder (220 – 350 μL)] [3, 4] were carefully withdrawn, and their volumes measured with a microsyringe, and analyzed for phosphatidylcholine, cholesterol, and bile salt content. In selected experiments, the sealed ultracentrifuge tube was remixed by inversion and subjected to gel chromatography as described below, either immediately or after incubation for 8 or 11.5 hrs at 37 °C.

6.1.3 Gel Chromatography

A prepacked Pharmacia HR10 / 30 Superose 6 column (Pharmacia - LKB, Piscataway, NJ) was pre-equilibrated with aqueous solutions containing 0.15 M sodium chloride, 3 mM sodium azide, and 8 or 11 mM sodium taurocholate, corresponding to IMC values of model biles containing 3 g/dL total lipid, 10 mol% Ch, and a TC/(TC+EYPC) ratio of 0.6 and 0.7, respectively [43]. A 500-μL model bile sample (200 μL for replicates) was injected onto the column, and eluted at 37 °C with the same aqueous solution at a flowrate of 0.5 mL/min (Pharmacia P-500 pump) [35]. Fractions (1 mL) were analyzed for phosphatidylcholine and cholesterol content.

6.1.4 Lipid Analysis

Cholesterol was measured with a cholesterol oxidase method (Sigma, St. Louis, MO). Phosphatidylcholine was analyzed as inorganic phosphorus using the method of Bartlett [7]. Bile salt was analyzed by the 3α-hydroxysteroid dehydrogenase assay described by Turley and Dietschy [168]. Results are given as the mean of 2 – 4 determinations, $\pm$ the standard deviation.

6.1.5 Quasi-Elastic Light Scattering (QELS)

The light-scattering apparatus consisted of a 2-W argon laser (Lexel model 95), a goniometer, and an autocorrelator (model BI - 9000 AT, Brookhaven Instruments, Holtsville, NY). All measurements were performed with a wavelength of 514.5 nm at 90°. Model bile samples (1.5 to 2 mL) were filtered through 0.22 μm sterile filters to remove dust particles, and kept at 37 °C using a circulating water bath during measurement. Effective diffusivities of the particles were obtained from the measured autocorrelation functions using the non-negatively constrained least-square analysis [58]. The mean hydrodynamic radii, $\bar{R}_h$, of the particles were calculated using the Stokes-Einstein equation [36].

6.2 Results

6.2.1 Centrifugal Separation of Mixed Micelles and Vesicles

To identify conditions under which mixed micelles could be separated from vesicles by ultracentrifugation, *type A micellar biles* were adjusted to densities of 1.03, 1.05, and 1.07 g/mL. The composition of this model bile lies within the one-phase micellar region of the TC-PL-Ch pseudo-ternary equilibrium phase diagram [26], and both simple bile salt micelles and mixed micelles are present. Table 6.1 shows the EYPC concentration in each fraction after 8 hrs of ultracentrifugation at various medium densities. Sedimentation of mixed micelles is more rapid at 1.03 g/mL than at 1.05 g/mL, as demonstrated by the steeper concentration gradient across the ultracentrifuged solution. In fact, at 1.07 g/mL, the trend in the variation of EYPC concentration is reversed, indicating that mixed micelles are less dense than the aqueous medium. Using the EYPC concentration and measured volume of each fraction, the distribution of EYPC among the four fractions can be calculated and is shown in Figure 6-1. Even at a medium density of 1.03 g/mL, the top fraction still contains 2.5 % of total EYPC after 8 hrs of ultracentrifugation, indicating that separation of mixed micelles may not be satisfactory. Figure 6-2 shows the distribution of Ch and EYPC after the duration of ultracentrifugation was extended to 13 hrs (medium density = 1.03 g/mL). The percent of total EYPC in the top fraction was substantially reduced from 2.5 % to 0.2 %, which corresponds to a EYPC concentration of only 0.3 mM in the top fraction. An increase in total lipid concentration did not substantially alter the separation. For a model bile containing 10 g/dL total lipid, 2 mol% Ch, and a TC/(TC+EYPC) ratio of 0.7 ([TC] = 113.5 mM, [EYPC] = 48.6 mM, [Ch] = 3.3 mM), 2 % of total EYPC was found in the top fraction after 13 hrs of ultracentrifugation at a density of 1.03 g/mL (data not shown). The slightly higher percent EYPC found in the top fraction is most likely due to the increased viscosity of the bile.

A system containing only unilamellar vesicles (Ch/EYPC = 1.0) was ultracentrifuged at a density of 1.03 g/mL for 2, 4, and 13 hrs. The percent Ch and EYPC

Table 6.1: EYPC concentrations (mM) in the four fractions after ultracentrifugation at various medium densities.

	Density (g/mL)		
Fraction Volume (μL)	1.03	1.05	1.07
50	4.0	8.3	14.3
100	10.7	11.5	12.7
200	11.7	11.2	11.4
Remainder (220 – 350)	15.9	13.0	12.0

Note: Micellar biles (3 g/dL, 2 mol% Ch, TC/(TC+EYPC) = 0.7) were adjusted to various densities by direct addition of sucrose. After ultracentrifugation for 8 hrs (42,000 rpm, 37 °C), four fractions were withdrawn carefully, and their volumes were measured with a microsyringe. Measurements were performed in duplicate, with an average standard deviation of 0.8 mM.

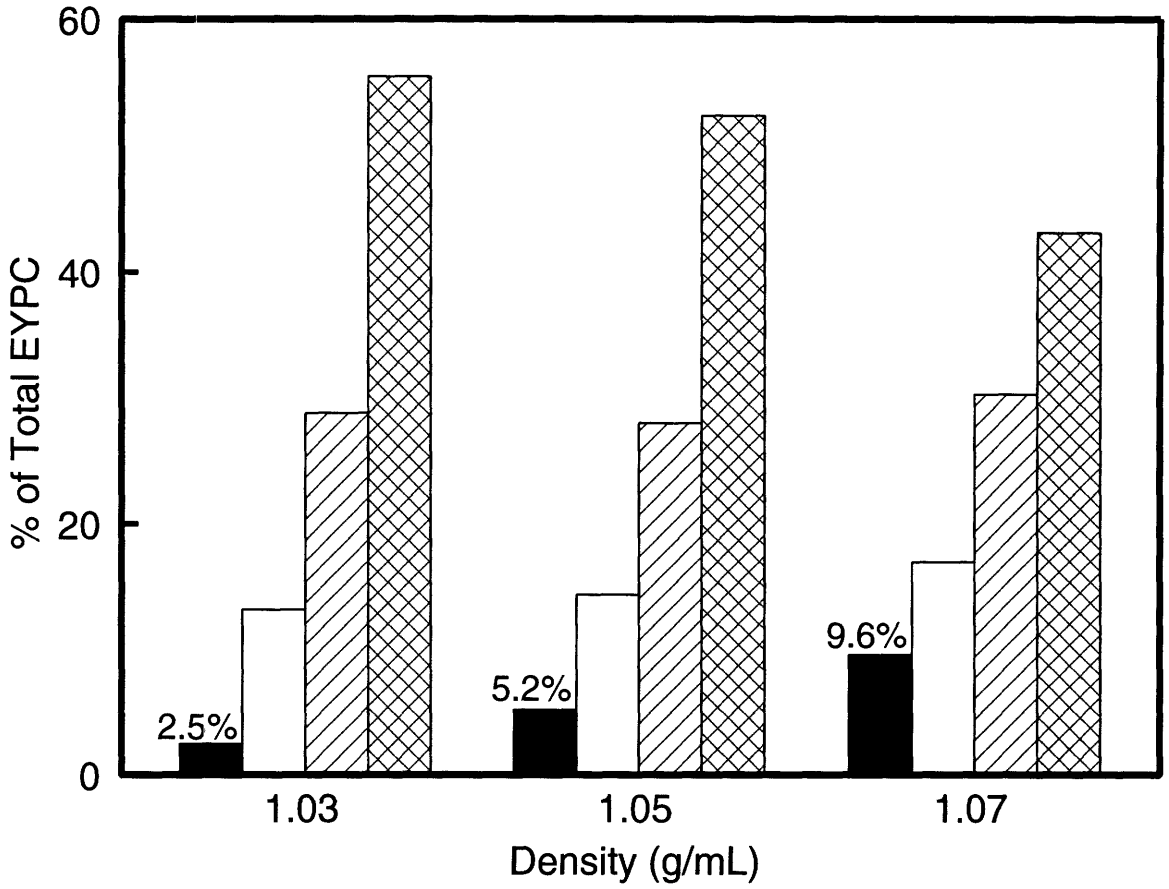

Figure 6-1: Effect of varying the density of the medium on the distribution of EYPC in micellar biles (3 g/dL, 2 mol% Ch, TC/(TC+EYPC) = 0.7) after 8 hrs of ultracentrifugation. Four fractions were removed: top 50 μL (black bars), 100 μL (white bars), 200 μL (striped bars), and remainder (220 - 350 μL) (cross-hatched bars). Only 2.5 % of total EYPC was found in the top 50-μL fraction in the 1.03 g/mL case, as compared to 9.6 % in the 1.07 g/mL case, indicating that mixed micelles sediment at a much faster rate in a medium density of 1.03 g/mL.

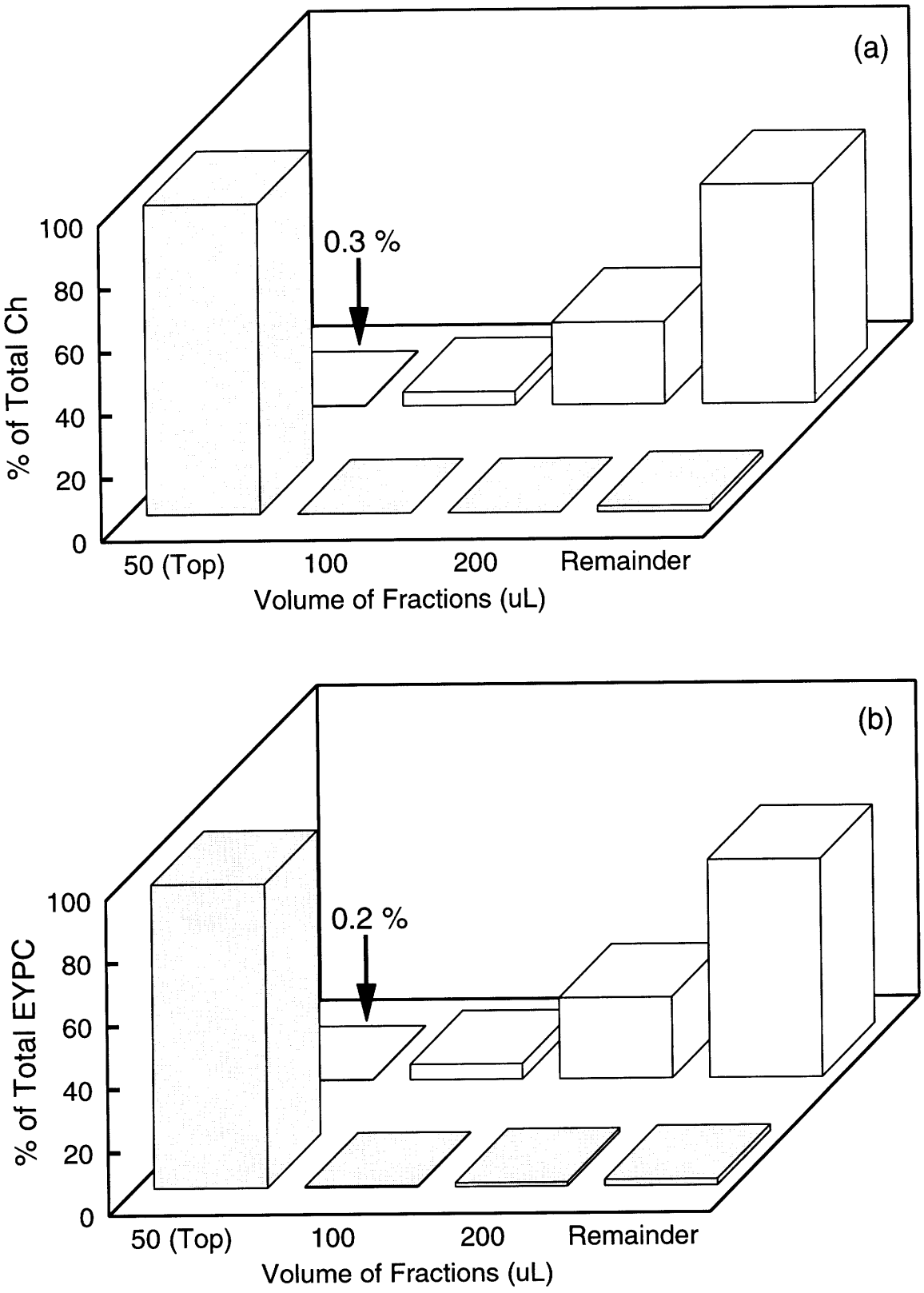

Figure 6-2: Distributions of Ch (a) and EYPC (b) in a vesicle suspension (grey bars, n = 3) and micellar bile (3 g/dL, 2 mol% Ch, TC/(TC+EYPC) = 0.7) (white bars, n = 2) after ultracentrifugation for 13 hrs at a density of 1.03 g/mL. Greater than 96 % of Ch and EYPC were found in the top 50-μL fraction of the vesicle suspension, while only 0.2 % was found in the corresponding fraction of the micellar bile. The average standard deviations are 0.4 % and 2.1 % for Ch and EYPC in the vesicle suspension, respectively, and 1.4 % and 0.6 % for Ch and EYPC in the micellar bile, respectively.

in the top fraction increased from 73 % after 2 hrs, to 98 and 96 %, respectively, after 4 hrs, remaining unchanged upon further ultracentrifugation (see Figures 6-2(a) and 6-2(b)). In contrast, only 0.3 % of Ch and 0.2 % of EYPC were found in the same top fraction after 13 hrs of ultracentrifugation of *type A micellar bile*. Consequently, under these conditions (density of 1.03 g/dL, 13 hrs of ultracentrifugation), ultracentrifugation would separate mixed micelles and vesicles quantitatively. The top fraction would contain more than 96 % of vesicular lipids, with contamination by only 0.3 % of micellar lipids. Thus, these conditions were used in all subsequent ultracentrifugation studies.

The sedimentation of simple micelles at 1.03 g/mL was also examined. As Figure 6-3 shows, a shallow gradient in bile salt concentration forms in a simple micellar solution (10 mM TC, 0.15 M sodium chloride, 3 mM sodium azide) after 13 hrs of ultracentrifugation. Accordingly, simple micelles also sediment due to the density difference between simple micelles and the aqueous medium, but much more slowly than the larger mixed micelles.

6.2.2 Comparison between Ultracentrifugation and Gel Chromatography

Ch-supersaturated model biles containing 3 g/dL total lipid, TC/(TC+EYPC) ratios of 0.6 and 0.7, and 10 mol% Ch were subjected to gel chromatography and ultracentrifugation under optimal conditions to separate mixed micelles and vesicles quantitatively, as determined above. Table 6.2 displays the vesicular Ch content and the Ch/EYPC ratio found in vesicles. The percent Ch in vesicles was found to be significantly higher by ultracentrifugation than by gel chromatography for both TC/(TC+EYPC) ratios examined ($p < 0.001$), but the measured Ch/EYPC ratios were found not to differ significantly ($p > 0.1$). In a model bile (3 g/dL, 10 mol% Ch, TC/(TC+EYPC) = 0.7) with 8 wt% sucrose added after 30 minutes of incubation at 37 °C, 24 % ± 1 % (n = 2) of Ch was found in the vesicular fraction by gel chromatography, a value similar to that in the absence of sucrose (22 ± 2 %). Thus,

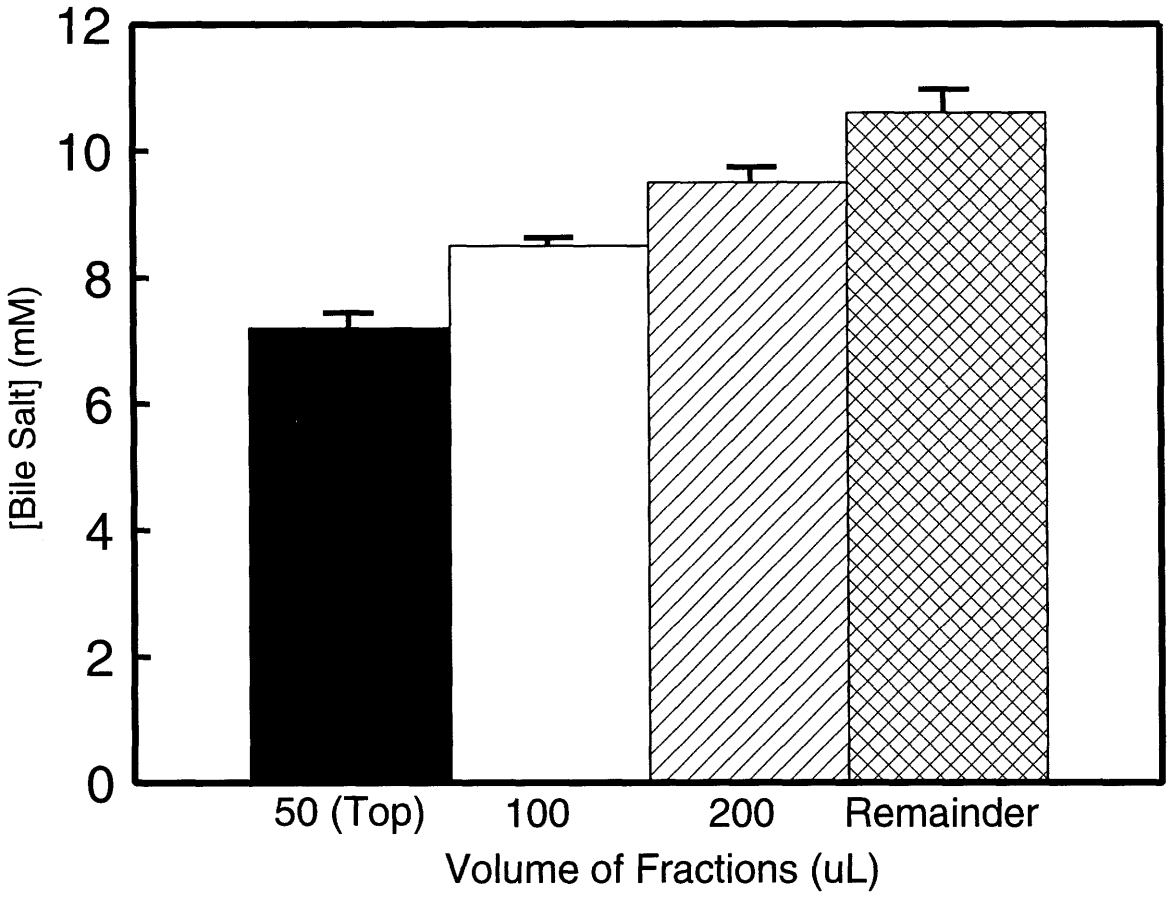

Figure 6-3: Distribution of bile salt among the four fractions in a simple micellar solution after ultracentrifugation. When a 10 mM TC solution was ultracentrifuged at 42,000 rpm and 37 °C for 13 hrs, using a medium density of 1.03 g/mL, a shallow gradient of bile salt concentration was formed. Measurements were performed in triplicate.

Table 6.2: Percent of total Ch and Ch/EYPC ratio in vesicles as measured by ultracentrifugation and gel chromatography.

	Vesicular Ch (%)		Ch/EYPC Ratio	
TC/(TC+EYPC)	Ultracentrifugation	Chromatography	Ultracentrifugation	Chromatography
0.6	31 ± 2	19 ± 2	1.0 ± 0.04	1.0 ± 0.3
0.7	40 ± 5	22 ± 2	1.3 ± 0.2	1.5 ± 0.2

Note: Ch-supersaturated model biles (3 g/dL, 10 mol% Ch, TC/(TC+EYPC) = 0.6 and 0.7) were subjected separately to ultracentrifugation (42,000 rpm, 37 °C, 1.03 g/mL, 13 hrs) and gel chromatography (Superose 6, 37 °C) (n = 3 and 4 for TC/(TC+EYPC) ratios of 0.6 and 0.7, respectively).

the presence of sucrose did not alter the Ch distribution significantly.

To better understand the systematic difference observed between ultracentrifugation and gel chromatography, the effect of duration of ultracentrifugation on the Ch distribution was examined. Model biles (3 g/dL, 10 mol% Ch, TC/(TC+EYPC) = 0.7) were ultracentrifuged at 1.03 g/mL for 6, 10, and 13 hrs, remixed immediately, and subjected to gel chromatography. Figure 6-4(a) shows the percent Ch in the vesicular fraction, as measured using gel chromatography, as a function of duration of ultracentrifugation. The percent Ch in vesicles increases gradually from 22 % (without ultracentrifugation) to 41 $\pm$ 1 % (n = 2) after 13 hrs of ultracentrifugation. Notably, the value obtained using gel chromatography after 13 hrs of ultracentrifugation is virtually identical to that obtained by ultracentrifugation for the same time period (40 $\pm$ 5 %, see Table 6.2).

Interpretation of the data presented above is aided by knowledge of the time course of the ultracentrifugal behavior of mixed micelles and vesicles. Vesicles rapidly float to the top fraction within 4 hrs of ultracentrifugation, whereas the smaller mixed micelles sediment much more slowly from this fraction. Therefore, a shorter duration of ultracentrifugation would tend to overestimate the percent Ch in vesicles, but the error would decrease with further duration of ultracentrifugation. As shown in Figure 6-4(a), exactly the opposite occurred, suggesting that an induced change in the thermodynamic state of the model bile during ultracentrifugation shifted Ch from mixed micelles to vesicles. It would, therefore, be logical that this alteration in Ch distribution would reverse upon removal of the centrifugal field. To examine this possibility, identical model biles (3 g/dL, 10 mol% Ch, TC/(TC+EYPC) = 0.7) were ultracentrifuged for 13 hrs, remixed, and then incubated at 37 °C for 8 and 11.5 hrs prior to gel chromatography. Figure 6-4(b) demonstrates that, after 8 hrs of incubation at 37 °C, 33 % of the total Ch is found in vesicles, with this value decreasing further to 31 % after 11.5 hrs of incubation. By comparison with the value of 22 % Ch found in vesicles without ultracentrifugation, it can be inferred that the model bile relaxes towards its original state after ultracentrifugation induces a non-equilibrium state.

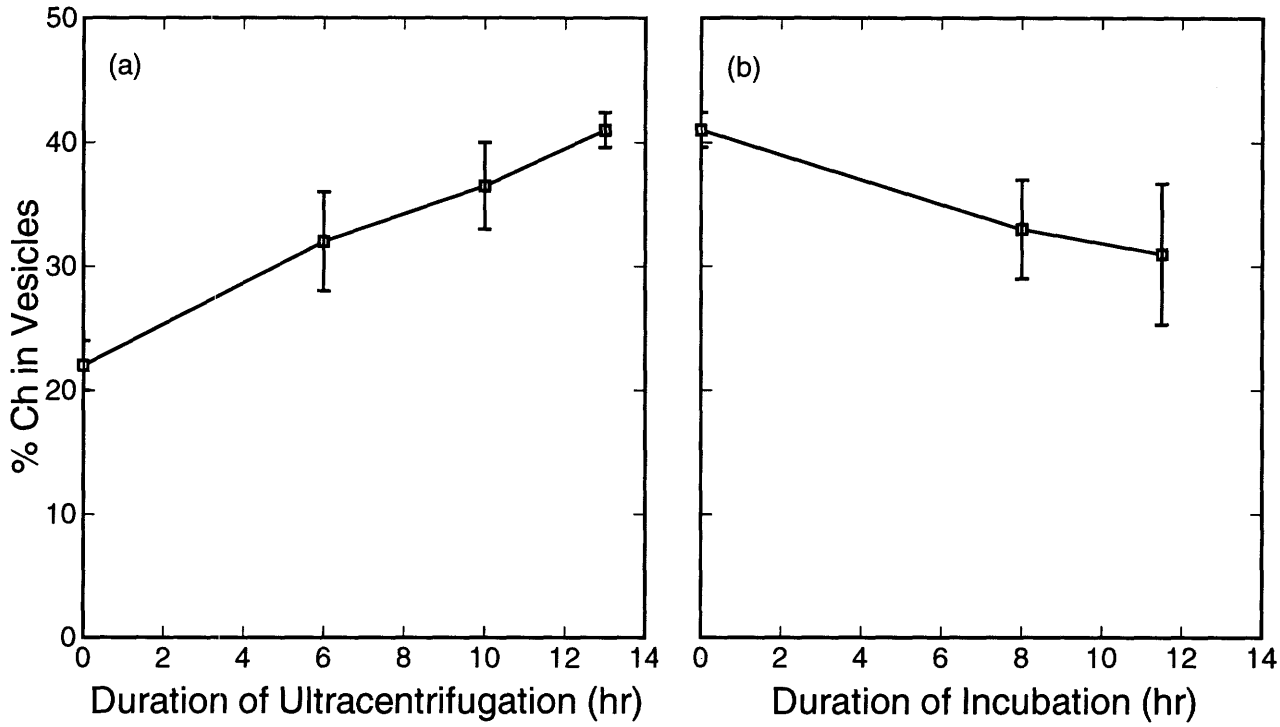

Figure 6-4: Effect of duration of ultracentrifugation (a) and incubation (b) on the percent Ch in vesicles (measured in duplicate). (a): model biles (3 g/dL, 10 mol% Ch, TC/(TC+EYPC) = 0.7) were ultracentrifuged for various durations, remixed, and subjected to gel chromatography immediately; (b): model biles of identical composition were ultracentrifuged for 13 hrs, remixed, and subjected to gel chromatography after various periods of incubation at 37 °C. The vesicular Ch increased gradually during ultracentrifugation, but decreased towards the original value upon incubation after ultracentrifugation.

6.2.3 Phase Alteration During Ultracentrifugation

A Ch-unsaturated *type B micellar bile* (CSI $\approx$ 0.97) [26] was ultracentrifuged for 13 hrs at a medium density of 1.03 g/mL. The composition of this model bile lies just below the saturation line that defines the one-phase micellar region of the TC-PL-Ch pseudo-ternary phase diagram, and at equilibrium this bile contains only simple and mixed micelles. Figure 6-5(a) demonstrates that the gel chromatography elution profile showed only a micellar peak prior to ultracentrifugation. Accordingly, QELS measurements showed a single particle population with a $\bar{R}_h$ value of 33 Å, consistent with the expected size of mixed micelles [110]. However, after ultracentrifugation, a narrow translucent band appeared beneath the meniscus in the top 50-μL fraction. When the model bile was immediately remixed and subjected to gel chromatography, a vesicle peak appeared in the elution profile, in addition to mixed micelles (see Figure 6-5(b)). Chemical analysis of the eluted fractions showed that the vesicular fraction contained 9 % of total Ch, with a Ch/EYPC ratio of 0.9. QELS measurements confirmed a bimodal particle size distribution, with particle $\bar{R}_h$ values of 38 Å and 395 Å, the latter consistent with the expected size of unilamellar vesicles [111, 153].

6.3 Discussion

Separation of mixed micelles and vesicles by ultracentrifugation is based on the observation that mixed micelles are denser than vesicles [3, 4, 99, 169]. Underlying this technique are the assumptions that: (i) the density of the aqueous medium can be adjusted to a value between those corresponding to mixed micelles and vesicles, so that vesicles will move in a direction *opposite* to that of mixed micelles under the influence of the centrifugal field, and (ii) the inert substances used to generate the gradient (sucrose in this case) do not alter molecular self-association in the system. From the first assumption, a quantitative separation implies that the top fraction of the ultracentrifuged solution should be devoid of mixed micelles. Using a micellar bile (*type A*) and a vesicle suspension separately, we have demonstrated that, at a density of 1.03 g/mL, vesicles indeed float to the top rapidly, while mixed micelles

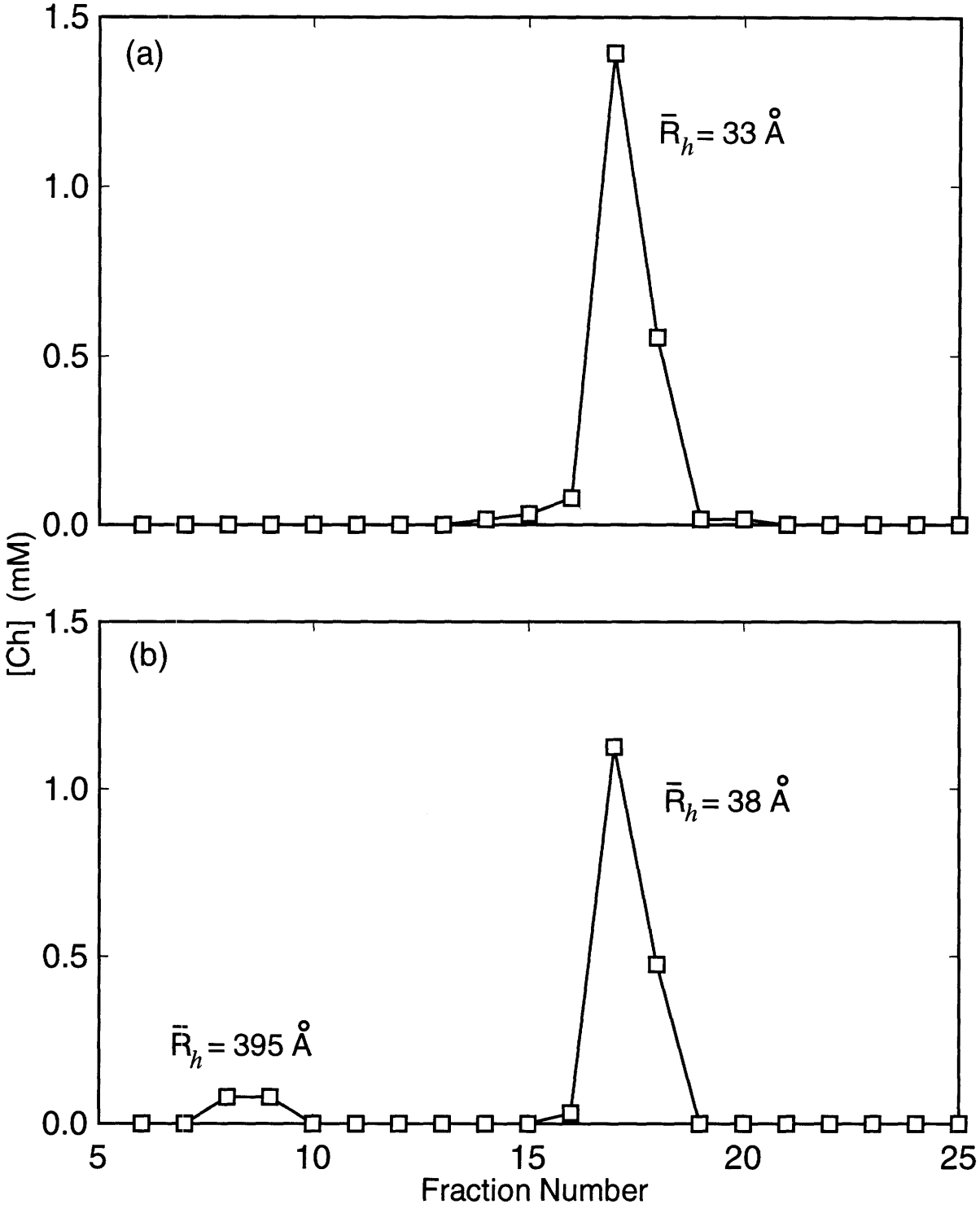

Figure 6-5: Cholesterol elution profile of model bile (3 g/dL, 7 mol% Ch, TC/(TC+EYPC) = 0.7, CSI = 0.97) before (a) and after (b) ultracentrifugation. Using QELS, a single particle population ($\bar{R}_h$ = 33 Å) was present before ultracentrifugation, but two particle populations ($\bar{R}_h$ = 38 Å and 395 Å) were detected after ultracentrifugation, consistent with the appearance of a vesicle peak in the gel chromatography profile after ultracentrifugation.

sediment towards the bottom under a centrifugal field. The fact that vesicles float at a much faster rate than that corresponding to micelle sedimentation is mainly due to the large size difference between the two lipid aggregates. Using a $\bar{R}_h$ value of 395 Å and a density of 1.02 g/mL (for a conservative estimate), the sedimentation coefficient [142] of vesicles is 33 Svedberg units (1 Svedberg unit = 10^{-13} seconds), whereas that of mixed micelles is only 0.8 Svedberg units. A noteworthy point is that the sedimentation coefficient also depends on the viscosity of the liquid medium; since the viscosity of native biles can vary within a wide range due to the presence of different proteins and mucous contents, application of ultracentrifugation to native biles may be inappropriate. Previously, Amigo and colleagues [3] demonstrated that the second assumption is valid, namely, that neither sucrose nor metrizamide alters the chromatographic elution profile in vesicles in native biles, a finding that was confirmed in the present study using model biles.

Despite demonstrating that these assumptions are valid and that the conditions used could quantitatively separate vesicles and mixed micelles, a progressive increase in the proportion of vesicular Ch with longer durations of ultracentrifugation was observed. This could not be attributed to incomplete separation of micelles and vesicles, since extending the duration of ultracentrifugation increased the systematic overestimation of vesicular cholesterol as compared to gel chromatography. Indeed, when the model bile was remixed and incubated after ultracentrifugation, the system relaxed towards its original state, and the percent Ch in vesicles returned to the original value. In gel chromatography, both the percent Ch in vesicles as well as the Ch/PL ratio are affected by changes in the eluant bile salt concentration [66]. Similarly, as demonstrated in Figure 6-3, the concentration of bile salt monomers and simple micelles at individual points along the ultracentrifugation-induced gradient differed from that of the unperturbed bile. More specifically, ultracentrifugation creates a zone in the top fraction that is depleted in bile salts, as shown in Figure 6-3. The sedimentation of simple TC micelles in a centrifugal field has also been analyzed theoretically by solving the proper partial differential equation governing the mass balance in the system. Using parameters corresponding to the actual experimental conditions, rea-

sonably good agreement was found between the predicted concentration profile (not shown) and the measured concentration profile shown in Figure 6-3. This clearly indicates that the experimental profile shown in Figure 6-3 is indeed generated by the centrifugal field used in this study. Accordingly, during ultracentrifugation, the relative composition of the top fraction shifts toward higher EYPC and Ch contents and lower TC contents, with the associated formation of vesicles as observed experimentally (Figure 6-5). More hydrophobic bile salts, such as taurodeoxycholate, are also found in native biles. However, these bile salts form larger simple micelles as compared to taurocholate, which should magnify the effect of a non-uniform bile salt concentration, and hence enhance the discrepancy between gel chromatography and ultracentrifugation. In contrast, during gel chromatography using the correct IMC, the lipid aggregates, including simple bile salt micelles, are not under the influence of any centrifugal field, and the concentration of simple micelles remains constant throughout the column. Consequently, during ultracentrifugation, changes in the local composition is believed to give rise to a new thermodynamic state, as compared to that of the original model bile sample, and hence, alter the distribution of Ch between the lipid aggregates.

Previous observations in the literature also support the conclusion that ultracentrifugation can alter the relative proportions of biliary micelles and vesicles. Ulloa and colleagues found [169] that a very high proportion of biliary Ch was solubilized in vesicles at a relatively modest degree of biliary supersaturation (CSI value of 1.08). Since simple and mixed micelles solubilize 100 % of cholesterol present at the micellar phase limit and unsaturated vesicles are rapidly transformed into mixed micelles [34], the observation by Ulloa and colleagues that 71 % of cholesterol is present in vesicles [169] is inconsistent with the pseudo-ternary equilibrium phase diagram. Using a different protocol with prolonged (60 hrs) ultracentrifugation, Sahlin and colleagues found [149] that unsaturated, presumably micellar, biles with median CSI values of 0.51 and 0.65, contained 28 and 18 %, respectively of total Ch in vesicles. Both these groups found that the molar ratio of vesicular Ch/phospholipid was less than one, indicating that the Ch saturation of vesicles was less than unity, the limit of

cholesterol solubility in PL [21, 149]. Thus, observations by other groups showed unexpectedly high proportions of cholesterol in vesicles that appear to be unsaturated with cholesterol, and are consistent with the finding that a different thermodynamic state is induced during ultracentrifugation.

The effect of an induced concentration gradient on the equilibrium phase behavior of a system in an ultracentrifuge has indeed been discussed thoroughly in earlier theoretical studies [143]. In addition to the existence of a concentration gradient, as discussed above, the potential induced by the centrifugal field also plays an important role in determining the phase equilibrium in an ultracentrifuge [45, 46]. The chemical potential of a component in an ultracentrifuge depends not only on the local composition, but also on the potential that results from the centrifugal field, which is proportional to $r^2\omega^2$, where r is the distance from the axis of rotation and ω is the angular velocity. In fact, as pointed out by Rossen and colleagues [143], the phase diagram of a system can be distorted by a centrifugal field, and the extent of distortion depends on the difference in this field potential across the solution. Of note, these authors also indicated explicitly that using ultracentrifugation to separate interspersed phases runs the danger of altering their composition or number, which is exactly what was observed in the present study. Perhaps the most clear-cut demonstration of this shift in thermodynamic state during ultracentrifugation is the creation of vesicles from a Ch-unsaturated micellar bile (*type B*). This observation shows that, during ultracentrifugation, the local composition in the model bile moves across the saturation line in the TC-PL-Ch pseudo-ternary equilibrium phase diagram, thus entering a metastable region where vesicles constitute a possible phase.

6.4 Concluding Remarks

In view of the results of the present study, and the theoretical considerations discussed above, caution should be exercised in interpreting previous ultracentrifugation studies reporting the distribution of Ch between vesicles and mixed micelles in model and native biles. In particular, the very high percent Ch in vesicles found by ultra-

centrifugation may be a result of a systematic increase induced by this technique. Gel chromatography is believed to be more reliable in preserving the original distribution of cholesterol and vesicle composition. However, this technique may not be applicable in some cases. For example, in model biles containing tauroursodeoxycholate, the vesicles that form are so large that they may not even pass through the void space in the chromatographic column. In such cases, ultracentrifugation seems to be the only alternative. In addition, gel chromatography tends to be more tedious in the sense that the IMC of each model bile must be measured separately, which can be quite time-consuming for a large number of bile samples. It would therefore be desirable if one could still utilize ultracentrifugation, while minimizing its deficiency. In the following chapter, a modification of the ultracentrifugation technique will be described, which allows us to more accurately estimate the distribution of cholesterol, as well as the vesicular cholesterol content, in model biles. The modified ultracentrifugation technique and gel chromatography will then be utilized to study the effects of, and the interactions among, four physiological variables, namely, total lipid content, bile salt to EYPC ratio, Ch content, and bile salt hydrophobicity, on the vesicle composition and the distribution of cholesterol between vesicles and mixed micelles using a two-level factorial experiment.

Chapter 7

Factorial Experimental Study of Cholesterol Distribution and Vesicle Composition

As discussed in chapters 1 and 6, the distribution of cholesterol between vesicles and mixed micelles, as well as the vesicle composition, play an important role in cholesterol nucleation [66, 67, 136]. By knowing how certain physiological variables, such as total lipid content and cholesterol content, affect the distribution of cholesterol and vesicle composition, one may eventually be able to alter the propensity of lithogenic bile towards cholesterol nucleation. The traditional "one-variable-at-a-time" approach in experimental research often lacks the ability to reveal the interactions among several process variables. This chapter describes the application of factorial experimental design to the study of vesicle composition, as well as the distribution of cholesterol between vesicles and mixed micelles in model bile [180]. In a two-level factorial design, for example, the value of each variable is set at one of two levels (high and low). For k variables, therefore, there are 2^k combinations. Instead of varying only one variable at a time, however, the values of the variables are varied simultaneously from one experimental condition to another. In other words, there are no two experimental conditions that differ in the value of only one variable. Indeed, it is this simultaneous variation that allows us to study readily the interactions among the variables, and

provides useful information in a relatively short time. The principles of statistical experimental design will be illustrated by going through the actual experiments and data analysis involved. However, the discussion here is by no means exhaustive; the interested reader is referred to Ref. 16 for a general overview of this subject.

To study the distribution of cholesterol and the vesicular Ch/PL ratio, the vesicles must be separated from mixed micelles. In chapter 6, ultracentrifugation was compared to gel chromatography with respect to the separation of vesicles and mixed micelles in bile, and it was found that ultracentrifugation may elevate the vesicular cholesterol content due to the creation of a bile salt depletion zone in the top fraction. Although gel chromatography is believed to be more reliable in preserving the original distribution of cholesterol, it may not be applicable in some cases. For example, in model biles containing tauroursodeoxycholate, the vesicles are so large that they may not be able to pass through the void space in the chromatographic column. In this case, ultracentrifugation seems to be the only alternative. In addition, gel chromatography tends to be more tedious in the sense that the inter-mixed micellar / vesicular bile salt concentration (IMC) of each model bile must be measured separately, which can be time-consuming when dealing with a large number of bile samples. It will therefore be desirable if one can still utilize the principle of centrifugation, but minimize the effect of the bile salt depletion zone on the distribution of cholesterol. In this study, the ultracentrifugation technique is modified for the separation of vesicles and mixed micelles. The modification is based on the premise that, by reducing the mobility of simple and mixed micelles in a centrifugal field, the effect of centrifugation on the distribution of cholesterol, which is mainly due to the creation of a bile salt depletion zone in the top fraction (see chapter 6), can be considerably minimized. After briefly discussing the modified ultracentrifugation technique, a statistical experimental study on the distribution of cholesterol between vesicles and mixed micelles, as well as on the vesicular Ch/PL ratio, in model biles will be presented. In addition, by detailing the procedures involved in this methodology and illustrating its ability to extract useful information, this study also serves another important purpose: demonstrating the application of a systematic experimental methodology in medical

research.

7.1 Materials and Methods

Sodium tauroursodeoxycholate (TUDC) was obtained from Calbiochem (San Diego, CA) and purified by ether extraction. All the other materials are the same as described in chapter 6.

7.1.1 Model Bile Preparation

Model biles were prepared by the method of coprecipitation. In brief, stock solutions of the three lipid components were mixed in appropriate amounts and dried under a stream of nitrogen. The lipid mixtures were then dissolved in chloroform, dried again under nitrogen, and finally dried under vacuum for 24 hrs. Dried lipid films were resuspended in 0.15 M sodium chloride/3 mM sodium azide aqueous solution, mixed, and incubated at 37 °C for 30 minutes. For the development of the modified ultracentrifugation technique, the following solutions were used: (1) Ch-unsaturated micellar bile containing 3 g/dL total lipid, 2 mol% Ch, and a TC/(TC+EYPC) ratio of 0.7 ([TC] = 34.1 mM, [EYPC] = 14.6 mM, [Ch] = 1.0 mM), (2) aqueous solution containing 11 mM TC, 0.15 M sodium chloride, and 3 mM sodium azide, and (3) vesicular suspension containing 1 mg/mL total lipid and a Ch/EYPC molar ratio of 1:1. The vesicle suspension was prepared by repeated extrusion as described in chapter 6. The composition of the Ch-unsaturated micellar bile (solution (1)) falls in the one-phase region of the pseudo-ternary TC-EYPC-Ch phase diagram [26] (see bottom region in Figure 1-5) and therefore it contains only simple and mixed micelles. In addition, Ch-supersaturated model biles of various compositions as given in Table 7.1 were used for comparison between the modified ultracentrifugation technique and gel chromatography. The compositions of the Ch-supersaturated model biles used in the statistical experimental study are given in Table 7.2. The compositions of these Ch-supersaturated model biles are all within the metastable two-phase region (see shaded region in Figure 1-5) above the one-phase micellar region, and therefore they

Table 7.1: Percent of total Ch and Ch/EYPC ratio in vesicles as measured by modified ultracentrifugation (MU) and gel chromatography (GC).

Model Bile			R_{Ch} (%)		Ch/EYPC	
Number	TLC (g/dL)	TC / TC+EYPC	MU	GC	MU	GC
1	3	0.7	23.6 ± 2.5 (8)	22.0 ± 2.0 (4)	1.53 ± 0.13 (8)	1.5 ± 0.2 (4)
2	3	0.6	20.1 ± 5.3 (8)	19.0 ± 2.0 (3)	1.05 ± 0.12 (8)	1.0 ± 0.3 (3)
3	1	0.6	93.9 ± 0.8 (2)	97.5 ± 0 (2)	0.35 ± 0.01 (2)	0.35 ± 0.06 (2)
4	6	0.6	41.7 ± 1.6 (5)	36.0 ± 0 (2)	1.49 ± 0.10 (5)	1.52 ± 0.08 (2)

Note: TLC: total lipid content, TC: taurocholate, Ch: cholesterol, EYPC: egg-yolk phosphatidylcholine. Ch-supersaturated model biles were subjected separately to modified ultracentrifugation (42,000 rpm, 37 °C, 16 wt% sucrose, 2 or 4 hrs) and gel chromatography (Superose 6, 37 °C). All model biles contain 10 mol% Ch except for number 4, which contains 13 mol% Ch. Results are given as mean ± standard deviation (number of replicates).

Table 7.2: Experimental conditions and measured responses for the 2^4 two-level factorial design.

Run	TLC (g/dL)	BS / BS+EYPC	mol% Ch	Bile Salt	R_{Ch} (%)	Ch/EYPC	Replicates
1	6	0.8	13	TC	50.3 ± 2.3	2.13 ± 0.15	4
2	1	0.8	13	TUDC	76.6 ± 2.3	1.15 ± 0	6
3	6	0.6	13	TUDC	66.6 ± 2.4	0.82 ± 0.10	5
4	1	0.6	13	TC	72.8 ± 5.7	0.67 ± 0.09	4
5	6	0.8	10	TUDC	75.2 ± 1.5	1.23 ± 0.08	6
6	1	0.8	10	TC	69.3 ± 4.0	1.60 ± 0.13	3
7	6	0.6	10	TC	13.8 ± 3.8	1.27 ± 0.34	4
8	1	0.6	10	TUDC	90.0 ± 1.9	0.37 ± 0	3
9	6	0.8	13	TUDC	89.1 ± 0.2	1.15 ± 0.02	3
10	1	0.8	13	TC	80.3 ± 3.1	1.41 ± 0.04	4
11	6	0.6	13	TC	41.7 ± 1.6	1.49 ± 0.10	5
12	1	0.6	13	TUDC	94.9 ± 3.2	0.45 ± 0.01	3
13	6	0.8	10	TC	39.6 ± 2.7	2.58 ± 0.26	5
14	1	0.8	10	TUDC	61.8 ± 3.2	0.95 ± 0.03	3
15	6	0.6	10	TUDC	46.3 ± 1.3	0.78 ± 0.02	3
16	1	0.6	10	TC	95.7 ± 2.2	0.35 ± 0.04	4

Note: TLC: total lipid content, BS: bile salt, EYPC: egg-yolk phosphatidylcholine, Ch: cholesterol, TC: taurocholate, TUDC: tauroursodeoxycholate. The distribution of cholesterol, R_{Ch}, is defined in Eq. (7.1). The measured responses, R_{Ch} and Ch/PL ratio, are given as mean ± standard deviation.

contain vesicles, mixed micelles, and simple micelles.

7.1.2 Modified Ultracentrifugation

The densities of the model biles were adjusted to approximately 1.06 g/mL by direct addition of 16 wt% sucrose [141]. Samples were centrifuged in 0.8-mL Ultra-Clear tubes (Beckman Instruments, Palo Alto, CA) at 42,000 rpm, 37 °C, for 2 or 4 hrs (Beckman L8-55 ultracentrifuge, SW50.1 horizontal swinging bucket rotor, maximum $g \approx 200{,}000$). Four fractions [top (50 – 100 μL), 100 μL, 200 μL, and remainder (200 – 350 μL)] were carefully withdrawn from the centrifuged solution, and their volumes were measured using a microsyringe. Note that, unlike the ultracentrifugation technique described in chapter 6, the precise volume of the top fraction is not so critical here. In the previous ultracentrifugation technique, the operating conditions are so selected that the top fraction is clear of mixed micelles and contains only vesicles. Accordingly, any volume that is larger than that required to include all the vesicles may be contaminated with mixed micelles. In the modified technique, however, the vesicular cholesterol content is estimated by subtracting the micellar cholesterol concentration from the measured cholesterol concentration in the top fraction. In this case, then, any cholesterol in the top fraction that is carried by mixed micelles will not be counted as vesicular cholesterol. As will be discussed in a later section, since the mixed micelles do not sediment significantly in the modified technique, the micellar cholesterol concentration can be estimated by the cholesterol concentration in the bottom fractions.

7.1.3 Separation of Vesicles and Mixed Micelles

For the TC-containing model biles, vesicles and mixed micelles were separated using either gel chromatography (Pharmacia HR10 / 30 Superose 6 column, Pharmacia - LKB, Piscataway, NJ), or modified ultracentrifugation as described above. Note that the two methods yielded comparable results, as will be shown later in the discussion of the modified ultracentrifugation technique. Indeed, in some experiments involving

TC model biles, both methods were used as a check. The general procedure for gel chromatography has been described in chapter 6. The IMC value for each model bile, which is required in the pre-equilibration buffer and the eluant, was measured using centrifugal ultrafiltration [42]. Modified ultracentrifugation was used exclusively for TUDC-containing model biles, since, as mentioned earlier, the vesicles are too large for gel chromatography to be implemented in this case.

7.2 Statistical Experimental Design

7.2.1 Response and Process Variables

There are two responses of interest: (i) the distribution of cholesterol between vesicles and mixed micelles, and (ii) the Ch/EYPC molar ratio in vesicles. The distribution of cholesterol, denoted as R_{Ch}, is expressed as

$$R_{Ch} = \frac{\text{Amount of cholesterol in vesicles}}{\text{Total amount of cholesterol in model bile}} \times 100\% \tag{7.1}$$

There are four physiological variables of interest: (1) total lipid content, (2) bile salt (BS) to EYPC molar ratio, expressed as BS/(BS+EYPC), (3) cholesterol content (mol% Ch), and (4) the type of bile salt. The first three variables define the composition of a model bile, and are expected to play a role in determining the responses described above. The type of bile salt is included in this study because native bile contains a mixture of bile salts. The two bile salts selected for this study, TUDC and TC, differ in their hydrophobicity [21], which should affect the solubilization of cholesterol in vesicles and mixed micelles. As will be discussed in the following paragraph, the values of these variables were set at either high or low levels, which are tabulated in Table 7.3. Note that the symbols, $\tilde{x}_i$ (i = 1 to 4), in Table 7.3 are assigned arbitrarily for notation purposes. The high and low levels were determined based on the physiological values found in native biles [21], and were chosen to encompass the widest ranges possible. There are other physiological variables, such as calcium concentration [89, 118] and protein content, that may play a role in

Table 7.3: High and low levels for the process variables.

Symbols	Variables	High	Low	Units
$\tilde{x}_1$	TLC	6	1	g/dL
$\tilde{x}_2$	BS/(BS+EYPC)	0.8	0.6	mole/mole
$\tilde{x}_3$	mol% Ch	13	10	mole %
$\tilde{x}_4$	Bile Salt Type	TUDC	TC	

Note: TLC: total lipid content, BS: bile salt, Ch: cholesterol, EYPC: egg-yolk phosphatidylcholine, TC: taurocholate, TUDC: tauroursodeoxycholate.

determining the distribution of cholesterol and the Ch/EYPC ratio. In particular, it has been suggested that protein concentration is related to the metastability of bile [31, 66, 158] and that certain proteins may promote or inhibit cholesterol nucleation in bile [20, 60, 94, 151]. A wealth of literature is available on this subject, and the interested reader is referred to Ref. [65] and references therein for further details.

7.2.2 Two-Level Factorial Design

The two-level factorial design is shown in Table 7.2. Since we have four variables, there are $2^4 = 16$ experimental runs in total. The design was divided into two blocks, each consisting of eight experimental runs; within each block, the experiments were performed in random order. As indicated in Table 7.2, replicate experiments were performed so that a standard deviation can be obtained for each experimental condition. The results obtained for this experimental design were analyzed using a regression analysis. However, in order to ensure that the estimated coefficients of the variables can be compared on an equal basis, the values of the variables were coded so that they became 1 and -1 for the high and low levels, respectively. This coding procedure also allows for the use of qualitative variables, which can be arbitrarily assigned a value of 1 or -1. In the present study, for example, TUDC and TC were represented as 1 and -1, respectively. From a physical point of view, the high and low levels for the type of bile salt can be thought of as representing the hydrophobicity of the bile salt. The coded variables are dimensionless and can be obtained using the following formula:

$$x_i = \frac{\tilde{x}_i - \frac{1}{2}(\text{high level} + \text{low level})}{\frac{1}{2}(\text{high level} - \text{low level})} \tag{7.2}$$

where $\tilde{x}_i$ (i =1 to 4) is the actual variable given in Table 7.3, and x_i (i = 1 to 4) is the corresponding coded variable, having a value of either 1 or -1 for the high and low levels, respectively. To estimate the effect of each variable, and the interactions among them, the following model was fitted to the data using the coded variables:

$$
\begin{aligned}
y \;=\; & \beta_0 + \beta_1 x_1 + \beta_2 x_2 + \beta_3 x_3 + \beta_4 x_4 \\
& + \beta_{12} x_1 x_2 + \beta_{13} x_1 x_3 + \beta_{14} x_1 x_4 + \beta_{23} x_2 x_3 + \beta_{24} x_2 x_4 + \beta_{34} x_3 x_4 \\
& + \beta_{123} x_1 x_2 x_3 + \beta_{124} x_1 x_2 x_4 + \beta_{134} x_1 x_3 x_4 + \beta_{234} x_2 x_3 x_4 \\
& + \beta_{1234} x_1 x_2 x_3 x_4 \qquad (7.3)
\end{aligned}
$$

where y is the response, that is, the distribution of cholesterol, R_{Ch}, or the Ch/EYPC ratio. The coefficient, β_i, reflects the individual effect of each variable, x_i, β_{ij}'s reflect the two-term interactions between variables x_i and x_j, and, similarly, β_{ijk}'s and β_{ijkl} reflect the three-term and four-term interactions, respectively. Note that the magnitude of the various coefficients reflect the relative importance of each variable as well as their interactions. The model fitting was performed using the SAS statistical software package (SAS Institute Inc., Cary, NC). However, since we are fitting sixteen runs to sixteen coefficients, this is equivalent to solving sixteen equations for sixteen unknowns (the various β's). The significance of each coefficient was assessed by estimating the confidence interval. For example, for the coefficient, β_i, the $(1-\alpha)$ confidence interval can be written as $\beta_i \pm t_{\nu,\alpha/2}\, S(\beta_i)$, where $t_{\nu,\alpha/2}$ is the abscissa value of the t distribution having a degree of freedom, $\nu = \sum_{j=1}^{m}(n_j - 1)$, and an upper tail probability of $\alpha/2$, m is the number of experimental runs ($m = 16$ in this study), n_j is the number of replicates at the j^{th} run, and $S(\beta_i)$ is the standard deviation of the coefficient, β_i. In a two-level factorial experiment, all the coefficients have the same standard deviation, which is equal to $(\sigma^2/2^k)^{1/2}$, where σ^2 is an estimate of the pure error variance, and k is the number of variables ($k = 4$ in this study). The pure error variance can be estimated as $\sigma^2 = \sum_{j=1}^{m}(n_j - 1)\sigma_j^2/\nu$, where σ_j is the standard deviation at the j^{th} experimental run [16]. If the confidence interval for a particular coefficient includes zero as a plausible value, then that coefficient was treated as insignificant. The confidence intervals were calculated using a level of significance of 95 %, that is, $\alpha = 0.05$.

7.3 Results

7.3.1 Modified Ultracentrifugation

As discussed in chapter 6, in ultracentrifugation, sedimentation of both simple micelles and mixed micelles may result in a bile salt depletion zone in the top fraction, causing a shift in thermodynamic state of the model bile and altering the distribution of cholesterol between vesicles and mixed micelles. A logical modification is therefore to reduce the mobility of the micelles in the centrifugal field, and then to subtract the background micellar cholesterol concentration from the measured cholesterol concentration in the top fraction. In principle, this may be achieved by adjusting the density of the suspending medium to match, at least approximately, that of the micelles, coupled with shortening the duration of centrifugation. Because of the reduced density difference between the micelles and the suspending medium, the micelles should not sediment appreciably even in a strong centrifugal field. The shorter duration of centrifugation should reduce the extent of sedimentation of micelles, particularly for simple micelles due to their small size. On the other hand, by increasing the density of the suspending medium, one also increases the density difference between the vesicles and the suspending medium, which should force the vesicles to float more rapidly to the top.

As shown in chapter 6, the density of mixed micelles falls between 1.05 and 1.07 g/mL. Therefore, as a first approximation, we adjusted the density to approximately 1.06 g/mL by direct addition of 16 wt% sucrose. A vesicle suspension (1 mg/mL total lipid, Ch:EYPC = 1:1) and a micellar bile (3 g/dL total lipid, 2 mol% Ch, TC/(TC+EYPC) = 0.7) were centrifuged with 16 wt% sucrose at 42,000 rpm and 37 °C for 2 hrs. Since the vesicle suspension contains only Ch/EYPC vesicles (no micelles), and, as mentioned earlier, the micellar bile contains only simple and mixed micelles (no vesicles) (see bottom one-phase region in Figure 1-5), this allows us to study the floatation of vesicles and the sedimentation of mixed micelles in a centrifugal field separately. The concentrations of cholesterol in the vesicle suspension and those of EYPC in the micellar bile are shown in Table 7.4. Note that 95 % of the

Table 7.4: Ch, EYPC, and TC distributions in vesicle suspension, micellar bile, and simple micellar solution, respectively, after centrifugation.

Fraction Volume (μL)	Vesicle Suspension [Ch] (mM)	Vesicle Suspension % Total Ch	Micellar Bile [EYPC] (mM)	Simple Micellar Solution [TC] (mM)
50 – 60 (Top)	6.7	95.3	10.6	8.4
100	0	0	10.5	8.6
200	0.1	4.7	10.8	8.6
265 – 320 (Remainder)	0	0	10.9	8.8

Note: the vesicle suspension and the micellar bile were centrifuged for 2 hrs with duplicate measurements. The simple micellar solution was centrifuged for 4 hrs with triplicate measurements. Centrifugation was performed with 16 wt% sucrose at 42,000 rpm and 37 °C; the average standard deviation is 0.2 mM.

total cholesterol is collected in the top fraction of the vesicle suspension. Since all the cholesterol is associated with vesicles, this indicates that almost all the vesicles have floated to the top under the stated conditions. In chapter 6, it was shown that when the density of the suspending medium is adjusted to 1.03 g/mL (8 wt% sucrose), only 73 % of total cholesterol is found in the top fraction after 2 hrs of centrifugation (see chapter 6). The increased percentage of cholesterol in the top fraction in the present study after the same duration of centrifugation is a result of the increased density difference between the vesicles and the suspending medium. On the other hand, the EYPC concentrations in the four fractions of the centrifuged micellar bile are very similar, demonstrating that, with 16 wt% sucrose and 2 hrs of centrifugation, the mixed micelles do not sediment significantly. Indeed, the duration had been extended to 4 hrs and only a slight increase ($\approx$ 0.5 mM) in EYPC concentration in the bottom fraction was observed (data not shown).

To study the sedimentation of simple micelles using 16 wt% sucrose, a simple micellar solution (11 mM TC) was centrifuged at 42,000 rpm and 37 °C for 4 hrs. The bile salt concentrations in the four fractions after centrifugation are also shown in Table 7.4. The concentration difference between the top and bottom fraction is only 0.4 mM, which implies that simple micelles are more or less unperturbed in the centrifugal field generated under the stated conditions. The fact that simple micelles do not move away from the top fraction, even after 4 hrs of centrifugation, should considerably reduce the effect of a bile salt depletion zone on the thermodynamic state of the model bile, and therefore prevent any significant shift of cholesterol between vesicles and mixed micelles.

These few studies on the mobility of individual biliary aggregates in a centrifugal field confirm the rationale behind the modification of the ultracentrifugal technique. Perhaps a more direct validation of this technique, however, is to compare the results obtained by this technique to those obtained by gel chromatography. Various Ch-supersaturated model biles with compositions given in Table 7.1 were subjected to gel chromatography and modified ultracentrifugation. The compositions of these model biles fall in the metastable two-phase region of the pseudo-ternary TC-EYPC-Ch

phase diagram [26] (see shaded region in Figure 1-5), and therefore they all contain both vesicles and mixed micelles. However, in modified ultracentrifugation, the top fraction of the centrifuged solution also contains mixed micelles, in addition to vesicles, and therefore part of the cholesterol content measured in the top fraction is associated with mixed micelles. Consequently, to estimate the amount of cholesterol in vesicles, the micellar cholesterol concentration is subtracted from the measured cholesterol concentration of the top fraction. Since, as shown earlier, the mixed micelles do not sediment significantly in modified ultracentrifugation, the micellar cholesterol concentration is taken as equal to the average cholesterol concentration of the bottom three fractions. As illustrated by the comparison in Table 7.1, the agreement between the two techniques is very satisfactory. Therefore, the modified ultracentrifugation technique is believed to yield compatible results, compared to gel chromatography, and can be used to estimate the distribution of cholesterol and the Ch/EYPC ratio in model biles.

7.3.2 Distribution of Cholesterol

The responses and their associated standard deviations measured at each experimental condition are tabulated in Table 7.2. As mentioned earlier, the model described in Eq. (7.3) was fitted to the data, and the values of the coefficients are shown in Table 7.5. The statistically insignificant coefficients are marked by a "x" in Table 7.5, based on a 95 % confidence interval as discussed earlier.

As shown in Table 7.5, within the range of investigation, the most significant physiological variable affecting the distribution of cholesterol is the total lipid content (x_1), with its coefficient, β_1, having a value of -13.68. Note that the coefficient, β_0, simply represents the average response of the sixteen runs. The fact that total lipid content is associated with a negative coefficient simply means that increasing the total lipid content reduces the percentage of cholesterol found in vesicles. The observed effect of increasing total lipid content on the distribution of cholesterol, R_{Ch}, may be a result of a decrease in the number of vesicles. It is well known that, in model bile, mixed micelles can solubilize more cholesterol as the total lipid content increases

Table 7.5: Estimated values of the coefficients for the distribution of cholesterol, R_{Ch}, and the vesicular Ch/EYPC ratio, obtained from the 2^4 design.

Coefficient	Estimate			
	R_{Ch}		Ch/EYPC	
β_0	66.50		1.15	
β_1	-13.68		0.28	
β_2	1.28	x	0.38	
β_3	5.04		0.01	x
β_4	8.56		-0.29	
β_{12}	9.45		-0.03	x
β_{13}	4.06		-0.04	x
β_{14}	7.91		-0.15	
β_{23}	1.26	x	-0.07	
β_{24}	-0.66	x	-0.12	
β_{34}	1.70		0.02	x
β_{123}	-4.21		-0.03	x
β_{124}	2.79		-0.03	x
β_{134}	-2.25		0	x
β_{234}	-0.83	x	0.07	x
β_{1234}	2.18		-0.01	x

Note: The values of the coefficients were obtained by fitting the model described in Eq. (7.3) to the data shown in Table 7.2. β_i is the coefficient for variable x_i, β_{ij} is the interaction between variables x_i and x_j, and so on. Ch: cholesterol, EYPC: egg-yolk phosphatidylcholine, x_1: total lipid content, x_2: BS/(BS+EYPC), x_3: mol% Ch, x_4: bile salt type. The insignificant coefficients are marked with "x".

[21]. In terms of the pseudo-ternary TC-EYPC-Ch phase diagram, this implies that the one-phase micellar region expands upon an increase of total lipid content, with its boundary moving towards the cholesterol apex (see bottom region in Figure 1-5). Accordingly, with a model bile containing a fixed percentage of bile salt, phospholipid, and cholesterol, corresponding to a fixed coordinate on the phase diagram shown in Figure 1-5, increasing the total lipid content results in a decrease in the relative proportion of vesicles compared to mixed micelles, and hence in a decrease in R_{Ch}. On the other hand, a decrease in R_{Ch} may also be a result of a reduced Ch/EYPC ratio in vesicles. However, as will be discussed later, increasing the total lipid content actually increases the Ch/EYPC ratio in vesicles, which implies that the decrease in R_{Ch} is most likely caused by an increase in the proportion of mixed micelles.

The second most important physiological variable in determining the distribution of cholesterol is the type of bile salt (x_4), with its coefficient, β_4, equal to 8.56. The positive value in this case indicates that switching from TC ($x_4 = -1$) to TUDC ($x_4 = 1$) results in an increase in R_{Ch}. This effect may be explained by the difference in hydrophobicity between TC and TUDC, and their interaction with EYPC molecules. The major difference between TC and TUDC is that TUDC contains a 7β-hydroxyl group, while TC contains a 7α-hydroxyl group. The presence of the 7α-hydroxyl group in TC results in the TC molecule having distinct hydrophobic and hydrophilic regions, since in this case, all three hydroxyl groups in the molecules reside on one side of the fused-ring structure. In contrast, a 7β-hydroxyl group in TUDC makes the molecule less distinctive regarding the hydrophobic and hydrophilic regions, rendering it more hydrophilic than TC, as measured by reverse-phase high-performance liquid chromatography [21]. In a TC-EYPC-Ch mixed micelle, the hydrophobic moieties of the EYPC molecules, which contain aliphatic chains of 16 to 18 carbons, interact favorably with the hydrophobic regions of the TC molecules. In a TUDC-EYPC-Ch mixed micelle, however, the interaction between EYPC and TUDC is less favorable, owing to the lower hydrophobicity of TUDC. Consequently, TUDC has a lower capability of incorporating EYPC into mixed micelles, causing the EYPC to form other microstructures in the solution, namely, Ch/EYPC vesicles.

In addition to the effects of individual variables, the interactions between two variables often play an important role in a process. What exactly does it mean by interaction? In the context of statistical experimental design, interaction means that the effect of one variable on a particular response is dependent on the level of other variables. Consider again Table 7.5. Among all the two-variable interactions, β_{12} has the largest value (9.45), followed by $\beta_{14} = 7.91$. This means that the effect of total lipid content (x_1) actually depends on the levels of BS/(BS+EYPC) (x_2) and on the type of bile salt (x_4). Table 7.6 shows the average values of R_{Ch} at the four combinations of x_1 and x_2, that is, [-1,-1], [-1,1], [1,-1], and [1,1]. The average value of R_{Ch} at each combination was calculated by averaging all R_{Ch} values having the corresponding combination of x_1 and x_2. For example, referring to Table 7.2, the average value of R_{Ch} at $[x_1,x_2]$ = [-1,-1] is equal to (72.8+90.0+94.9+95.7)/4. Note that when BS/(BS+EYPC) is at the high level ($x_2 = 1$ or $\tilde{x}_2 = 0.8$), the difference between the average values of R_{Ch} at high and low total lipid contents (x_1) is only 8.4. In contrast, when BS/(BS+EYPC) is at the low level ($x_2 = -1$ or $\tilde{x}_2 = 0.6$), this difference is 46.3. *In other words, reducing the total lipid content at a lower bile salt to phospholipid ratio results in a much more drastic increase in the percentage of vesicular cholesterol.* Also shown in Table 7.6 is the interaction between x_1 and x_4. As shown in the table, when the total lipid content is at the low level ($x_1 = 1$ or $\tilde{x}_1 = 1$ g/dL), switching from TC ($x_4 = -1$) to TUDC ($x_4 = 1$) does not seem to make much difference on the average R_{Ch} value, whereas at the high level of total lipid content ($x_1 = 1$ or $\tilde{x}_1 = 6$ g/dL), the average R_{Ch} value increases by 90 % upon switching from TC to TUDC. *This implies that switching the type of bile salt from TC to TUDC is much more effective at high total lipid content in increasing R_{Ch} than at low total lipid content.*

Although there are other coefficients, including β_3, β_{123}, and other two-term and three-term interactions, that are significant in the sense that their 95 % confidence intervals do not include zero as a plausible value, they are relatively less important when compared to the coefficients discussed above. For example, mol% Ch (x_3) can affect the distribution of cholesterol between vesicles and mixed micelles, since its

Table 7.6: Average values of the distribution of cholesterol, R_{Ch} (%), at various experimental conditions.

x_1	x_2		x_4	
	-1	1	-1	1
-1	88.4	72	79.5	80.8
1	42.1	63.6	36.4	69.3

Note: Each value corresponds to the average of four experimental runs having the same combination of the specified process variables. x_1: total lipid content, x_2: BS/(BS+EYPC), x_4: bile salt type.

coefficient, $\beta_3 = 5.04$, is statistically significant. However, comparing the magnitude of β_1 and β_3, one expects mol% Ch to have much less influence on the distribution of cholesterol compared to that of total lipid content, x_1. Similarly, the three-term interaction between total lipid content (x_1), BS/(BS+EYPC) (x_2), and mol% Ch (x_3) is statistically significant, since $\beta_{123} = -4.21$, but it is not as important as the two-term interaction between total lipid content (x_1) and BS/(BS+EYPC) (x_2). Because these variables and interactions are only of secondary importance, they will not be discussed any further.

7.3.3 Vesicular Ch/EYPC Ratio

The second response of interest in is the Ch/EYPC ratio in vesicles. Again, Eq. (7.3) was fitted to the data given in Table 7.2 as described before, and the values of the coefficients are tabulated in Table 7.5. The most important individual effect in this case is BS/(BS+EYPC) (x_2), with its coefficient, β_2, having a value of 0.38. This is followed by total lipid content (x_1) and the type of bile salt (x_4), with $\beta_1 = 0.28$ and $\beta_4 = -0.29$, respectively. The effects of the total lipid content and BS/(BS+EYPC) are probably due to a preferential incorporation of phospholipid, compared to cholesterol, in mixed micelles. As mentioned earlier, an increase in total lipid content results in the formation of a larger proportion of mixed micelles. Similarly, as BS/(BS+EYPC) increases, the mixed micelles may also be enriched with bile salt. In both cases, more EYPC molecules are needed in the mixed micelles in order to regulate the chain packing requirement in the aggregates. Consequently, more EYPC molecules may be drawn to mixed micelles, compared to cholesterol, because of the flexibility of their aliphatic chains. Since fewer EYPC molecules are available to form vesicles, the Ch/EYPC ratio in vesicles rises accordingly. Indeed, this preferential incorporation of phospholipid has been suggested in a previous study [67]. The effect of the type of bile salt on the vesicular Ch/EYPC ratio is also due to the difference in the interaction between TUDC and EYPC and that between TC and EYPC, as alluded to in the discussion of the distribution of cholesterol. The decreased hydrophobicity of TUDC makes the interaction between bile salt and EYPC in mixed micelles less fa-

vorable, pushes the EYPC molecules into vesicles, and lowers the vesicular Ch/EYPC ratio. Note that the effect of mol% Ch on vesicular Ch/EYPC ratio is very small ($\beta_3 = 0.01$), compared to other individual effects. However, one point to bear in mind is that the insignificance of mol% Ch in affecting the vesicular Ch/EYPC ratio may also be due to the fact that the selected range of mol% Ch is too narrow for this particular response.

The values of the coefficients in Table 7.5 also indicate that, when compared to the individual effects, all the two-variable interactions in this case are quite weak. The two relatively more significant two-variable interactions are between total lipid content (x_1) and the type of bile salt (x_4) ($\beta_{14} = -0.15$), and between BS/(BS+EYPC) (x_2) and the type of bile salt (x_4) ($\beta_{24} = -0.12$). The interactions among these variables are not too surprising, since total lipid content, BS/(BS+EYPC), and the type of bile salt are all quite important individually, as discussed above. The interactions between x_1 and x_4, and between x_2 and x_4 are shown in Table 7.7. The average value of the Ch/EYPC ratio at each combination of the variables was calculated in a similar manner as described in the case of R_{Ch}. As shown in Table 7.7, using TC as the bile salt ($x_4 = -1$), changing the total lipid content from 1 g/dL ($x_1 = -1$) to 6 g/dL ($x_1 = 1$) increases the average values of Ch/EYPC by 85 %, whereas with TUDC ($x_4 = 1$), the same change in total lipid content produces only a 37 % increase. *In other words, increasing total lipid content with TC can increase the vesicular Ch/EYPC ratio much more significantly than with TUDC.* Similarly, using TC as the bile salt ($x_4 = -1$), the average Ch/EYPC ratio increases by 103 % when BS/(BS+EYPC) is increased from 0.6 ($x_2 = -1$) to 0.8 ($x_2 = 1$), while only a 84 % increase is realized when TUDC ($x_4 = 1$) is used. *This shows that increasing the BS/(BS+EYPC) ratio is more effective in increasing the vesicular Ch/EYPC ratio with TC rather than TUDC.*

Finally, note that all the interactions involving three terms or more are statistically insignificant. This is consistent with the observation regarding the distribution of cholesterol, where higher-order interactions are relatively unimportant compared to individual effects and two-term interactions. Indeed, in most situations, three-terms

Table 7.7: Average values of the vesicular Ch/EYPC ratio at various experimental conditions.

x_4	x_1		x_2	
	-1	1	-1	1
-1	1.01	1.87	0.95	1.93
1	0.73	1.00	0.61	1.12

Note: Each value corresponds to the average of four experimental runs having the same combination of the specified process variables. x_1: total lipid content, x_2: BS/(BS+EYPC), x_4: bile salt type, Ch: cholesterol, EYPC: egg-yolk phosphatidylcholine.

and higher-order interactions can be neglected, which would require fewer runs in an experimental design. This is actually the rationale behind the so-called fractional factorial design, which is beyond the scope of this study. The interested reader is referred to Ref. 16 for further discussions on this subject.

7.4 Discussion

Using nucleation time as a response variable, previous studies [89, 158] have identified the importance of bile concentration, or equivalently of total lipid content, in cholesterol nucleation in bile. These findings suggested that increased total lipid content results in a decrease in nucleation time, that is, concentrated bile is more prone to cholesterol nucleation. In addition, Kibe and co-workers also found a dramatic decrease in nucleation time with increasing BS/PL ratio [89]. The relation between the metastability of bile and total lipid content and BS/PL ratio can also be seen by measuring the cholesterol thermodynamic activity [32, 103], which was found to increase with total lipid content and BS/PL ratio. This study reveals that total lipid content, indeed, plays an important role in determining the distribution of cholesterol, as well as the vesicular Ch/EYPC ratio. However, the effects on these two responses are opposite. Increasing total lipid content reduces the relative amount of cholesterol in vesicles compared to mixed micelles, but increases the vesicular Ch/EYPC ratio. On the other hand, increasing BS/(BS+EYPC) increases the vesicular Ch/EYPC ratio, but has no significant effect on R_{Ch}. Taking all these observations into consideration, it appears that nucleation time, or the metastability, of bile is more correlated to the vesicular Ch/EYPC ratio than to the distribution of cholesterol. In fact, by plotting the Ch/EYPC ratio versus R_{Ch}, it can be shown that no correlation seems to exist between R_{Ch} and the vesicular Ch/EYPC ratio. The effects of the type of bile salt on the distribution of cholesterol and Ch/EYPC ratio may be explained satisfactorily by the interactions between EYPC and bile salt. Specifically, hydrophobic bile salts such as TC interact more favorably with the hydrophobic moieties of EYPC, thus attracting more EYPC to mixed micelles. Consequently, switching from TUDC to

TC would result in a higher vesicular Ch/EYPC ratio and lower R_{Ch}.

Perhaps the most attractive feature of factorial experimental design is its ability to reveal interactions among the variables. A major advantage of identifying the interactions among the physiological variables is that one may be able to magnify, or reduce, the effect of one variable on a particular response by varying *other variables.* Take the vesicular Ch/EYPC ratio, for example. As revealed by this statistical experimental study, the most important physiological variable in determining the vesicular Ch/EYPC ratio is the ratio between bile salt and phospholipid. Intuitively, then, one would try to lower this ratio in order to attain a low vesicular Ch/EYPC ratio. However, the results of this study also indicate that the effect of BS/(BS+EYPC) depends on the type of bile salt. Consequently, instead of just significantly reducing BS/(BS+EYPC), which may not be feasible sometimes, another strategy is to lower BS/(BS+EYPC) and switch to a more hydrophobic bile salt simultaneously. A possible advantage of this strategy is that one may not need to change each variable by much, compared to varying just one variable, to achieve the same result.

As mentioned earlier, other physiological variables such as protein content and calcium concentration may also be important in determining the kinetics of cholesterol nucleation in bile. Although not included in the present study, the effect of these variables may also be investigated using factorial experiments, either as a separate study, or as an extension to the present study. To study only protein content and calcium concentration in a separate study is quite straight forward, since the methodology involved is identical to that described here. The disadvantage of a separate study involving only these two variables is that the interactions between protein content or calcium concentration and other variables such as bile salt to phospholipid ratio will be excluded. To incorporate protein content and calcium concentration as an extension to the present study, however, it may be more practical to employ fractional factorial design instead of a complete factorial design [16], since a complete design would require $2^6 = 64$ experimental runs. Fractional factorial design, as the name implies, is a fraction of the complete design. Using a fractional design can reduce the number of experimental runs required at the expense of information

involving higher-order interactions among the variables. However, as pointed out earlier, higher-order interactions are usually quite insignificant compared to individual effects and two-term interactions, and such a loss of information is therefore often tolerable.

The two-level factorial design presented in this study is not meant to reveal the detailed behavior of the response. Since each variable in the design is set at only two levels, this strategy cannot reveal possible nonlinear behaviors in the response surface. To study the nonlinear behavior of a particular response, at least three levels must be used for each variable in the design. There are a number of very efficient higher-order designs available in the literature, and the interested reader is referred to Ref. 16 for further details. As demonstrated in this study, two-level factorial design is a very powerful methodology in terms of identifying the relative importance of the variables and the interactions among them. If a functional relation is desired, however, then a two-level factorial design should serve only as a starting point for further investigation.

7.5 Concluding Remarks

In summary, this chapter has presented a systematic experimental study on the effects of various physiological variables on the distribution of cholesterol between vesicles and mixed micelles and the vesicular Ch/EYPC ratio. The main contribution of the work presented in this chapter is that one can compare quantitatively the relative importance of each physiological variable, and, more importantly perhaps, identify the interactions among these variables in determining the responses of interest. In particular, it was found that total lipid content has a significant but opposite effect on the distribution of cholesterol and on the vesicular Ch/EYPC ratio. Increasing the total lipid content reduces the percentage of cholesterol in vesicles while raising the vesicular Ch/EYPC ratio. The BS/(BS+EYPC) ratio is the most important variable in determining the vesicular Ch/EYPC ratio, but does not seem to be significant regarding the distribution of cholesterol. The hydrophobicity of bile salt affects both

the distribution of cholesterol and the vesicular Ch/EYPC ratio, presumably through the interactions with the hydrophobic moieties of the phospholipids. In addition, this study also reveals that the effect of total lipid content on the distribution of cholesterol depends strongly on the BS/(BS+EYPC) ratio as well as on the bile salt hydrophobicity, while the effect of the bile salt hydrophobicity on the vesicular Ch/EYPC ratio is dependent on the total lipid content and the BS/(BS+EYPC) ratio. The results of this experimental study not only are consistent with previous observations, but also illustrate the importance of understanding the interactions among the various physiological variables. Knowledge of these interactions should be helpful in cholesterol gallstone research. More specifically, as illustrated using the Ch/EYPC ratio as an example, one may be able to manipulate more than one physiological variable simultaneously in order to alter certain responses of interest. In addition to the distribution of cholesterol and the Ch/EYPC ratio, other responses may also be important. One of these responses may be the cholesterol thermodynamic activity in bile. As alluded to earlier, a significant correlation appears to exist between the cholesterol thermodynamic activity and the metastability of bile. Statistical experimental design can be used in this case to study how the cholesterol thermodynamic activity is affected by certain physiological variables, and what one should do to alter its value.

This chapter concludes the experimental studies of cholesterol solubilization in model bile. The following chapter will summarize the main results of this thesis, as well as discuss future research directions in the area of mixed surfactant systems.

Chapter 8

Conclusions and Future Research Directions

This thesis was motivated by several important theoretical and experimental aspects of vesicular systems. In the study of complex fluids, for example, mixed surfactant vesicles represent an important class of self-assembling microstructures. In industry, vesicles are currently being utilized as encapsulating devices for cosmetic products and food ingredients, and are also potentially important in the controlled delivery of drugs. In medicine, the formation of cholesterol gallstones is closely related to the formation of mixed vesicles in bile. All these important areas demand a better and more fundamental understanding of the formation and stability of mixed surfactant vesicles. The detailed findings pertaining to both the theoretical and experimental studies conducted as part of this thesis have already been covered at length in the previous chapters, and therefore, will not be repeated here. Instead, below, I will summarize the central elements and results of the work conducted as part of this thesis.

8.1 Thesis Summary

On the theoretical front, a detailed molecular-thermodynamic theory was developed in chapter 2 to describe the formation of mixed cationic/anionic surfactant vesicles.

The theory is based on a detailed modeling of the various free-energy contributions associated with vesiculation. The key elements of this theory include: (i) calculation of the free energy associated with packing of the surfactant tails in the vesicle hydrophobic region, which explicitly accounts for the vesicular geometry in the context of a mean-field approach, where the presence of finite curvature plays a major role in determining the distribution of molecules between the outer and inner vesicle leaflets, (ii) development of approximate expressions for the surface potentials of a charged vesicle, and their subsequent utilization in the evaluation of the vesicle electrostatic free energy, which greatly enhances the computational efficiency in the minimization of g_{ves}, and (iii) application of an equation of state for a two-dimensional hard-disk mixture, based on the scaled-particle theory, to model the steric repulsions between the surfactant heads, which provides a more accurate and realistic estimation of g_{steric}.

Because of this detailed molecular description, the theory permits one to gain considerable insight into the underlying mechanism of vesicle stabilization, including the relative importance of, and the interplay between, the various free-energy contributions to vesiculation. In addition, since the theory accounts explicitly for the molecular nature of a vesicle, it is applicable over the entire vesicle size range. Moreover, the theory also allows for possible extensions to account for the presence of other self-assembling structures possessing relatively small sizes, such as, mixed micelles. Using the CTAB/SOS mixture as an example in chapter 4, it was found that the molecular structure of the surfactants, indeed, plays a central role in a rigorous description of vesiculation. This is reflected by the importance of the distribution of molecules in the minimization of g_{ves} of finite-sized vesicles. In addition, by varying the tail-length asymmetry between the cationic and anionic surfactants, it was also found, in chapter 5, that energetically stabilized vesicles can form in highly asymmetric surfactant mixtures such as those containing CTAB and SPS. The formation of these small vesicles is mainly due to the ability of the shorter hydrophobic tails to cover the exposed hydrocarbon/water vesicle interfaces as the vesicle curvature increases, without incurring a high packing free-energy penalty. On the other hand, in mixtures such as those containing CTAB and SPDS, where the surfactant tail-

length asymmetry is small, g_{ves} of a finite-sized vesicle is always higher than that corresponding to a planar bilayer. In this case, vesicles are stabilized by the entropy of mixing, and they tend to be large and widely distributed in size. The theory also reveals that the optimum vesicle composition reflects a delicate balance between the entropic and energetic factors responsible for vesiculation. More specifically, as the surfactant tail lengths become comparable, the transfer free energy, g_{tr}, does not depend strongly on composition. This causes the entropic factor, which depends on the surfactant monomer concentrations, to become more dominant in determining the optimum vesicle composition. This situation is similar to that in which salt is added to a cationic/anionic surfactant mixture. In that case, the contribution from the energetic factor is decreased via a reduction in the electrostatic free-energy penalty.

On the experimental front, the research was more geared towards the medically relevant problem of cholesterol gallstone formation. I first performed a systematic comparison between two techniques currently used to separate vesicles and mixed micelles in bile: ultracentrifugation and gel chromatography (see chapter 6). The results show that ultracentrifugation overestimates the percentage of cholesterol in vesicles, mainly due to the formation of a bile salt depletion zone in the top fraction of the centrifuged solution, which is, in turn, caused by the sedimentation of simple and mixed micelles. In an attempt to develop a more reliable centrifugal separation method, the ultracentrifugation technique was modified by adjusting the density of the suspending medium to be similar to that of the micelles, thus minimizing the mobility of the micelles in a centrifugal field (see chapter 7). This modification significantly reduces the sedimentation of micelles, and considerably minimizes the artifactual elevation of vesicular cholesterol.

Using both modified ultracentrifugation and gel chromatography to separate the biliary aggregates, a factorial experimental study was performed to investigate the effects of four physiological variables, namely, total lipid content, bile salt to phospholipid ratio, cholesterol content, and the type of bile salt, on two responses: vesicle composition and the distribution of cholesterol between biliary aggregates. Among the four physiological variables examined, it was found that: (i) total lipid content

has a significant but opposite effect on the distribution of cholesterol and on the vesicular Ch/EYPC ratio, (ii) BS/(BS+EYPC) ratio is the most important variable in determining the vesicular Ch/EYPC ratio, but not in determining the distribution of cholesterol, and (iii) the hydrophobicity of bile salt affects both the distribution of cholesterol and the vesicular Ch/EYPC ratio, presumably through interactions with the hydrophobic moieties of the phospholipids. One advantage of the factorial experiments, as exemplified by the results obtained in this thesis, is that it can rank the variables according to their relative importance in determining the values of the responses, thus allowing us to understand quantitatively the contribution of each variable. More important, however, is the fact that factorial experimental studies are able to identify the interactions among these variables. In particular, significant interactions were found between total lipid content and the type of bile salt (or bile salt hydrophobicity) in both the distribution of cholesterol and the vesicular Ch/EYPC ratio. Knowing these interactions, one may be able to manipulate more than one physiological variable simultaneously in order to alter certain responses of interest, such as the vesicular Ch/EYPC ratio.

Although the findings summarized in the preceding paragraphs represent important contributions, both to the theoretical modeling and understanding of mixed surfactant vesicles, as well as to the experimental study of biliary systems, much work remains to be done in both areas. From a theoretical point of view, in spite of the details involved in the molecular modeling of mixed vesicles, there are still several aspects in the molecular-thermodynamic theory that would benefit from further improvement. From an experimental standpoint, the application of two-level factorial experiments described in this thesis can be viewed as a starting point for many future studies. And, finally, as mentioned in chapter 1, the theory developed in this thesis can, indeed, be applied to biliary systems, thus providing a theoretical basis in that area. Below, I will discuss in more detail some ideas for future theoretical and experimental research.

8.2 Future Directions for Theoretical Work

Future theoretical work may be broadly divided into two categories: (i) improvement of the molecular-thermodynamic theory developed as part of this thesis, and (ii) application of the theory to various systems. This section will discuss some of these issues in more detail.

8.2.1 Molecular Model of Vesiculation

As discussed in chapter 2, the free energy of vesiculation, g_{ves}, is composed of five free-energy contributions (see Eq. (2.4)). Various assumptions have been made in the evaluation of these free-energy contributions, and therefore, in an effort to improve this molecular model, an obvious starting point is to relax some of these assumptions. In the calculation of the transfer free energy, g_{tr}, for example, one needs to calculate the free energy associated with mixing the surfactant molecules in each leaflet, g_m (see Eq. (2.5) in chapter 2). In the present theory, g_m is calculated, as a first approximation, by assuming ideal mixing. The assumption of ideal mixing in each vesicle leaflet, however, may be restrictive in cases where specific interactions exist between the surfactant heads. Specific interactions between surfactant heads have, indeed, been proposed in previous studies [146, 147, 148] as a mechanism for energetic stabilization of small vesicles. Osborne-Lee and co-workers have suggested a simple treatment for nonideal mixing within mixed nonionic/anionic micelles [133]. In this treatment, the surface of the mixed micelle is represented by a planar lattice, and the lattice partition function is expressed as a function of the contact energy between the unlike components. Extending this treatment to vesicles, then, each vesicle leaflet may be represented by a planar lattice, and analogous expressions for the partition functions associated with each leaflet may be derived accordingly[1]. Although such treatment will invariably introduce more parameters, such as the contact energy, into the theory, it should be a feasible first step in accounting for nonideal mixing within

[1] A word of caution here is that nonideal mixing may also affect the calculation of some of the other free-energy contributions to vesiculation, since ideal mixing was also assumed in the present theory in the calculation of these free energies (see chapter 2).

each vesicle leaflet. The possibility of nonideal mixing would result in a constraint on the leaflet compositions (X_{oA} and X_{iA}), in addition to the constraint imposed by the mass balance in a vesicle as given in Eq. (F.4) in appendix F, which, in turn, would affect the distribution of molecules, f. In other words, in addition to satisfying Eq. (F.4) for a given value of F, the leaflet compositions will also depend on whether the unlike contact, that is, the contact between the heads of surfactants A and B, is more (or less) favorable than the pure-component contacts (A-A and B-B contacts). Consequently, the distribution of molecules, f, may be different as a result of this new mixing nonideality, compared to that corresponding to ideal mixing, and therefore, g_{ves}, which depends strongly on f, may also change accordingly.

In the present theory, the evaluation of the electrostatic free energy, g_{elec}, is based on the assumption that the nonlinear Poisson-Boltzmann equation provides an accurate relation between the surface potentials and the surface charge densities. As discussed in chapter 3, however, the PB equation itself is based on certain assumptions, one of which, in particular, is the assumption of point-sized ions. Neglecting the size of the ions in solution does not seem to be too restrictive, at least for entropically-stabilized vesicles, since their radii are usually larger than 300 Å[87], which is much larger than the size of a typical counterion ($\approx$ 1 or 2 Å). In the case of energetically-stabilized vesicles, however, where the vesicle radius is of the order of 50 Å, the size of the counterions may play a role. More importantly, however, is the fact that the neglect of ion size restricts the ability of the present theory to reveal the effect of different counterions on the vesicle properties and the phase behavior, a feature which has been observed experimentally [74]. Perhaps the simplest way to incorporate finite ion-size effects, within the context of the PB equation, is through the use of the Stern model [13]. In the Stern model, the macroion (in this case, the self-assembled microstructure) is surrounded by a layer of counterions, whose thickness reflects the radius of the counterion. Within this layer, referred to as the Stern layer, the electrostatic potential varies linearly with the spatial coordinate, while the spatial potential profile follows that prescribed by the PB equation outside this layer. By varying the thickness of the Stern layer, therefore, one can account for the fact that different

counterions have different sizes. The Stern model has, indeed, been applied to the modeling of ionic micelles [155, 156, 157], and its application to vesicles should be considered as the first step towards improving the accuracy of evaluating g_{elec}. Other totally different and more sophisticated approaches, such as those using the integral equation theory [11, 44, 134], may also be used in the treatment of the vesicle electrostatic free energy. However, these approaches involve rather complex computational procedures, and considerable effort may be required to incorporate them into the molecular-thermodynamic model described in this thesis.

Another aspect that may require further analysis is the steric free energy associated with the surfactant heads. Recall that, in the present theory, the surfactant heads are treated as hard disks, characterized by their cross-sectional area, $a_{h,k}$ ($k = A$ and B). This was acceptable in the present studies since the heads of all the surfactants examined are quite compact. However, this may not be appropriate in dealing with chain-like surfactant heads, as already mentioned in chapter 2. In particular, when this theory is applied to the model biliary system, where the vesicles are mainly composed of phosphatidylcholine and cholesterol (and a small amount of bile salt), the flexible choline heads of the phosphatidylcholine molecules also require special attention regarding their steric repulsions. One alternative in treating the steric free energy is to adopt the mean-field approach which was used for the calculation of the packing free energy, g_{pack}. In other words, one can view the flexible surfactant heads as being similar to the surfactant tails; namely, instead of packing tails in the vesicle hydrophobic region, the surfactant heads can be "packed" in the aqueous regions beyond the hydrocarbon/water vesicle interfaces. In this sense, therefore, the surfactant heads can be treated as short polymers grafted onto a surface [27, 28, 29, 114]. One disadvantage of this treatment, however, is the increased complexity with respect to the computational procedure, a problem also found in the tail-packing calculations. Recall, from chapter 2, that g_{pack} is generated for a fixed number of vesicle configurations, and that at any other configuration, g_{pack} is obtained by interpolation. The main reason for this procedure is the long time requirement in the computation of g_{pack}, which is, in turn, due to the fact that one has to enumerate a large number of

chain conformations, as discussed in chapter 2.

8.2.2 Entropy of Mixing, G_m, and Interaction Free Energy, G_{int}

Another important area that requires further consideration is the evaluation of the entropy associated with mixing the vesicles, monomers, and water molecules, as well as the characterization of the interactions among these entities. As stated in chapter 2, the present theory incorporates the ideal entropy of mixing, and neglects the inter-aggregate interactions, mainly due to the fact that the systems of interest are very dilute. When the condition of a dilute system is no longer valid, however, one must modify the modeling approach for G_m and G_{int} in order to obtain a more realistic description of the vesicle suspension. Such a situation may arise when the theory is applied to the model biliary system, where the total concentration of the lipid components (bile salt, phospholipid, and cholesterol) can be higher than 10 g/dL. The entropy of mixing in a vesicle suspension can, in fact, be rather complex. Since the size difference between the vesicles, the surfactant monomers, and the water molecules is quite large, the ideal mixing model, which depends only on the number concentrations of the various species, may not be appropriate in this case. Other entropy models have been used in previous studies of micellar solutions [81, 122, 124, 139], and they may be adapted to estimate the entropy of a vesicle suspension as a starting point. Another approach in the estimation of G_m is to treat the various species as hard spheres of different sizes. Adopting this point of view, theories describing mixtures of hard spheres may be applied in the calculation of G_{mix} [84, 122, 150].

In addition to calculating G_m, the hard-sphere representation is also useful in estimating the interaction free energy, G_{int}, among the various species. In this case, the vesicles can be treated as individual colloidal particles[2], and the methodologies often used in the analysis of colloidal stability can be applied here [172, 176]. More

[2]As a first approximation, the interactions involving the surfactant monomers may be neglected due to their small size compared to that of vesicles.

specifically, G_{int} can be approximated by the potential energy acting among these particles through a background of water. This potential is, indeed, the so-called potential of mean force [105], and its calculation depends on the pair potential functions describing the interactions between the various species. When water is treated as a background, the pair potential functions between the various species are "effective" pair potential functions in the sense that they are acting through a medium (water) instead of through vacuum. Borrowing concepts from the studies of colloidal stability, then, the DLVO (Derjaguin-Landau-Verwey-Overbeek) potential can be used as a first approximation [171]. Simply speaking, the DLVO potential is composed of an attractive part and a repulsive part. The attractive component, which is usually modeled as a van der Waals attraction, tends to bring the particles together. On the other hand, the repulsive component, which may include electrostatic repulsions, tends to push the particles apart. Consequently, the interactions among the various species will depend on the relative magnitudes of these two components in the pair potential function, as well as on the distances between the particles. Although this particle-level treatment is quite promising in an attempt to account for the interactions among the vesicles in a vesicle suspension, its accuracy will depend on the proper modeling of the pair potential functions. A detailed discussion on this subject, however, is beyond the scope of this chapter, and the interested reader is referred to Refs. 105 and 171 for additional information.

8.2.3 Global Phase Behavior of Surfactant Mixtures

In addition to improving the molecular-thermodynamic theory, as discussed in the preceding sections, future theoretical work may also include the application of the theory to other surfactant mixtures. Within this category of future work, the most important and interesting undertaking, I believe, should be the incorporation of other microstructures, such as, mixed micelles, into the theory, so that one can study the global phase behavior of a surfactant mixture. In the discussion of energetically-stabilized vesicles in chapter 5, I emphasized the point that the theory does not predict the actual formation of small vesicles in those systems. Indeed, in order to

predict what microstructures will actually form in a given surfactant mixture, the theory should also be able to predict the free energies of formation of other possible microstructures, such as, mixed micelles, so that these can then be compared with each other. A nice feature of the present theory, which has already been alluded to in chapter 1, is that it is capable of incorporating other microstructures, regardless of their sizes. Accordingly, the first step in this direction should be the application of the theory to mixed micelles, which can then be incorporated in the study of the global phase behavior of surfactant mixtures. The application to mixed micelles is quite straightforward, since the free-energy contributions associated with vesiculation are also found in mixed micellization.

8.2.4 Application to the Biliary System

The incorporation of mixed micelles is not only important in the general areas of colloid and interface science and complex fluids, but also in the theoretical study of the biliary system. This point should be quite clear by now, considering the fact that, as discussed in chapter 1, bile contains both mixed micelles and vesicles, which share the task of solubilizing cholesterol. More importantly, by incorporating the formation of mixed micelles into the theory, the free energy of model bile, and hence the chemical potential of cholesterol, can be calculated. Why do we want to calculate the chemical potential of cholesterol in model bile? Medical researchers have been trying to find an index that can clearly distinguish between normal bile and abnormal bile with respect to their susceptibilities towards cholesterol gallstone formation. From a clinical standpoint, the advantage of having such an index is that preventive measures may be taken before the actual formation of cholesterol gallstones. Even if prevention is not feasible, a high-risk patient can be monitored more regularly so that early detection of cholesterol gallstones may be possible, which, in turn, should greatly facilitate any medical treatments. Cholesterol supersaturation in bile was initially believed to be a sufficient requirement for cholesterol nucleation [2], which led to the use of the cholesterol supersaturation index (CSI) [23, 26] as a standard measure of the supersaturation in both native and model biles. In 1973, however,

Holzbach and co-workers [79] studied the biliary cholesterol contents of 80 individuals and found that about 70 % of the normal individuals had supersaturated biles. This demonstrated that supersaturation alone does not provide a clear indication of the susceptibility towards cholesterol gallstone formation.

Since nucleation is the first step in the birth of a crystal, it is reasonable to expect that the nucleation rate should be an effective indicator of cholesterol gallstone formation. In 1979, Holan and co-workers [78] devised the so-called "nucleation time" measure (see chapter 6 for the definition)[3], and it has been used in many studies to characterize the metastability of biles [32, 66, 89, 131]. However, measurements involving nucleation are particularly prone to error due to sample contamination, and extreme care is necessary to obtain accurate results. The statistical nature of nucleation also calls for many repeated measurements, which makes the routine use of nucleation time as an index of metastability rather tedious.

Thermodynamic principles of phase equilibrium imply that the chemical potential of cholesterol constitutes the major driving force for cholesterol crystal nucleation in bile [104]. Indeed, cholesterol monomer activity, a measure of cholesterol chemical potential, appears to better reflect the propensity for cholesterol crystal nucleation than the widely used CSI [32, 103]. Consequently, if one can calculate the chemical potential of cholesterol in bile, it may be used as a rigorous index of bile metastability. Since chemical potential is a fundamental thermodynamic quantity, its value should be independent of the experimental procedures used. This, in turn, should allow for results obtained from various studies to be compared on a common basis.

8.3 Future Directions for Experimental Work

The factorial experimental design described in chapter 7 represents an initial step towards a systematic investigation on the formation of cholesterol gallstones in bile. Further experimental efforts are required to shed more light on the mechanism of

[3]Note that the nucleation time, as defined here, does not really measure the true time for the appearance of a *nucleus*, since by the time that a crystal is observed, considerable crystal growth may have already occurred [93].

cholesterol gallstone formation in bile, which may eventually provide guidelines for the treatment and prevention of this disease. Below, I will discuss some of the future steps that may be taken to advance our knowledge in this area.

8.3.1 Non-Linear Behavior — Higher-Order Design

As discussed in chapter 7, a two-level factorial design is unable to reveal any nonlinear behavior in the response surface. To obtain more detailed information on the response surface, therefore, higher-order designs are necessary. For example, to study the quadratic behavior of the variables, at least three levels are required in the design. However, increasing the number of levels also implies that one has to perform more experimental runs. For four variables, for example, $3^4 = 81$ experimental runs are required. This large number of experimental runs makes a complete three-level design rather impractical. Indeed, a more efficient approach in higher-order design is the so-called fractional factorial design [16], which has been referred to in chapter 7. A fractional factorial design requires only a fraction of the number of experimental runs needed in a complete design. The rationale behind such a strategy is that, as discussed in chapter 7, interactions involving three variables or more are usually unimportant, and therefore it is not critical for an experimental design to be able to reveal the information regarding these interactions. Because the information available in a fractional design is usually not as well-defined as that in a complete design, however, additional efforts may be required to interpret the data. Nevertheless, a fractional, higher-order design should provide us with valuable information on the response surface, and should, therefore, be an important next step following the two-level design described in this thesis. Many higher-order designs, such as the central-composite design [17] and the Box-Behnken design [15], are available in the literature, and the interested reader is referred to the cited references for further details.

8.3.2 Thermodynamic Activity of Cholesterol

The thermodynamic activity of cholesterol is basically a measure of the cholesterol chemical potential in bile, whose importance in the study of cholesterol gallstone formation has already been discussed in the preceding section on future theoretical work. Because of its fundamental significance and its close relation to the nucleation of cholesterol, it is important to understand how the various physiological variables affect its value. Experimental techniques have been developed recently to measure cholesterol monomer activity in bile [32, 76, 85, 103, 131], which allows us to apply the experimental design methodology in this case, using the measured cholesterol monomer activity as a response. This study should begin with a two-level factorial study in order to identify the most important variables, and then proceed with higher-order designs as described above. The main objective in this study is to find out how cholesterol monomer activity responds to changes in the physiological variables of interest, so that one may be able to alter its value in an effort to lower the propensity towards cholesterol nucleation.

As more cholesterol monomer activity data are collected, one may be able to develop a statistical model to describe the relation between cholesterol monomer activity and the physiological variables involved. Such a statistical model is useful in the sense that it can predict, within the range of investigation, the cholesterol monomer activity for a given condition, and should therefore provide a powerful tool in the prevention of cholesterol gallstones. In this statistical modeling effort, however, it is important that the responses be measured at conditions other than those prescribed in the factorial design. This is to ensure that the statistical model so developed can describe the behavior of the response as broadly as possible, since data measured in two- and three-level factorial experiments only permit the fitting of up to quadratic terms in the statistical model.

8.4 Concluding Remarks

The work presented in this thesis represents a significant effort in advancing our knowledge in the area of mixed surfactant systems and the formation of cholesterol gallstones in bile. The findings obtained in this thesis should contribute to our theoretical understanding of the formation of mixed surfactant vesicles, as well as to our experimental knowledge on cholesterol solubilization in bile. It is also hoped that this thesis will serve as a gateway for further studies, both theoretical and experimental, in the area of mixed surfactants that will prove to be challenging and rewarding for future generations of researchers.

Appendix A

Size and Composition Distribution

Consider a vesicle suspension formed by mixing two surfactant components, A and B, with water. The vesicle suspension, which now contains vesicles of all sizes and compositions, can be viewed as a multi-component system, whose total Gibbs free energy can be written as

$$G = N_w\mu_w + N_{1A}\mu_{1A} + N_{1B}\mu_{1B} + \sum_{n,F} N_{n,F}\mu_{n,F} \tag{A.1}$$

where N_w, N_{1A}, and N_{1B} are the number of water molecules, A monomers, and B monomers, respectively, μ_w, μ_{1A}, and μ_{1B} are the corresponding chemical potentials, and $N_{n,F}$ and $\mu_{n,F}$ are the number and chemical potential of vesicles characterized by aggregation number, n, and composition, F. Note that, in Eq. (A.1), vesicles characterized by a particular set of n and F values are treated as separate solute species [38, 173], and that the summation runs over all n and F. At equilibrium at constant temperature and pressure, the total Gibbs free energy, G, attains a minimum with respect to variations in N_w, N_{1A}, N_{1B}, and $N_{n,F}$, that is, $\delta G = 0$. Accordingly,

$$\delta G = \mu_w\delta N_w + \mu_{1A}\delta N_{1A} + \mu_{1B}\delta N_{1B} + \sum_{n,F} \mu_{n,F}\delta N_{n,F} = 0 \tag{A.2}$$

For a system containing a given amount of water, and surfactant components A and B, N_w, N_A, and N_B are constant. Accordingly,

$$\delta N_w = 0 \tag{A.3}$$

$$\delta N_A = \delta N_{1A} + \sum_{n,F} nF\delta N_{n,F} = 0 \tag{A.4}$$

$$\delta N_B = \delta N_{1B} + \sum_{n,F} n(1-F)\delta N_{n,F} = 0 \tag{A.5}$$

Substituting Eqs. (A.3), (A.4), and (A.5) in Eq. (A.2), yields

$$-\mu_{1A}\sum_{n,F} nF\delta N_{n,F} - \mu_{1B}\sum_{n,F} n(1-F)\delta N_{n,F} + \sum_{n,F}\mu_{n,F}\delta N_{n,F} = 0 \tag{A.6}$$

or

$$\sum_{n,F}[\mu_{n,F} - nF\mu_{1A} - n(1-F)\mu_{1B}]\delta N_{n,F} = 0 \tag{A.7}$$

Since $\delta N_{n,F} \neq 0$, Eq. (A.7) indicates that, at equilibrium, the following relation is satisfied

$$\frac{\mu_{n,F}}{n} = F\mu_{1A} + (1-F)\mu_{1B} \tag{A.8}$$

Using the assumptions of ideal mixing and negligible interactions, the chemical potentials of the solute species involved can be expressed as

$$\mu_{1A} = \mu^o_{1A} + kT\ln X_{1A} \tag{A.9}$$

$$\mu_{1B} = \mu^o_{1B} + kT\ln X_{1B} \tag{A.10}$$

$$\mu_{n,F} = \mu^o_{n,F} + kT\ln X(n,F) \tag{A.11}$$

where μ^o_{1A}, μ^o_{1B}, and $\mu^o_{n,F}$ are the standard-state chemical potentials of surfactant A monomers, surfactant B monomers, and vesicles characterized by n and F, respectively, and X_{1A}, X_{1B}, and $X_{n,F}$ are the corresponding mole fractions. Substituting Eqs. (A.9), (A.10), and (A.11) in Eq. (A.8), denoting $\mu^o_{n,F}/n$ as $\tilde{\mu}^o_{n,F}$, and rearranging, one obtains Eq. (2.2) in chapter 2.

The above derivation for the vesicle size and composition distribution in a vesicle

suspension is, indeed, identical to that for the case of a two-component mixed micellar system. This reflects the fact that, in both cases, the self-assembling aggregates, that is, vesicles and mixed micelles, are treated as individual solute species regardless of their internal structures. In this sense, then, the difference between vesicles and mixed micelles comes at the level of the standard state, that is, at the level of the free energy of vesiculation or micellization, in which the internal structures of these aggregates are explicitly accounted for. The main difference between vesiculation and micellization is that there are two aggregated environments in a vesicle (the outer and inner leaflets), while there is only one in a mixed micelle. Consequently, as the monomers assemble to form a vesicle, they can, in principle, go into either the outer or inner leaflet. However, as stated in chapter 2, the free energy of vesiculation, g_{ves}, is calculated as an explicit function of n and F only, and the other independent variables, X_{oA}, f, and t_b, are determined by minimizing g_{ves} before hand. This is actually a simplifying approximation. In other words, it is assumed that the distributions in X_{oA}, f, and t_b are so narrow that all the vesicles having the same aggregation number, n, and composition, F, will have identical values of X_{oA}, f, and t_b. The monomers will therefore distribute between the two leaflets as they assemble to form an isolated vesicle, such that the chemical potential of component k is the same in the outer and inner leaflets. This is, in fact, equivalent to treating an isolated vesicle as a system containing two "phases" (the outer and inner leaflets). At equilibrium, where the Gibbs free energy attains its minimum value, the chemical potential of any component must then be identical in all phases.

Appendix B

Chain Packing in a Vesicle

The packing of surfactant tails in a vesicle is somewhat different from that in a micelle or planar bilayer. Unlike a micelle, a vesicle contains two hydrocarbon/water interfaces on which the surfactant tails can anchor, and unlike a planar bilayer, the compositions of the outer and inner leaflets of a vesicle need not be the same. Consequently, the average conformation of a molecule in the outer leaflet can be different from that in the inner leaflet. In an attempt to facilitate the calculation of the packing free-energy contribution, some useful expressions specific to a finite-radius vesicle are presented in this appendix,

Consider Eq. (2.12) in chapter 2. Instead of solving this integral equation, Eq. (2.12) can be discretized to a finite number of layers in the vesicle bilayer. Thus, suppose that the vesicle bilayer is divided into L layers of identical thickness, t_v, between R_o and R_i. One can then rewrite Eq. (2.12) as

$$\sum_{k=A,B} [f X_{ok} \langle \phi_{ok}(i) \rangle + (1-f) X_{ik} \langle \phi_{ik}(i) \rangle] = m(i) \tag{B.1}$$

where $\langle \phi_{ok}(i) \rangle$ ($\langle \phi_{ik}(i) \rangle$) is the configurational-average segment volume in layer i due to component k in the outer (inner) leaflet, and $m(i)$ is the volume available in layer i. The configurational-average segment volumes can be expressed more explicitly as

follows

$$\langle \phi_{ok}(i) \rangle = \sum_{\alpha_k} P(\alpha_k) \phi_{ok}(\alpha_k, i) \tag{B.2}$$

$$\langle \phi_{ik}(i) \rangle = \sum_{\xi_k} P(\xi_k) \phi_{ik}(\xi_k, i) \tag{B.3}$$

where α_k and ξ_k denote the conformation of component k in the outer and inner leaflets, respectively. The volume available in layer i can be expressed as

$$\begin{aligned} m(i) &= \int_{r_i}^{r_i+t_v} a(r)dr \\ &= \int_{r_i}^{r_i+t_v} \frac{3v_t r^2}{R_o^3 - R_i^3} dr \end{aligned} \tag{B.4}$$

where $v_t = Fv_A + (1-F)v_B$ is the volume per molecule in the hydrophobic region, and v_A and v_B are the tail volumes of components A and B, respectively. Using the relation $r_i = R_i + (L-i)t_v$, Eq. (B.4) can be reduced, after some rearrangement, to the following expression

$$m(i) = \frac{v_t}{\gamma^2 + 3\gamma + 3} \left\{ \frac{3}{L} + \frac{3\gamma}{L^2}(2L - 2i + 1) + \frac{\gamma^2}{L^3}[3(L-i)(L-i+1) + 1] \right\} \tag{B.5}$$

where $\gamma = t_v/R_i$ accounts for the curved geometry of a vesicle bilayer. Note that, as $R_i \to \infty$, that is, as the vesicle bilayer becomes planar, $\gamma \to 0$, and $m(i) = v_t/L$, which is uniform throughout the bilayer and independent of the vesicle radius.

The probability of conformation, α_k, can be written, in the discretized form, as [159, 160]

$$P(\alpha_k) = \frac{1}{y_{ok}} \exp\left[-\beta\epsilon(\alpha_k) - \beta \sum_{i=1}^{L} \pi(i)\phi_{ok}(\alpha_k, i) \right] \tag{B.6}$$

where y_{ok} is the partition function for component k in the outer leaflet, $\beta = 1/kT$, and $\pi(i)$ is the so-called lateral pressure in layer i. A corresponding expression can be written for the probability of conformation, ξ_k, in the inner leaflet. Substituting Eqs. (B.2), (B.3), (B.5), and (B.6) in Eq. (B.1), one obtains L equations and L

unknowns, that is, $\pi(i), i = 1 \ldots L$ [1]. In this study, all the possible conformations of a tail are enumerated using the rotational isomeric state model [53]. Note, however, that in a vesicle bilayer, the segment volume distribution in the outer leaflet, $\phi_k(\alpha_k, i)$, is not necessarily the same as that in the inner leaflet, $\phi_k(\xi_k, i)$, even though α_k and ξ_k denote the same bond sequence and orientation of a molecule of component k. Consequently, in evaluating the configurational-average segment volumes using Eqs. (B.2) and (B.3) in the solution of Eq. (B.1), $\langle\phi_{ok}(i)\rangle$ and $\langle\phi_{ik}(i)\rangle$ must be calculated separately.

As indicated in chapter 2, the present theory explicitly accounts for the curvature of a vesicle bilayer in the calculation of the packing free energy, g_{pack}. However, the predicted results presented in chapter 4 indicates that the vesicles formed by CTAB and SOS are indeed quite large, and their configuration closely resembles that of a planar bilayer. This may justify the approximation of the vesicle bilayer by a planar bilayer in the calculation of the packing free-energy contribution. A two-component planar bilayer can be characterized by only two variables: thickness and composition. The packing free energies of a planar bilayer containing C16 and C8 tails are shown in Table B.1 as well as in Figure B-1, as a function of the thickness of the hydrophobic region, t_b, and the composition, F. As shown in Figure B-1, the bilayer packing free energy, g^{∞}_{pack}, rises sharply towards small values of F and large values of t_b. This sharp rise is due to the fact that as the bilayer becomes thicker and more depleted in the longer C16 chains, it is more difficult to satisfy the uniform-density constraint. In other words, the shorter C8 chains have to stretch more and locate themselves in the proper orientations so as to reach the center of the bilayer. This, in turn, results in a significant loss of entropy, and therefore in an increase in packing free energy. On the other hand, as the bilayer becomes thinner and richer in C16 chains, g^{∞}_{pack} also increases slightly. This small increase in g^{∞}_{pack} is mainly due to an increase in the internal energy of the chains, which is a result of an increased number of gauche bonds required to fit the longer C16 chains in a thinner bilayer. A statistical model of the

[1] As explained in Ref. 159, there are, indeed, only $L - 1$ independent equations, due to the conservation of chain volume.

free-energy surface shown in Figure B-1 has been fitted using a stepwise-regression analysis. Specifically, this yields

$$\begin{aligned} g_{pack}^{\infty} &= 5.836F^4 - 19.241F^3\tilde{t_b} + 33.503F^2\tilde{t_b}^2 - 24.630F\tilde{t_b}^3 + 7.935\tilde{t_b}^4 \\ &\quad - 12.606F^2\tilde{t_b} + 11.764F\tilde{t_b}^2 - 5.371\tilde{t_b}^3 + 2.84F^2 + 0.545 \end{aligned} \tag{B.7}$$

where g_{pack}^{∞} is the packing free energy of a planar bilayer, $\tilde{t_b} = t_b/\ell_{A,max}$ is the scaled bilayer thickness, and $\ell_{A,max}$ is the fully-extended length of a C16 chain ($\approx$ 20.5 Å). Although not used in the present study, Eq. (B.7) can be adopted to simplify the calculation of g_{pack}, at least in the large-radius limit. Note that Eq. (B.7) is *strictly* valid within the range of bilayer thicknesses between 12 and 22 Å, and a range of compositions between 0.1 and 1.0.

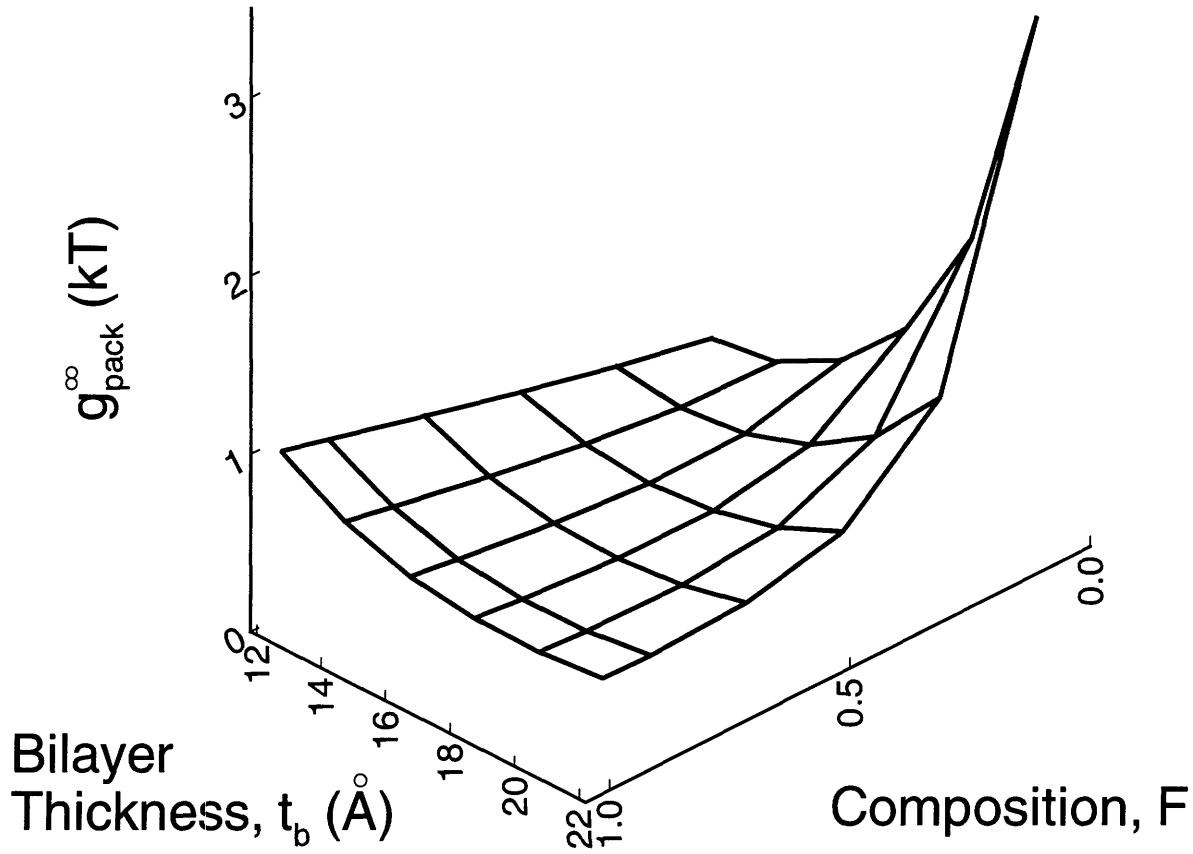

Figure B-1: Predicted variation of the packing free energy of a planar bilayer, g^{∞}_{pack}, containing C16 and C8 tails as a function of vesicle composition, F, and bilayer thickness, t_b.

Table B.1: Packing free energy of a planar bilayer, g^{∞}_{pack} (kT/molecule), containing C16 and C8 tails as a function of the vesicle composition, F, and the bilayer thickness, t_b. The vesicle composition is defined as the fraction of C16 in the vesicle.

Vesicle	Bilayer Thickness, t_b, (Å)					
Composition, F	12	14	16	18	20	22
0.1	0.374	0.426	0.617	0.980	1.665	3.094
0.3	0.487	0.440	0.476	0.598	0.826	1.230
0.5	0.616	0.507	0.470	0.500	0.587	0.750
0.7	0.754	0.597	0.517	0.504	0.528	0.622
0.9	0.895	0.699	0.587	0.548	0.553	0.601
1.0	0.967	0.753	0.628	0.578	0.572	0.608

Appendix C

Steric Free Energy

The scaled-particle theory equation of state for a hard-disk mixture can be written as [56]

$$\frac{\Pi}{\rho kT} = \frac{1}{1-\eta} + \frac{\pi}{4\rho}\frac{(\sum_k \rho_k d_k)^2}{(1-\eta)^2} \tag{C.1}$$

where Π is the surface pressure, d_k and ρ_k are the hard-disk diameter and number density of component k, respectively, $\rho = \sum_k \rho_k$ is the total number density of the system, and η is the packing fraction of the system, defined as

$$\eta = \frac{\pi}{4}\sum_k \rho_k d_k^2 \tag{C.2}$$

Note that Eq. (C.1) accounts only for repulsions between the hard disks. The packing fraction, η, can also be expressed as $\eta = N\bar{a}_h/A$, where N is the total number of molecules, A is the total area, and $\bar{a}_h$ is the molar-average hard-disk area, defined as

$$\bar{a}_h = \sum_k X_k a_{h,k} \tag{C.3}$$

where X_k and $a_{h,k} = \pi d_k^2/4$ are the mole fraction and hard-disk area of component k, respectively. Equation (C.1) can now be rewritten as

$$\frac{\Pi}{\rho kT} = 1 + \frac{NA\bar{a}_h - N^2\bar{a}_h^2 + \pi NA\bar{d}^2/4}{(A - N\bar{a}_h)^2} \tag{C.4}$$

where the molar-average hard-disk diameter, $\bar{d}$, is defined as

$$\bar{d} = \sum_k X_k d_k \tag{C.5}$$

Applying Eq. (2.21) in chapter 2 to the outer steric-repulsion surface, and using Eq. (C.4) and the definition $\Pi^{id}/\rho kT = 1$, one obtains

$$g_{steric,o} = -kT \int_{\infty}^{A_o} \frac{(N_o \bar{a}_{ho} - N_o^2 \bar{a}_{ho}^2/A_o + \pi N_o \bar{d}_o^2/4)}{(A_o - N_o \bar{a}_{ho})^2} dA_o \tag{C.6}$$

where $g_{steric,o} = G_{steric,o}/N_o$ is the outer steric free energy per molecule in the outer leaflet, $G_{steric,o}$ is the total outer steric free energy, $N_o = nf$ is the number of molecules in the outer leaflet, $\bar{a}_{ho} = \sum_{k=A,B} X_{ok} a_{h,k}$ is the outer molar-average hard-disk area, and $\bar{d}_o = \sum_{k=A,B} X_{ok} d_k$ is the outer molar-average hard-disk diameter. The integration in Eq. (C.6) can be carried out readily to yield

$$g_{steric,o} = kT \left[\frac{\pi \bar{d}_o^2/4}{a_o' - \bar{a}_{ho}} - \ln\left(1 - \frac{\bar{a}_{ho}}{a_o'}\right) \right] \tag{C.7}$$

An expression similar to Eq. (C.7) can be written for the inner leaflet, that is

$$g_{steric,i} = kT \left[\frac{\pi \bar{d}_i^2/4}{a_i' - \bar{a}_{hi}} - \ln\left(1 - \frac{\bar{a}_{hi}}{a_i'}\right) \right] \tag{C.8}$$

In Eqs. (C.7) and (C.8), a_o' (a_i') is the area per molecule at the outer (inner) steric-repulsion surface. Note that, although the hard-disk area, $a_{h,k}$, and diameter, d_k, depend only on the structures of the surfactant molecules, the corresponding molar-average quantities for the outer and inner leaflets can be different since X_{ok} and X_{ik} need not be the same. Finally, the steric free energy per molecule in the vesicle can be expressed as

$$g_{steric} = f g_{steric,o} + (1 - f) g_{steric,i} \tag{C.9}$$

and Eq. (2.24) in chapter 2 can be obtained by substituting Eqs. (C.7) and (C.8) in Eq. (C.9).

Appendix D

Electrostatic Free Energy

As mentioned in chapter 2, Eq. (2.27) corresponds only to an approximation in the calculation of the electrostatic free energy. The rationale behind such an approximation is to keep our molecular model simple, yet provide a reasonable thermodynamic description of a vesicle suspension. The more accurate approach in the calculation of g_{elec} is to charge the four surfaces simultaneously (see Figure 2-2(a)), although the actual application of this approach can be tedious because it requires a numerical integration of the Poisson-Boltzmann equation at each charging step. This appendix will discuss in more detail the approximations involved in the derivation of Eq. (2.27).

Consider the four charged surfaces shown in Figure 2-2(a). The total electrostatic free energy associated with charging these surfaces can be written as follows [171]

$$G_{elec} = \int_0^1 (\psi_1 Q_{1f} + \psi_2 Q_{2f} + \psi_3 Q_{3f} + \psi_4 Q_{4f}) d\lambda \qquad \text{(D.1)}$$

where ψ_j and Q_{jf}, $j = 1, \ldots, 4$, is the electrical potential and final charge on the surfaces denoted by R_j in Figure 2-2(a), respectively, and λ is the charging parameter. Equation (D.1) simply describes the charging of the four surfaces from zero to their corresponding final charges. The four surface potentials are related to each other through the following two boundary conditions,

$$\epsilon_w \left(\frac{R_1 R_2}{R_2 - R_1} \right) (\psi_2 - \psi_1) - \epsilon_h \left(\frac{R_2 R_3}{R_3 - R_2} \right) (\psi_3 - \psi_2) \;=\; Q_{2f} \lambda \qquad \text{(D.2)}$$

$$\epsilon_h \left(\frac{R_2 R_3}{R_3 - R_2}\right)(\psi_3 - \psi_2) - \epsilon_w \left(\frac{R_3 R_4}{R_4 - R_3}\right)(\psi_4 - \psi_3) = Q_{3f}\lambda \qquad \text{(D.3)}$$

where ϵ_w (ϵ_h) is the permittivity in water (hydrocarbon). Next, ψ_2 and ψ_3 are expressed in terms of ψ_1 and ψ_4. After some rearrangements of Eqs. (D.2) and (D.3), one obtains

$$\psi_2 \frac{\epsilon_w}{D}\left[1 + \frac{\epsilon_h D}{\xi \epsilon_w}\left(\frac{R_2}{R_1} + \frac{R_2}{R_4}\right)\right] = \frac{Q_{2f}\lambda}{R_1 R_2} + \psi_1 \frac{\epsilon_w}{D}\left[1 + \frac{\epsilon_h D R_2}{\xi \epsilon_w R_4}\right] + \psi_4 \frac{\epsilon_h R_3}{\xi R_1} + \frac{\epsilon_h D(Q_{2f} + Q_{3f})\lambda}{\xi \epsilon_w R_1 R_4} \qquad \text{(D.4)}$$

and

$$\psi_3 = \frac{(Q_{2f} + Q_{3f})\lambda D}{R_3 R_4 \epsilon_w} - \frac{R_1 R_2}{R_3 R_4}(\psi_2 - \psi_1) + \psi_4 \qquad \text{(D.5)}$$

where ξ is defined as $\xi = R_3 - R_2$, and D is the gap distance, defined as $D = R_2 - R_1 = R_4 - R_3$. Since the vesicle radii are usually much larger than D and ξ, ψ_2 and ψ_3 can be approximated by the following expressions

$$\psi_2 \approx \psi_1 + \psi_4 \frac{\epsilon_h D R_3}{\epsilon_w \xi R_1} + \frac{Q_{2f} D \lambda}{\epsilon_w R_1 R_2} + \frac{\epsilon_h D^2 Q_{3f}\lambda}{\epsilon_w^2 \xi R_1 R_4} \qquad \text{(D.6)}$$

and

$$\psi_3 \approx \psi_4 + \frac{Q_{3f} D \lambda}{\epsilon_w R_3 R_4} \qquad \text{(D.7)}$$

Substituting Eqs. (D.6) and (D.7) in Eq. (D.1), and using the definition $R_2 = R_1 + D$ and $R_4 = R_3 + D$, one obtains

$$\begin{aligned} G_{elec} = n g_{elec} = & \int_0^1 \psi_1 (Q_{1f} + Q_{2f}) d\lambda + \int_0^1 \psi_4 \left[Q_{4f} + Q_{3f}\left(1 + \frac{\epsilon_h D R_3 Q_{2f}}{\epsilon_w \xi R_1 Q_{3f}}\right)\right] d\lambda \\ & + \frac{Q_{2f}^2 D}{2\epsilon_w R_1^2 (1 + D/R_1)} + \frac{Q_{3f}^2 D}{2\epsilon_w R_3^2 (1 + D/R_3)}\left(1 + \frac{\epsilon_h D R_3 Q_{2f}}{\epsilon_w \xi R_1 Q_{3f}}\right) \end{aligned} \qquad \text{(D.8)}$$

Recall that the net charges, Q_o' and Q_i', appearing in Eq. (2.27) (see chapter 2) are defined as $Q_o' = Q_{3f} + Q_{4f}$ and $Q_i' = Q_{1f} + Q_{2f}$. Comparing Eq. (D.8) to Eq. (2.27), it can be seen that the approximation in Eq. (2.27) is due to the factor $\epsilon_h D R_3 Q_{2f}/\epsilon_w \xi R_1 Q_{3f}$. The ratio Q_{2f}/Q_{3f} appearing in this factor depends on the composition asymmetry between the two leaflets. As discussed in chapter 4, however,

the composition asymmetry is typically very small. In addition, R_1 and R_3 are of the same order of magnitude, and the typical values of ϵ_w, ϵ_h, D, and ξ are 80, 2.5, 1 Å, and 20 Å, respectively. Consequently, the factor $\epsilon_h D R_3 Q_{2f}/\epsilon_w \xi R_1 Q_{3f}$ is of the order of 10^{-3}, which is much smaller than unity. This approximation should therefore introduce little error in the calculation of g_{elec}. The second approximation comes in when the four charged surfaces of a vesicle (see Figure 2-2(a)) are replaced with two (outer and inner) surfaces in the calculation of the surface potentials (see Figure 2-2(c)), that is, we estimate ψ_1 and ψ_4 by ψ_i and ψ_o, respectively. The mathematical details of the two-surface configuration has been given in an earlier study [177], and therefore it will not be repeated here. To analyze the error involved, it suffices to consider the boundary conditions in the solution of the nonlinear PB equation. Consider again Figure 2-2(a). The boundary condition at R_1 can be written as

$$\epsilon_w \kappa_w \left.\frac{d\psi_{ia}}{dx}\right|_{R_1} - \epsilon_w \kappa_w \left.\frac{d\psi_{ig}}{dx}\right|_{R_1} = 4\pi q_1 \tag{D.9}$$

where κ_w is the inverse Debye screening length, ψ_{ia} is the potential in the inner aqueous region, ψ_{ig} is the potential in the inner gap region between R_1 and R_2, and q_1 is the surface charge density at R_1. Here, the gap region is assumed to be filled with pure water, thus having a permittivity, ϵ_w. A similar boundary condition at R_2 can be written as follow

$$\epsilon_w \kappa_w \left.\frac{d\psi_{ig}}{dx}\right|_{R_2} - \epsilon_h \kappa_w \left.\frac{d\psi_{hc}}{dx}\right|_{R_2} = 4\pi q_2 \tag{D.10}$$

where ψ_{hc} is the potential in the hydrophobic region between R_2 and R_3. The potential gradients at R_1 and R_2 in the inner gap region are related through the following relation

$$\left.\frac{d\psi_{ig}}{dx}\right|_{R_1} = \left(\frac{R_2}{R_1}\right)^2 \left.\frac{d\psi_{ig}}{dx}\right|_{R_2} \tag{D.11}$$

Equation (D.11) results from the assumption that there is no ion accumulation in the gap region. This assumption was made mainly for simplicity, but its validity may be justified by the fact that the value of D (1 – 2 Å) is comparable to the typical size of

a counterion. Using Eqs. (D.10) and (D.11), Eq. (D.9) can be rewritten as

$$\epsilon_w \kappa_w \left.\frac{d\psi_{ia}}{dx}\right|_{R_1} - \left(\frac{R_2}{R_1}\right)^2 \epsilon_h \kappa_w \left.\frac{d\psi_{hc}}{dx}\right|_{R_2} = 4\pi q_1' \tag{D.12}$$

where $q_1' = (Q_{1f}+Q_{2f})/4\pi R_1^2$ is the net charge density evaluated at R_1. This equation can be compared to the boundary condition at the inner surface in the two-surface configuration, which states that [177]

$$\epsilon_w \kappa_w \left.\frac{d\psi_{ia}}{dx}\right|_{R_1} - \epsilon_h \kappa_w \left.\frac{d\psi_{hc}}{dx}\right|_{R_1} = 4\pi q_1' \tag{D.13}$$

In the special case where $D = 0$, Eq. (D.12) is identical to Eq. (D.13), which is quite obvious since in that case the "four-surface" configuration is identical to the two-surface configuration. For $D \neq 0$, then, the approximation involves an additional term, $(2D/R_1)(d\psi_{hc}/dx)|_{R_2}$, which should be small for a typical vesicle since R_1 is usually much larger than D. A similar situation can be found at the outer surface. The validity of these approximations can be better judged by comparing the electrostatic free energy obtained by using Eq. (2.27), denoted as $g_{elec}^{(2)}$, to that obtained by using Eq. (D.1), denoted as $g_{elec}^{(4)}$. In using Eq. (D.1), the nonlinear PB equation was solved to obtain the four surface potentials at each charging stage. Figure D-1 shows graphically such a comparison. The agreement between the values obtained by both approaches is very good for up to 4 kT, which should cover the range of electrostatic free energies encountered in the present study.

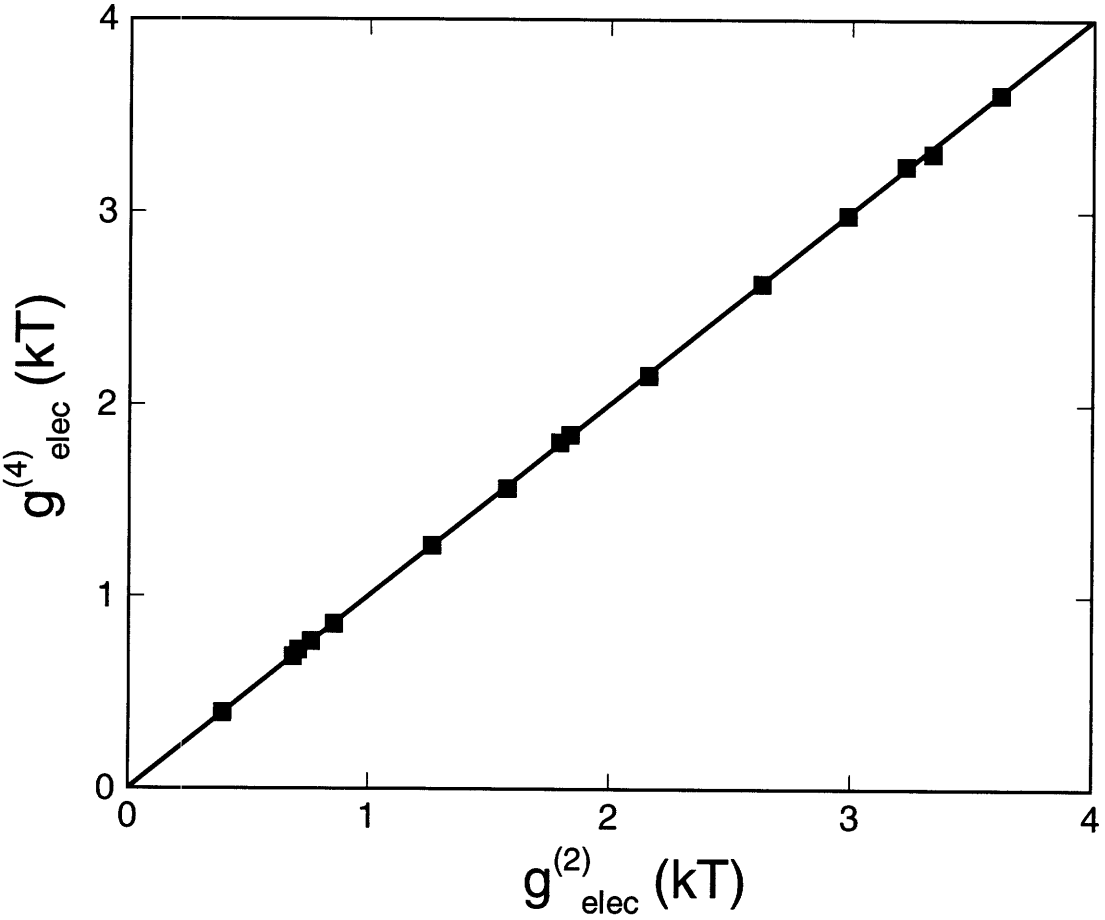

Figure D-1: Comparison between the predicted electrostatic free energy per molecule obtained by using Eq. (D.1), $g^{(4)}_{elec}$, and that obtained by using Eq. (2.27), $g^{(2)}_{elec}$. The parameters used in this comparison are as follows: $T = 298$ K, $R_o = 565$ Å, $R_i = 520$ Å, $f = 0.55$, $n = 200000$, $d_{ch,A} = 2.5$ Å, and $d_{ch,B} = 3.8$ Å. The ion concentration in solution is 0.001 M.

Appendix E

Summary of Model Equations

1. **Transfer Free Energy,** g_{tr} [Eq. (2.5)]

$$g_{tr} = F\Delta\mu_{tr,A} + (1-F)\Delta\mu_{tr,B} + g_m$$

$\Delta\mu_{tr,k}$ and g_m can be obtained by using Eqs. (2.6) and (2.7), respectively.

2. **Packing Free Energy,** g_{pack} [Eqs. (2.9) and (2.10)]

$$g_{pack} = \sum_{k=A,B} [fX_{ok}\mu_{ok} + (1-f)X_{ik}\mu_{ik}] - \mu^f_{pack}$$

μ_{ok} and μ_{ik} are calculated by extending the mean-field approach of Szleifer and co-workers [159, 160], which involves enumerating all the chain conformations, and solving the uniform-density constraint equations for the lateral pressures in the outer and inner vesicle leaflets.

3. **Interfacial Free Energy,** g_σ [Eq. (2.14)]

$$g_\sigma = f\bar{\sigma}_o(a_o - a_o^*) + (1-f)\bar{\sigma}_i(a_i - a_i^*)$$

$\bar{\sigma}_o$ can be obtained by using Eqs. (2.17) and (2.19), while $\bar{\sigma}_i$ can be obtained by using Eqs. (2.18) and (2.20).

4. **Steric Free Energy,** g_{steric} [Eq.(2.24)]

$$\frac{g_{steric}}{kT} = f\left[\frac{\pi\bar{d}_o^2/4}{a'_o - \bar{a}_{ho}} - \ln\left(1 - \frac{\bar{a}_{ho}}{a'_o}\right)\right] + (1-f)\left[\frac{\pi\bar{d}_i^2/4}{a'_i - \bar{a}_{hi}} - \ln\left(1 - \frac{\bar{a}_{hi}}{a'_i}\right)\right]$$

$\bar{d}_o$, $\bar{d}_i$, $\bar{a}_{ho}$, and $\bar{a}_{hi}$ can be obtained by using the definitions given in Eqs. (C.3) and (C.5) in Appendix 2.2.4.

5. **Electrostatic Free Energy,** g_{elec} [Eq. (2.27)]

$$ng_{elec} = \frac{Q_{2f}^2 D}{2\epsilon_w R_1^2(1 + D/R_1)} + \frac{Q_{3f}^2 D}{2\epsilon_w R_3^2(1 + D/R_3)} + \int_0^1 [\psi_i(\lambda)Q'_i + \psi_o(\lambda)Q'_o]d\lambda$$

The surface potentials, ψ_o and ψ_i, can be obtained from Eqs. (32) and (33) in Ref. 177.

Appendix F

Geometric Constraints in a Vesicle

The five geometric constraints that relate the ten variables, n, F, a_o, a_i, f, X_{oA}, X_{iA}, R_o, R_i, and t_b (see chapter 2), are written below

$$\frac{4}{3}\pi(R_o^3 - R_i^3) = n[Fv_A + (1-F)v_B] \quad \text{(F.1)}$$

$$4\pi R_o^2 = nfa_o \quad \text{(F.2)}$$

$$4\pi R_i^2 = n(1-f)a_i \quad \text{(F.3)}$$

$$F = fX_{oA} + (1-f)X_{iA} \quad \text{(F.4)}$$

$$t_b = R_o - R_i \quad \text{(F.5)}$$

where v_A and v_B are the tail volumes of components A and B, respectively, in the hydrophobic region. Equations (F.1), (F.2), and (F.3) simply describe the conservation of total volume, outer surface area, and inner surface area, respectively. Equation (F.4) results from the mass balance of component A in the vesicle, and Eq. (F.5) is merely the definition of the bilayer thickness (see Figure 2-1). Note that the bilayer thickness in our model is just the thickness of the hydrophobic region between the two hydrocarbon/water interfaces, and it would be smaller than most experimentally measured bilayer thicknesses, which usually include the head-group region. Knowing n, F, X_{oA}, f, and t_b, the remaining five variables, namely, R_o, R_i, a_o, a_i, and X_{iA}, can then be calculated using Eqs. (F.1) – (F.5).

Appendix G

Derivation of Analytical Expressions for the Surface Potentials

The approximate analytical expressions for the outer and inner surface potentials of a charged vesicle are derived in this appendix. Consider Eqs.(3.21) and (3.22) presented in chapter 3. Specifically,

$$s_o - \frac{\gamma}{X_o^2}(y_3 - y_1) = 2\sinh(\frac{y_3}{2})\left[1 + \frac{2}{X_o}\frac{1}{\cosh(y_3/2)+1}\right] \tag{G.1}$$

$$s_i + \frac{\gamma}{X_i^2}(y_3 - y_1) = 2\sinh(\frac{y_1}{2})\left[1 - \frac{2}{X_i}\frac{\cosh(y_3/2) - \cosh(y_o/2)}{\sinh^2(y_1/2)}\right] \tag{G.2}$$

where

$$s_o = \frac{4\pi\sigma_o ez}{\epsilon_3\kappa_w kT} \tag{G.3}$$

$$s_i = \frac{4\pi\sigma_i ez}{\epsilon_1\kappa_w kT} \tag{G.4}$$

$$\gamma = \frac{\epsilon_2}{\epsilon_w}\left(\frac{1}{X_i} - \frac{1}{X_o}\right)^{-1} \tag{G.5}$$

In what follows, the surface potentials, $y_{3,o}$ and $y_{1,i}$, are abbreviated as y_3 and y_1, respectively, for clarity. Equation (G.1) can be rewritten as

$$s_o - \frac{\gamma}{X_o^2}(y_3 - y_1) = 2\sinh(\frac{y_3}{2}) + \frac{4}{X_o}\tanh(\frac{y_3}{4}) \tag{G.6}$$

For small y_3, one may approximate $\tanh(y_3/4)$ by the leading-order term, $y_3/4$. This approximation may seem rather restrictive at first glance, since the difference between $\tanh(y)$ and y reaches 30 % at $y = 1$, corresponding to an outer surface potential of only about 100 mV. Since $\tanh(y)$ approaches a constant value of 1 as y increases, the error of this approximation is expected to scale as y at large y. However, $\sinh(y)$ scales as the exponential of y at large y, which implies that $\sinh(y_3/2)$ will become the dominant term on the right-hand side of Eq. (G.6) as y_3 becomes large. As a result, the accuracy in the approximation of $\tanh(y_3/4)$ will not be important. Indeed, using $X_o = 1$, the largest error in evaluating the right-hand side of Eq. (G.6), due to this approximation of $\tanh(y_3/4)$, is only about 10 %, which occurs at $y_3 \approx 5$. The function, $\sinh(y_3/2)$, can also be linearized around the potential, y_3^o, which corresponds to a vesicle having an electrically neutral interior. The corresponding equation for this condition can be written as follows

$$s_o = 2\sinh(\frac{y_3^o}{2})\left[1 + \frac{4}{X_o}\frac{1}{\cosh(y_3^o/2)+1}\right]^{\frac{1}{2}} \tag{G.7}$$

where y_3^o is the outer surface potential when the interior of the vesicle is electrically neutral. Note that this is equivalent to setting y_3 equal to y_1 in Eq. (G.1) [1]. The solution to Eq. (G.7) is given in Ref. 48. Specifically,

$$y_3^o = 2\ln[z_3 + (z_3^2 - 1)^{\frac{1}{2}}] \tag{G.8}$$

where

$$z_3 = \cosh(\frac{y_3}{2}) = \left[\left(1 + \frac{2}{X_o}\right)^2 + \frac{s_o^2}{4}\right]^{\frac{1}{2}} - \frac{2}{X_o} \tag{G.9}$$

[1] Equation (G.1) is an approximate expression obtained by linearizing the square-root term.

Using this linearization and the approximation for $\tanh(y_3/4)$ discussed above, one obtains Eq. (3.28) in chapter 3, where

$$A_3 = 2\sinh(\frac{y_3^o}{2}) - y_3^o\cosh(\frac{y_3^o}{2}) \tag{G.10}$$

$$B_3 = \cosh(\frac{y_3^o}{2}) \tag{G.11}$$

For Eq. (G.2), the function, $\cosh(y_o/2)$, is first approximated by expanding around $y_o = 0$. To retain the dependence on y_o, we keep the second-order term (the first non-vanishing term that contains y_o). Equation (G.2) can then be written as

$$s_i + \frac{\gamma}{X_i^2}(y_3 - y_1) = 2\sinh(\frac{y_1}{2}) - \frac{4}{X_i}\tanh(\frac{y_1}{4}) + \frac{y_o^2}{2X_i}\frac{1}{\sinh(y_1/2)} \tag{G.12}$$

Applying approximations similar to those discussed above, one obtains Eq. (3.29) in chapter 3, where

$$A_1 = 2\sinh(\frac{y_1^o}{2}) - y_1^o\cosh(\frac{y_1^o}{2}) \tag{G.13}$$

$$B_1 = \cosh(\frac{y_1^o}{2}) \tag{G.14}$$

$$y_1^o = 2\ln[z_1 + (z_1^2 - 1)^{\frac{1}{2}}] \tag{G.15}$$

$$z_1 = \left[\left(1 - \frac{2}{X_i}\right)^2 + \frac{s_i^2}{4}\right]^{\frac{1}{2}} + \frac{2}{X_i} \tag{G.16}$$

The center-point potential, y_o, can now be expressed in terms of y_1 and y_3 from Eq. (3.29), which yields

$$y_o^2 = \left[(s_i - A_1) - y_1\left(\frac{\gamma}{X_i^2} - \frac{1}{X_i} + B_1\right) + y_3\frac{\gamma}{X_i^2}\right] X_i(A_1 + B_1 y_1) \tag{G.17}$$

One can now invert Eq. (3.23) in chapter 3, which yields

$$y_o \approx \tilde{y}_1 - \hat{Y}_3\tilde{y}_1^3 \tag{G.18}$$

where

$$\tilde{y}_1 = y_1/Y_1 \tag{G.19}$$

$$\hat{Y}_3 = Y_3/Y_1 \tag{G.20}$$

with Y_1 and Y_3 given in Eqs. (3.24) and (3.25), respectively. Note that Eq. (G.18) is valid for small $\tilde{y}_1$, which should be a good approximation for large X_i, since Y_1 increases exponentially with X_i. Substituting Eqs. (G.18) and (3.32) in Eq. (G.17), one obtains

$$(\tilde{y}_1 - \hat{Y}_3\tilde{y}_1^3)^2 = (E + FY_1\tilde{y}_1)X_i(A_1 + B_1Y_1\tilde{y}_1) \tag{G.21}$$

where

$$E = (s_i - A_1) + \frac{\gamma X_o^2(s_o - A_3)}{X_i^2(\gamma + X_o + B_3X_o^2)} \tag{G.22}$$

$$F = \frac{1}{X_i^2}\left[\frac{\gamma^2}{\gamma + X_o + B_3X_o^2} - (\gamma - X_i + B_1X_i^2)\right] \tag{G.23}$$

After some rearrangement, one obtains a polynomial in $\tilde{y}_1$ as given in Eq. (3.30) in chapter 3.

In order to obtain a simpler analytical solution, let us neglect the fourth- and sixth-order terms in Eq. (3.30) for the moment. This truncation should be valid for small $\tilde{y}_1$, an approximation which was already used in the inversion of Eq. (3.23). It is noteworthy that by truncating the polynomial to only the second-order term, we are, indeed, applying the linearized Poisson-Boltzmann equation to the interior of the vesicle, which has the solution $y_o = \tilde{y}_1$. To make full use of Tenchov's expression, which contains the first nonlinear correction to the linear solution, however, one needs to keep at least the fourth-order term in Eq. (3.30), and this will undoubtedly complicate any attempt to find an analytical expression. Nevertheless, the truncated polynomial can be written as

$$\tilde{y}_1^2 + \frac{(A_1F + B_1E)X_iY_1}{(B_1FY_1^2X_i - 1)}\tilde{y}_1 + \frac{A_1EX_i}{(B_1FY_1^2X_i - 1)} = 0 \tag{G.24}$$

The solution to Eq. (G.24) is given by Eq. (3.31) in chapter 3. The root of this quadratic equation is chosen to yield the correct limit as X_i and X_o approach infinity. One can show that, as X_i and X_o approach infinity, Eq. (3.31) can be reduced to $\tilde{y}_1Y_1 = y_{1,i} = -E/F$, which corresponds to the solution to Eqs. (3.28) and (3.29)

given in chapter 3. Specifically, consider Eq. (3.31) in chapter 3

$$\tilde{y}_1 \approx -\frac{(A_1F + B_1E)Y_1}{2(B_1FY_1^2 - 1/X_i)} \pm \frac{1}{2}\left\{\left[\frac{(A_1F + B_1E)Y_1}{(B_1FY_1^2 - 1/X_i)}\right]^2 - \frac{4A_1E}{(B_1FY_1^2 - 1/X_i)}\right\}^{\frac{1}{2}} \quad \text{(G.25)}$$

As X_i approaches infinity, the square-root term in Eq. (G.25) can be approximately written as

$$\left\{\frac{(A_1F - B_1E)^2}{(B_1FY_1)^2}\right\}^{\frac{1}{2}} \quad \text{(G.26)}$$

or

$$\frac{A_1F - B_1E}{B_1FY_1} \quad \text{(G.27)}$$

Substituting Eq. (G.26) in Eq. (G.25), with the limit $X_i \to \infty$, one obtains

$$\tilde{y}_1 \approx -\frac{E}{FY_1} \quad \text{(G.28)}$$

or

$$y_{1,i} \approx -\frac{E}{F} \quad \text{(G.29)}$$

Note that in going from the expression in (G.26) to that in (G.27), it is assumed that the numerator in (G.27) is positive, and in this case, the positive root is chosen in Eq. (G.25) (the root with a positive sign in front of the square-root term) to obtain Eq. (G.29). If, however, the numerator in (G.27) is negative, as may be the case when s_i is negative, then the negative root in Eq. (G.25) should be used in order to obtain Eq. (G.29), since in this case the term $(B_1E - A_1F)$ in (G.27) is positive.

To show that Eq. (G.29) is indeed the solution to Eqs. (3.28) and (3.29) given in chapter 3, we first rewrite E and F (see Eqs. (G.22) and (G.23)) in the limit $X_o, X_i \to \infty$, that is,

$$E \approx (s_i - A_1) + \frac{(\gamma/X_i^2)(s_o - A_3)}{(\gamma/X_o^2 + B_3)} \quad \text{(G.30)}$$

$$F \approx \frac{(\gamma/X_oX_i)^2}{(\gamma/X_o^2 + B_3)} - (\frac{\gamma}{X_i^2} + B_1) \quad \text{(G.31)}$$

Note that the terms γ/X_o^2 and γ/X_i^2 are inversely proportional to the bilayer thickness and are, therefore, finite. As $X_o, X_i \to \infty$, one can express Eqs. (3.28) and (3.29) as

$$s_o - \frac{\gamma}{X_o^2}(y_{3,o} - y_{1,i}) \approx A_3 + y_{3,o}B_3 \tag{G.32}$$

$$s_i + \frac{\gamma}{X_i^2}(y_{3,o} - y_{1,i}) \approx A_1 + y_{1,i}B_1 \tag{G.33}$$

From Eqs. (G.29) and (G.33), $y_{3,o}$ and $y_{1,i}$ can be expressed as

$$y_{3,o} = \frac{s_o - A_3}{B_3 + \gamma/X_o^2} + \frac{\gamma/X_o^2}{B_3 + \gamma/X_o^2} y_{1,i} \tag{G.34}$$

$$y_{1,i} = \frac{s_i - A_1}{B_1 + \gamma/X_i^2} + \frac{\gamma/X_i^2}{B_1 + \gamma/X_i^2} y_{3,o} \tag{G.35}$$

Substituting Eq. (G.34) in Eq. (G.35), and performing some rearrangement, one obtains

$$\left[B_1 + \frac{\gamma}{X_i^2} - \frac{(\gamma/X_o X_i)^2}{\gamma/X_o^2 + B_3}\right] y_{1,i} = (s_i - A_1) + \frac{(\gamma/X_i^2)(s_o - A_3)}{\gamma/X_o^2 + B_3} \tag{G.36}$$

or

$$-F y_{1,i} = E \tag{G.37}$$

$$y_{1,i} = -\frac{E}{F} \tag{G.38}$$

Bibliography

[1] M.H. Abraham. Thermodynamics of solution of homologous series of solutes in water. *J. Chem. Soc. Faraday Trans. 1*, 80:153, 1984.

[2] W.H. Admirand and D.M. Small. The physicochemical basis of cholesterol gallstone formation in man. *J. Clin. Invest.*, 47:1043, 1968.

[3] L. Amigo, C. Covarrubias, and F. Nervi. Rapid isolation of vesicular and micellar carriers of biliary lipids by ultracentrifugation. *J. Lipid Res.*, 31:341, 1990.

[4] L. Amigo, C. Covarrubias, and F. Nervi. Separation and quantitation of cholesterol carriers in native bile by ultracentrifugation. *Hepatology*, 12:130S, 1990.

[5] D. Andelman, T. Kawakatsu, and K. Kawasaki. Equilibrium shape of two-component unilamellar membranes and vesicles. *Europhys. Lett.*, 19:57, 1992.

[6] D. Andelman, M. Kozlov, and W. Helfrich. Phase transitions between vesicles and micelles driven by competing curvatures. *Europhys. Lett.*, 25:231, 1994.

[7] G.R. Bartlett. Phosphorus assay in column chromatography. *J. Biol. Chem.*, 234:466, 1959.

[8] J. Bentz. Electrostatic potential between concentric surfaces: Spherical, cylindrical, and planar. *J. Colloid Interf. Sci.*, 90:164, 1982.

[9] M. Bergström and J.C. Eriksson. The energetics of forming equilibrated bilayer vesicles. *Langmuir*, 12:624, 1996.

[10] D. Blankschtein, G.M. Thurston, and G.B. Benedek. Phenomenological theory of equilibrium thermodynamic properties and phase separation of micellar solutions. *J. Chem. Phys.*, 85:7268, 1986.

[11] L. Blum. Primitive electrolytes in the mean spherical approximation. In H. Eyring and D. Henderson, editors, *Theoretical Chemistry: Advances and Perspectives*, volume 5, page 1. Academic Press, New York, 1980.

[12] J.O'M. Bockris and A.K.N. Reddy. *Modern Electrochemistry. Volume 1.* Plenum Press, New York, 1970.

[13] J.O'M. Bockris and A.K.N. Reddy. *Modern Electrochemistry. Volume 2.* Plenum Press, New York, 1970.

[14] C.J.F Böttcher. *Theory of Electric Polarization. Vol. I.* Elsevier Publishing Co., Amsterdam, 1973.

[15] G.E.P. Box and D.W. Behnken. Some new three level designs for the study of quantitative variables. *Technometrics*, 2:455, 1960.

[16] G.E.P. Box, W.G. Hunter, and J.S. Hunter. *Statistics for Experimenters.* John Wiley & Sons, New York, 1978.

[17] G.E.P. Box and K.B. Wilson. On the experimental attainment of optimum conditions. *J. Roy. Stat. Soc., Ser. B*, 13:1, 1951.

[18] J.E. Brady, D.F. Evans, B. Kachar, and B.W. Ninham. Spontaneous vesicles. *J. Am. Chem. Soc.*, 106:4279, 1984.

[19] L.L. Brasher, K.L. Herrington, and E. Kaler. Electrostatic effects on the phase behavior of aqueous cetyltrimethylammonium bromide and sodium octyl sulfate mixtures with added sodium bromide. *Langmuir*, 11:4267, 1995.

[20] N. Busch and R.T. Holzbach. Crystal growth-inhibiting proteins in bile. *Hepatology*, 12:195S, 1990.

[21] D.J. Cabral and D.M. Small. Physical chemistry of bile. In J.G. Forte, editor, *Handbook of Physiology - The Gastrointestinal System III*, chapter 31, page 621. American Physiological Society, New York, 1989.

[22] T.R. Carale, Q.T. Pham, and D. Blankschtein. Salt effects on intramicellar interactions and micellization of nonionic surfactants in aqueous solutions. *Langmuir*, 10:109, 1994.

[23] M.C. Carey. Critical tables for calculating the cholesterol saturation of native bile. *J. Lipid Res.*, 19:945, 1978.

[24] M.C. Carey and M.J. Cahalane. Whither biliary sludge? *Gastroenterology*, 95:508, 1988.

[25] M.C. Carey and J.T. LaMont. Cholesterol gallstone formation. 1. Physical-chemistry of bile and biliary lipid secretion. In H. Popper and F. Schaffner, editors, *Progress in Liver Diseases, Vol. X*, chapter 7, page 139. W.B. Saunders Co., Philadelphia, 1992.

[26] M.C. Carey and D.M. Small. The physical chemistry of cholesterol solubility in bile: Relationship to gallstone formation and dissolution in man. *J. Clin. Invest.*, 61:998, 1978.

[27] M.A. Carignano and I. Szleifer. Statistical thermodynamic theory of grafted polymeric layers. *J. Chem. Phys.*, 98:5006, 1993.

[28] M.A. Carignano and I. Szleifer. Pressure isotherms, phase transition, instability, and structure of tethered polymers in good, θ, and poor solvents. *J. Chem. Phys.*, 100:3210, 1994.

[29] M.A. Carignano and I. Szleifer. Structural and thermodynamic properties of end-grafted polymers on curved surfaces. *J. Chem. Phys.*, 102:8662, 1995.

[30] S. Carnie, J.N. Israelachvili, and B.A. Pailthorpe. Lipid packing and transbilayer asymmetries of mixed lipid vesicles. *Biochim. Biophys. Acta*, 554:340, 1979.

[31] K. Chijiiwa, I. Hirota, and H. Noshiro. High vesicular cholesterol and protein in bile are associated with formation of cholesterol but not pigment gallstones. *Dig. Dis. Sci.*, 38:161, 1993.

[32] K. Chijiiwa, R. Kiyosawa, and F. Nakayama. Cholesterol monomer activity correlates with nucleation time in model bile. *Clin. Chim. Acta*, 178:181, 1988.

[33] S. Chiruvolu. *Microstructure of Vesicle-Forming Surfactant and Lipid Solutions.* PhD thesis, University of California Santa Barbara, 1994.

[34] D.E. Cohen, M. Angelico, and M.C. Carey. Structural alterations in lecithin-cholesterol vesicles following interactions with monomeric and micellar bile salts: Physical-chemical basis for subselection of biliary lecithin species and aggregative states of biliary lipids during bile formation. *J. Lipid Res.*, 31, 1990.

[35] D.E. Cohen and M.C. Carey. Rapid (1 hour) high performance gel filtration chromatography resolves coexisting simple micelles, mixed micelles, and vesicles in bile. *J. Lipid Res.*, 31:2103, 1990.

[36] D.E. Cohen, M.R. Fisch, and M.C. Carey. Principles of laser light-scattering spectroscopy: Applications to the physiochemical study of model and native biles. *Hepatology*, 12:113S, 1990.

[37] D.E. Cohen, E. Kaler, and M.C. Carey. Cholesterol carriers in human bile: are "lamellae" involved? *Hepatology*, 18, 1993.

[38] J.M. Corkill, J.F. Goodman, T. Walker, and J. Wyer. The multiple equilibrium model of micelle formation. *Proc. Roy. Soc. A.*, 312:243, 1969.

[39] J.E. Curry, S.E. Feller, and D.A. McQuarrie. A variational solution of the non-linear Poisson-Boltzmann equation inside a spherical cavity. *J. Colloid Interf. Sci.*, 143:527, 1991.

[40] J.M. Donovan and M.C. Carey. Separation and quantitation of cholesterol "carriers" in bile. *Hepatology*, 12:94S, 1990.

[41] J.M. Donovan and A.A. Jackson. Rapid determination by centrifugal ultrafiltration of the inter-mixed micellar/vesicular (non-lecithin associated) bile salt concentrations in model bile: Influence of Donnan equilibrium effect. *J. Lipid Res.*, 34:1121, 1993.

[42] J.M. Donovan, A.A. Jackson, and M.C. Carey. Molecular species composition of the inter-mixed micellar/vesicular bile salt concentrations in model bile. Dependence upon hydrophilic-hydrophobic balance. *J. Lipid Res.*, 34:1131, 1993.

[43] J.M. Donovan, N. Timofeyeva, and M.C. Carey. Influence of total lipid concentration, bile salt:lecithin ratio, and cholesterol content on inter-mixed micellar/vesicular (non-lecithin-associated) bile salt concentration in model bile. *J. Lipid Res.*, 32:1501, 1991.

[44] D.M. Duh and A.D.J. Haymet. Integral equation theory for charged liquids: Model 2-2 electrolytes and the bridge function. *J. Chem. Phys.*, 97:7716, 1992.

[45] A. Duyndam and T. Odijk. Equilibrium distribution of linear micellar aggregates in a gravitational or centrifugal field. *Langmuir*, 9, 1993.

[46] A. Duyndam and T. Odijk. Dynamic sedimentation of linear micellar aggregates in a centrifugal field. *J. Chem. Phys.*, 100, 1994.

[47] E. Egberts, S. Marrink, and H.J.C. Berendsen. Molecular dynamics simulation of a phospholipid membrane. *Eur. Biophys. J.*, 22:423, 1994.

[48] D.F. Evans, D.J. Mitchell, and B.W. Ninham. Ion binding and dressed micelles. *J. Phys. Chem.*, 88:6344, 1984.

[49] D.F. Evans and B.W. Ninham. Ion binding and the hydrophobic effect. *J. Phys. Chem.*, 87:5025, 1983.

[50] E. Feitosa, A.A. Neto, and H. Chaimovich. Integration of the nonlinear Poisson-Boltzmann equation for charged vesicles in electrolytic solutions. *Langmuir*, 9:702, 1993.

[51] J.H. Fendler. *Membrane Mimetic Chemistry.* Wiley, New York, 1982.

[52] M.P.A. Fisher and M. Wortis. Curvature corrections to the surface tension of fluid drops: Landau theory and a scaling hypothesis. *Phys. Rev. B*, 29:6252, 1984.

[53] P.J. Flory. *Statistical Mechanics of Chain Molecules.* Hanser Publishers, Munich, 1989.

[54] A. Fogden, D.J. Mitchell, and B.W. Ninham. Undulations of charged membranes. *Langmuir*, 6:159, 1990.

[55] A. Fogden and B.W. Ninham. The bending modulus of ionic lamellar phases. *Langmuir*, 7:590, 1991.

[56] D.P. Fraser, M.J. Zuckermann, and O.G. Mouritsen. Theory and simulations for hard-disk models of binary mixtures of molecules with internal degrees of freedom. *Phys. Rev. A*, 43:6642, 1991.

[57] N.E. Gabriel and M.F. Roberts. Spontaneous formation of stable unilamellar vesicles. *Biochemistry*, 23:4011, 1984.

[58] E.F. Grabowski and I.D. Morrison. Particle size distributions from analyses of quasi-elastic light-scattering data. In B.E. Dahneke, editor, *Measurement of Suspended Particles by Quasi-Elastic Light Scattering*, chapter 7, page 199. John Wiley & Sons, New York, 1983.

[59] G. Gregoriadis, editor. *Liposome Technology. Volume II: Entrapment of Drugs and Other Materials.* CRC Press, Boca Raton, second edition, 1988.

[60] A.K. Groen. Nonmucous glycoproteins as pronucleating agents. *Hepatology*, 12:189S, 1990.

[61] D.W.R. Gruen. A model for the chains in amphiphilic aggregates. 1. Comparison with a molecular dynamics simulation of a bilayer. *J. Phys. Chem.*, 89:146, 1985.

[62] D.W.R. Gruen. A model for the chains in amphiphilic aggregates. 2. Thermodynamic and experimental comparisons for aggregates of different shape and size. *J. Phys. Chem.*, 89:153, 1985.

[63] G. Gunnarsson, B. Jönsson, and H. Wennerström. Surfactant association into micelles. An electrostatic approach. *J. Phys. Chem.*, 84:3114, 1980.

[64] Z. Halpern, M.A. Dudley, A. Kibe, M.P. Lynn, A.C. Breuer, and R.T. Holzbach. Rapid vesicle formation and aggregation in abnormal human biles. *Gastroenterology*, 90:875, 1986.

[65] P.R. Harvey and S.M. Strasberg. Will the real cholesterol-nucleating and -antinucleating proteins please stand up? *Gastroenterology*, 104:646, 1993.

[66] P.R.C. Harvey, G. Sömjen, T. Gilat, S. Gallinger, and S.M. Strasberg. Vesicular cholesterol in bile. Relationship to protein concentration and nucleation time. *Biochim. Biophys. Acta*, 958:10, 1988.

[67] P.R.C. Harvey, G. Sömjen, M.S. Lichtenberg, C. Petrunka, T. Gilat, and S.M. Strasberg. Nucleation of cholesterol from vesicles isolated from bile of patients with and without cholesterol gallstones. *Biochim. Biophys. Acta*, 921:198, 1987.

[68] S. Hashimoto, J.K. Thomas, D.F. Evans, S. Mukherjee, and B.W. Ninham. Unusual behavior of hydroxide surfactants. *J. Colloid Interf. Sci.*, 95:594, 1983.

[69] H. Hauser. Spontaneous vesiculation of uncharged phospholipid dispersions consisting of lecithin and lysolecithin. *Chem. Phys. Lipids*, 43:283, 1987.

[70] M.J. Haye and C. Bruin. Molecular dynamics study of the curvature correction to the surface tension. *J. Chem. Phys.*, 100:556, 1994.

[71] J.B. Hayter. A self-consistent theory of dressed micelles. *Langmuir*, 8:2873, 1992.

[72] W. Helfrich. Elastic properties of lipid bilayers: Theory and possible experiments. *Z. Naturforsch.*, 28c:693, 1973.

[73] W. Helfrich. Size distributions of vesicles: The role of the effective rigidity of membranes. *J. Phys.*, 47:321, 1986.

[74] K.L. Herrington. *Phase Behavior and Microstructure in Aqueous Mixtures of Oppositely Charged Surfactants.* PhD thesis, University of Delaware, 1994.

[75] K.L. Herrington, E.W. Kaler, D.D. Miller, J.A. Zasadzinski, and S. Chiruvolu. Phase behavior of aqueous mixtures of dodecyltrimethylammonium bromide (DTAB) and sodium dodecyl sulfate (SDS). *J. Phys. Chem.*, 97:13792, 1993.

[76] W.I. Higuchi, P.H. Lee, K. Takayama, U.K. Jain, and N.A. Mazer. Cholesterol monomer activity and its role in understanding cholesterol saturation and crystallization. *Hepatology*, 12:88S, 1990.

[77] T.L. Hill. Statistical thermodynamics of the transition region between two phases. I. Thermodynamics and quasi-thermodynamics. *J. Chem. Phys.*, 56:526, 1952.

[78] K.R. Holan, R.T. Holzbach, R.E. Hermann, A.M. Cooperman, and W.J. Claffey. Nucleation time: A key factor in the pathogenesis of cholesterol gallstone disease. *Gastroenterology*, 77:611, 1979.

[79] R.T. Holzbach, M. Marsh, M. Olszewski, and K. Holan. Cholesterol solubility in bile: Evidence that supersaturated bile is frequent in healthy bile. *J. Clin. Invest.*, 52:1467, 1973.

[80] J.N. Israelachvili. *Intermolecular and Surface Forces.* Academic Press, London, second edition, 1991.

[81] J.N. Israelachvili, D.J. Mitchell, and B.W. Ninham. Theory of self-assembly of hydrocarbon amphiphiles into micelles and bilayers. *J. Chem. Soc. Faraday Trans. 2*, 72:1525, 1976.

[82] J.N. Israelachvili, D.J. Mitchell, and B.W. Ninham. Theory of self-assembly of lipid bilayers and vesicles. *Biochim. Biophys. Acta*, 470:185, 1977.

[83] M. Iwamatsu. The surface tension and Tolman's length of a drop. *J. Phys.: Condens. Matter*, 6:L173, 1994.

[84] G. Jackson and J.S. Rowlinson. Phase equilibria in model mixtures of spherical molecules of different sizes. *J. Chem. Soc. Faraday Trans. 1*, 82:3461, 1986.

[85] U.K. Jain, W.I. Higuchi, P.H. Lee, and C.L. Liu. A rapid method for the measurement of cholesterol thermodynamic activity in bile salt-lecithin-cholesterol solutions. *J. Pharm. Sci.*, 82:714, 1993.

[86] E.W. Kaler, K.L. Herrington, A.K. Murthy, and J.A.N. Zasadzinski. Phase behavior and structures of mixtures of anionic and cationic surfactants. *J. Phys. Chem.*, 96:6698, 1992.

[87] E.W. Kaler, A.K. Murthy, B.E. Rodriguez, and J.A.N. Zasadzinski. Spontaneous vesicle formation in aqueous mixtures of single-tailed surfactants. *Science*, 245:1371, 1989.

[88] T. Kawakatsu, D. Andelman, K. Kawasaki, and T. Taniguchi. Phase transitions and shapes of two component membranes and vesicles I: Strong segregation limit. *J. Phys. II (France)*, 3:971, 1993.

[89] A. Kibe, M.A. Dudley, Z. Halpern, M.P. Lynn, A.C. Breuer, and R.T. Holzbach. Factors affecting cholesterol monohydrate crystal nucleation time in model systems of supersaturated bile. *J. Lipid Res.*, 26:1102, 1985.

[90] M. Kléman. Remarks on a possible elasticity of membranes and lamellar media: Disordered layers. *Proc. R. Soc. Lond. A*, 347:387, 1976.

[91] F.O. Koenig. On the thermodynamic relation between surface tension and curvature. *J. Chem. Phys.*, 18:449, 1950.

[92] Y. Kondo, H. Uchiyama, N. Yoshino, K. Nishiyama, and M. Abe. Spontaneous vesicle formation from aqueous solutions of didodecyldimethylammonium bromide and sodium dodecyl sulfate mixtures. *Langmuir*, 11:2380, 1995.

[93] F.M. Konikoff, D.S. Chung, J.M. Donovan, D.M. Small, and M.C. Carey. Filamentous, helical, and tubular microstructures during cholesterol crystallization from bile. *J. Clin. Invest.*, 90:1155, 1992.

[94] J.T. LaMont and M.C. Carey. Cholesterol gallstone formation. 1. Pathobiology and pathomechanics. In H. Popper and F. Schaffner, editors, *Progress in Liver Diseases, Vol. X*, chapter 7, page 165. W.B. Saunders Co., Philadelphia, 1992.

[95] M.A. Lampert and R.U. Martinelli. Solution of the Poisson-Boltzmann equation in the interior of charged, spherical and cylindrical vesicles. I. The high-charge limit. *Chemical Physics*, 88:399, 1984.

[96] D.D. Lasic. Liposomes. *American Scientist*, 80:20, 1992.

[97] D.D. Lasic. *Liposomes: From Physics to Applications.* Elsevier Publishing Co., Amsterdam, 1993.

[98] J.L. Lebowitz, E. Helfand, and E. Praestgaard. Scaled particle theory of fluid mixtures. *J. Chem. Phys.*, 43:774, 1965.

[99] S.P. Lee, H.Z. Park, H. Madani, and E.W. Kaler. Partial characterization of a non-micellar system of cholesterol solubilization in bile. *Am. J. Physiology*, 252:G374, 1987.

[100] D. Lichtenberg and Y. Barenholz. Liposomes: Preparation, characterization, and preservation. In *Methods of Biochemical Analysis, Vol.33*, page 337. Wiley, New York, 1992.

[101] D.R. Lide. *CRC Handbook of Chemistry and Physics.* CRC Press, Boca Raton, FL, 71st edition, 1990.

[102] Z. Lin, M. He, L.E. Scriven, and H.T. Davis. Vesicle formation in electrolyte solutions of a new cationic siloxane surfactant. *J. Phys. Chem.*, 97:3571, 1993.

[103] C.L. Liu, U.K. Jain, P.H. Lee, N.A. Mazer, and W.I. Higuchi. Cholesterol thermodynamic activity, quasielastic light scattering, and polarizing microscopy

studies in aqueous taurocholate-lecithin solutions supersaturated with cholesterol. *J. Colloid Interf. Sci.*, 165:411, 1994.

[104] J. Lothe and G.M. Pound. Statistical mechanics of nucleation. In A.C. Zettlemoyer, editor, *Nucleation*, chapter 3, page 109. Marcel Dekker, Inc., New York, 1969.

[105] W.G. MacMillan and J.E. Mayer. The statistical thermodynamics of multicomponent systems. *J. Chem. Phys.*, 13:276, 1945.

[106] R.A. Marcus. Calculation of thermodynamic properties of polyelectrolytes. *J. Chem. Phys.*, 23:1057, 1955.

[107] S. Marrink and H.J.C. Berendsen. Simulation of water transport through a lipid membrane. *J. Phys. Chem.*, 98:4155, 1994.

[108] G.A. Martynov. Solution of the nonlinear Poisson-Boltzmann equation for a sphere. *Colloid Journal (USSR)*, 38:995, 1976.

[109] S. May and A. Ben-Shaul. Spontaneous curvature and thermodynamic stability of mixed amphiphilic layers. *J. Chem. Phys.*, 103:3839, 1995.

[110] N.A. Mazer, G.B. Benedek, and M.C. Carey. Quasielastic light-scattering studies of aqueous biliary lipid systems. Mixed micelle formation in bile salt-lecithin solutions. *Biochemistry*, 19:601, 1980.

[111] N.A. Mazer and M.C. Carey. Quasi-elastic light-scattering studies of aqueous biliary lipid systems. Cholesterol solubilization and precipitation in model bile solutions. *Biochemistry*, 22:426, 1983.

[112] D.A. McQuarrie. *Statistical Mechanics.* Harper & Row, New York, 1975.

[113] M. Mille and G. Vanderkooi. Electrochemical properties of spherical polyelectrolytes II. Hollow sphere model for membranous vesicles. *J. Colloid Interf. Sci.*, 61:455, 1977.

[114] S.T. Milner, T.A. Witten, and M.E. Cates. Theory of the grafted polymer brush. *Macromolecules*, 21:2610, 1988.

[115] D.J. Mitchell and B.W. Ninham. Micelles, vesicles and microemulsions. *J. Chem. Soc. Faraday Trans. 2*, 77:601, 1981.

[116] D.J. Mitchell and B.W. Ninham. Electrostatic curvature contributions to interfacial tension of micellar and microemulsion phases. *J. Phys. Chem.*, 87:2996, 1983.

[117] D.J. Mitchell and B.W. Ninham. Curvature elasticity of charged membranes. *Langmuir*, 5:1121, 1989.

[118] E.W. Moore. Biliary calcium and gallstone formation. *Hepatology*, 12:206S, 1990.

[119] D.C. Morse and S.T. Milner. Fluctuations and phase behavior of fluid membrane vesicles. *Europhys. Lett.*, 26:565, 1994.

[120] A.K. Murthy, E.W. Kaler, and J.A. Zasadzinski. Spontaneous vesicles from aqueous solutions of aerosol ot and choline chloride compounds. *J. Colloid Interf. Sci.*, 145:598, 1991.

[121] R. Nagarajan. Micellization of binary surfactant mixtures: Theory. In P.M. Holland and D.N. Rubingh, editors, *Mixed Surfactant Systems*, chapter 4, page 54. American Chemical Society, Washington,D.C., 1992.

[122] R. Nagarajan. Modelling solution entropy in the theory of micellization. *Colloids Surfaces A: Physicochem. Eng. Aspects*, 71:39, 1993.

[123] R. Nagarajan and E. Ruckenstein. Critical micelle concentration: A transition point for micellar size distribution. *J. Colloid Interf. Sci.*, 60:221, 1977.

[124] R. Nagarajan and E. Ruckenstein. Aggregation of amphiphiles as micelles or vesicles in aqueous media. *J. Colloid Interf. Sci.*, 71:580, 1979.

[125] R. Nagarajan and E. Ruckenstein. Theory of surfactant self-assembly: A predictive molecular thermodynamic approach. *Langmuir*, 7:2934, 1991.

[126] A.E. Nielsen and P.S. Bindra. The effect of curvature on interfacial tension in liquid systems measured by homogeneous nucleation. *Croatica Chemica Acta*, 45:31, 1973.

[127] M.J.P. Nijmeijer, C. Bruin, A.B. van Woerkom, and A.F. Bakker. Molecular dynamics of the surface tension of a drop. *J. Chem. Phys.*, 96:565, 1992.

[128] Y.J. Nikas, S. Puvvada, and D. Blankschtein. Surface tensions of aqueous nonionic surfactant mixtures. *Langmuir*, 8:2680, 1992.

[129] B.W. Ninham and D.F. Evans. The rideal lecture: Vesicles and molecular forces. *Faraday Discuss. Chem. Soc.*, 81:1, 1986.

[130] B.W. Ninham, D.F. Evans, and G.J. Wei. The curious world of hydroxide surfactants. spontaneous vesicles and anomalous micelles. *J. Phys. Chem.*, 87:5020, 1983.

[131] H. Noshiro, K. Chijiiwa, and I. Hirota. Activity of cholesterol in human gallbladder bile in relation to nucleation of cholesterol monohydrate crystals. *Clin. Chim. Acta*, 205:167, 1992.

[132] H. Ohshima, T.W. Healy, and L.R. White. Accurate analytic expressions for the surface charge density / surface potential relationship and double-layer potential distribution for a spherical colloidal particle. *J. Colloid Interf. Sci.*, 90:1, 1982.

[133] I.W. Osborne-Lee, R.S. Schechter, W.H. Wade, and Y. Barakat. A new theory and new results for mixed nonionic-anionic micelles. *J. Colloid Interf. Sci.*, 108:60, 1985.

[134] C.W. Outhwaite. Equilibrium theory of electrolyte solutions. *Stat. Mech.: A Specialist Periodical Report*, 2:188, 1975.

[135] N.R. Pattinson and B.A. Chapman. Distribution of biliary cholesterol between mixed micelles and nonmicelles in relation to fasting and feeding in humans. *Gastroenterology*, 91:697, 1986.

[136] Y. Peled, Z. Halpern, B. Eitan, G. Goldman, F. Konikoff, and T. Gilat. Biliary micellar cholesterol nucleates via the vesicular pathway. *Biochim. Biophys. Acta*, 1003:246, 1989.

[137] J.L. Pope. Crystallization of sodium taurocholate. *J. Lipid Res.*, 8:146, 1967.

[138] S. Puvvada and D. Blankschtein. Molecular-thermodynamic approach to predict micellization, phase behavior and phase separation of micellar solutions. I. Application to nonionic surfactants. *J. Chem. Phys.*, 92:3710, 1992.

[139] S. Puvvada and D. Blankschtein. Theoretical and experimental investigations of micellar properties of aqueous solutions containing binary mixtures of nonionic surfactants. *J. Phys. Chem.*, 96:5579, 1992.

[140] S. Puvvada and D. Blankschtein. Thermodynamic description of micellization, phase behavior, and phase separation of aqueous solutions of surfactant mixtures. *J. Phys. Chem.*, 96:5567, 1992.

[141] Weast R.C. *CRC Handbook of Chemistry and Physics.* CRC Press, Boca Raton,FL, 67th edition, 1986.

[142] D. Rickwood and G.D. Birnie. Introduction: Principles and practices of centrifugation. In G.D. Birnie and D. Rickwood, editors, *Centrifugal Separations in Molecular and Cell Biology*, page 1. Butterworths & Co., London, 1978.

[143] W.R. Rossen, H.T. Davis, and L.E. Scriven. Sedimentation of molecular solutions in the ultracentrifuge: I. Equilibrium phase behavior. *J. Colloid Interf. Sci.*, 113, 1986.

[144] J.S. Rowlinson and B. Widom. *Molecular Theory of Capillarity.* Oxford University Press, New York, 1982.

[145] H.Y. Saad and W.I. Higuchi. Water solubility of cholesterol. *J. Pharm. Sci.*, 54:1205, 1965.

[146] S.A. Safran, F.C. MacKintosh, P.A. Pincus, and D. Andelman. Spontaneous vesicle formation by mixed surfactants. *Progr. Colloid Polym. Sci.*, 84:3, 1991.

[147] S.A. Safran, P.A. Pincus, and D. Andelman. Theory of spontaneous vesicle formation in surfactant mixtures. *Science*, 248:354, 1990.

[148] S.A. Safran, P.A. Pincus, D. Andelman, and F.C. MacKintosh. Stability and phase behavior of mixed surfactant vesicles. *Phys. Rev. A*, 43:1071, 1991.

[149] S. Sahlin, P. Thyberg, J. Ahlberg, B. Angelin, and K. Einarsson. Distribution of cholesterol between vesicles and micelles in human gallbladder bile: Influence of treatment with chenodeoxycholic acid and ursodeoxycholic acid. *Hepatology*, 13:104, 1991.

[150] J.J. Salacuse and G. Stell. Polydisperse systems: Statistical thermodynamics, with applications to several models including hard and permeable spheres. *J. Chem. Phys.*, 77:3714, 1982.

[151] B.F. Smith. Gallbladder mucin as a pronucleating agent for cholesterol monohydrate crystals in bile. *Hepatology*, 12:183S, 1990.

[152] G.J. Sömjen and T. Gilat. A non-micellar mode of cholesterol transport in human bile. *FEBS Letters*, 156:265, 1983.

[153] G.J. Sömjen and T. Gilat. Contribution of vesicular and micellar carriers to cholesterol transport in human bile. *J. Lipid Res.*, 26:699, 1985.

[154] G.J. Sömjen, E. Wachtel, O. Warshavskaya, R. Rosenberg, and T. Gilat. Comparison of ultracentrifugation and chromatography for the separation and quantitation of cholesterol carriers in model and human hiles [abstract]. *Hepatology*, 18, 1993.

[155] D. Stigter. On the adsorption of counterions at the surface of detergent micelles. *J. Phys. Chem.*, 68:3603, 1964.

[156] D. Stigter. Micelle formation by ionic surfactants. III. Model of stern layer, ion distribution, and potential fluctuations. *J. Phys. Chem.*, 79:1008, 1975.

[157] D. Stigter. Micelle formation by ionic surfactants. IV. Electrostatic and hydrophobic free energy from stern-gouy ionic double layer. *J. Phys. Chem.*, 79:1015, 1975.

[158] S.M. Strasberg, J.L. Toth, S. Gallinger, and P.R.C. Harvey. High protein and total lipid concentration are associated with reduced metastability of bile in an early stage of cholesterol gallstone formation. *Gastroenterology*, 98:739, 1990.

[159] I. Szleifer. *Statistical Thermodynamics of Amphiphilic Aggregates.* PhD thesis, Hebrew University, 1988.

[160] I. Szleifer, A. Ben-Shaul, and W.M. Gelbart. Statistical thermodynamics of molecular organization in mixed micelles and bilayers. *J. Chem. Phys.*, 86:7094, 1987.

[161] Y. Talmon, D.F. Evans, and B.W. Ninham. Spontaneous vesicles formed from hydroxide surfactants: Evidence from electron microscopy. *Science*, 221:1047, 1983.

[162] C. Tanford. *The Hydrophobic Effect: Formation of Micelles and Biological Membranes.* John Wiley & Sons, New York, 1973.

[163] T. Taniguchi, K. Kawasaki, D. Andelman, and T. Kawakatsu. Equilibrium shape deformations of two-component vesicles. *Cond. Matt. Materials Comm.*, 1:75, 1993.

[164] T. Taniguchi, K. Kawasaki, D. Andelman, and T. Kawakatsu. Phase transitions and shapes of two component membranes and vesicles II: Weak segregation limit. *J. Phys. II (France)*, 4:1333, 1994.

[165] B.G. Tenchov, R.D. Koynova, and B.D. Raytchev. The electrical double layer inside a spherical aqueous cavity: A comparison between exact numerical and approximate analytical solutions. *J. Colloid Interf. Sci.*, 102:337, 1984.

[166] H.G. Thomas. *Experimental and Theoretical Studies of Phase Transitions and Micellar Size Distributions in Ternary Surfactant Systems.* PhD thesis, Massachusetts Institute of Technology, 1995.

[167] R.C. Tolman. The effect of droplet size on surface tension. *J. Chem. Phys.*, 17, 1949.

[168] S.D. Turley and J.M. Dietschy. Re-evaluation of the 3α-hydroxysteroid dehydrogenase assay for total bile acids in bile. *J. Lipid Res.*, 19:924, 1978.

[169] N. Ulloa, J. Garrido, and F. Nervi. Ultracentrifugal isolation of vesicular carriers of biliary cholesterol in native human and rat bile. *Hepatology*, 7:235, 1987.

[170] K.J. van Erpecum, G.P. van Berge Henegouwen, B. Stoelwinder, Y.M.G. Schmidt, and F.L.H. Willekens. Bile concentration is a key factor for nucleation of cholesterol crystals and cholesterol saturation index in gallbladder bile of gallstone patients. *Hepatology*, 11:1, 1990.

[171] E.J.W. Verwey and J.Th.G. Overbeek. *Theory of the Stability of Lyophobic Colloids.* Elsevier Publishing Co., New York, 1948.

[172] V. Vlachy and J.M. Prausnitz. Donnan equilibrium. Hypernetted-chain study of one-component and multicomponent models for aqueous polyelectrolyte solutions. *J. Phys. Chem.*, 96:6465, 1992.

[173] H. Wennerström and B. Lindman. Micelles. Physical chemistry of surfactant association. *Phys. Rep.*, 52:1, 1979.

[174] L.R. White. Approximate analytic solution of the Poisson-Boltzmann equation for a spherical colloidal particle. *J. Chem. Soc. Faraday Trans. 2*, 73:577, 1977.

[175] M. Winterhalter and W. Helfrich. Bending elasticity of electrically charged bilayers: Coupled monolayers, neutral surfaces, and balancing stresses. *J. Phys. Chem.*, 96:327, 1992.

[176] A. Yethiraj, C.K. Hall, and R. Dickman. Interaction between colloids in solutions containing dissolved polymer. *J. Colloid Interf. Sci.*, 151:102, 1992.

[177] P.K. Yuet and D. Blankschtein. Approximate expressions for the surface potentials of charged vesicles. *Langmuir*, 11:1925, 1995.

[178] P.K. Yuet and D. Blankschtein. Molecular - thermodynamic modeling of mixed cationic/anionic vesicles. *Langmuir*, 1995. submitted.

[179] P.K. Yuet and D. Blankschtein. Effect of surfactant tail-length asymmetry on the formation of mixed surfactant vesicles. *Langmuir*, 1996. submitted.

[180] P.K. Yuet, D. Blankschtein, and J.M. Donovan. Study of cholesterol distribution and vesicle composition in model bile using two-level factorial experimental design. *Hepatology*, 1996. submitted.

[181] P.K. Yuet, D. Blankschtein, and J.M. Donovan. Ultracentrifugation systematically overestimates vesicular cholesterol in bile. *Hepatology*, 1996. in press.